INVESTIGATING THE RESPONSE OF LIGHT-FRAME WOOD STUD WALLS WITH AND WITHOUT BOUNDARY CONNECTIONS TO BLAST LOADS

by

Christian Viau

Thesis submitted to the
Faculty of Graduate and Postdoctoral Studies
in partial fulfillment of the requirements for the degree of

Master of Applied Science

in Civil Engineering

Under the auspices of the Ottawa-Carleton Institute for Civil Engineering

uOttawa

University of Ottawa

ABSTRACT

Most of the research on high strain rate effects on wood since the 1950s has been on impact loading. Very limited work has been conducted on full-scale wood specimens under blast loading. In North America, the prevalence of these structures makes them susceptible to unintended blast effects. The question on how to retrofit and protect these structures against blast loads has still not been addressed adequately, and design provisions for new wood structures against blast are not comprehensive.

Far-field explosion effects were simulated using the University of Ottawa shock tube. Twenty-five light-frame wood stud walls were tested dynamically. The research program aimed to determine the response of light-frame wood stud walls to blast loads that correspond to the heavy to blow-out damage levels. The results showed that, under idealized simply supported end conditions, the stud walls failed in flexure. Under heavier loads, ripping of sheathing commonly used in light-frame wood structures was observed, which caused premature failure of the assembly because the load was not fully distributed to the studs. The use of stiffer sheathing or reinforcing the sheathing provided a better load path and the wall was capable of reaching its full capacity. The effect of using realistic boundary connection details was investigated, and the results showed that typical connection detailing performed poorly under blast loads. Designed steel brackets connecting the studs to the rim-joist allowed for the studs to reach their full capacity. An analytical single degree-of-freedom model was generated using material properties obtained from static testing. The model was validated using the experimental results from the shock tube testing. Also, a catcher system consisting of welded-wire-mesh was incorporated into the wall system in order to diminish debris throw.

ACKNOWLEDGEMENTS

The process of writing this thesis allowed me to exponentially develop from whom I was two years ago. Such an arduous task not only necessitated self-dedication from myself, but also the assistance, friendship, and guidance provided by many individuals and organizations.

First and foremost, I would like to thank my thesis supervisor, Dr. Ghasan Doudak, for his time, patience, and energy invested in me and my project. Without his guidance and financial support, particularly when expensive equipment was destroyed during laboratory testing, this thesis could not have been written and completed with its inherent quality and thoroughness.

I would like to recognize the financial support received throughout my master's, specifically from the Natural Sciences and Engineering Research Council of Canada, the Province of Ontario (OGS), and the University of Ottawa. This financial aid allowed me to focus solely on my research and coursework, making the overall experience significantly better.

I'd like to take this opportunity to acknowledge Mr. Daniel Lacroix, for all the help and guidance he has provided me since day one. Special thanks go to Mr. Eric Jacques, for providing me and everyone in blast engineering with an invaluable analysis tool, *RCBlast*, as well as for his technical backing throughout testing. To those who accepted my plea for help in the laboratory, especially during evenings and weekends, I am forever appreciative of your help: Mr. Pedro Guimarães, Mr. Arthur Manieri, Mr. Jose Barreiro, Mr. Samuel Clémot-Dupont, Mr. Alexandre Lafontaine, Ms. Madelyn Pos, Mr. Rémi St-Amour, and Mr. Frédéric Dagenais.

Last but certainly not least, I give countless thanks to my mother, father, and brother, for believing in and supporting me throughout the process of writing this thesis. Without your constant affection and moral support, all of this could not have been possible. Encore une fois, merci à vous.

TABLE OF CONTENTS

LIST OF TABLES

LIST OF FIGURES

NOTATIONS

Symbol	Definition
I^+	Positive impulse
I^-	Negative impulse
A	Loaded area
B	Rotational restraint constant
c	Damping coefficient
DIF	Dynamic increase factor
DIF_{MOE}	Dynamic increase factor on the modulus of elasticity
DIF_{MOR}	Dynamic increase factor on the modulus of rupture
D_{max}	Average maximum displacement
$D_{max\text{-}EXP.}$	Average maximum experimental displacement
$D_{max\text{-}SDOF}$	SDOF-predicted maximum displacement
EA_f	Axial stiffness of the flange
EA_w	Axial stiffness of the web
$\overline{EA_f}$	Modified axial stiffness of the flange
EI_{PCA}	Bending stiffness with PCA
EI_w	Bending stiffness of the web
f(x,t)	Distributed load per unit length relative to time
F(t)	External forcing function
f_b	Specified 5^{th} percentile design strength in bending
F_o	Peak pressure in idealized triangular forcing function
h	Distance between centroids
k	Stiffness
K_D	Load duration factor
K_H	System effect factor
K_L	Lateral stability factor
K_L	Load transformation factor
K_{LM}	Load-mass transformation factor
K_m	Mass transformation factor
K_R	Resistance transformation factor
K_{Sb}	Service condition factor in bending
K_T	Treatment factor
K_{Zb}	Size effect factor in bending
L	Clear span
L_f	Distance between sheathing gaps
m	Mass

$\bar{m}(x)$	Distributed mass
M_p	Ultimate moment capacity
μ	Ductility ratio
$\emptyset(x)$	Shape function
P_R	Peak reflected pressure
P_s	Incident pressure
R(y)	Resistance function
R_e	Elastic resistance
R_u	Ultimate resistance
S	Interlayer stiffness
S_D	Dynamic bending strength
SIF	Strength increase factor
S_{PCA}	Section modulus with PCA
S_S	Static bending strength
t	Time
t_a	Arrival time of shock wave
t_d	Idealized positive phase duration
T_{max}	Average time-to-maximum
$T_{max\text{-}EXP.}$	Maximum average experimental time-to-maximum
$T_{max\text{-}SDOF}$	Maximum SDOF-predicted time-to-maximum
t_o	Positive phase time duration
t_o^-	Negative phase time duration
W	Uniformly distributed load
x_e	Elastic limit
x_{max}	Maximum displacement
y	Displacement
$\dot{y}$	Velocity
$\ddot{y}$	Acceleration
Δ	Mid-span deflection
ω	Natural frequency
ϕ	Material resistance factor

Acronym	Definition
ASD	Allowable stress design
ASTM	American Society for Testing and Materials
ATD	Anthropomorphic test device
COV	Coefficient of variation
CSA	Canadian Standards Association
CSL	Coated structural lumber
EN 1995	Eurocode 5 : Design of timber structures
FEA	Finite element analysis
FRP	Fibre-reinforced polymer
HSS	Hollow structural section
LLRS	Lateral Load Resisting System
LOP	Level of protection
LRFD	Load and resistance factor design
LSL	Laminated strand lumber
LVDT	Linear variable differential transducer
MOE	Modulus of elasticity
MOR	Modulus of rupture
NBCC	National Building Code of Canada
NDS	National Design Specification
O/C	On-center
OSB	Oriented strand board
PCA	Partial composite action
P-I	Pressure-impulse
POI	Point of interest
PSL	Parallel strand lumber
SD	Standard deviation
SDOF	Single degree-of-freedom
SEA	South-East Asia
SPF	Spruce-pine-fir
TNT	Trinitrotoluene
USAF	United States Air Force
UTM	Universal testing machine
WWM	Welded wire mesh

CHAPTER 1 - Introduction

1.1 Background

In recent times, environmental hazards to structures, such as earthquakes, strong winds, tsunamis, etc., have become well understood and documented by researchers, engineers and government officials. Consequently, the necessary design guidelines against these loads are now well established and continue to be optimized with the increase interest in these fields of research. Blast loading, on the other hand, is more difficult to quantify and has only recently regained interest from the research community primarily due to recent deliberate attacks (e.g. World Trade Center (2001), Oklahoma City bombing (1995)) or accidental explosions (e.g. Lac-Mégantic rail disaster (2014), Texas City Refinery explosion (2005)). Blast loads are known to cause significant structural damage and loss of human life. Provisions have been enacted around the world and documents are now available for designers to design against blast loads and their effects on structures (DHS, 2011; USADD, 2009; USADD 2008; USACE, 2008; Office of the Deputy Prime Minister, 2004).

1.2 Research needs

Most published research on the topic of blast is related to reinforced concrete and steel structures; little to no research has been done explicitly on wood structures. This is due to the lack of any inherent blast resistant properties: wood is relatively light (approximately 5x lighter than concrete, 17x lighter than steel) and is generally considered a brittle material. However, with the advancement in timber technology and the introduction of engineered wood products, taller and larger wood structures are now being constructed. Several Canadian provinces have enacted new provisions to allow the use of timber in construction, such as the “Wood First Act” in British Columbia, which requires wood to be considered as the primary building material in all new publicly funded buildings (Government of BC, 2009) and Ontario, where the newly amended Ontario Building Code now permits mid-rise buildings (up to six storeys) to be made entirely out of wood (Government of Ontario, 2014).

While the current building code of Canada (NRC, 2015) does not require the design against blast loads, the Canadian Standard Association (CSA) has published a standard which addresses blast

load analysis and design requirements (CSA, 2012). This standard addresses design considerations for various materials, including timber. It should be noted, however, that the research utilized to produce the design provisions for timber structures has been based on very limited research, most of which were conducted on small scale clear specimens (Jansson, 1992; Spencer, 1978).

The method by which the current standard calculates the dynamic strength of timber is by multiplying the static design strength of a single stud (no sheathing or load-sharing contribution) by a strength increase factor and a dynamic increase factor. The former deals with the fact that a blast scenario is a rare load case and therefore design level capacity values are too conservative to be considered in such a rare event and the latter deals with the increase in strength due to strain rate effects. While the blast code considers material strength increase, it does not consider any load-sharing contribution brought on by the connectivity between multiple load-bearing elements and sheathing. Effects on stiffness is also ignored, due to lack of research on this topic.

Published research has focused primarily on the understanding of the overall behaviour and response to blast of timber specimens and assemblies under simply supported end conditions. While these tests have contributed greatly to current knowledge, they have neglected to take into account realistic boundary conditions including the connections between the wall and the floors above and below it. The connection between subsystems in a light-frame wood structure is a very critical part of the overall system and one can therefore not simply assume that they are able to withstand blast loads. Detailing a wood stud wall for blast loads may not be adequate if the connections are not considered, since the main assumption is that flexural failure will occur in the load-bearing element; this capacity may not be reached if the connection fails prematurely. The current study investigates both typical as well as engineered connections to establish their behaviour and effect on the performance of the wall subsystem.

While the blast wave of any blast load is often considered as the main danger to a structure, flying debris and fragment are the main cause of occupant injuries (Bogosian & Avanessian, 2004). The current CSA standard states that any component, whether structural or non-structural shall be designed and detailed so that the risk of flying debris is reduced (CSA, 2012). Flying debris is very difficult to quantify and an alternative method for mitigating the adverse effect of debris is by

designing and detailing a catcher system that encapsulates and contains the debris throw. Such a system is also being investigated in the current study.

1.3 Light-frame wood stud walls

Wood is widely available, has a relative low cost as a construction material, is easy to use, and is durable when properly designed (Mamlouk & Zaniewski, 2011). Our harsh Canadian winters promote growth rings that are typically stronger than what is found in wood from warmer forests. These facts explain why the use of light-frame wood stud walls is so prevalent in North America, especially in residential construction.

Light-frame wood stud walls generally consist of four main components: studs, top and bottom plates, sheathing, and mechanical fasteners. The studs are the main load-bearing elements, usually consisting of 38 x 140 mm (2 x 6 in. nominal) visually graded lumber, with a spacing that is often based on code provisions or traditional practice. These studs are held in placed, in part, by a single bottom plate and two top plates with the same dimensions as the studs. The assembly is then covered (or sheathed) with plate elements, such as oriented strand board (OSB) or plywood. These usually come in panels of 1.22 x 2.44 m (4 x 8 ft.). Finally, all components are held together with mechanical fasteners, consisting typically of nails, however, screws or staples are also used. This creates a highly redundant system, due in part to the repetitious nature of the load-bearing elements and the connectivity between them. A visual representation of a wall subsystem is shown in Figure 1.1.

1.4 Blast loading

1.4.1 Types of blast loading

When an explosion occurs, a large amount of energy is released from the source, the majority of which is in the form of a shock-wave. This energy can be chemical, physical, or nuclear in nature. Radiation, fragments, or other entities may accompany the blast wave, depending on the source of the blast. Most research, however, has focused on physical and chemical explosions, as nuclear attacks on structures are extremely rare. There are two types of energy release mechanisms: deflagration and detonation. Deflagration occurs when the burning process rate of the energy source is slower than the speed of sound (i.e. subsonic). Detonation occurs when the burning

process rate exceeds the speed of sound (i.e. supersonic) (Krauthammer, 2008). In both processes, the fuel in question is transformed from a solid or liquid to a gas. High explosives, such as TNT or nitroglycerin, typically produce a detonation, whereas volatile gases produce deflagration. Detonations produce the shock wave that is most hazardous to structures as these types of explosions do not require any additional source of fuel to propagate through a medium, since the required energy is already provided or present once the burning process is initiated. Figure 1.2 documents the detonation of TNT that occurred as part of a series of tests by the US government as part of Operation Sailor Hat (1965). The white blast-wave is visible on the water surface and a shock condensation cloud appears above the source of detonation. Pressure waves created by a deflagration are typically smaller in magnitude to a shock wave, as additional energy source is required so that the pressure wave may propagate. However, in a highly concentrated or confined area (e.g. refining or petrochemical plants), a deflagration can be just as hazardous as a detonation (Cormie et al., 2009).

1.4.2 Shock wave characteristics

Focusing on the shock waves produced by a detonation, it is important to understand the fundamentals of how a shock wave is formed, how it propagates, and how it interacts with structures.

Once detonation occurs, a shock wave will be initiated and it will propagate in all direction in a spherical or hemispherical profile, depending on its location relative to the ground. As the blast wave travels away from the source, a reduction in the pressure and an increase in the overall blast duration will occur. This initial shock front is known as the “positive phase” and will generally have the greatest effect on the structure. Due to the overexpansion of the air particles brought on by the positive phase, a vacuum will be created due to the lower-than-ambient pressure. This is known as the “negative phase” pressure wave. This phase is generally longer in duration, but typically has much less effects on the structure. Oftentimes, designers completely ignore the effects of any other phases besides the initial positive phase (Dusenberry, 2010). This may be adequate for most design cases where the structural element is designed for multidirectional loading (such as a column) but may not be adequate in case of unidirectional loading (such as a design of window anchorage). Following the negative phase, a return to ambient pressure is experienced.

The effects of shock waves on structures are complicated in nature but are usually simplified during analysis. As the shockwave arrives at the structure, the incident pressure (the pressure which was created by the detonation) increases, due to the continuous arrival of air particles which further compresses the air surrounding the structure. This is known as the reflected pressure. The reflected pressure-time history is typically idealized as a sharp and sudden rise in pressure. The reflected pressure would gradually decrease until the end of the positive phase, which then marks the beginning of the negative phase. Plotting the relationship between reflected pressure and time (i.e. pressure-time history curves), designers are able to determine the two key parameters in any blast analysis, namely peak positive reflected pressure and positive impulse. Impulse is a direct measurement of the amount of energy brought on by a shock wave and is defined as the area under the pressure-time history curve. There can be positive and negative impulses, as calculated by Equations 1.1 and 1.2, respectively. All of these parameters and blast properties are shown in Figure 1.3.

$$I^+ = \int_{t_a}^{t_a+t_o} P_s(t)dt \qquad \text{Equation 1.1}$$

$$I^- = \int_{t_a+t_o}^{t_a+t_o+t_o^-} P_s(t)dt \qquad \text{Equation 1.2}$$

1.5 Dynamic analysis methods

1.5.1 Overview

The short time duration of a blast load, compared with other loadings such as dead loads, live load, earthquake loads, and wind loads, implies that the inertial forces and the kinetic energy cannot be neglected in the analysis of a structure. The use of an equivalent static approach to analyze blast loading is generally not acceptable. On the other hand, the uncertainties associated with blast loads and the material properties (especially for wood) justify the use of simplified modelling techniques such as single degree-of-freedom (SDOF). Official documents have recently established the SDOF methodologies for carrying out these types of analysis and their limitations (USACE, 2008; USADD, 2008) which have been shown to accurately predict the behaviour of various structural elements subjected to blast loads (e.g. Lacroix, 2013; Parlin, 2010; Lloyd, 2010).

1.5.2 Closed-form SDOF analysis

The close-form solution of a typical SDOF system consists of solving the following equation of motion:

$$m\ddot{y} + c\dot{u} + ky = F(t) \qquad \text{Equation 1.3}$$

Where the system is represented as having a mass of "m", a damping coefficient of "c", a stiffness of "k", and a forcing function which is dependent on time, "F(t)". The unknowns are y, $\dot{y}$, and $\ddot{y}$, which represent the displacement, velocity, and acceleration, respectively. A visual representation of Equation 1.3 is shown in Figure 1.4. In blast, it is often reasonable to assume that damping is negligible (Jansson, 1992; Biggs, 1964). Therefore, the close-form solution of Equation 1.3, assuming that F(t) can be represented as a triangular loading function with a time duration of t_d and with a peak pressure of F_o, is:

$$y(t) = \frac{F_o}{k}\left(\frac{\sin(\omega t)}{\omega t_d} - \cos(\omega t) - \frac{t}{t_d} - \ +1\right) \qquad \text{Equation 1.4}$$

Where ω represents the natural frequency of the system, in rad/sec. The main assumption in using this method and solution is that the mass of the system is concentrated at a single point and that the forcing function is applied at that particular point. These assumptions are not realistic, as structural components are continuous with a distributed mass, stiffness, and forcing function. Ignoring these discrepancies can introduce significant error into analysis (USADD, 2008).

In order to circumvent the shortcomings of traditional SDOF analysis described in the previous section, the system can be transformed into an equivalent SDOF system. This is done by selecting a point of interest (POI), where the mass, stiffness, and applied force of the real system are lumped (Biggs, 1964). Research has shown that light-frame wood stud walls tend to vibrate and deflect in the first mode shape, therefore making the assumption of this particular deflected shape appropriate (Polensek & Schimel, 1991). Transformation factors are calculated in order to transform the real system into an equivalent SDOF system. Equation 1.5 presents the equation of motion for the equivalent SDOF system, which includes the mass transformation factor, K_m, the resistance transformation factor, K_R, the load transformation factor, K_L, and the resistance term, R(y).

$$K_M m\ddot{y}(t) + K_R R(y) = K_L A P_R \left(1 - \frac{t}{t_d}\right) \quad \text{Equation 1.5}$$

Due to the fact that the negative phase is not considered, when time is equal or greater than the positive phase (t_d), the value of the forcing function is set to zero. P_R is the peak positive reflected pressure, while A is the loaded area. The transformation factors are calculated by equalling the kinetic energy, potential energy, and work done by the force to that of the equivalent SDOF system. This yields the following relationships:

$$K_M = \frac{\int_0^L \bar{m}(x)\emptyset^2(x)dx}{\int_0^L \bar{m}(x)dx} \quad \text{Equation 1.6}$$

$$K_L = \frac{\int_0^L f(x,t)\emptyset(x)dx}{\int_0^L f(x,t)dx} \quad \text{Equation 1.7}$$

Where $\bar{m}(x)$ is the distributed mass, $\emptyset(x)$ is the shape function based on the first mode deflected shape, $f(x,t)$ is the distributed load per unit length relative to time. K_R is taken as equal to K_L, due to the fact that resistance is the internal force going against the external force, trying to bring it back to initial position and therefore will typically be distributed similarly to the applied load (USADD, 2008). The format of the equivalent system is made simpler by describing a single transformation factor, defined as the ratio of the mass and load factors, as shown Equation 1.8, and yielding an equivalent SDOF system equation with a single transformation factor, as can be seen in Equation 1.9.

$$K_{LM} = \frac{K_M}{K_L} \quad \text{Equation 1.8}$$

$$K_{LM} m\ddot{y}(t) + R(y) = A P_R \left(1 - \frac{t}{t_d}\right) \quad \text{Equation 1.9}$$

1.5.3 Resistance curve

The resistance-deflection relationship is an essential part of any dynamic analysis since the physical response of a structural element can be directly correlated to its resistance curve. Resistance curves are typically modelled as linear or non-linear; therefore proper understanding of the material considered is key to choosing a suitable resistance curve.

1.5.4 Pressure-Impulse (P-I) diagrams

P-I diagrams are perhaps one of the most effective tools in determining the performance level and overall response of any type of structural assembly under the effect of pressure-impulse combinations. Usually generated via single degree-of-freedom formulations, assuming a certain failure mode and criteria, they allow for the plotting of iso-damage curves which separate regions that correlate to defined damage levels. An example of a typical P-I diagram is shown in Figure 1.5.

There are three different loading regimes in a P-I diagram: impulsive, dynamic, and quasi-static (Figure 1.6). In the impulsive regime, the load duration is usually short relative to response time. In other words, the load is applied and removed in a timeframe that does not allow the structure to respond. The quasi-static regime, on the other hand, has significantly longer load duration. The load does not dissipate before the response of the structure is attained. The response of the structure under this regime depends largely on its stiffness and the peak load. Finally, the dynamic regime is more complex, due to the fact that it is largely influenced by load duration, response time, and loading history (Krauthammer, 2008).

The CSA blast standard defines the iso-damage regions by ductility ratio and support rotation. Ductility ratio is defined as the ratio between maximum deformation and apparent elastic deformation while taking dynamic effects into account, as shown in Equation 1.10 (CSA, 2012). These response limits can be viewed in Table 1.1.

$$\mu = \frac{x_{max}}{x_e} \qquad \text{Equation 1.10}$$

1.6 Research objectives

The objective of this research project is to assess the behaviour of light-frame wood stud walls when subjected to blast loads that would cause hazardous and blowout levels of damage. In addition to focusing on simply supported end conditions, to establish a baseline for the flexure behaviour of the wall system, effort is also made to develop potential retrofits for any shortcomings observed during testing. In detail, the goals of this project are to:

1) Investigate the behaviour of light-frame wood walls exposed to blast loading in the high and blow-out regions, and develop appropriate material predictive models for the wall system including those with realistic connections;
2) Investigate and propose viable retrofit options for typical sheathing deficiencies and propose catcher system options to deal with debris;
3) Determine if typical connection detailing for stud walls are adequate for blast and propose viable retrofit options for stud wall connectors, and;
4) Determine the validity of and possibly refine CSA S850 provisions.

1.7 Scope

The stated research objectives will be achieved by the following course of actions:

- Carry out a detailed literature review on the behaviour of light-frame wood stud walls when subjected to impact and blast loading, model different stud walls aspects (strain rate effects, partial composite action, support restraint), and investigate existing retrofitting techniques;
- Determine the capacity and stiffness of a batch of studs and build twenty-five walls from said batch;
- Test the twenty-five walls dynamically using the University of Ottawa shock-tube and establish the damage level for each wall;
- Dynamically test various wall-sheathing setups for possible retrofit options;
- Simulate real-life connection details and determine via dynamic testing how typical connection perform when subjected to blast loading;
- Propose and dynamically test retrofit options for connection;
- Develop a material predictive model based on component properties obtained from static testing;
- Experimentally determine the nail-slip relationship between the studs and sheathing in order to apply partial composite action to the analytical model;
- Verify the applicability of code provisions and most recent research results concerning dynamic increase factors, and;
- Discuss the results, code implications, and make suggestions for code provision improvements.

1.8 Structure of thesis

Chapter 1 presented an introduction regarding the topics of blast loading, light-frame wood stud walls, as well as the research needs and objectives.

Chapter 2 presents a literature review on a number of studies that have been performed on the dynamic behaviour of wood, analytical modelling of wood elements subjected to blast, and existing retrofit techniques.

Chapter 3 presents a description of the experimental program that was utilized during the course of the research.

Chapter 4 presents the experimental program results, including static bending tests (both destructive and non-destructive) of studs and sheathing coupons, nail-slip testing for the connectivity between the studs and various sheathings, as well as dynamic tests performed on light-frame wood stud walls with various components (sheathing types, support conditions, etc.).

Chapter 5 presents the analytical modelling techniques and methodologies utilized in order to create a non-linear material predictive model. Also displayed in this chapter are the different model parameters tested and compared with each other. Analytical results are also presented.

Chapter 6 presents the discussion of both experimental and analytical results. Focus will be on the analytical portion of the work performed.

Chapter 7 presents the implications of the blast standard, including a direct comparison between the provisions provided by the code and the ones recommended in Chapter 5 and Chapter 6.

Chapter 8 presents a summary of the most significant research findings. It also presents the unanswered questions from the work that has been done, as well as possible new research topics that the current research has unveiled.

The Appendix presents detailed summaries of all performed dynamics tests, which includes test and analysis results.

Table 1.1 : Response limits for wood structures (CSA, 2012)

Element type	B1		B2		B3		B4	
	μ_{max}	θ_{max}	μ_{max}	θ_{max}	μ_{max}	θ_{max}	μ_{max}	θ_{max}
Flexure	1	—	2	—	3	—	4	—
Combined flexure and compression	1	—	2	—	2	—	2	—
Axial compression‡	—	—	—	—	—	—	1	2.4°

* *Where a dash (—) is shown, the corresponding parameter is not applicable as a response limit.*
† *Values shown are based on very limited test data; use specific test data if available.*
‡ *Ductility ratio is based on axial deformation rather than lateral deformation.*

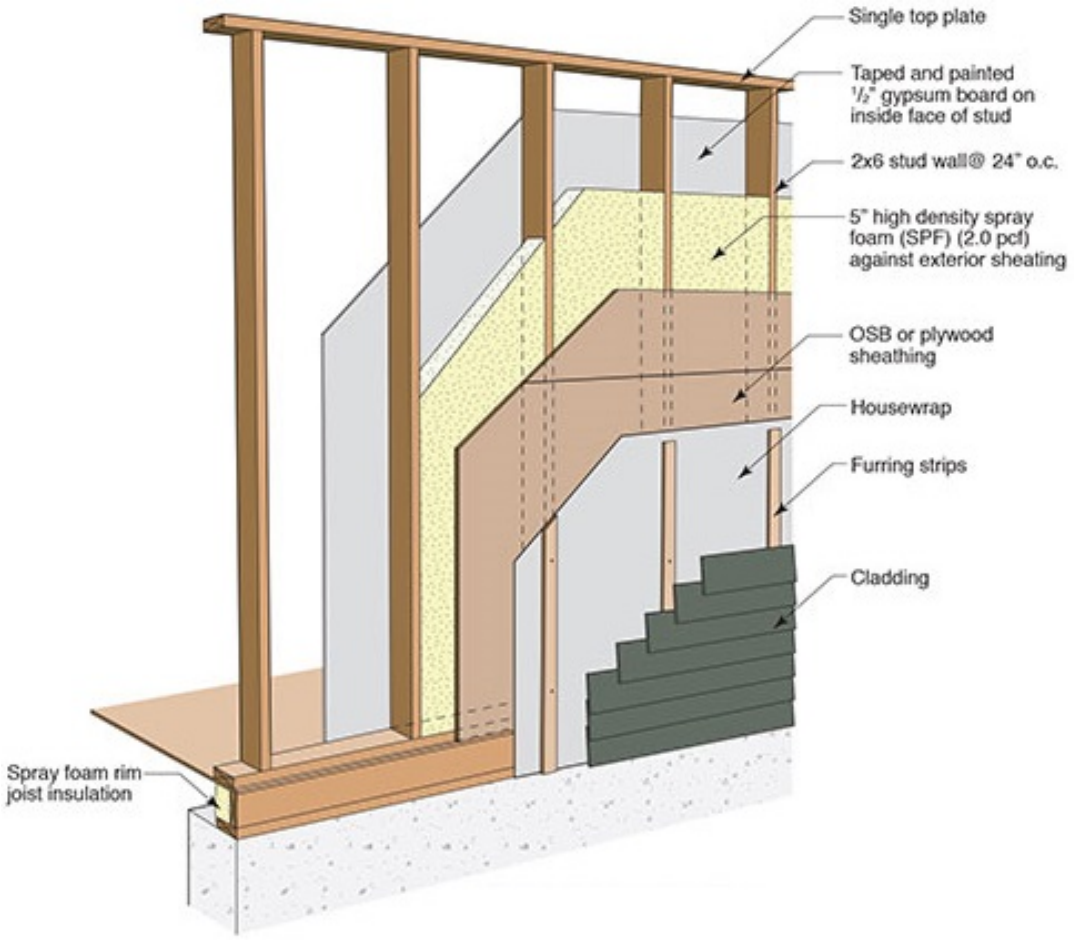

Figure 1.1 : Typical light-frame wood stud wall assembly (buildingscience.com, 2008)

Figure 1.2 : Detonation of 500 tons of TNT (Operation Sailor Hat, 1965)

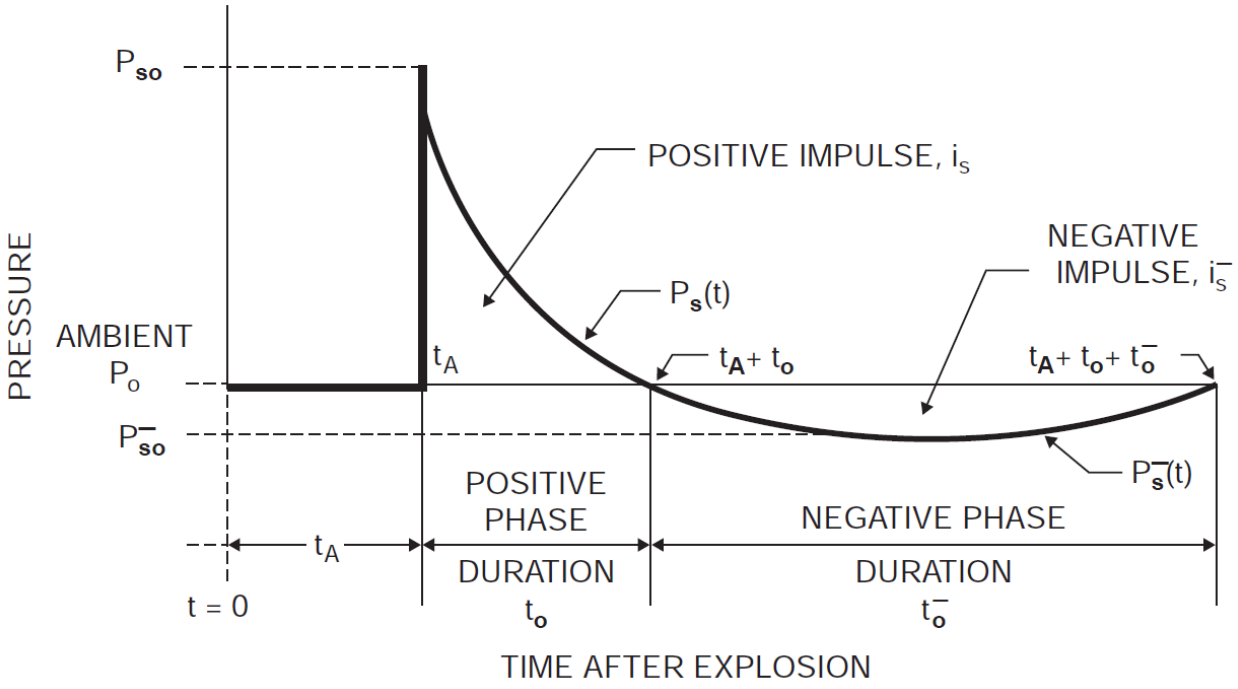

Figure 1.3 : Typical pressure-time history of a blast wave (Dusenberry, 2010)

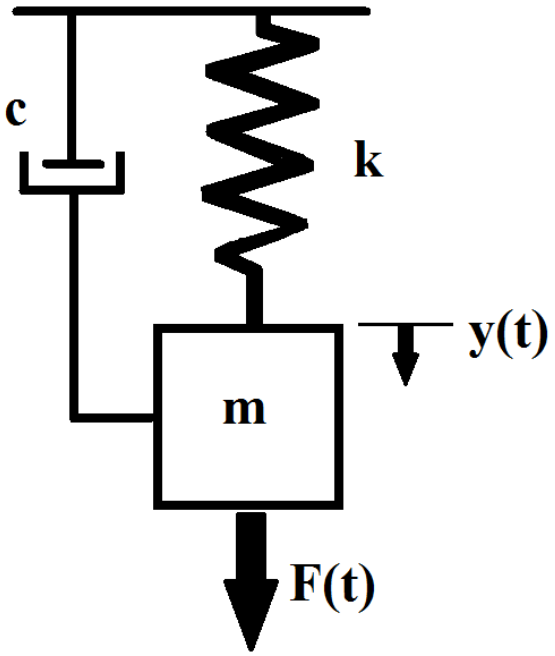

Figure 1.4 : Typical damped SDOF system

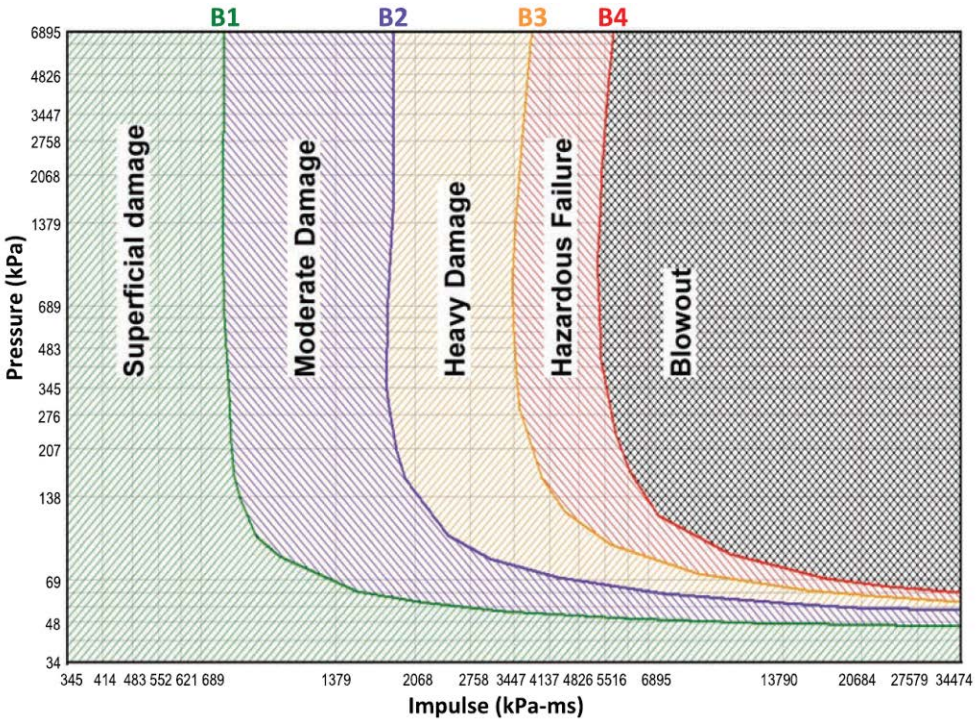

Figure 1.5 : Typical P-I diagram (CSA, 2012)

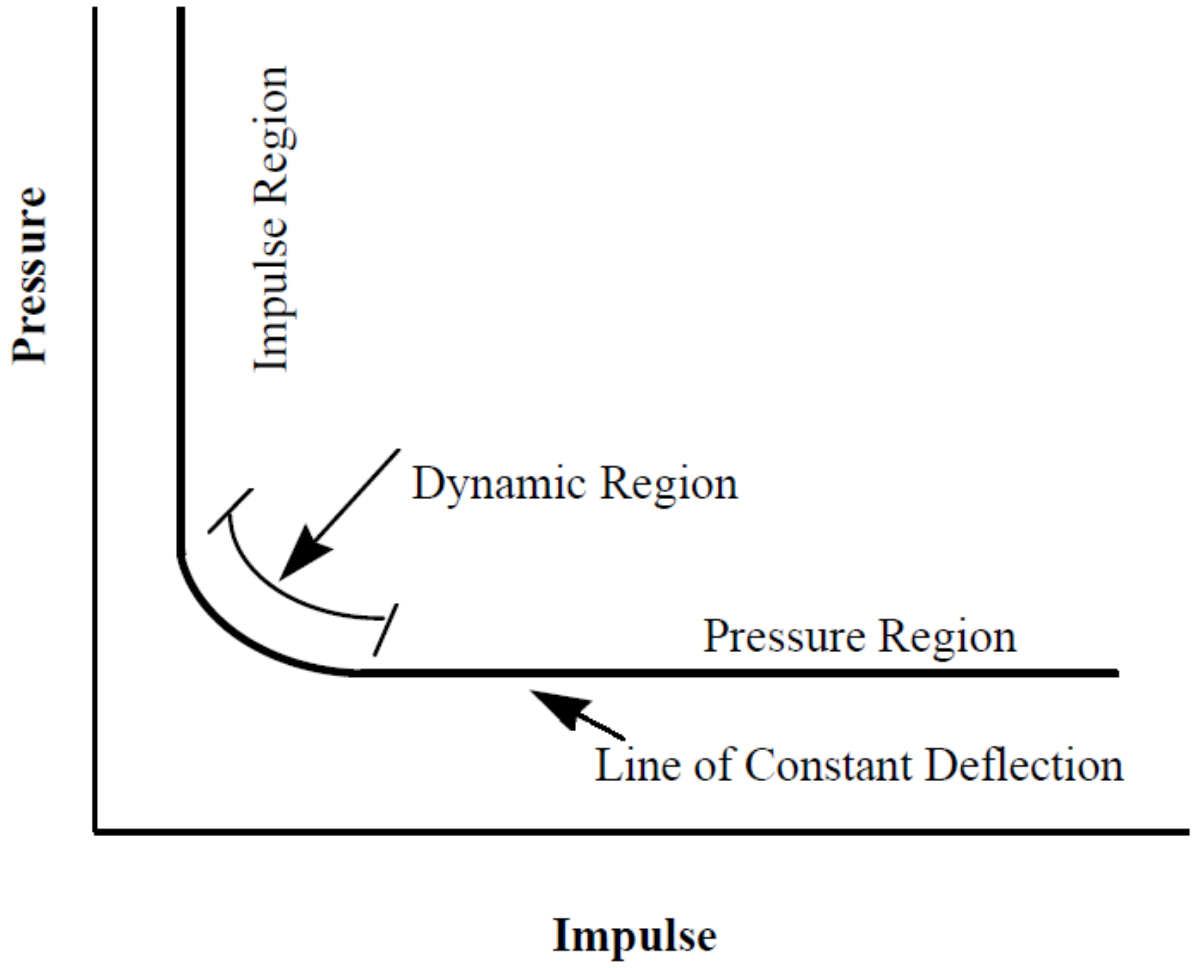

Figure 1.6 : Different response regimes (USACE, 2008)

CHAPTER 2 - Literature Review

2.1 Behaviour of wood under impact loading

Early research performed on wood regarding the effects of load duration and rate-of-loading was focused primarily on impact loading (i.e. relatively high magnitude loads applied during a very short time duration). Some of the first reports produced stem from the US Department of Agriculture, dating back to the 1950s. The testing took place prior to the in-grade testing (Barrett & Lau, 1994) where it was recognized that only full-size samples can truly reflect the behaviour of wood members. The impact tests were conducted on small size and clear (i.e. free from defects) specimens, therefore were not representative of that from what is used in industry. A study was conducted at the Forest Products Laboratory, where the effects of rapid loading on the compressive and flexural strength of wood specimens were investigated (Liska, 1950). Two softwood and two hardwood species were tested, both free of defects and as straight grained as possible. The testing took place in a time duration range of 0.3 – 750 s. The results of these tests on the compressive and flexural strengths showed an increase as the time to maximum load decreased. This increase was reported to be in the range of 10 – 40 % of the control time to maximum load duration. No significant change in the modulus of elasticity was observed throughout these tests.

Nadeau and Bennett (1982) conducted impact tests on clear specimens of Douglas-Fir wood in order to determine the effects of the rate-of-loading (strain rate) and the duration of load on the strength of wood. Of particular interest to the researchers was the effects of the test sample-relative strength (i.e. comparing the top percentile and the bottom percentile results). Half of the specimens were intentionally notched on the tension face through the use of a saw, to promote flexural failure and investigate the effects of initial cracks on the response. The testing program's strain rate range was $3.2E^{-7}$ – $8.4E^{-3}$ s^{-1} for the notched specimens and $3.2E^{-7}$ – $6.5E^{-2}$ s^{-1} for the unnotched specimens. It was determined that, depending on the strain rate, there was an increase in ultimate strength varying from 10 % to 30% for the unnotched specimens, which is comparable to similar testing performed previously (Spencer, 1978). Nadeau and Bennett (1982) reported rate-of-loading effects in the stronger specimens, but observed that these effects were absent in the weaker specimens. The authors concluded that there are two specific regions where the response to impact loads differs; the high stressing-rate region, where strength is independent of the strain rate, and

the low stressing-rate region where strength is highly influenced by crack growth. The boundary between these two regions shifts to lower overall stressing rates as the initial strength decreases. This is due to the fact that initially weaker specimens typically already have developed micro-cracks and are less affected by crack growth.

Another study which looked at the variation of the effects of strain rate dependence on the quality of wood came to the conclusion that dynamic strength increase was typically found in higher-quality lumber (Jansson, 1992). It was observed that the failure mode was highly dependent on the quality of the tested specimens and that specimens with knots would most of the time fail in flexural at the zone near the knot. The failure modes would also shift from a crack-dependent failure to a brasher failure, which is independent of the presence of cracks, as the time to failure decreased.

Parallel strand lumber tested under impact loading reported an average dynamic strength increase of 30 % for an average strain rate of approximately 3.1 s^{-1}. Due to the nature of PSL, two kinds of failure occurred; flexural failure on the tension face of the test specimen and shear/debonding failure at the interface between the laminates. It was noted that due to the impact strength of the hammer, crushing of wood fibres near the impact zone most likely caused a decrease in apparent bending strength which could not be quantified (Sukontasukkul et al., 2000).

2.2 Behaviour of wood structures under simulated and actual blast loads

Information on how wood behaves under high strain rates is limited when compared to other constructions materials such as reinforced concrete and structural steel. Furthermore, most studies on blast testing on timber structures are classified and inaccessible for research and design purposes. This chapter highlights the important findings that have been obtained so far in this area, and identifies gaps in knowledge that formed the main driver for the current research study.

2.2.1 Shock tube testing of individual wood studs – University of Ottawa, 2013

The behaviour of visually graded lumber studs subjected to a simulated blast load was investigated in an experimental testing program (Jacques et al., 2013). Simulated blast waves were generated through the use of the University of Ottawa's shock tube, which allows for the testing of mid-to-full-scale specimens against blast loads. The goal of the research was to determine the apparent

dynamic increase factors on material properties and to validate a single degree-of-freedom (SDOF) model.

Static testing results were compared with those determined from dynamic testing in order to determine dynamic effects. For a strain rate range of 0.1 – 1.0 s^{-1}, an average dynamic increase factor on the modulus of rupture (DIF_{MOR}) and modulus of elasticity (DIF_{MOE}) of 1.41 and 1.14, respectively, was found. Statistical analysis showed that while the dynamic effect on the MOR was substantive, the dynamic effects observed on average on the MOE and strain-at-failure were insignificant due to the large variability in results and the high amount of scatter within the relatively small sample size. It was noted by the authors, however, that to maintain stress-strain compatibility, an increase in the MOR would dictate that the strain-at-failure would have to experience an increase as well. SDOF modelling results proved that this simple analysis tool could effectively model the behaviour of wood studs. The authors concluded that a linear-elastic resistance curve captured well the overall dynamic response of the individual studs to the shock wave.

2.2.2 Shock tube testing of light-frame wood stud walls – University of Ottawa, 2013

Full-scale static tests were conducted and the results were compared with those obtained from the shock tube testing in order to determine the apparent dynamic increase factors on the MOR and MOE (Lacroix & Doudak, 2014). These dynamic tests were conducted in a strain rate range of 0.12 – 0.55 s^{-1} which yielded an average DIF_{MOR} and DIF_{MOE} of 1.40 and 1.18, respectively. The boundary conditions were simply supported in order to keep the focus on the behaviour of the stud walls, as well as simplify the modelling process. These tests results were used in the validation of a SDOF model, which was able to predict dynamic wall response with reasonable accuracy. Analysis results showed that a bi-linear curve could effectively model the wall behaviour. The ductility was assumed to stem mostly from the mechanical fasteners attaching the sheathing panel to the framing elements. The motivator of this research was, in part, to extend the study described in 2.2.1 as well as the study undertaken by Lacroix (2013) to include the behaviour of complete walls composed of framing elements, sheathing and fasteners.

Lacroix and Doudak (2014) presented an empirical equation to determine the DIF_{MOR} for wood studs as a function of strain rate by comparing results from different studies in the literature

including data obtained from impact tests. This equation is stated to only be valid for a strain rate range of $1.67E^{-1} – 1.65E^{3}$ s^{-1}:

$$DIF_{MOR} = 1.46 + 0.1 \log_{10} \dot{\varepsilon} \qquad \text{Equation 2.1}$$

2.2.3 Coated structural lumber and laminated strand lumber – University of Maine, 2010

During the development of the *Vehicle Bomb Mitigation Guide* (USAF, 2006), tests were conducted on coated structural lumber (CSL) and laminated strand lumber (LSL) in part for its use in the retrofitting of South-East Asia huts, a type of temporary shelter for USAF members during operations overseas. CSL consists of visually graded lumber coated with Fibre-reinforced polymer (FRP) along its longitudinal direction. The goal was to increase ductility, minimize debris, and to facilitate repairs after a blast event. Full-scale tests were conducted on CSL shelters where the predominant failure mode was established to be in the wall and roof-to-wall interface, as shown in Figure 2.1. This is due to the placement of the FRP reinforcement, which caused failure in the connection. Uncoated LSL was chosen as a possible material option in order to retrofit the CSL systems at their critical sections (Syron, 2010). High strain rate compression tests were conducted on LSL specimens. The strain rate range varied from $1E^{-5} – 1E^{-3}$ s^{-1}. A compressive strength increase factor in the ranges of 1.31 – 1.37 and 1.16 – 1.41 was found in the longitudinal and transverse directions, respectively.

2.3 Existing retrofit options for light-frame wood stud walls

While wood enjoys the inherent earthquake-resisting property due to its light weight, this inherent material property is its bane when it comes to resisting blast loads. Also, wood is considered a brittle material (except in compression) and therefore its blast resisting properties may need to be enhanced in some cases to either introduce higher capacity or more ductility.

2.3.1 Sheathing deficiencies and debris

A study on structural/non-structural elements in a blast (Bogosian & Avanessian, 2004) has provided data that shows that debris is the primary injury/death causing mechanism. Utilizing anthropomorphic test devices (ATDs), the relationship between blunt trauma injury levels and

blast pressure/impulse was numerically quantified. It was shown that wood stud walls could potentially create moderate-to-high injury levels. The injuries incurred was determined to be lower than the potential injury a window panel could cause. This is due to the fact that the stud debris tended to strike the test dummies at chest level, whereas window panels tended to strike at head level. These tests were based on the assumption that the top and bottom connections failed and the stud-wall would essentially fly as a single entity.

The South-East Asia huts described earlier in section 2.1.3 were considered to be blast deficient and various retrofitting options were considered. The United States Air Force (USAF) produced a report that described tests and retrofits that were performed (USAF, 2006). The performance rating of various retrofits was based on potential personnel injury and fatality, as well as the probability associated with these criterions. The SEA huts consisted of dimensional lumber sheathed with plywood, and included some openings, such as doors and windows. A before-and-after shot of a typical test is shown in Figure 2.2. Results showed that structural damage and component failure did not correlate with a high probability of injuries and fatalities. Rather, structural collapse of the hut did. It was noted, however, that while the correlation between structural failure and injuries were insignificant, debris hazards were still present in the SEA huts. While this may seem counter-intuitive, the authors noted that debris hazard calculations are highly dependent on the positions of the personnel. In order to mitigate this, the report suggested removing windows, making sure that the doors open to the outside, adding additional sheets of plywood on both the interior and exterior walls, and reinforcing the bottom of the walls and bottom truss chords with additional dimensional lumber.

Lacroix (2013) tested five walls with 11 mm (7/16 in.) thick OSB as sheathing and five with 18.5 mm (3/4 in.) plywood as sheathing. Exposed to various blast waves, plywood walls performed significantly better than those sheathed with OSB. When pressures exceeded approximately 35 kPa, the OSB walls began to suffer from ripping in the sheathing and on some shots, flying sheathing debris was observed. An example of this type of damage is shown in Figure 2.3. In some tests, the OSB sheathing failed before or with the studs, resulting in incomplete load distribution to the load-bearing elements (i.e. studs). Due to the fact that the sheathing acts as a load distributor and contributes to the overall capacity of the wall assembly, this effect was detrimental to the overall system capacity and performance. The plywood walls did not produce any sheathing debris

and damage to the sheathing was limited to minor cracking. It was concluded that 11 mm OSB is not appropriate for use in assemblies designed to resist blast loading. Since this study was limited to pressure levels that induced low, moderate and heavy damage in the walls, and premature tearing of the OSB panels was only observed at the high-pressure shots, it was deemed appropriate in the current study to investigate whether the sheathing is capable of transferring the pressure to the studs at higher pressure levels.

A recent study (Lacroix et al., 2013) investigated possible retrofits of both the studs and the sheathing. Two sheathing retrofits were investigated, both involving 18.5 mm (3/4 in.) plywood. One retrofit was for new construction, when the walls were built with plywood directly onto the studs. The other retrofit was for a retrofitting scenario for pre-existing light-frame wood stud walls with OSB, where sheets of plywood were to be screwed atop the existing OSB. Compared to the previous study, where nail pull-out was prominent, no pull-out was observed in these tests. The walls with the added plywood panel were found to be stiffer than the walls with only OSB or plywood, and had an average maximum stud displacement which was 18 % less than that of the plywood-only walls. During the modelling phase of the study, both retrofits showed an increase in capacity and stiffness over the reference OSB-only wall.

2.3.2 Boundary connection deficiencies

A recent study found that a typical stud wall assembly, when exposed to blast loading, will experience failure at the connections (Sorensen & McGill, 2011). This contributes greatly in creating flying debris, where the whole stud wall becomes airborne and can potentially strike occupants and cause injuries and fatalities. Maintaining the connection between the floors and the actual studs is important for not only reducing the chances of progressive collapse but to also reduce the chances of flying debris (USACE, 2008). These fastener capacities are typically inexpensive and have published capacity values provided by the manufacturers.

Shock-tube testing at the University of Ottawa has led to the development of a prototypical wood stud retrofit system, consisting of a specially designed hanger fastener, which provides connectivity between the stud-wall and the floors, and tension rod strengthening system, thereby increasing the overall per stud capacity (Lloyd & Jacques, 2011). As shown in Figure 2.4, the connectors consist of steel hangers that are installed at the ends of each stud and that connects to

typical blocking or rim-joist members. This provides an effective load path and an innovative way to distribute the load into the diaphragm. The authors tested typically connected stud walls as well as retrofitted walls. The typically connected stud walls failed in combined flexural and fastener pull-out. As expected, this type of failure caused the wall to become a projectile, travelling in excess of 8 m/s. The retrofitted walls performed very well and no connection failure was observed.

2.4 Static and dynamic modelling of wood stud walls

It has been shown that while a light-frame wood stud wall is an assembly composed of various components with different connectivity between them, proper techniques and modelling methods have been developed in order to capture the very complicated processes and interactions and model the walls as simple elements (e.g. Lacroix, 2013; Parlin, 2010).

2.4.1 Partial composite action between the wood studs and sheathing

The connections between the sheathing and load-bearing framing elements cannot be considered rigid, but rather semi-rigid, depending on various parameters such as the fasteners used, the density of the materials, and the ratio of the MOE between the materials connected. While a conservative approach would be to neglect this action and merely base response and capacity entirely on the load-bearing elements (i.e. studs/joists), it has been shown that doing so would be overly conservative (Lacroix, 2013). Initially developed for floor systems, the same theory can be used in a wall systems since both systems are loaded out-of-plane under uniformly distributed loads. Using this knowledge, theoretical and experimental quantifications of this partial connectivity have been developed.

Early testing conducted at the Forest Product Laboratory showed that floors had much larger capacity and stiffness than those calculated from traditional beam theory methods. The researchers determined that a T-section with proper parameters could be utilized to model floor behaviour, in a linear-elastic fashion (Polensek et al., 1972). Reported increases in capacity and stiffness varied from 1.50 to 2.44 and 1.15 to 2.04, respectively.

McCutcheon (1977) developed a method in which an assumed T-beam would be utilized to model the behaviour of sheathed wood floors. The experimental component of this research program consisted of seven floors loaded with uniformly distributed load. The deflection of each joist was

measured and compared with the theoretical values obtained from the developed method. Twenty-two out of twenty-nine calculated T-beam deflections were within 5 % of the experimental deflections. The author noted that the interlayer gaps should be taken into account through the use of a simple modification factor. McCutcheon (1984) extended his T-section methodology for systems with sheathing on both sides, effectively utilizing an I-beam with partially connected flanges. Experimental data from these tests on both T-beams and I-beams showed that they could provide a system stiffness increase from 9 % to 109 %. The author noted that a floor-joist system is relatively insensitive to changes in the interlayer stiffness, acknowledging that an increase by a factor of 2.5 would only yield a 6 % decrease in deflections. Similarly, a decrease of interlayer stiffness by a factor of 2.5 would only increase the deflections by 16 %.

2.4.2 Modelling of wood stud wall end conditions

First attempts at modelling the complexity of the dynamic interaction between the stud wall, bottom/top plates, and foundation was highly non-linear and time consuming. A computer program consisting of FEA, multi-linear material models, and a step-by-step procedure was used to predict the behaviour of the connection system of a typical stud wall (Polensek & Schimel, 1986). What was of interest in this study was the determination of a value for the rotational restraint at the ends of stud walls when exposed to wind loads and to determine if enough restraint actually existed in the typical construction methods. Nine full-scale wood stud walls were tested with variations in end conditions in order to validate the computer program, as well as determine possible retrofits for increasing support restraints. The authors observed that as-built walls exhibited an average rotational restraint of 2 %, but that providing additional nailing and extending the sheathing passed the bottom and top plates could increase the support restraint by 13 %. The coefficient of support decreased with increasing lateral loading and became negligible at a lateral pressure of 7.2 kPa.

Bulleit and his collaborators created a simple linear-elastic method in order to capture the complexity and non-linearity of the connectivity of stud walls (Bulleit et al., 2005). Modelling a stud as a simply supported T-beam with partial composite action occurring between the sheathing and the load-bearing stud, the authors modelled the end connections as two equal stiffness rotational springs. Using classical beam deflection theory, an equation for mid-span deflection was determined with an added variable for the stiffness of the rotational springs. Testing and analysis was performed on five stud walls with 12.7 mm (1/2 in.) plywood. Results showed that typically

built wood stud walls had negligible support restraint, which confirmed the findings of McCutcheon (1984). However, adding additional nails, and thereby increasing the rotational stiffness of the connections, would consequently increase the ultimate out-of-plane strength; one configuration in which additional nails were used to connect the sheathing to the top and bottom plates provided a rotational restraint, thereby increasing the stud wall capacity.

2.4.3 Modelling the behaviour of light-frame wood stud walls

Studies have shown that in free vibration tests, typical stud T-sections showed a tendency to vibrate under the 1st mode shape, even when the variability of the MOE in a stud wall assembly was large (Polensek & Schimel, 1991). Experimental testing and SDOF modelling has also been performed on light-frame wood stud walls, which resulted in good agreement between analytical and experimental data (Lacroix & Doudak, 2013). It was observed in these tests that, under a blast load, all studs would reach their maximum displacement at approximately the same time (i.e. they were in sync) but afterwards would become out-of-sync in terms of vibration, due to variations in material properties. In terms of viscous damping, Polensek and Schimel (1991) showed that damping would vary from 2 % - 9 % in static cyclic tests. It is expected that, in dynamic loading, especially in the range of blast, damping would be negligible relative to the effects of inertial forces. In previous impact testing, it was also determined that damping effects in these very short duration tests was negligible, since only the first cycle is typically of interest (Jansson, 1992; Biggs, 1964).

2.5 Summary

This chapter presented an overview on the brief knowledge base that currently exists on wood behaviour when exposed to short duration loads (impact and blast), its associated strengths and shortcomings in terms of performance, and the current knowledge gaps. While recent interests in the effects of blast loads on wood have produced full-scale testing data which has contributed to the blast standard (CSA, 2012), major unknowns still exist when it comes to designing a wood structure against blast or when retrofitting existing wood structures; the latter being of great importance due to the prevalence of light-frame wood buildings in North America. As shown in this chapter, the majority of the current published and established literature on strain rate effects of wood is from impact testing on clear specimens. While these tests have shown that there is a

significant correlation between strength and strain rate, they are not representative of what is used in construction. Jacques et al. (2013), Lacroix (2013), Parlin (2010) and Syron (2010) have all performed full-scale tests which resulted in general agreement that wood experiences a dynamic increase in its capacity under various high strain rates. Specifically, Jacques et al. (2013) and Lacroix (2013) have both concluded that a dynamic increase factor of 1.4 is applicable on strength. They also observed an apparent dynamic increase factor on the stiffness.

Wood members with typical dimensions used as wall studs, when loaded out-of-plane, will experience flexural failure. This allows researchers to use simple and practical analysis tools, such as single degree-of-freedom modelling to capture overall behaviour, without the need for more advanced modelling methods. While most modelling performed so far assumed idealized connections, established mechanics-based methods, such as partial composite action and support restraint, can be integrated into any analytical model and could capture complex interactions that occur in the assemblies. This would result in a more accurate and representative analytical model. Studies have shown that typically connected stud walls can be modelled as simply supported, since the end connections typically do not provide much rotational restraint (Bulleit et al., 2005; Polensek & Schimel, 1986). Tests have also shown that typical connections often fail prior to the studs in a blast scenario (Sorensen & McGill, 2011; USACE, 2008). The question remains whether the current guidelines are appropriate for a blast loading scenario due to the fact that the current blast code (CSA S850) takes on a relatively simple performance-based design approach. Retrofits developed by government agencies (USAF, 2006), and researchers (Lacroix et al., 2013; Lloyd & Jacques, 2011) have shown that there exists many possible solutions in overcoming the inherent blast deficiencies that typical wood assemblies have. Integration the rotational restraints into a SDOF model has been established (Bulleit et al. 2005) and can potentially affect the overall response of the stud wall.

While the research focus has been on the flexural response of wood specimens, it has been implicitly implied that the specimen will in fact receive the load. Little to no work has been conducted on how severe blast loads (i.e. pressure-impulse combinations that yield hazardous-blowout damage levels) can affect the sequence of failure in typical stud wall assemblies. While it is important to get a general sense of performance in terms of how the overall system performs and reacts to these loads, the complex and highly non-linear interaction between the various

subsystems is usually ignored. Determining how manipulating these subsystems can affect the overall response of the wall (e.g. stiffer sheathing, tougher connections, sheathing-stud joints, etc.) and can further increase performance levels is still unclear and presents an opportunity to refine current blast provisions. While most provisions and studies have deemed SDOF analysis viable for blast analysis, additional research gaps exist in terms of the scope of applicability and accuracy of the single degree-of-freedom (SDOF) analysis method when modelling these assemblies under blowout damage levels. The current study will attempt to verify if existing knowledge on the response of wood stud walls applies when dealing with high damage levels. The study will also propose simple design solutions to the discussed shortcomings of typical wood stud walls. All of this will be done by taking on a holistic approach in order to understand the individual element performance (i.e. how every wall component behaves separately from each other), followed by the dynamic testing of the wall in its complete form. Finally, based on current analysis techniques, integrating the simple elements and their properties into an analytical model that can be used by designers and researchers as a prediction tool for the response of fully idealized light-frame wood stud walls.

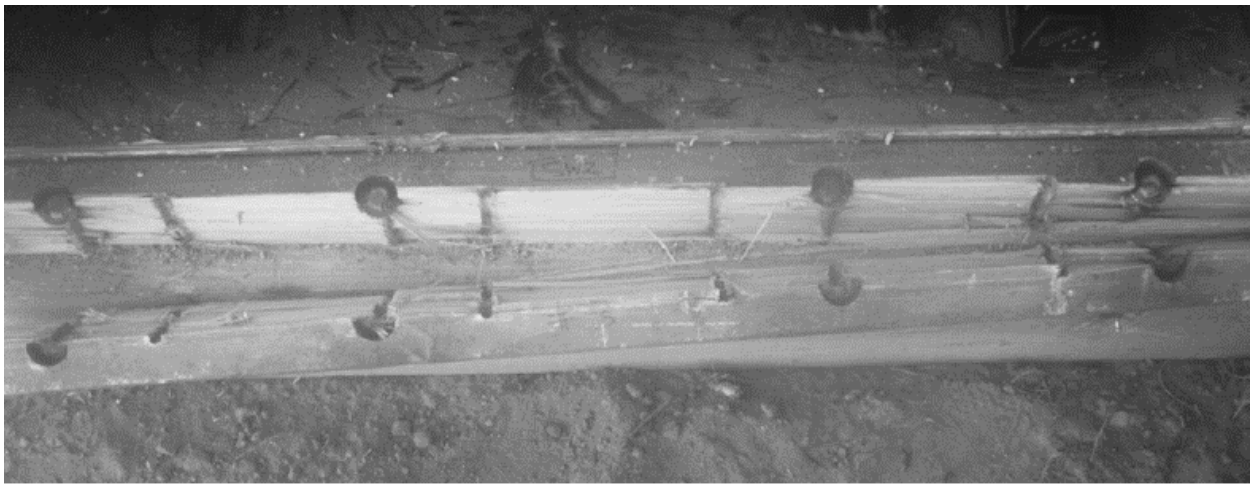

Figure 2.1 : Damaged CSL connection plates (Syron, 2010)

Figure 2.2 : SEA hut before (left) and after (right) testing (USAF, 2006)

Figure 2.3 : Damaged OSB sheathing (Lacroix, 2013)

Figure 2.4 : End hanger retrofit unit (Lloyd & Jacques, 2011)

CHAPTER 3 - Experimental Program

3.1 General

A total of twenty-five light-frame wood stud walls were dynamically tested to destruction. This section will provide an overview on the experimental phase of the study, which can be divided into static and dynamic testing.

Twenty-one light-frame wood stud walls consisting of 38 x 140 mm (2 x 6 in.) spruce-pine-fir (SPF) No. 2 visually graded lumber, spaced at 406 mm on center with one top and one bottom plate, were tested to failure under dynamic loading. Of those twenty-one walls, thirteen were sheathed with 11 mm OSB, four with 18.5 mm plywood, and the remaining four with both 11 mm OSB and 18.5 mm plywood. The walls sheathed with OSB and plywood only utilized 50 mm long nails with a diameter of 2.87 mm to connect the sheathing to the framing. The remaining four walls were detailed as possible retrofit option, with plywood panels screwed atop the pre-existing OSB panels with 76 mm long screws with a diameter of 4.2 mm. Complete details regarding the three wall configurations are shown in Figures 3.1 to 3.3.

Additionally, four light-frame wood stud walls consisting of 38 mm x 184 mm (2 x 8 in.) spruce-pine-fir (SPF) No. 2 visually graded lumber sheathed with 11 mm OSB with similar construction details were also tested dynamically to destruction. The sheathing was connected to the studs using 50 mm long nails with a diameter of 2.87 mm. The motivation for using 38 x 184 mm studs, albeit an uncommon size for light-frame stud walls, is twofold: a designer may consider increasing the size of the framing elements in areas where the blast load is high and typical framing sizes (i.e. 2 x 4s and 2 x 6s) may not be sufficient, and to investigate whether the sheathing element is capable of transferring the load to the main resisting elements. The latter point is important mainly because designers (based on current design provisions) are more likely to focus on the framing (wall stud) design only, while a breach in the sheathing element would constitute a premature failure in the wall and the ultimate capacity of the studs would not be reached. If a premature failure is anticipated in the sheathing, a reinforcement of the sheathing panel might be necessary and for that purpose a retrofit of the system would be required. 152 mm x 152 mm x 11.1 mm^2 welded wire mesh (WWM) was placed either between the OSB and the studs (to enhance the sheathing performance), or on the outside face of the studs to act as a “catcher system” was investigated.

When utilized as sheathing reinforcement, the WWM grid was secured to the sheathing mainly by clamping action brought on by the sheathing fasteners. When installed as a catcher system, heavy-duty staples were used to attach it to the tension face of the studs. In both applications, off-the-shelf steel plates were used to further secure the ends of the WWM to the top and bottom wall plates, to ensure that the integrity of the retrofit is maintained. More details regarding these two wall configurations are shown in Figures 3.4 and 3.5

When nails were used to connect sheathing to the framing elements, they were fastened using a grid pattern of 150 mm (field and edge). This was meant to reduce nail withdrawal during rebound (Lacroix, 2013). The walls with both OSB and plywood sheathing required the use of screws spaced at 300 mm on center in order to effectively connect the additional sheathing panel. All twenty-five walls measured 2070 mm in width, 2108 mm in height, and had a clear span of 2032 mm. The end conditions varied, with sixteen walls having idealized pinned end condition, two with typical toe-nailed connections as per Part 9 of the National Building Code of Canada 2010, and the remaining seven being connected with various steel connectors. The way by which these connections were detailed is shown in Figures 3.6 and 3.7. A summary of all the dynamic test configurations can be found in Table 3.1.

3.2 Sheathing coupon testing

Eighty 76 mm by 330 mm (3 x 13 in.) specimens of OSB and plywood sheathing were tested to destruction in order to determine their static modulus of elasticity (MOE) and modulus of rupture (MOR). These tests were conducted in accordance with the American Society for Testing and Materials (ASTM) for Evaluating Properties of Wood-Base Fiber and Particle Panel Materials (ASTM, 2006). A point load was applied at mid-span at a constant rate and the mid-span deflection was recorded. The test setup as well as typical failure mode are shown in Figure 3.8. The tests were conducted until an ultimate failure of the specimen was reached. Half of the specimens consisted of OSB and the other half of plywood. The number of specimens tested was determined using the ASTM standard for Sampling and Data-Analysis for Structural Wood and Wood-Based Products (ASTM, 2010).

3.3 Load-displacement relationship of typical timber joints

Typical sheathing-nail-stud joints were reproduced and tested under tensile loading using a universal testing machine (UTM) in order to determine the load-slip relationship for the nail joint connecting the sheathing panel to the stud. Three different joint configurations were used in the full-scale dynamic wall tests. A total of thirty tests, ten for each configuration, were carried-out, according to ASTM standard (ASTM, 2012). For each test, the load and joint displacement was measured. Two linear variable displacement transducers (LVDTs), one on each side, were used to measure overall joint slip. The test setup and typical failure mode are shown in Figure 3.9.

3.4 Stud static bending tests

The modulus of elasticity (MOE) of 220 studs was measured with the use of a handheld grader (Brookhuis Micro-Electronics) as well as a non-destructive preloading technique of the studs within their elastic limit. Twenty-five studs were randomly selected and tested to destruction under four-point loading in order to determine the modulus of rupture (MOR). These tests were done in accordance with the ASTM standard for Static Tests of Lumber in Structural Sizes (ASTM, 2009). As shown in Figures 3.10 and 3.11, a two-point load was applied at the third points of each stud. Lateral bracing was provided at mid-span and at the point of bearing, in order to eliminate any possibility of lateral-torsional buckling occurring during the test. Simply supported end conditions were provided through the use of a simple steel plate rotating about a pin. The load application points were made of a dense wood material in order to reduce wood crushing. The load was measured using a load cell positioned in between the hydraulic jack and the load-distribution frame. Mid-span deflections were measured by a compact string pot wire gauge with a 300 mm stroke.

3.5 Wall dynamic testing

This section will describe how the simulated blast loads were generated through the use of the University of Ottawa's shock tube, a unique device which can generate shock waves similar to that of bomb blasts and high pressure waves. The methodology and the full-scale test setup will be discussed as well.

3.5.1 Description of the shock tube

The shock tube is a testing apparatus capable of reproducing shock waves similar to those found in the far-field detonation of high-explosives. The shock tube consists of three main components: the driver section, the spool section, and the expansion section. These different sections are shown in Figure 3.12. The mechanism used in the tests is referred to as a double diaphragm firing system, where sheets of aluminum foils are used to separate the three sections. The thicknesses and quantity of aluminum foils are predetermined and depends on the pressure-impulse combination for which the specimen is subjected. Different driver lengths are available, from 305 to 5185 mm (1 to 17 ft.), which will yield different impulses, allowing the investigation of various types of blast waves. Upon the installation of the desired driver and aluminum foils, compressed air is introduced into the driver and diaphragm section. When the desired driver pressure is attained, the diaphragm is drained (i.e. air is allowed to escape through a control nozzle) until the set of aluminum foils separating the driver and diaphragm ruptures. This subsequently ruptures the other set of foils separating the diaphragm and the expansion section, which then allows for the release of the compressed air. This creates a shockwave that travels down the 6096 mm (20 ft.) long expansion section, where it eventually comes into contact with the test specimen. The opening of the expansion section is 2032 x 2032 mm (80 x 80 in.), which allows for testing of large- to full-scale specimens. In order to provide near-realistic conditions, where negative pressures are able to develop, twelve vents are positioned around the opening of the expansion section. The shock tube is capable of producing reflected pressures up to 100 kPa and impulses up to 2200 kPa-ms. Depending on driver pressure and length, the positive phase of the blast wave can vary from 5 to 70 ms. A driver length of 2745 mm (9 ft.) was used throughout testing. This was done to facilitate comparison between different kinds of sheathing, connections, and detailing used through the research program. The majority of walls tested by Lacroix (2013) were tested with a driver of such length, which allowed for a more direct comparison to be made.

3.5.2 Description of test setup

This section describes the test setup for the full-scale stud walls subjected to blast loading using the shock tube. Two kinds of test setups were used due to the different end conditions.

3.5.2.1 Simply supported walls test setup

The walls were attached to the end frame without the use of a load transfer device, since the sheathing panels acted as load distributor for their respective walls. In order to mimic simply supported end conditions, two steel angles were placed at the edge of the opening and braced to the shock tube frame through the use of four 76 x 76 mm hollow steel sections (HSS). The tip of the angles were aligned with the edge of the shock tube opening, allowing for the clear span to be 2032 mm, identical to the clear span for the static bending tests. These angles provided a rotational point of contact for the outside face of the wall, while also creating a gap between the wall and the shock tube frame, allowing the walls to rotate freely without creating any rotational restraint. To reduce crushing of wood and to allow sufficient rotation on the inside face of the wall (i.e. where the studs are exposed), 50 mm x 100 mm steel plates with rollers were attached to the backside of each stud. The centerline of the roller was aligned with the interface between the studs and the plates, as well as the angles. These rollers were in contact with a rectangular 76 mm x 152 mm HSS which clamps the wall to the shock tube frame. Detailed schematics of the simply supported test setup are shown in Figures 3.13 to 3.16.

3.5.2.2 Walls test setups with end connections

A similar test setup was utilized in order to test walls with end conditions that include connections. The top and bottom plates of the test specimens were connected to lumber pieces simulating floor rim joists. The rim joists were attached to the end frame of the shock tube using a hollow steel section (HSS). The blocking simulates typical boundary elements in light-frame wood floor construction and the clamping of the blocking to the shock tube simulates the in-plane stiffness of the floor diaphragm. The blocking, consisting of three 38 x 140 x 2070 mm lumber pieces connected to each other using 76 x 4.2 mm construction screws, was then slotted in order to allow the bolts, which support the 76 x 152 mm HSS used to clamp the blocking to the shock tube, to pass through unhindered. This detail is shown in Figure 3.17.

3.5.2.3 Measuring methods and equipment

The reflected pressure for each test was measured by two dynamic piezoelectric pressure sensors, placed strategically at the bottom and on the side of the shock tube opening. Strain gauges were used on the four middle studs of each wall in order to obtain strain data and determine the dynamic

failure point for each test. The area where the strain gauges were placed was hand-sanded and cleaned and a layer of epoxy was placed on the sanded area and allowed to dry. Once dry, the area was hand-sanded again. Strong adhesive was then used to physically glue the strain gauges onto the stud face. The exposed strain gauge was then covered with electrical and duct tape. The strain gauges used were general purpose 350 Ohm strain gauges, measuring 4.5 x 12.5 mm. Mid-span stud deflection for the four middle studs were obtained using 300 mm stroke LVDTs. These LVDTs were attached to a steel enclosing bracket, acting as a protective barrier for the LVDTs. The bracket was attached to a steel frame which in turn was attached to the outer frame of the shock tube. This made all measured displacements relative to the shock tube. The entirety of the setup (strain gauges, LVDTs, pressure sensors) was connected to a data acquisition system which recorded data at a sampling rate of 100 000 samples per second. The data acquisition system was also connected to a high-speed camera, capable of recording videos at a rate of 500 frames per second at a resolution of 800 x 600 pixels. The recording process was triggered by the pressure wave passing by the pressure sensors. The two complete test setups are shown in Figures 3.18 to 3.20. The strain gauge application process is shown in Figure 3.21.

During the testing, both the stud mid-span displacement as well as tension and compression side strain was measured. Although the LVDTs would continue to record stud displacement beyond the point of initial failure, they could not be utilized directly in order to determine the point at which the stud failed. The determination of ultimate failure was done through the use of strain gauges placed on the compression face of the studs, as shown in Figure 3.22.

Table 3.1 : Dynamic testing summary

<table>
<tr><th>Specimen</th><th>End conditions</th><th>Construction details (metric)</th></tr>
<tr><td>W1
W2
W3
W4</td><td rowspan="6">Simply supported</td><td>• 38 mm x 140 mm No. 2 SPF @ 406 mm O/C
• 11 mm OSB
• Nails, 50 mm x 2.87 mm @ 150 mm (field & edge)</td></tr>
<tr><td>W5
W6
W7
W8</td><td>• 38 mm x 140 mm No. 2 SPF @ 406 mm O/C
• 18.5 mm plywood
• Nails, 50 mm x 2.87 mm @ 150 mm (field & edge)</td></tr>
<tr><td>W9
W10
W11
W12</td><td>• 38 mm x 140 mm No. 2 SPF @ 406 mm O/C
• 11 mm OSB
• 18.5 mm plywood atop OSB
• Nails, 50 mm x 2.87 mm @ 150 mm (field & edge) (OSB)
• Screws, 76 mm x 4.2 mm @ 300 mm (field & edge) (plywood)</td></tr>
<tr><td>W13
W14</td><td>• 38 mm x 184 mm No. 2 SPF @ 406 mm O/C
• 11 mm OSB
• Nails, 50 mm x 2.87 mm @ 150 mm (field & edge)
• 152 mm x 152 mm x 11.1 mm^2 welded wire meshed between studs and OSB</td></tr>
<tr><td>W15
W16</td><td>• 38 mm x 184 mm No. 2 SPF @ 406 mm O/C
• 11 mm OSB
• Nails, 50 mm x 2.87 mm @ 150 mm (field & edge)
• 152 mm x 152 mm x 11.1 mm^2 welded wire meshed attached at exterior stud face</td></tr>
<tr><td>W17</td><td>82 mm nails @ 400 mm O/C (typical)</td><td rowspan="8">• 38 mm x 140 mm No. 2 SPF @ 406 mm O/C
• 11 mm OSB
• Nails, 50 mm x 2.87 mm @ 150 mm (field & edge)</td></tr>
<tr><td>W18</td><td>82 mm nails @ 150 mm O/C (typical)</td></tr>
<tr><td>W19</td><td rowspan="2">Simpson Strong-Tie® HU28</td></tr>
<tr><td>W20</td></tr>
<tr><td>W21</td><td rowspan="2">Simpson Strong-Tie® LJS26DS</td></tr>
<tr><td>W22</td></tr>
<tr><td>W23</td><td rowspan="2">Simpson Strong-Tie® LTS18</td></tr>
<tr><td>W24</td></tr>
<tr><td>W25</td><td>Simpson Strong-Tie® ML24Z</td></tr>
</table>

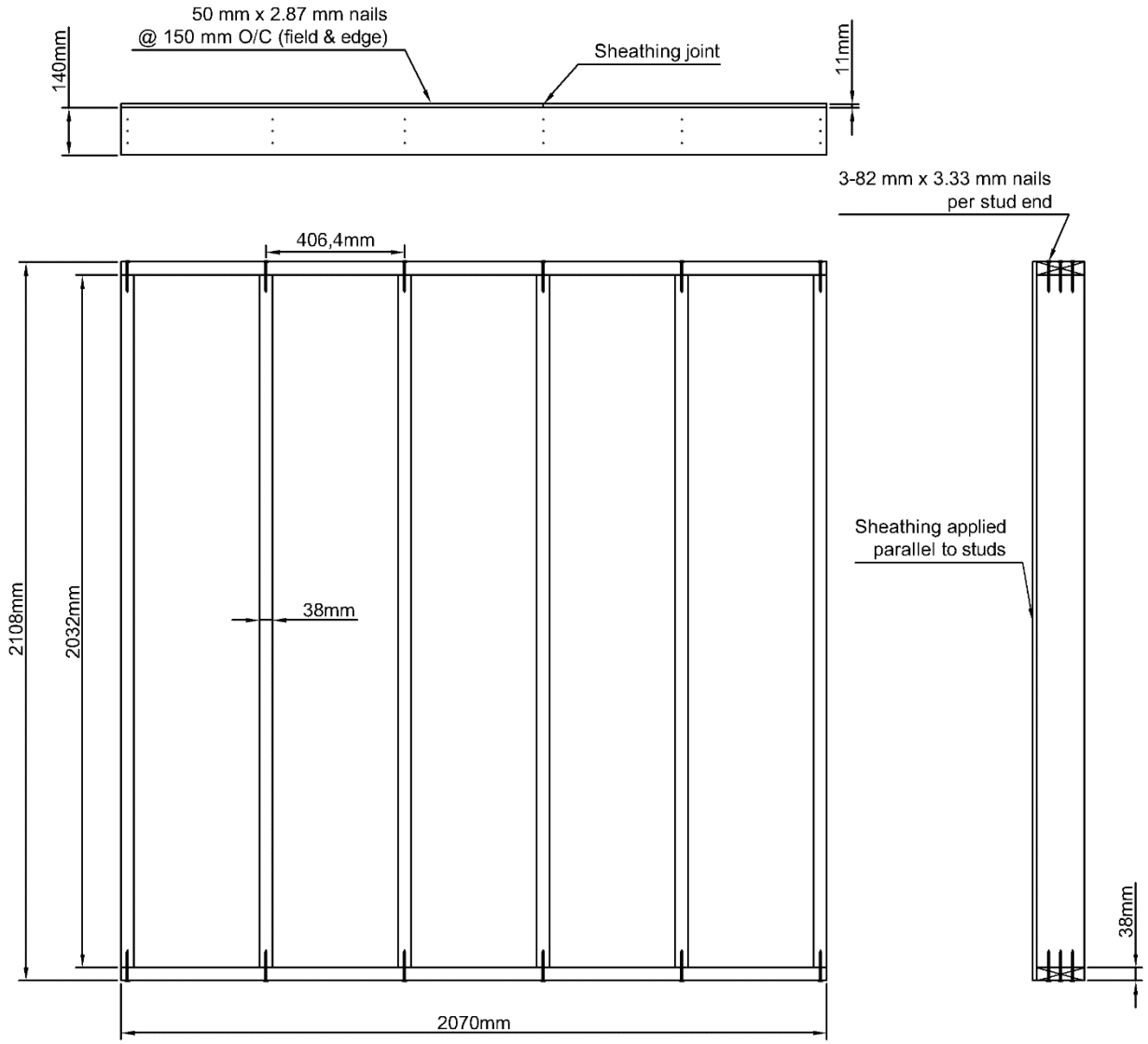

Figure 3.1 : 2 x 6 wall with OSB detailing

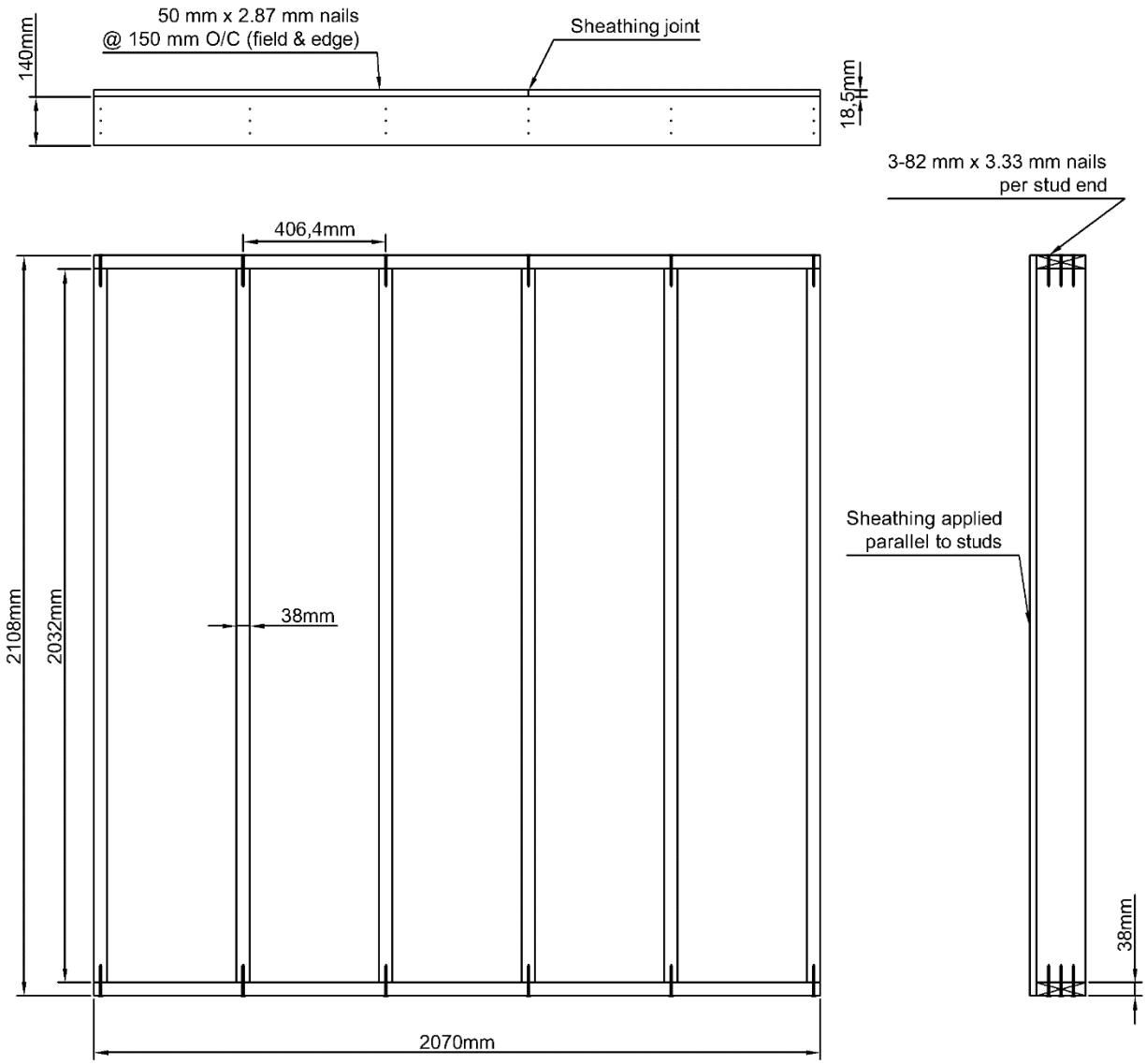

Figure 3.2 : 2 x 6 wall with plywood detailing

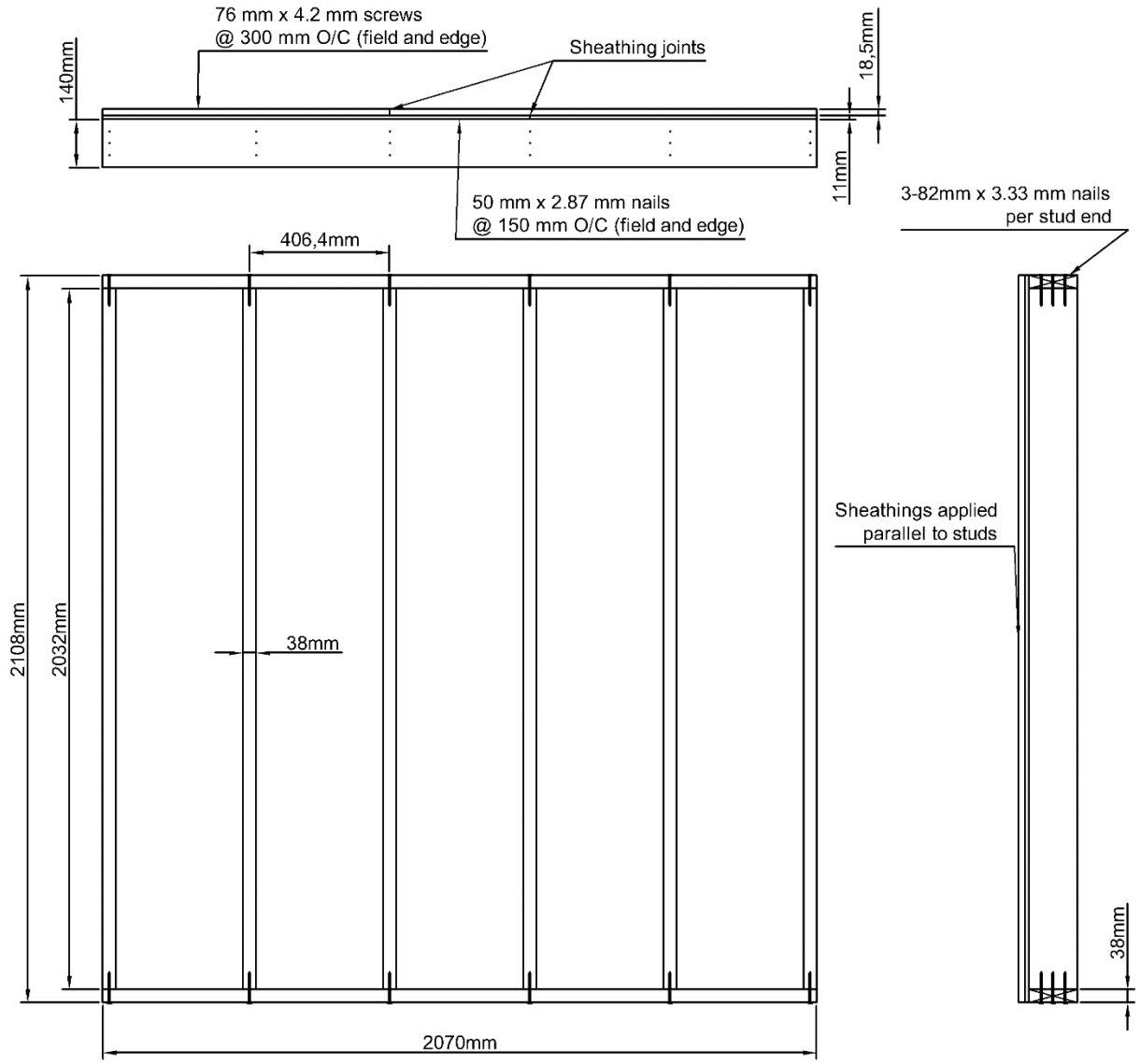

Figure 3.3 : 2 x 6 wall with OSB and plywood detailing

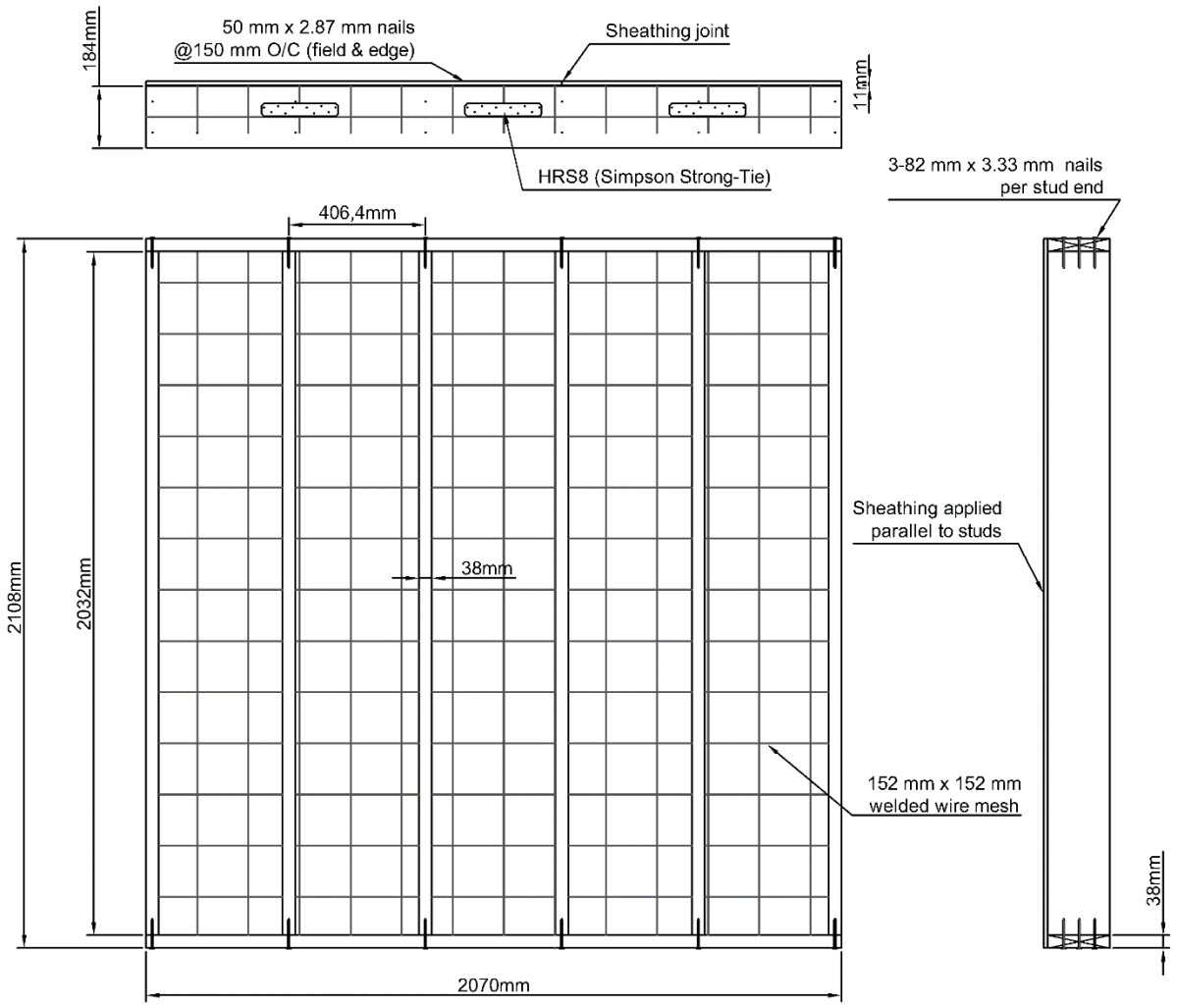

Figure 3.4 : 2 x 8 wall with WWM as OSB reinforcement

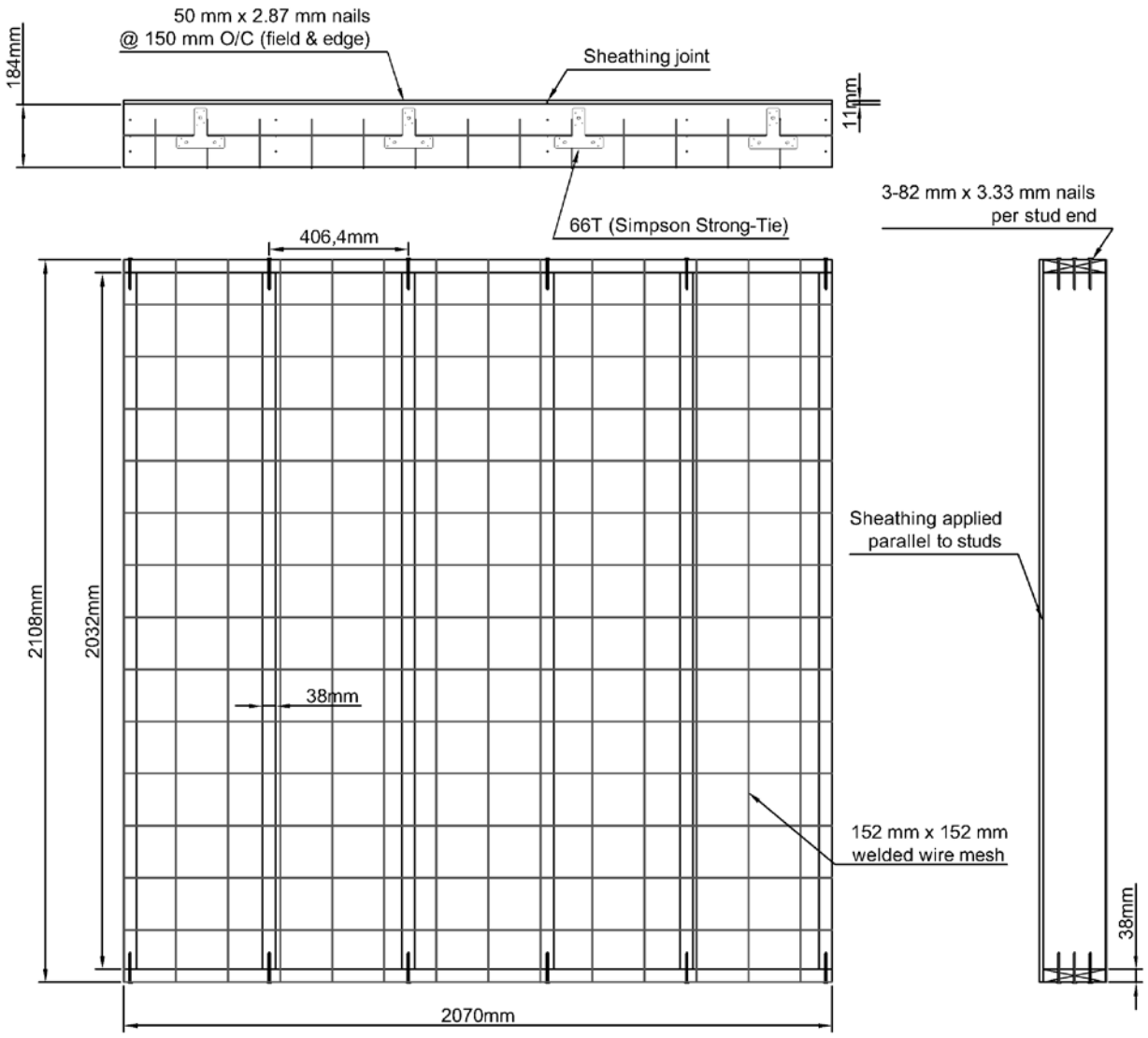

Figure 3.5 : 2 x 8 wall with WWM as catcher system

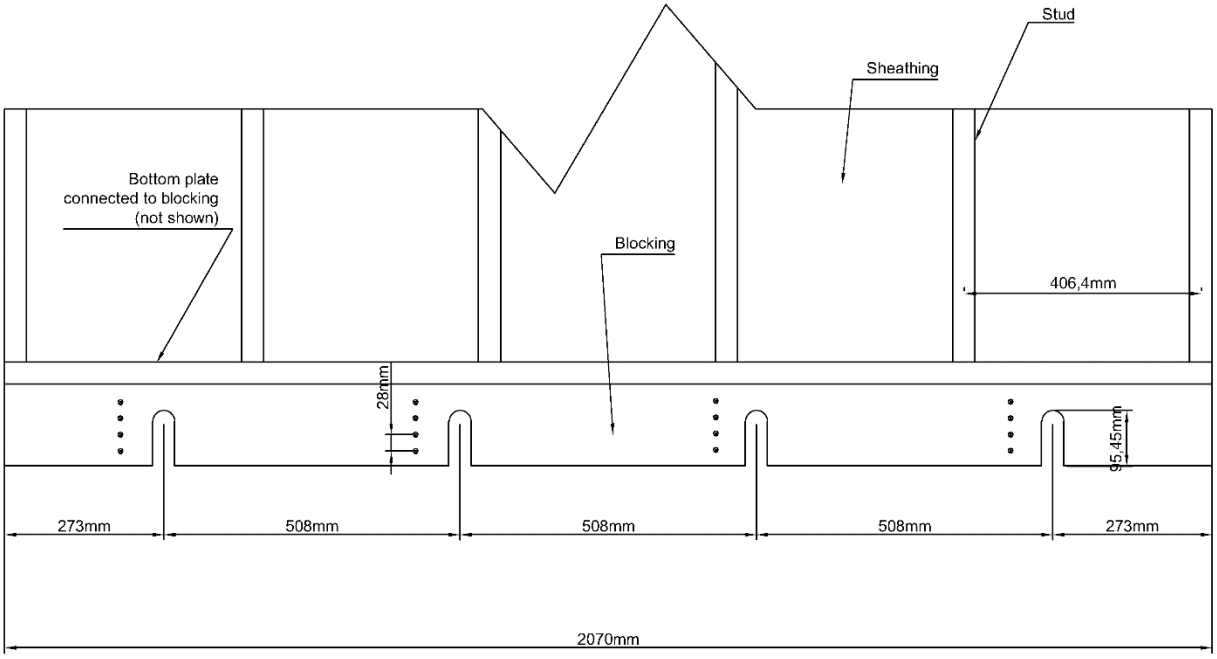

Figure 3.6 : Wall detail for typically and atypically connected walls – front view

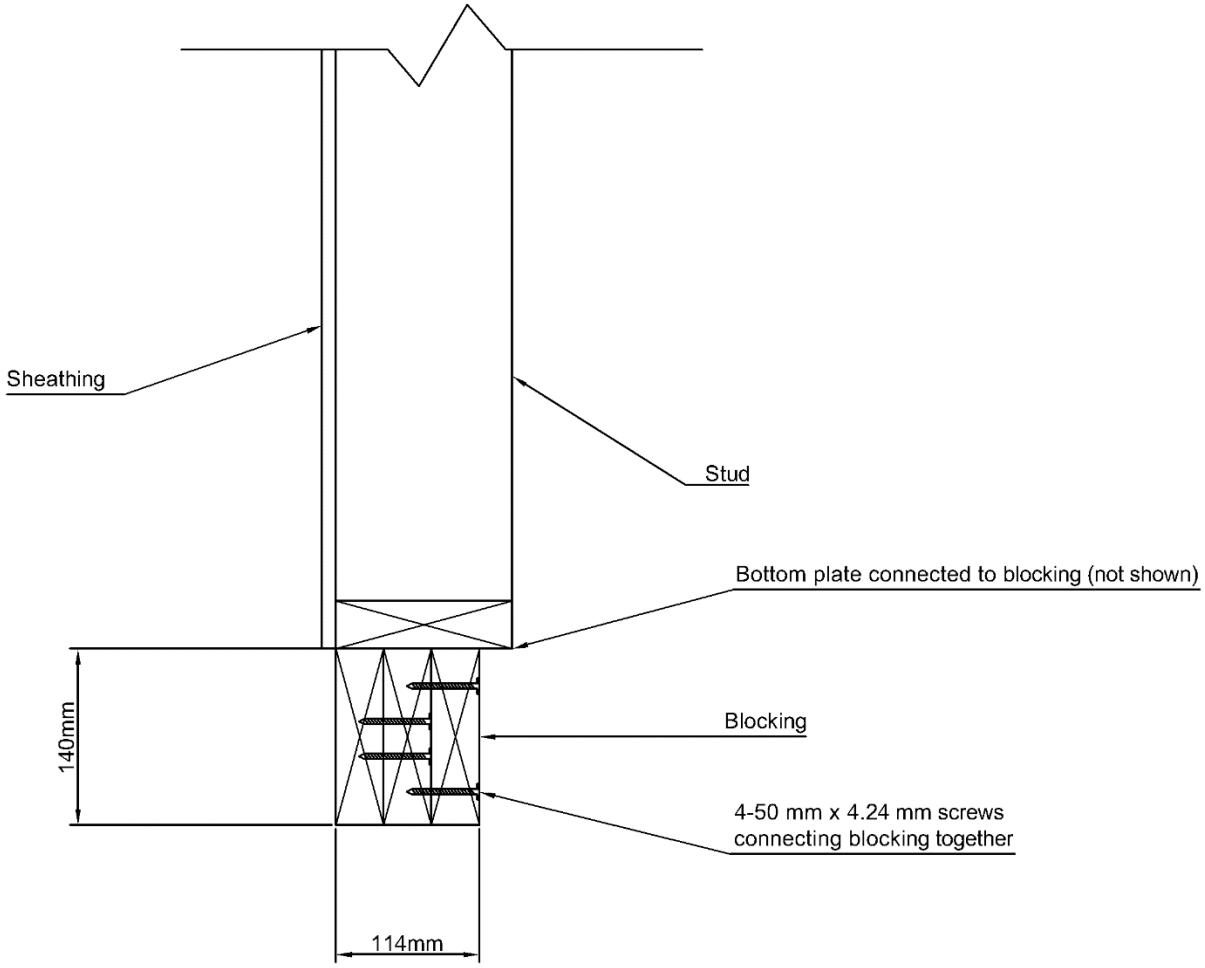

Figure 3.7 : Wall detail for typically and atypically connected walls – side view

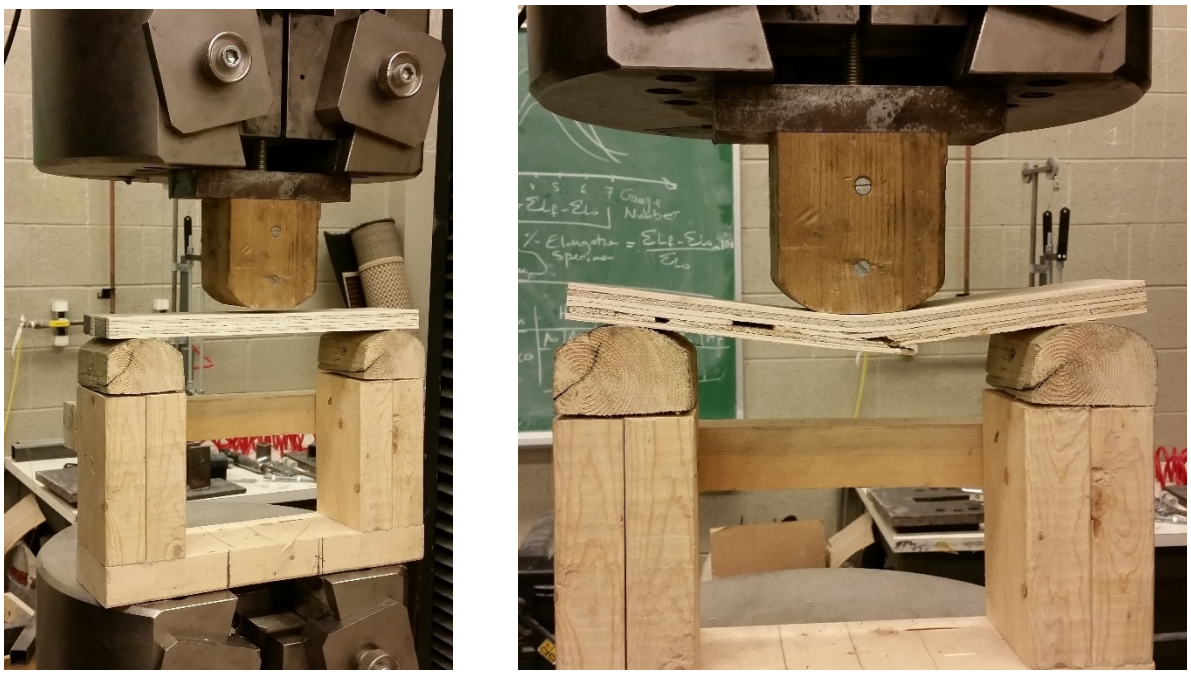

Figure 3.8 : Typical test setup and failure mode for sheathing coupon tests

Figure 3.9 : Typical test setup and failure mode for load-slip tests

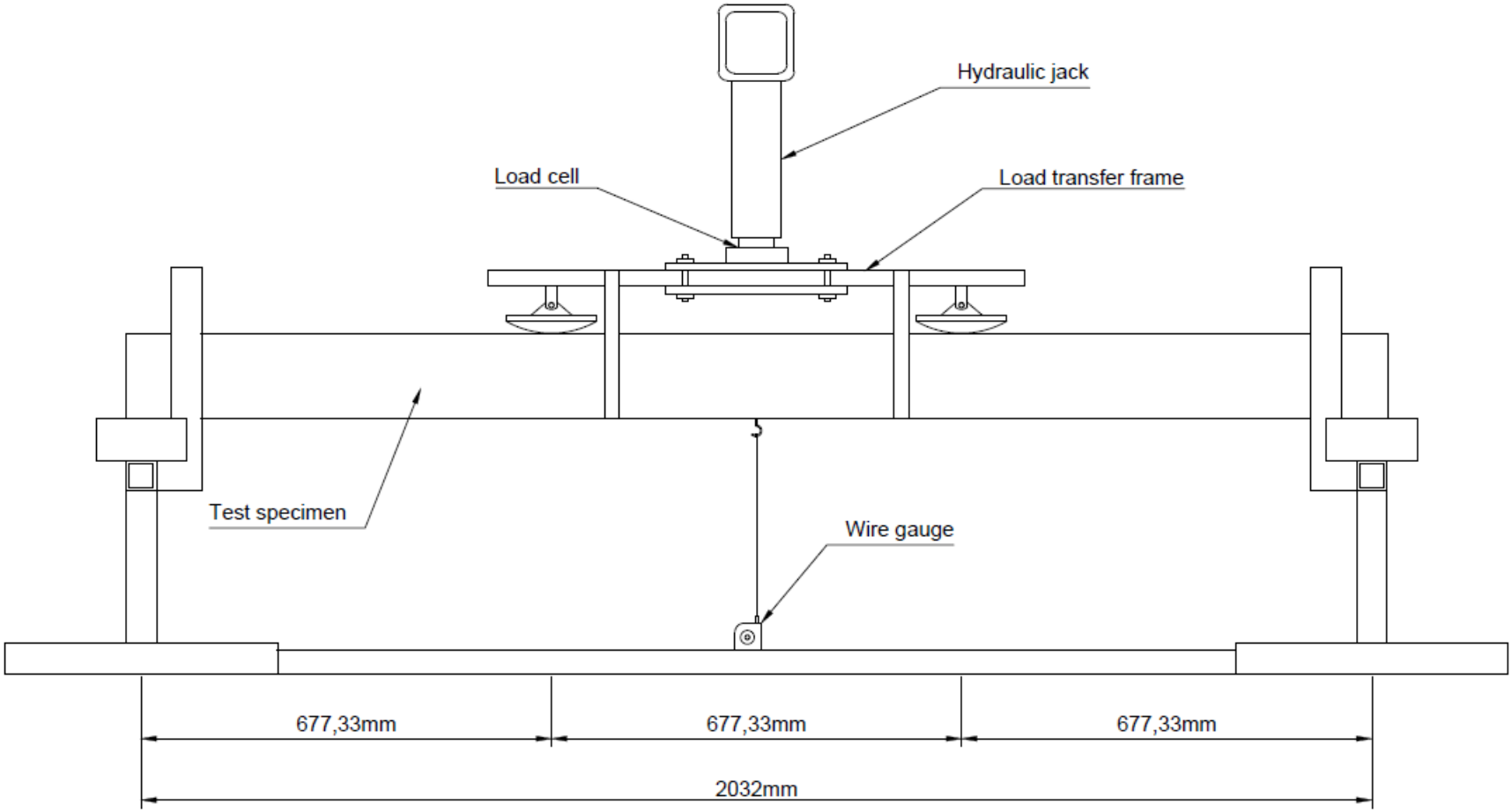

Figure 3.10 : Static bending test setup

A. Front view

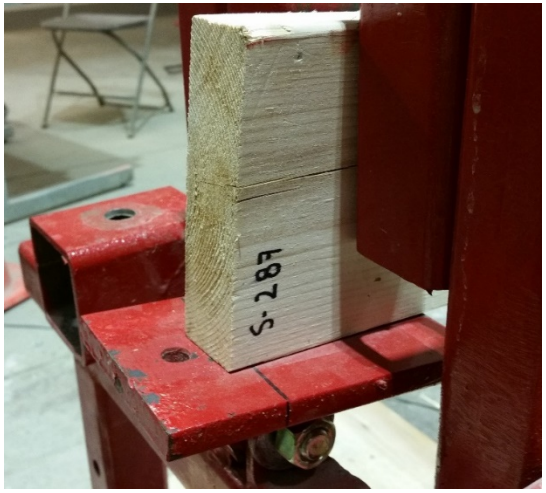

B. Idealized pin-ended conditions

C. Typical failure mode

Figure 3.11 : Static bending test setup

A. Spool and driver sections

B. Expansion section

C. End frame

Figure 3.12 : Shock tube components

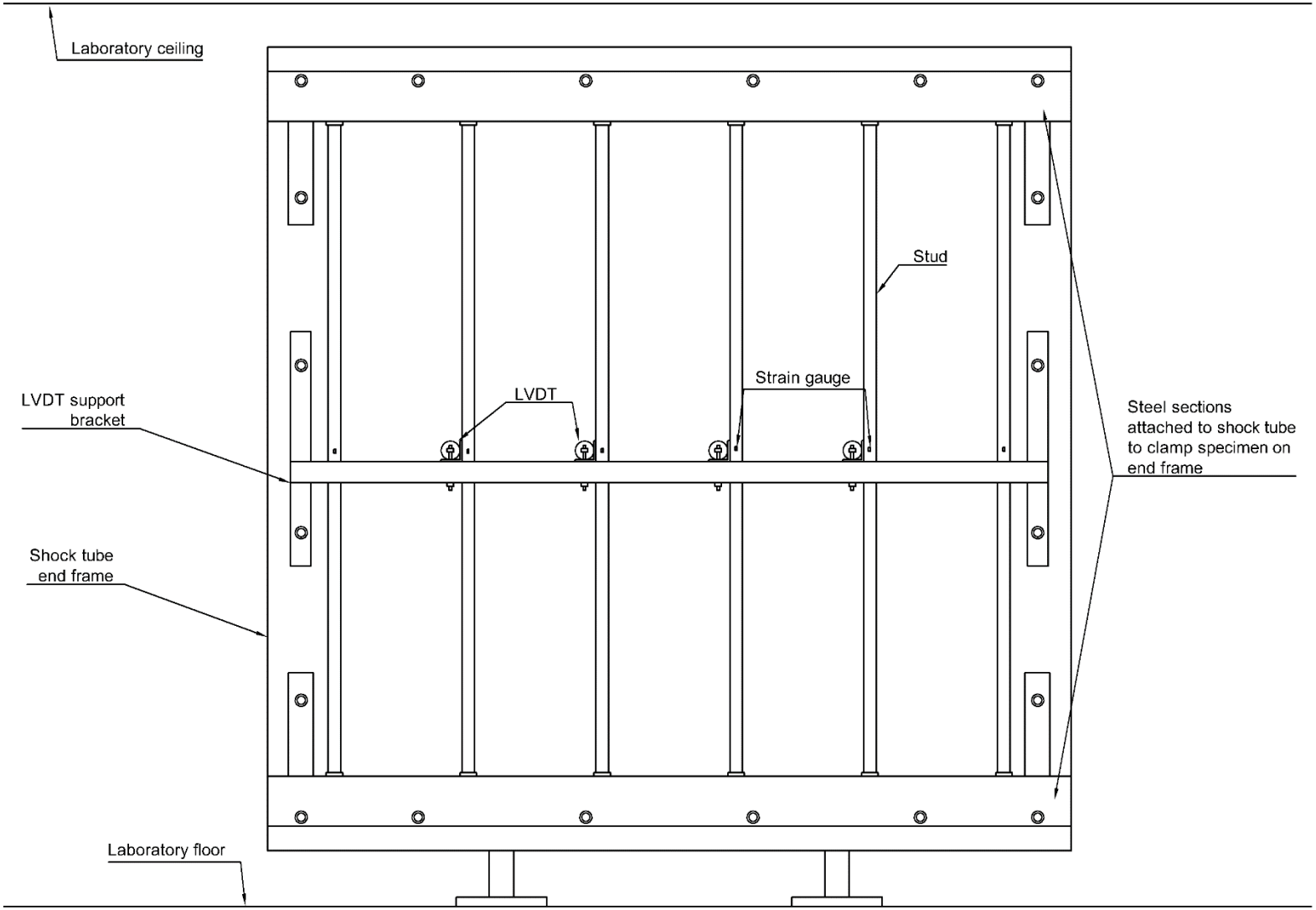

Figure 3.13 : Simply supported dynamic test setup – front view

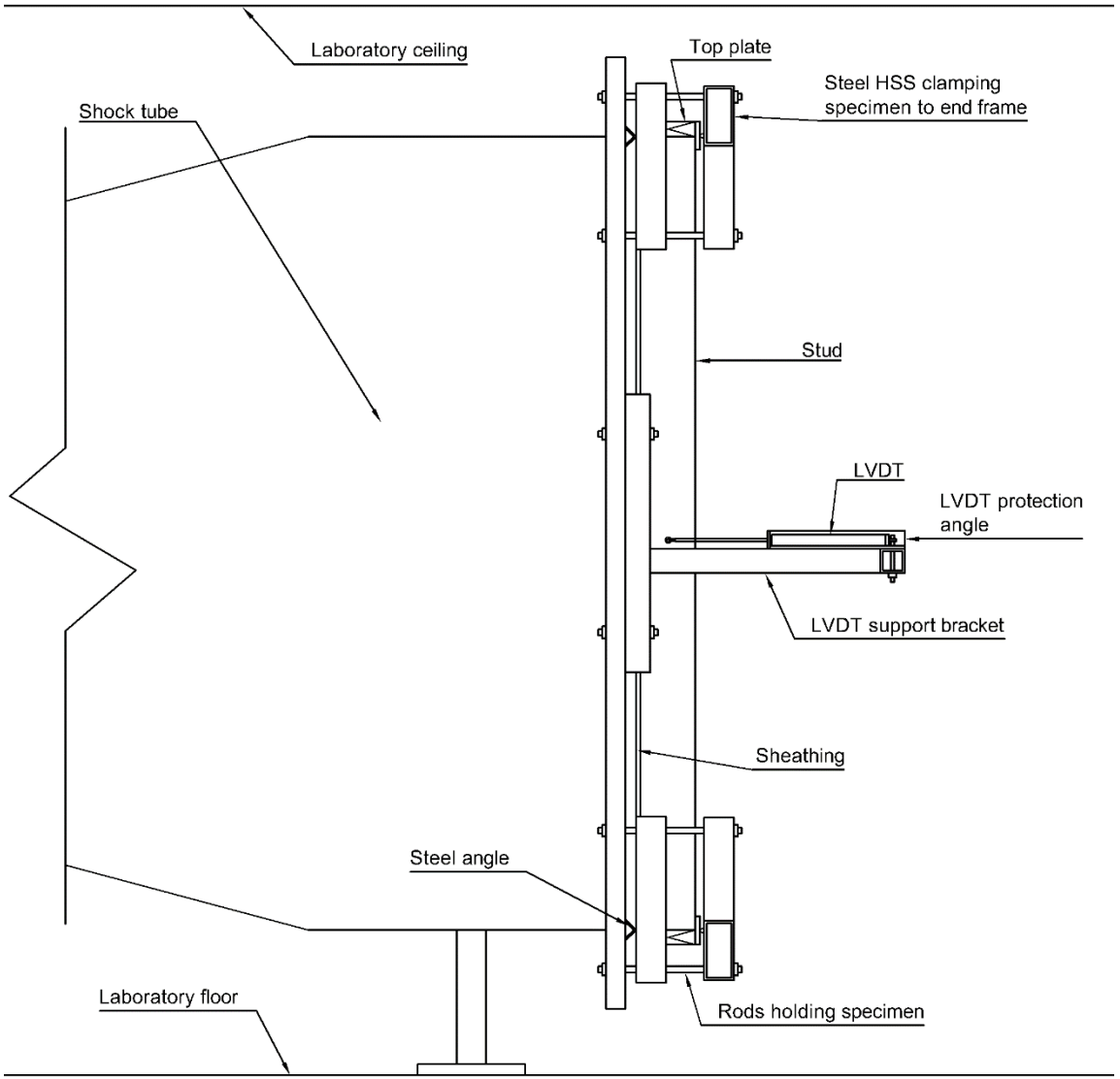

Figure 3.14 : Simply supported dynamic test setup – side view

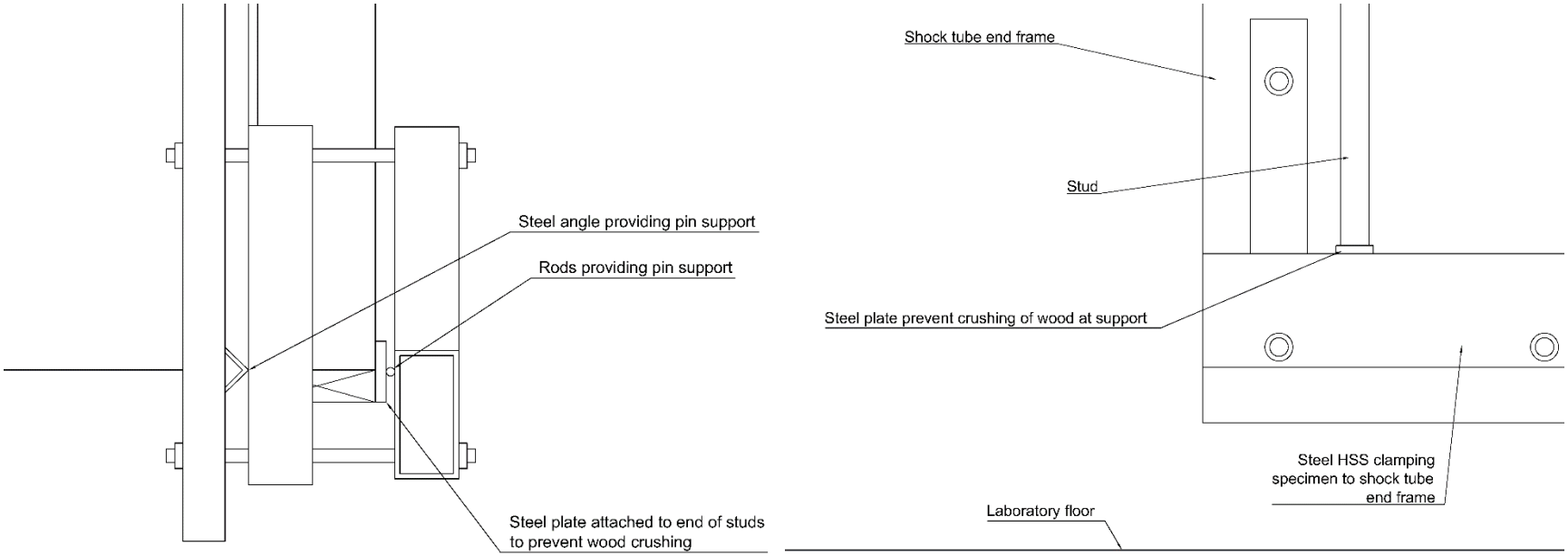

Figure 3.15 : Simply supported support condition details

A. Steel angles B. Steel roller plate

Figure 3.16 : Idealized simply supported support condition details

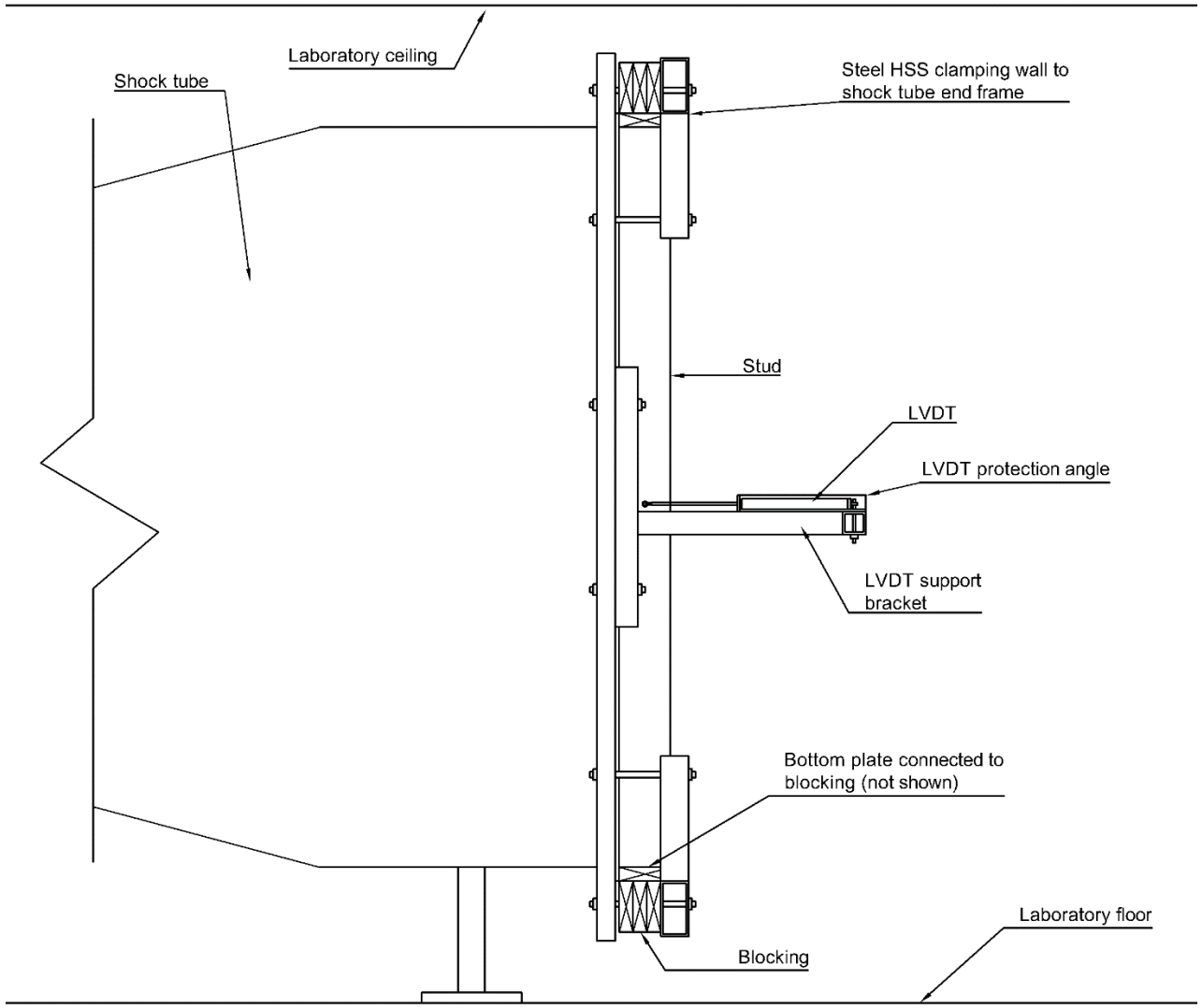

Figure 3.17 : Typically and atypically connected wall test setup – side view

A. Front view

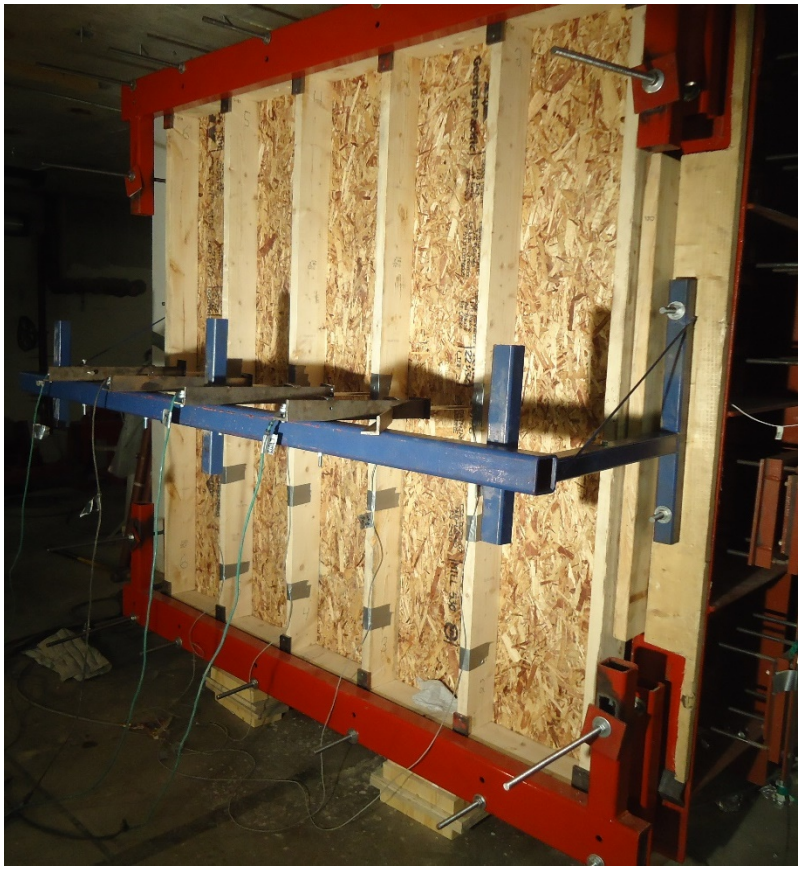

B. Oblique view

Figure 3.18 : Actual test setup for simply supported walls

A. Front view

B. Oblique view

C. Close-up of top-plate-to-blocking detail (side-view)

Figure 3.19 : Actual test setup for connected walls

A. WWM as sheathing reinforcement

B. WWM as catcher system

Figure 3.20 : Actual test setup for simply supported walls with WWM

A. Sanding of stud

B. Application of epoxy

C. Sanding of dried epoxy

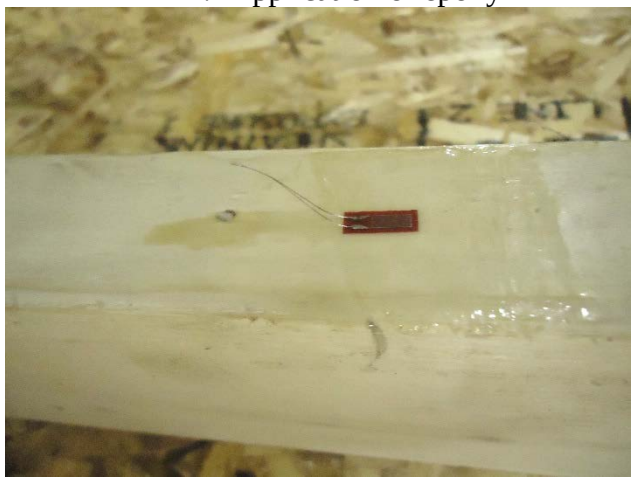

D. Application of strain gauge

Figure 3.21 : Strain gauge application process

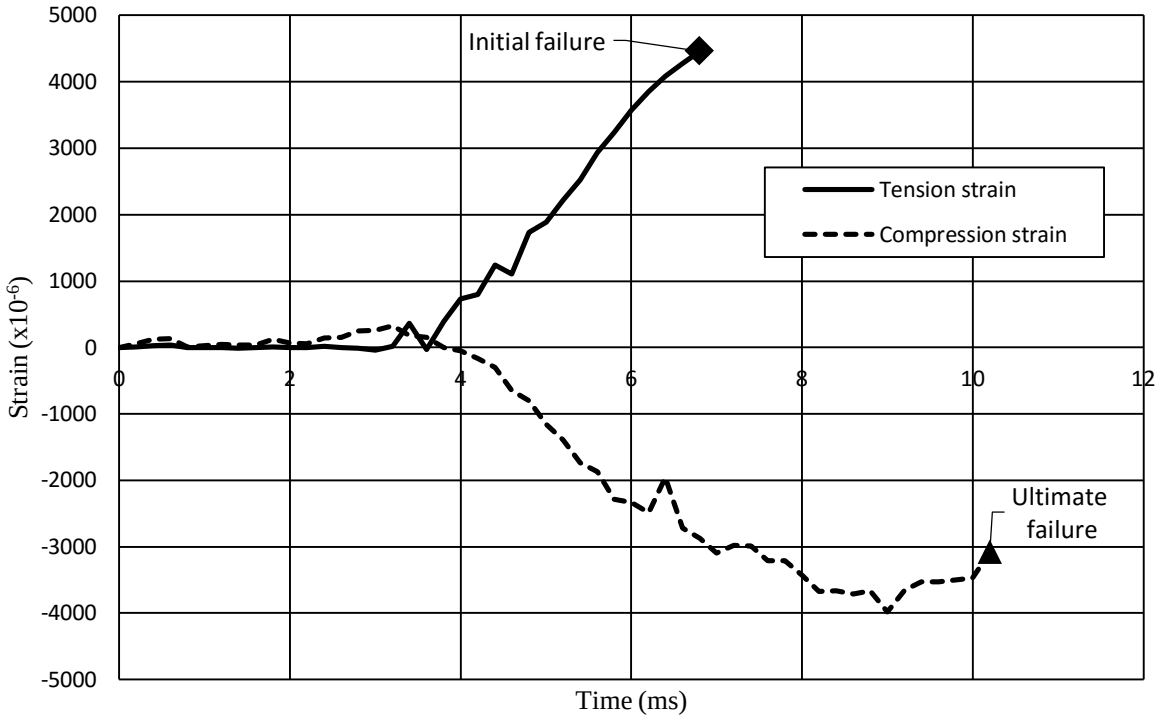

Figure 3.22 : Typical stud strain-time history

CHAPTER 4 - Experimental Results

4.1 General

The experimental results from both static and dynamic testing described in Chapter 3 are presented in this chapter. For static tests, presented results include the modulus of elasticity (MOE) and modulus of rupture (MOR) of the OSB and plywood coupons, as well as the results from individual stud bending tests. The load-displacement relationship of the sheathing-to-stud connection is also presented in this chapter. For the dynamic test, results for the behaviour of each wall is provided along with the pressure-impulse data to which each wall was subjected. Greater details of the dynamic test results can be found in the Appendix.

4.2 Static testing results

The results of this section are intended to be used as input material parameters in the modelling of the full-scale stud walls. Properties such as the modulus of rupture, modulus of elasticity, nail-slip between the studs and sheathing, as well as sheathing properties are important model inputs to be able to predict the behaviour of stud walls and various wall retrofit options.

4.2.1 Sheathing coupon testing results

The average MOE and MOR of the OSB and plywood coupons, along with the respective standard deviation (SD) and coefficient of variation (COV) are summarized in Table 4.1. Forty tests were conducted on OSB coupons and the results yielded an average MOE of 5020 MPa with a COV of 0.18. Figure 4.1 displays the results of the OSB coupons, along with the experimental average. The average MOR of the OSB coupons was determined to be 30.3 MPa with a COV of 0.22. These results are shown in Figure 4.2. Forty plywood coupons were also tested, which resulted in an average MOE of 4650 MPa with a COV of 0.12. These results are displayed in Figure 4.3. The average MOR of the forty plywood coupons was determined to be 49.8 MPa with a COV of 0.17. These results are displayed in Figure 4.4. A typical force-displacement relationship graph for an OSB coupon is shown in Figure 4.5. The average density of the OSB and plywood were determined to be 594.3 kg/m^3 and 429.5 kg/m^3, respectively with a COV of 0.05 for both material. The moisture content of the OSB coupons was 8.1 % with a COV of 0.13, while the moisture content of the plywood coupons were determined to be 8.6 % with a COV of 0.15.

4.2.2 Load-displacement relationship of typical timber joints

The behaviour of the sheathing-to-stud framing joints for all sheathing configurations tested in the full scale dynamic tests were investigated. Joint tests were performed on 11 mm OSB and 18.5 mm plywood using 50 mm long nails, as well as a configuration including 11 mm OSB with 50 mm nails with 18.5 mm plywood atop the OSB connected with 76 mm long construction screws. The nail and screw diameters are 2.87 mm and 4.2 mm, respectively. The initial stiffness was determined according to Yasumura & Kawai (1998) where the stiffness was calculated at the secant between 10 % and 40 % of the peak load. For timber shearwalls, this method has shown to produce realistic and accurate results, in comparison to other available methods (Muñoz et al., 2008). A typical load-displacement relationship graph for a sheathing-to-stud joint is shown in Figure 4.6. The average initial stiffness of the OSB joint was determined to be 1600 N/mm with a COV of 0.29. For the plywood joint, the average initial stiffness was determined to be 1750 N/mm with a COV of 0.39. The joint with both sheathing yielded an average of 3600 N/mm with a COV of 0.24.

4.2.3 Stud static bending testing results

A total of 220 studs were tested under four-point bending to determine their MOE and MOR. A total of 182 specimens consisted of 38 x 140 mm (2 x 6 in.) studs while the rest (38 specimens) consisted of 38 x 184 mm (2 x 8 in.) studs. The average MOE and MOR of the 38 x 140 mm studs were determined to be 9270 MPa with a COV of 0.18 and 35.6 MPa with a COV of 0.25, respectively. The 38 x 184 mm studs had an average MOE and MOR of 8830 MPa with a COV of 0.14 and 35.1 MPa with a COV of 0.19, respectively. These test results are shown in Figures 4.7 to 4.10, as well in summarized in Table 4.1. Figure 4.11 displays a typical force-displacement relationship graph for a stud tested destructively. Once all studs were tested, those tested non-destructively were randomly selected for the construction of twenty-five full-scale walls, which were tested dynamically in the shock tube.

The in-situ density and moisture content were measured for both sizes of the lumber. For the 2 x 6 in. studs, the average moisture content was determined to be 15.0 % while the average density was found to be 466.0 kg/m^3 with a COV of 0.16. The moisture content of the 2 x 8 in. studs was 17.2 % while the average density was found to be 514.7 kg/m^3 with a COV of 0.10.

4.3 Dynamic testing results

The following section summarizes the test results of the twenty-five walls tested dynamically. Table 4.2 summarizes all dynamic tests, including test result information such as the driver pressure, reflected pressure, reflected impulse, positive phase duration, average maximum stud displacement, average time to maximum displacement, average stud strain rate, and a quantified damage assessment for each wall. All stud displacement, strain, and time information pertain only to the four middle studs. Snapshots of videos recorded during testing will be present in the Appendix to display the progressive failure of the stud wall.

A typical pressure-impulse-time history relationship is shown in Figure 4.12. This graph is displayed in the Appendix for each wall. Figure 4.13 displays a typical stud displacement history for a typical test, including the reflected pressure. Complete test observations and details can be found in the Appendix.

Walls 1 – 16 were tested with simply supported end conditions, as to promote flexural failure of the studs; Walls 17 and 18 were tested with toe-nailed/nailed end conditions, as to reproduce current prescriptive wall end connection detailing for both seismic and non-seismic regions; Walls 19 – 25 were tested with different designed end connections, consisting of steel hangers, twist straps, and angles. All walls, excluding Wall 1 and 17, were subjected to only one pressure-impulse combination, in order to reduce the effect of damage accumulation, especially in the connections, in the results.

4.3.1 Wall 1: OSB sheathing with simply supported end conditions

Wall 1 was subjected to two different pressure and impulse combinations. For the first shot, a driver pressure of 68.9 kPa was used, which resulted in a reflected pressure of 13.7 kPa and a reflected impulse of 140.0 kPa-ms over a positive phase of 17.6 ms. An average maximum stud displacement of 17 mm was measured at an average time of 11.2 ms following the arrival of the primary shock wave. All studs remained elastic throughout this shot. Video review showed signs of nail withdrawal occurring at Stud 5, due to the negative pressure phase. The wall damage level was quantified as superficial.

For the second shot, a driver pressure of 296.5 kPa was used, which resulted in a reflected pressure of 54.2 kPa and a reflected impulse of 408.1 kPa-ms over a positive phase of 17.2 ms. An average maximum stud displacement of 53 mm was measured at an average time of 7.2 ms following the arrival of the primary shock wave. All but Stud 6 experienced total flexural failure and large amounts of debris was created. Cracking was observed on Stud 6. Viewing of the test video shows large rips forming in most of the sheathing upon the arrival of the initial shock wave. The wall damage level was quantified as blowout.

4.3.2 Wall 2: OSB sheathing with simply supported end conditions

A driver pressure of 275.8 kPa was used, which resulted in a reflected pressure of 46.5 kPa and a reflected impulse of 354.5 kPa-ms over a positive phase of 17.0 ms. An average maximum stud displacement of 54 mm was measured at an average time of 8.7 ms following the arrival of the primary shock wave. Stud 3, 4, and 6 failed, but did not create significant amounts of debris. Large amounts of rips in the sheathing around the undamaged studs were observed, which resulted in large amounts of sheathing debris. The wall damage level was quantified as blowout.

4.3.3 Wall 3: OSB sheathing with simply supported end conditions

A driver pressure of 306.8 kPa was used, which resulted in a reflected pressure of 50.4 kPa and a reflected impulse of 373.5 kPa-ms over a positive phase of 15.0 ms. An average maximum stud displacement of 58 mm was measured at an average time of 8.3 ms following the arrival of the primary shock wave. Stud 3 to 5 failed. Stud 4 created hazardous debris. Large amounts of rips in the sheathing around the undamaged studs were observed; this resulted in large amounts of sheathing debris. The wall damage level was quantified as blowout.

4.3.4 Wall 4: OSB sheathing with simply supported end conditions

A driver pressure of 310.3 kPa was used, which resulted in a reflected pressure of 56.4 kPa and a reflected impulse of 407.0 kPa-ms over a positive phase of 15.2 ms. An average maximum stud displacement of 52 mm was measured at an average time of 8.1 ms following the arrival of the primary shock wave. Stud 2 to 5 failed in flexure, with stud debris being produced and ejected at high velocity. Cracking at the ends of studs 1 and 6 was observed, likely due to the creation of a torque force by the sheathing under pressure. Most of the sheathing was blown off following the

arrival of the blast wave and significant debris of sheathing and stud elements was created. The wall damage level was quantified as blowout.

4.3.5 Wall 5: plywood sheathing with simply supported end conditions

A driver pressure of 275.8 kPa was used, which resulted in a reflected pressure of 48.1 kPa and a reflected impulse of 429.0 kPa-ms over a positive phase of 19.8 ms. An average maximum stud displacement of 55 mm was measured at an average time of 8.2 ms following the arrival of the primary shock wave. Stud 1 to 5 failed in flexure, with stud debris being produced and ejected at high velocity. Stud 6 suffered no visible damage. The smaller of the two sheathing sheets experienced a large rip at mid-span. A large gap was present at the sheathing joint along Stud 3. No noticeable sheathing debris was produced. The wall damage level was quantified as blowout.

4.3.6 Wall 6: plywood sheathing with simply supported end conditions

A driver pressure of 282.7 kPa was used, which resulted in a reflected pressure of 47.3 kPa and a reflected impulse of 437.2 kPa-ms over a positive phase of 19.4 ms. An average maximum stud displacement of 52 mm was measured at an average time of 9.4 ms following the arrival of the primary shock wave. All six studs failed in flexure, with stud debris being produced and ejected at high velocity. A significant rip in the sheathing was present near mid-span. A large gap was present at the sheathing joint along Stud 3. No noticeable sheathing debris was produced. The wall damage level was quantified as blowout.

4.3.7 Wall 7: plywood sheathing with simply supported end conditions

A driver pressure of 282.7 kPa was used, which resulted in a reflected pressure of 48.3 kPa and a reflected impulse of 434.2 kPa-ms over a positive phase of 19.6 ms. An average maximum stud displacement of 53 mm was measured at an average time of 8.4 ms following the arrival of the primary shock wave. All six studs failed in flexure, with stud debris being produced and ejected at high velocity. A significant rip in the sheathing was present near mid-span. A moderately sized gap was present at the sheathing joint along Stud 3. No noticeable sheathing debris was produced. The wall damage level was quantified as blowout.

4.3.8 Wall 8: plywood sheathing with simply supported end conditions

A driver pressure of 290.3 kPa was used, which resulted in a reflected pressure of 49.8 kPa and a reflected impulse of 465.2 kPa-ms over a positive phase of 19.6 ms. An average maximum stud displacement of 52 mm was measured at an average time of 6.9 ms following the arrival of the primary shock wave. Stud 2 to 6 failed, with Studs 2, 3, and 6 producing debris. A significant rip in the sheathing was present near mid-span. A large gap was present at the sheathing joint along Stud 3. No noticeable sheathing debris was produced. The wall damage level was quantified as blowout.

4.3.9 Wall 9: OSB and plywood sheathing with simply supported end conditions

A driver pressure of 310.3 kPa was used. A malfunction of the data acquisition system made it impossible to record the reflected pressure, impulse, stud displacement, or strain readings. Stud 2 to 6 failed, with Studs 2, 3, and 6 producing debris. A significant rip in the sheathing was present near mid-span. A large gap was present at the sheathing joint along Stud 3. No noticeable sheathing debris was produced. Nail withdrawal was observed along Stud 3 and 6. The wall damage level was quantified as blowout.

4.3.10 Wall 10: OSB and plywood sheathing with simply supported end conditions

A driver pressure of 326.1 kPa was used, which resulted in a reflected pressure of 49.7 kPa and a reflected impulse of 480.8 kPa-ms over a positive phase of 19.6 ms. An average maximum stud displacement of 52 mm was measured at an average time of 8.9 ms following the arrival of the primary shock wave. All six studs failed in flexure. Some stud debris was produced. A significant rip in the OSB layer was present near mid-span. Damage of the plywood sheet could be observed from inside the shock tube. No gap was present at the sheathing joint along Stud 3. Nail withdrawal was observed along Studs 3-5, with some screw puncture also occurring along those same studs. The wall damage level was quantified as blowout.

4.3.11 Wall 11: OSB and plywood sheathing with simply supported end conditions

A driver pressure of 407.5 kPa was used, which resulted in a reflected pressure of 65.1 kPa and a reflected impulse of 623.0 kPa-ms over a positive phase of 20.6 ms. An average maximum stud displacement of 66 mm was measured at an average time of 7.8 ms following the arrival of the primary shock wave. All six studs failed in flexure. Stud 1, 2, and 4 produced significant debris.

A significant rip in the OSB layer was present near mid-span. Damage of the plywood sheet could be observed from inside the shock tube. A small gap was present at the sheathing joint along Stud 3. Nail withdrawal was observed along Studs 1, 3, 5, and 6, with some screws having been punctured through the sheathing panels occurring along those same studs. The wall damage level was quantified as blowout.

4.3.12 Wall 12: OSB and plywood sheathing with simply supported end conditions

A driver pressure of 447.5 kPa was used, which resulted in a reflected pressure of 70.9 kPa and a reflected impulse of 654.1 kPa-ms over a positive phase of 21.4 ms. An average maximum stud displacement of 64 mm was measured at an average time of 8.0 ms following the arrival of the primary shock wave. All six studs failed in flexure and produced debris. The OSB layer suffered a large rip at mid-span. The plywood layer had major residual deflection at mid-span and was the only component holding the specimen up at the end of the test, however the axial capacity of the wall is estimated to be null. Overall wall residual deflection was approximately 600 mm. Damage of the plywood sheet could be observed from inside the shock tube. A moderate gap was present at the sheathing joint along Stud 3. Nail withdrawal and screws having been punctured through the sheathing panels was observed along all six studs. The wall damage level was quantified as blowout.

4.3.13 Wall 13: WWM reinforced OSB sheathing with simply supported end conditions

A driver pressure of 434.4 kPa was used, which resulted in a reflected pressure of 63.4 kPa and a reflected impulse of 571.7 kPa-ms over a positive phase of 22.0 ms. Stud displacements were not taken as a precautionary measure against damaging instrumentation. The time to maximum strain (and therefore displacement) was measured at an average time of 8.0 ms following the arrival of the primary shock wave. Studs 3 to 5 failed in flexure. Studs 2, 3, and 5 produced significant debris, while Stud 2 did not fail but was ejected from the wall due to top plate connection failure. Studs 1 and 6 received significant torque due to the asymmetrical connection of sheathing applied to only one side of each stud. Significant rips in the sheathing was prevalent throughout the wall section. The WWM prevented any major rips from occurring in the sheathing and developing into debris. The pressure was transferred entirely to the studs. The wall damage level was quantified as blowout.

4.3.14 Wall 14: WWM reinforced OSB sheathing with simply supported end conditions

A driver pressure of 303.4 kPa was used, which resulted in a reflected pressure of 51.2 kPa and a reflected impulse of 482.8 kPa-ms over a positive phase of 21.4 ms. An average maximum stud displacement of 42 mm was measured at an average time of 8.0 ms following the arrival of the primary shock wave. Studs 1 to 4 failed in flexure, while Studs 5 and 6 did not show visible signs of damage. Studs 1 to 3 produced significant debris. Significant rips in the sheathing was prevalent throughout the wall section. The WWM prevented any major rips from developing into debris, which promoted the distribution of pressure to the studs. Nail withdrawal was observed along Studs 1 to 3. The WWM itself seemed to have yielded, but did not suffer any significant damage. The wall damage level was quantified as blowout.

4.3.15 Wall 15: WWM catcher system with simply supported end conditions

A driver pressure of 297.9 kPa was used, which resulted in a reflected pressure of 47.6 kPa and a reflected impulse of 397.9 kPa-ms over a positive phase of 15.2 ms. An average maximum stud displacement of 38 mm was measured at an average time of 7.6 ms following the arrival of the primary shock wave. Only Stud 3 failed. No stud debris was created, and any sheathing debris was caught by the WWM. The entire sheathing layer was compromised, but significant residual axial capacity was maintained. The WWM prevented any major sheathing debris from being ejected from the wall. While the WWM did deflect, it was not damaged and was reused in another shot. The wall damage level was quantified as superficial.

4.3.16 Wall 16: WWM catcher system with simply supported end conditions

A driver pressure of 413.7 kPa was used, which resulted in a reflected pressure of 62.5 kPa and a reflected impulse of 437.1 kPa-ms over a positive phase of 14.0 ms. Since a significantly high pressure was used, no LVDTs were used to measure displacements, in order to prevent damaging them. The time to maximum strain (and therefore displacement) was measured at an average time of 7.0 ms following the arrival of the primary shock wave. None of the six studs failed, and no stud debris was created. The sheathing was completely blown off but all debris was caught by the WWM. The WWM prevented any major sheathing debris from being ejected from the wall. While the WWM did deflect in some areas, it was not damaged and was reused in another shot. The wall damage level was quantified as superficial since no significant damage was observed in the studs,

no debris was created and it was estimated that the studs retained their axial capacity. The wall damage level was quantified as superficial**.**

4.3.17 Wall 17: OSB sheathing with realistic nailed/toe-nailed end conditions

Wall 17 was subjected to two different pressure and impulse combinations. For the first shot, a driver pressure of 71.7 kPa was used, which resulted in a reflected pressure of 13.9 kPa and a reflected impulse of 139.2 kPa-ms over a positive phase of 16.6 ms. Since full connection failure was expected, no LVDTs were used to measure displacements in order to prevent damage to them. The time to maximum strain was measured at an average time of 10.0 ms following the arrival of the primary shock wave. All studs remained elastic throughout this shot. Nail withdrawal was observed at the sheathing joint along Stud 3. Full connection failure occurred at the top plate blocking, while 4 of the 6 fasteners in the bottom plate failed. All exposed fasteners displayed signs of yielding. The wall damage level was quantified as blowout, since the wall was no longer connected to its original blockings.

Since the wall components were not damaged, the wall was retested with new boundary connections. For the second shot, a driver pressure of 214.4 kPa was used, which resulted in a reflected pressure of 41.4 kPa and a reflected impulse of 302.5 kPa-ms over a positive phase of 16.0 ms. The time to maximum strain was measured at an average time of 7.0 ms following the arrival of the primary shock wave. All studs remained elastic throughout this shot. The stud wall was fully ejected from the end frame and travelled across to the laboratory wall. Full connection failure occurred at the top and bottom plates. All exposed fasteners displayed signs of yielding, with some being pulled out of the blocking. The wall damage level was quantified as blowout.

4.3.18 Wall 18: OSB sheathing with realistic nailed/toe-nailed end conditions

A driver pressure of 137.9 kPa was used, which resulted in a reflected pressure of 29.3 kPa and a reflected impulse of 234.6 kPa-ms over a positive phase of 17.4 ms. Since full connection failure was expected, no LVDTs were used to measure displacements in order to prevent damage to them. The time to maximum strain (and therefore connection failure) was measured at an average time of 8.9 ms following the arrival of the primary shock wave. All studs remained elastic throughout this shot. The stud wall was fully ejected from the end frame and travelled across to the laboratory. Full connection failure occurred at the top and bottom plates. All exposed fasteners displayed signs

of yielding, with some being pulled out of the blocking. The wall damage level was quantified as blowout.

4.3.19 Wall 19: OSB sheathing with retrofitted end conditions (HU28)

A driver pressure of 241.3 kPa was used, which resulted in a reflected pressure of 44.3 kPa and a reflected impulse of 387.3 kPa-ms over a positive phase of 19.8 ms. Since connection performance was not defined yet, no LVDTs were used to measure displacements in order to prevent damage to them. The time to maximum strain (and therefore maximum displacement) was measured at an average time of 5.0 ms following the arrival of the primary shock wave. Studs 2 – 5 failed in flexure while Studs 1 and 6 suffered no visible damage. Studs 2 and 4 produced hazardous debris. Significant damage was found throughout the bottom and top plates, with some screw withdrawal occurring in some connections. Damage can be described as splitting of the plates. Review of the test video showed that significant bottom and top plate rotation occurred, but residual displacement was reduced due to the connection detail. Significant sheathing debris was also created. The wall damage level was quantified as blowout.

4.3.20 Wall 20: OSB sheathing with retrofitted end conditions (HU28)

A driver pressure of 206.8 kPa was used, which resulted in a reflected pressure of 37.3 kPa and a reflected impulse of 341.5 kPa-ms over a positive phase of 18.4 ms. An average maximum stud displacement of 54 mm was measured at an average time of 8.7 ms following the arrival of the primary shock wave. Studs 2 – 5 failed in flexure while Studs 1 and 6 suffered no visible damage. No stud debris was created due in part to the connectors holding the stud halves in place. Moderate damage was found in both top and bottom plates, with the concentration of the most severe damage being in between Studs 3 and 4. Review of the test video showed that significant bottom and top plate rotation occurred. Significant sheathing debris was also created. The wall damage level was quantified as blowout.

4.3.21 Wall 21: OSB sheathing with retrofitted end conditions (LJS26DS)

A driver pressure of 213.7 kPa was used, which resulted in a reflected pressure of 39.5 kPa and a reflected impulse of 342.2 kPa-ms over a positive phase of 17.4 ms. An average maximum stud displacement of 42 mm was measured at an average time of 9.3 ms following the arrival of the primary shock wave. Studs 2 – 5 failed in flexure while Studs 1 and 6 suffered no visible damage.

Only Stud 4 created hazardous debris. Minor cracking was found in the bottom and top plates, mostly between Studs 1 to 3. Some screw withdrawal was observed at the bottom end of Stud 2. Significant sheathing debris was created. The wall damage level was quantified as blowout.

4.3.22 Wall 22: OSB sheathing with retrofitted end conditions (LJS26DS)

A driver pressure of 215.1 kPa was used, which resulted in a reflected pressure of 40.3 kPa and a reflected impulse of 364.4 kPa-ms over a positive phase of 18.8 ms. An average maximum stud displacement of 55 mm was measured at an average time of 8.2 ms following the arrival of the primary shock wave. Studs 2 – 5 failed in flexure while Studs 1 and 6 suffered no visible damage. No stud debris was created during the shot due in part by the connectors holding onto their respective stud-half. Cracking was located in the top plate between Studs 2 and 3. Screw withdrawal was observed at the ends of Stud 4 and 5. Review of the test video showed that residual displacement was reduced due to the connectors, when compared to other connectors and pin-pin conditions. Significant sheathing debris was also created. The wall damage level was quantified as blowout.

4.3.23 Wall 23: OSB sheathing with retrofitted end conditions (LTS18)

A driver pressure of 210.3 kPa was used, which resulted in a reflected pressure of 42.1 kPa and a reflected impulse of 328.9 kPa-ms over a positive phase of 18.0 ms. An average maximum stud displacement of 21 mm was measured at an average time of 6.8 ms following the arrival of the primary shock wave. Studs 3 – 5 failed in flexure while Studs 1, 2, and 6 suffered cracking near their ends due to row-shear failure occurring. Studs 3 to 5 created hazardous debris due to the fact that these connector did not perform well and generally caused splitting/row-shear failure to occur where they were connected to the studs. Stud 5's top connector ruptured which in part created debris. Review of the test video showed that the LVDT bracket partially stopped the stud debris from being propagated farther down the laboratory. Significant sheathing debris was also created. The wall damage level was quantified as blowout.

4.3.24 Wall 24: OSB sheathing with retrofitted end conditions (LTS18)

A driver pressure of 215.1 kPa was used, which resulted in a reflected pressure of 38.8 kPa and a reflected impulse of 318.0 kPa-ms over a positive phase of 18.0 ms. An average maximum stud displacement of 49 mm was measured at an average time of 6.8 ms following the arrival of the

primary shock wave. Studs 3 – 5 failed in flexure while Stud 1 had cracking near its ends due to row-shear failure. Studs 1 and 6 did not show visible signs of damage. No debris was generated, however this is due to the LVDT bracket keeping all stud debris within the shock tube. In reality, all 6 studs would have been ejected across the laboratory. Due to the asymmetrical nature of the connector, some twisting force was applied to the studs. Significant sheathing debris was also created. The wall damage level was quantified as blowout.

4.3.25 Wall 25: OSB sheathing with retrofitted end conditions (ML24Z)

A driver pressure of 211.0 kPa was used, which resulted in a reflected pressure of 39.1 kPa and a reflected impulse of 377.4 kPa-ms over a positive phase of 15.8 ms. An average maximum stud displacement of 32 mm was measured at an average time of 9.5 ms following the arrival of the primary shock wave. All six studs failed in flexure. Studs 2, 3, and 5 created hazardous debris. Connectors on almost all studs showed signs of yielding and screw withdrawal. No damage to either top or bottom plate was observed, mainly due to the fact that stud rotation took place about the connectors, and not between the plates and rim-joists themselves. Review of the test video showed that residual displacement was reduced due to the connectors, when compared to other connectors and pin-pin conditions. Splitting on at connection region on all six studs was observed. Significant sheathing debris was also created. The wall damage level was quantified as blowout.

Table 4.1 : Summary of OSB, plywood, and stud properties

	OSB		Plywood		2 x 6 studs		2 x 8 studs	
	Modulus of elasticity	**Modulus of rupture**	**Modulus of elasticity**	**Modulus of rupture**	**Modulus of elasticity**	**Modulus of rupture**	**Modulus of elasticity**	**Modulus of rupture**
Number of specimens	40	40	40	40	182	20	38	5
Average (MPa)	5020	30.3	4650	49.8	9270	35.6	8830	35.1
Standard deviation (MPa)	887	6.8	573	8.5	1658	9.0	1204	6.7
Coefficient of variation	0.18	0.22	0.12	0.17	0.18	0.25	0.14	0.19

Table 4.2 : Summary of dynamic tests

Test name	Wall mass (kg)	Driver pressure (kPa)	Reflected pressure (kPa)	Reflected impulse (kPa-ms)	Positive phase duration (ms)	Average stud failure displacement (mm)	Average time to max (ms)	Average strain rate (s^{-1})	Quantified wall damage
Wall_1_Shot_1	64.86	68.9	13.7	140.0	17.6	16.79	11.15	1.92E-1	Superficial
Wall_1_Shot_2	64.86	296.5	54.2	408.1	17.2	53.08	7.20	6.08E-1	Blowout
Wall_2_Shot_1	70.00	275.8	46.5	354.5	17.0	53.67	8.70	5.25E-1	Blowout
Wall_3_Shot_1	69.70	306.8	50.5	373.5	15.0	58.08	8.30	5.48E-1	Blowout
Wall_4_Shot_1	66.24	310.3	56.4	407.0	15.2	52.17	8.07	3.51E-1	Blowout
Wall_5_Shot_1	73.44	275.8	48.1	429.0	19.8	55.04	8.20	5.12E-1	Blowout
Wall_6_Shot_1	71.30	282.7	47.3	437.2	19.4	52.35	9.40	6.29E-1	Blowout
Wall_7_Shot_1	72.00	282.7	48.3	434.2	19.6	52.60	8.40	5.74E-1	Blowout
Wall_8_Shot_1	71.56	290.3	49.8	465.2	19.6	51.90	6.90	8.31E-1	Blowout
Wall_9_Shot_1	106.22	310.3	No data						Blowout
Wall_10_Shot_1	102.05	326.1	49.7	480.8	19.6	51.86	8.85	4.33E-1	Blowout
Wall_11_Shot_1	101.78	407.5	65.1	623.0	20.6	65.84	7.75	7.38E-1	Blowout
Wall_12_Shot_1	98.16	447.5	70.9	654.1	21.4	64.17	8.00	5.45E-1	Blowout
Wall_13_Shot_1	92.80	434.4	63.4	571.7	22.0	No data	8.00	9.05E-1	Blowout
Wall_14_Shot_1	92.90	303.4	51.2	482.8	21.4	41.68	8.00	3.69E-1	Hazardous
Wall_15_Shot_1	95.36	297.9	47.6	397.9	15.2	38.36	7.60	3.26E-1	Superficial
Wall_16_Shot_1	96.04	413.7	62.5	437.1	14.0	No data	7.00	4.30E-1	Superficial
Wall_17_Shot_1	68.46	71.7	13.9	139.2	16.6		9.95	1.52E-1	Blowout
Wall_17_Shot_2	68.46	214.4	41.4	302.5	16.0		6.98	3.20E-1	Blowout
Wall_18_Shot_1	68.66	137.9	29.3	234.6	17.4		8.85	2.28E-1	Blowout
Wall_19_Shot_1	73.24	241.3	44.3	387.3	19.8		5.00	5.88E-1	Blowout
Wall_20_Shot_1	73.54	206.8	37.3	341.5	18.4	53.63	8.70	5.03E-1	Blowout
Wall_21_Shot_1	69.76	213.7	39.5	342.1	17.4	42.00	9.30	5.19E-1	Blowout
Wall_22_Shot_1	71.78	215.1	40.3	364.4	18.8	55.47	8.20	6.94E-1	Blowout
Wall_23_Shot_1	70.80	210.3	42.1	328.9	18.0	20.54	6.80	3.14E-1	Blowout
Wall_24_Shot_1	72.13	215.1	39.1	318.0	18.0	48.81	6.80	3.58E-1	Blowout
Wall_25_Shot_1	72.54	211.0	39.1	377.4	15.8	31.66	9.50	4.36E-1	Blowout

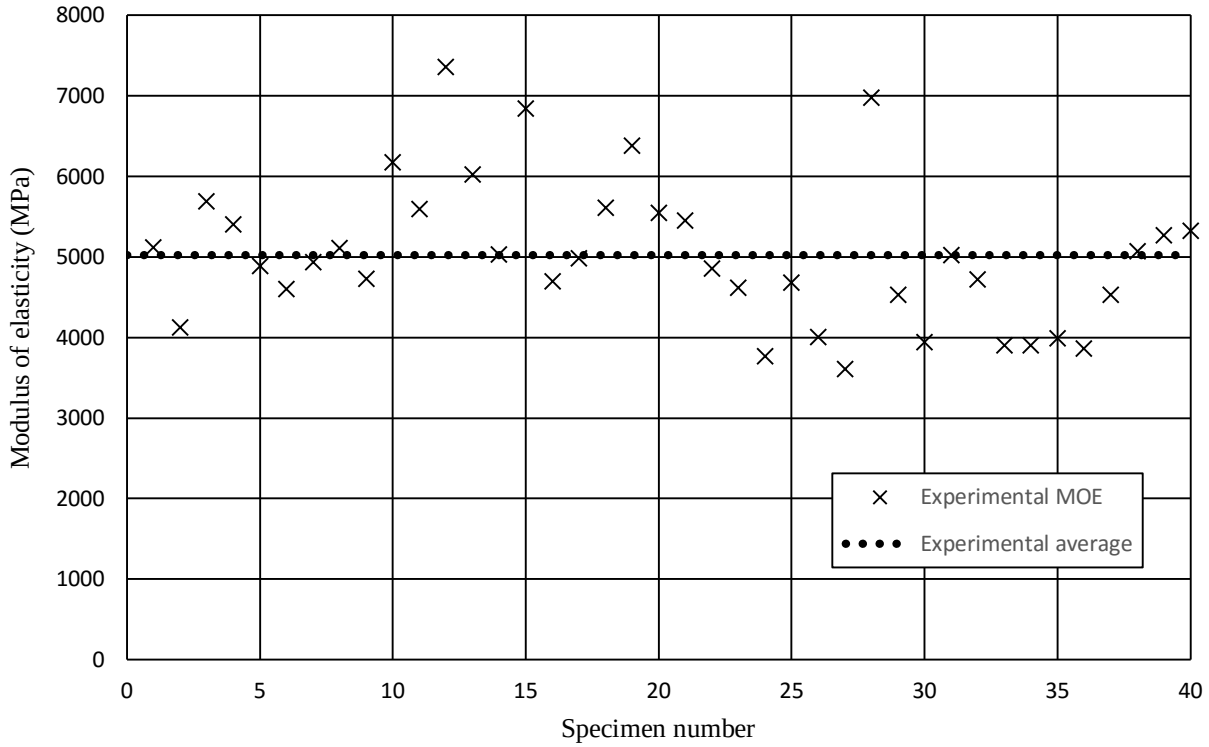

Figure 4.1 : Experimental MOE for OSB coupons

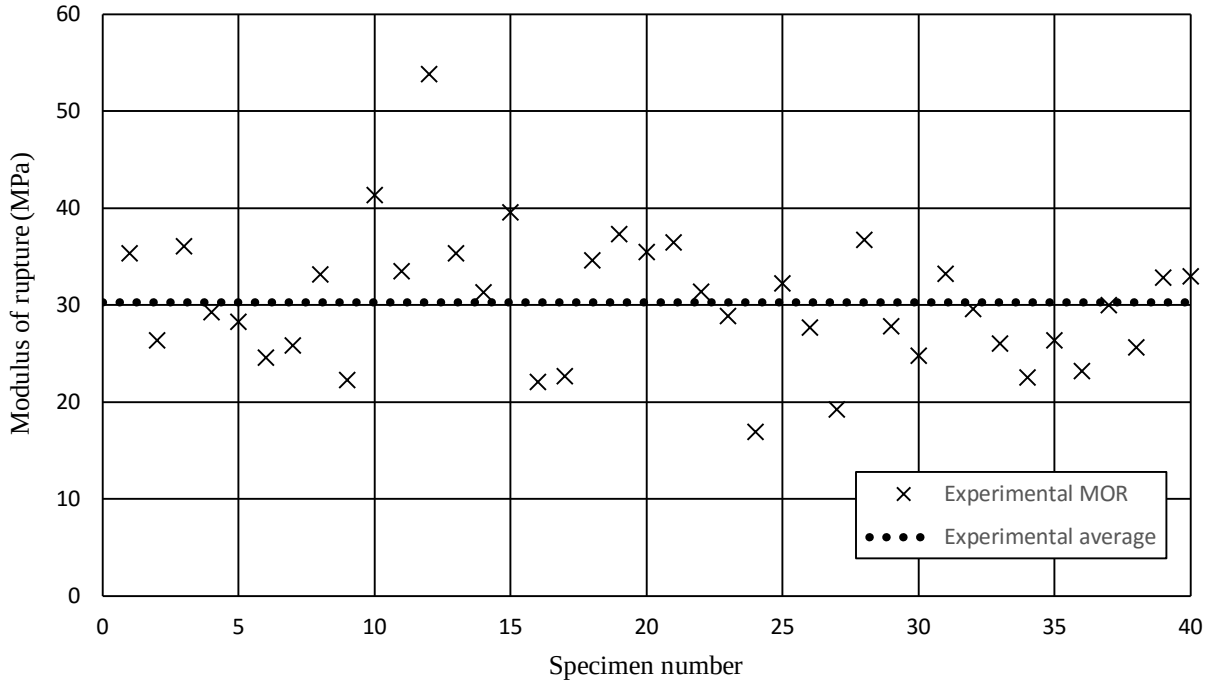

Figure 4.2 : Experimental MOR for OSB coupons

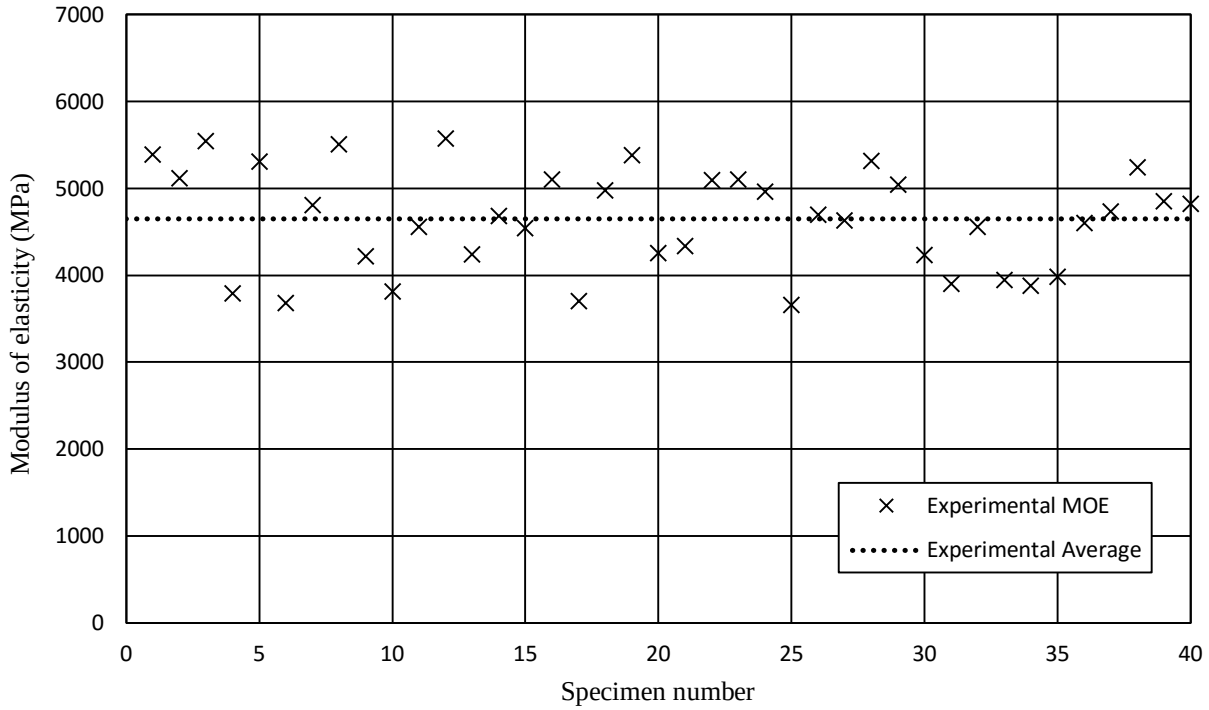

Figure 4.3 : Experimental MOE of plywood coupons

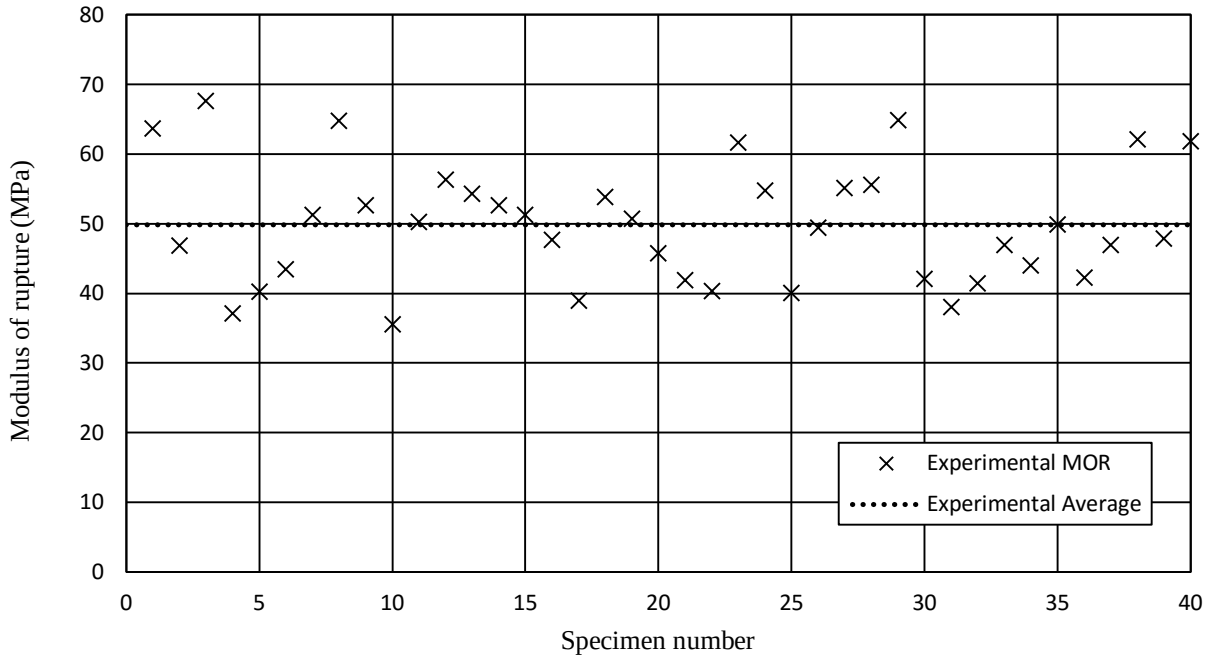

Figure 4.4 : Experimental MOR of plywood coupons

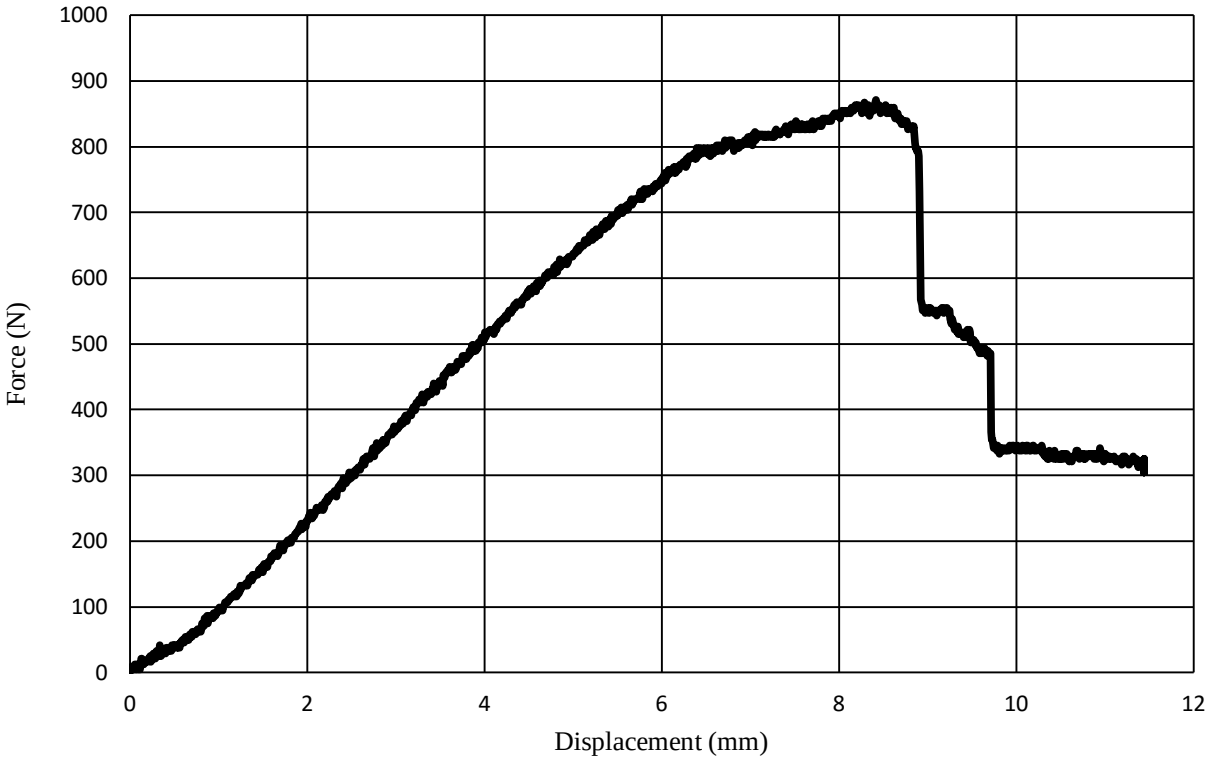

Figure 4.5 : Typical force-displacement history of OSB coupon

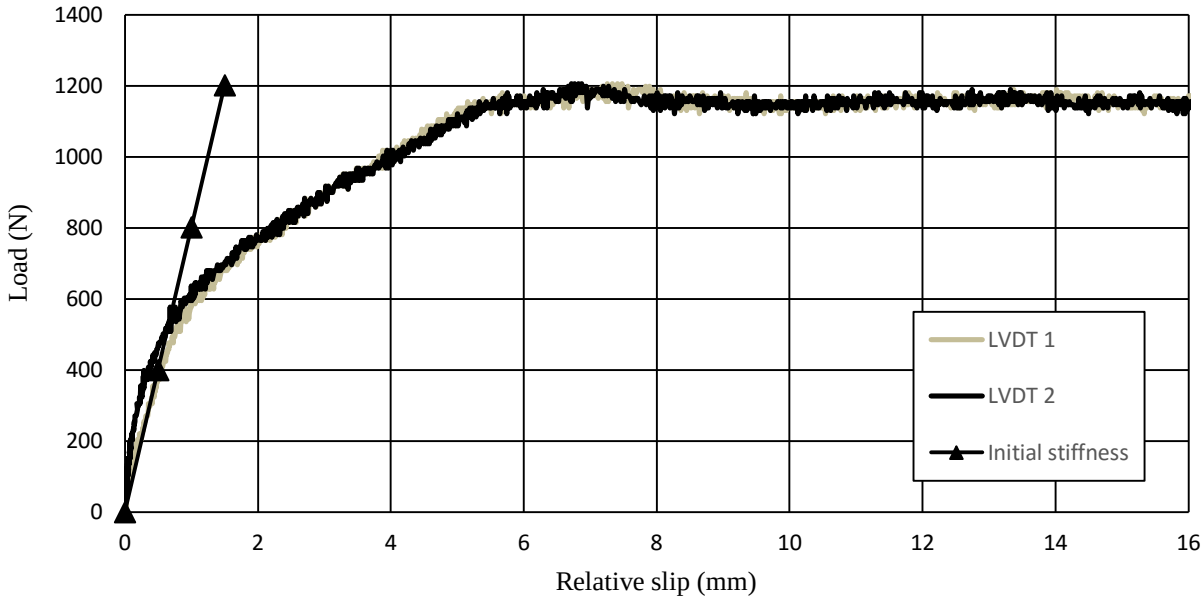

Figure 4.6 : Typical sheathing-stud load-slip history of plywood specimen

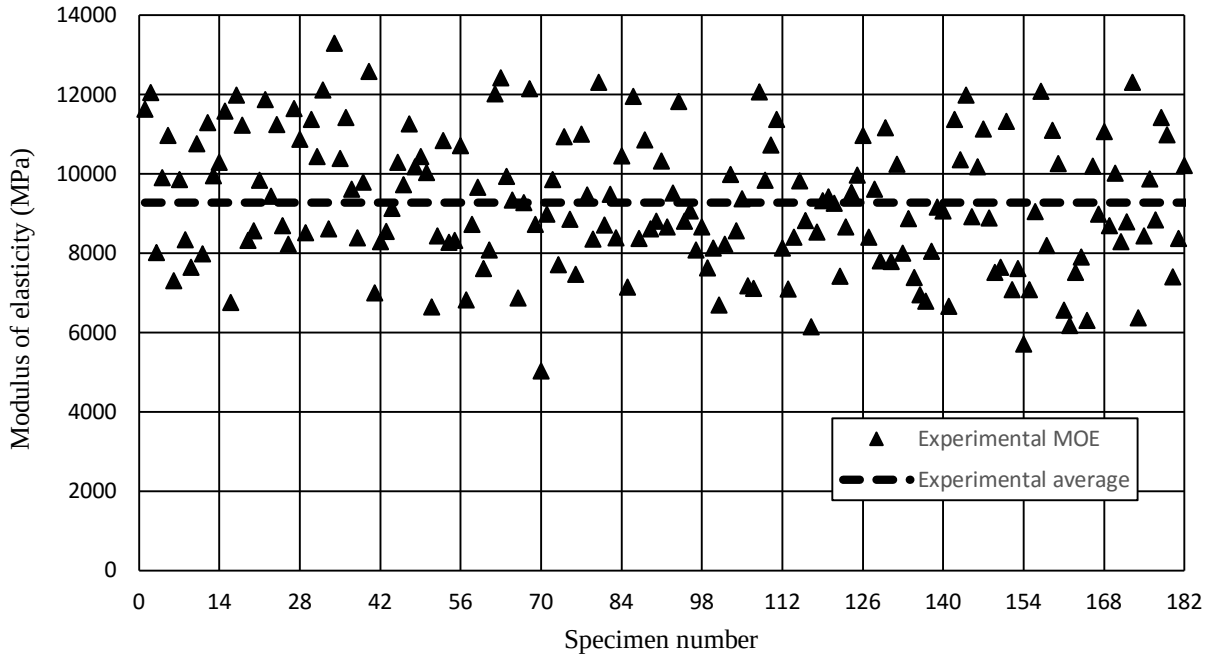

Figure 4.7 : Experimental MOE of 2 x 6 studs

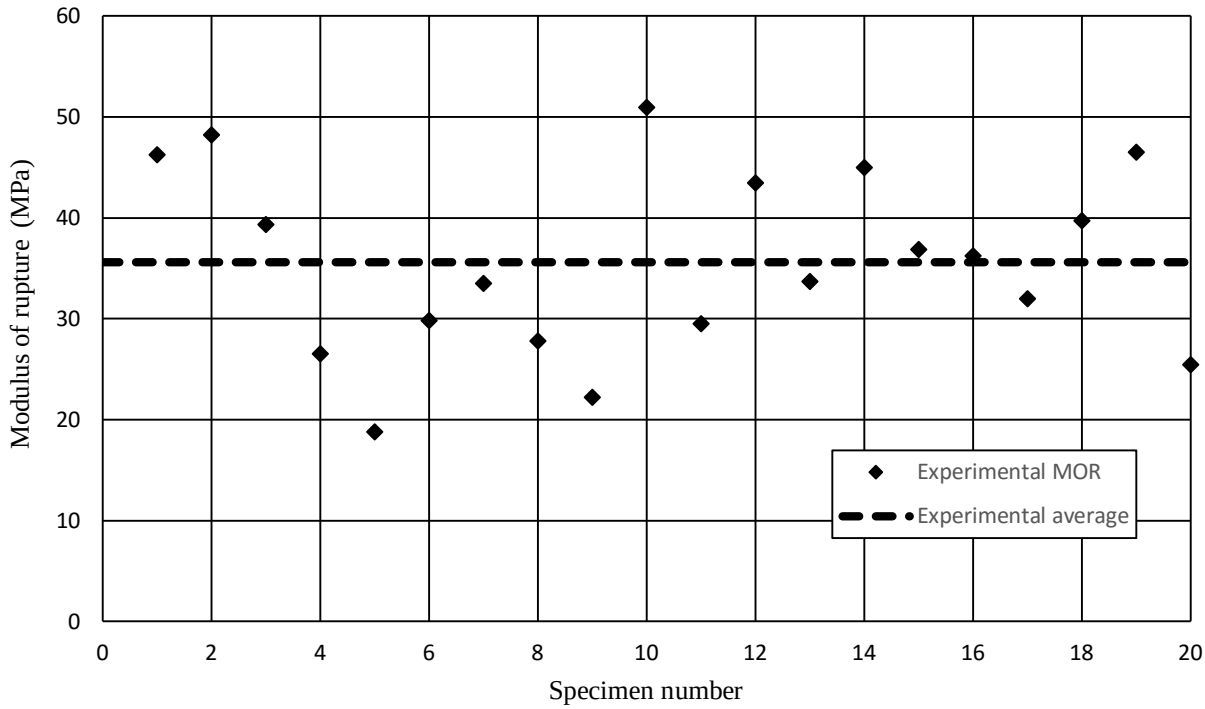

Figure 4.8 : Experimental MOR of 2 x 6 studs

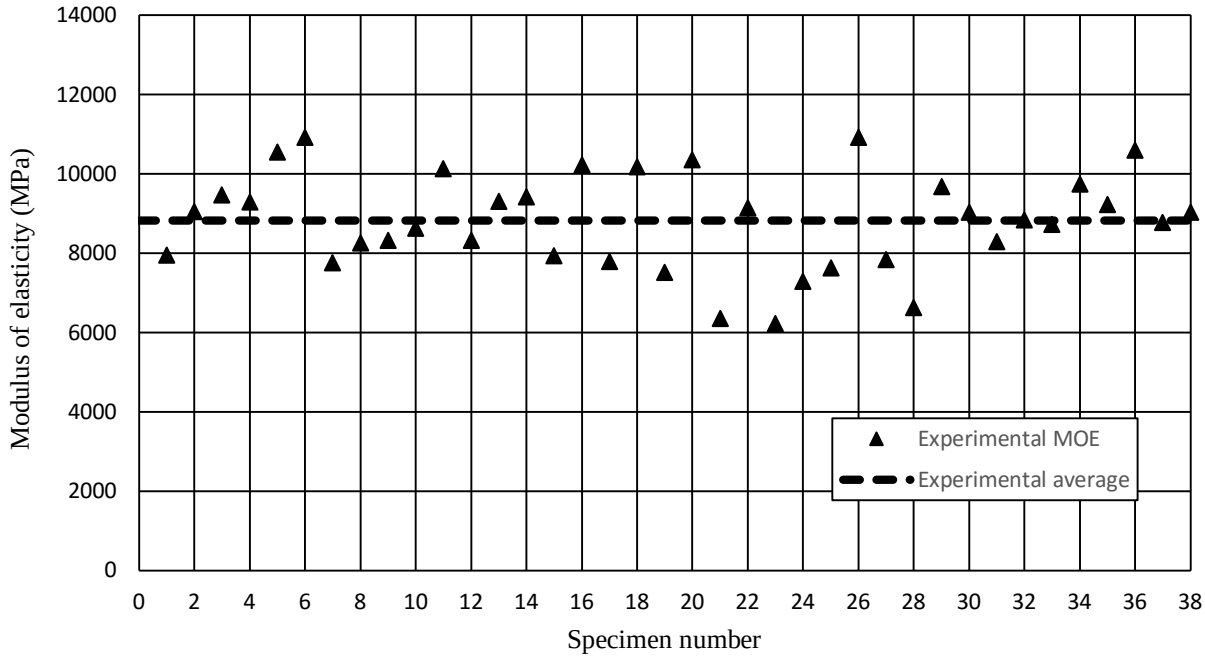

Figure 4.9 : Experimental MOE of 2 x 8 studs

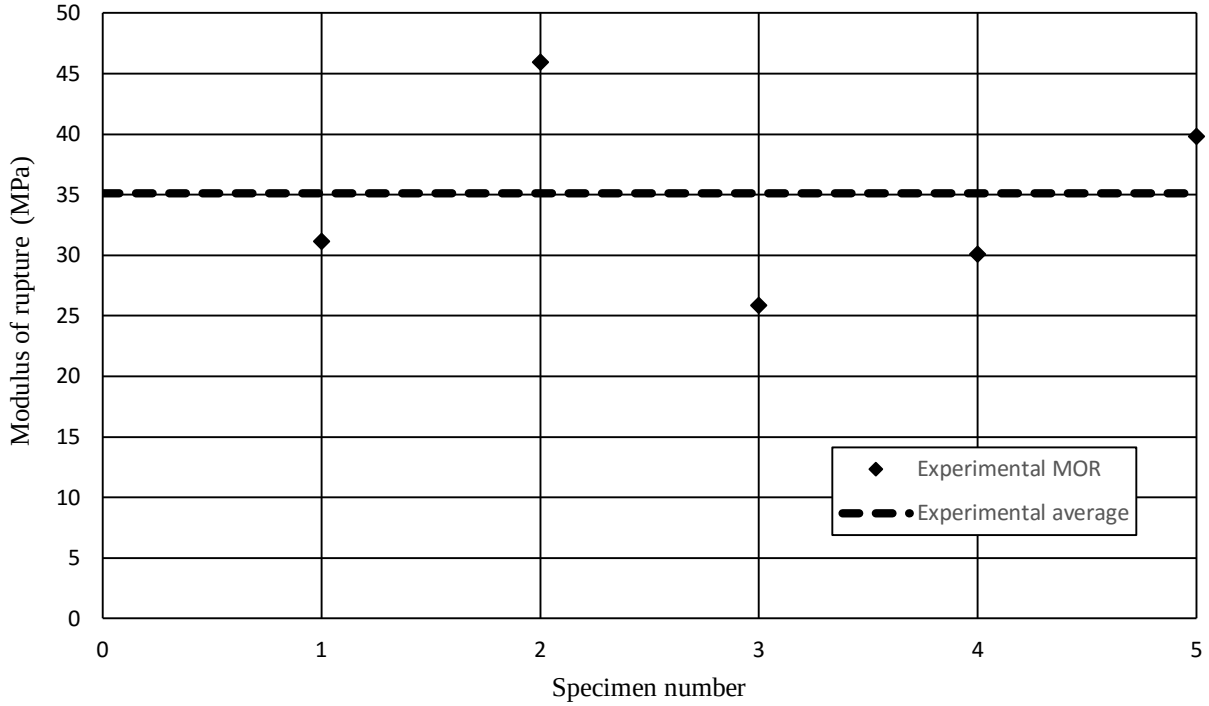

Figure 4.10 : Experimental MOR of 2 x 8 studs

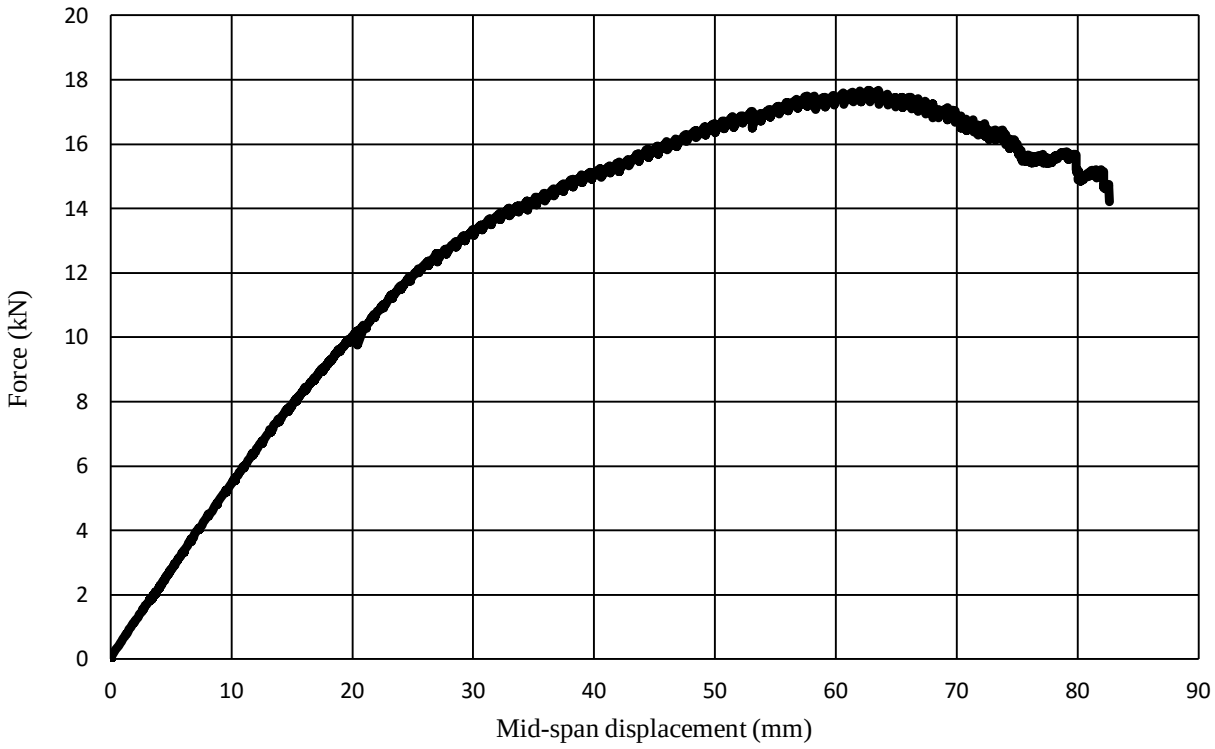

Figure 4.11 : Typical force-displacement history for static stud bending test

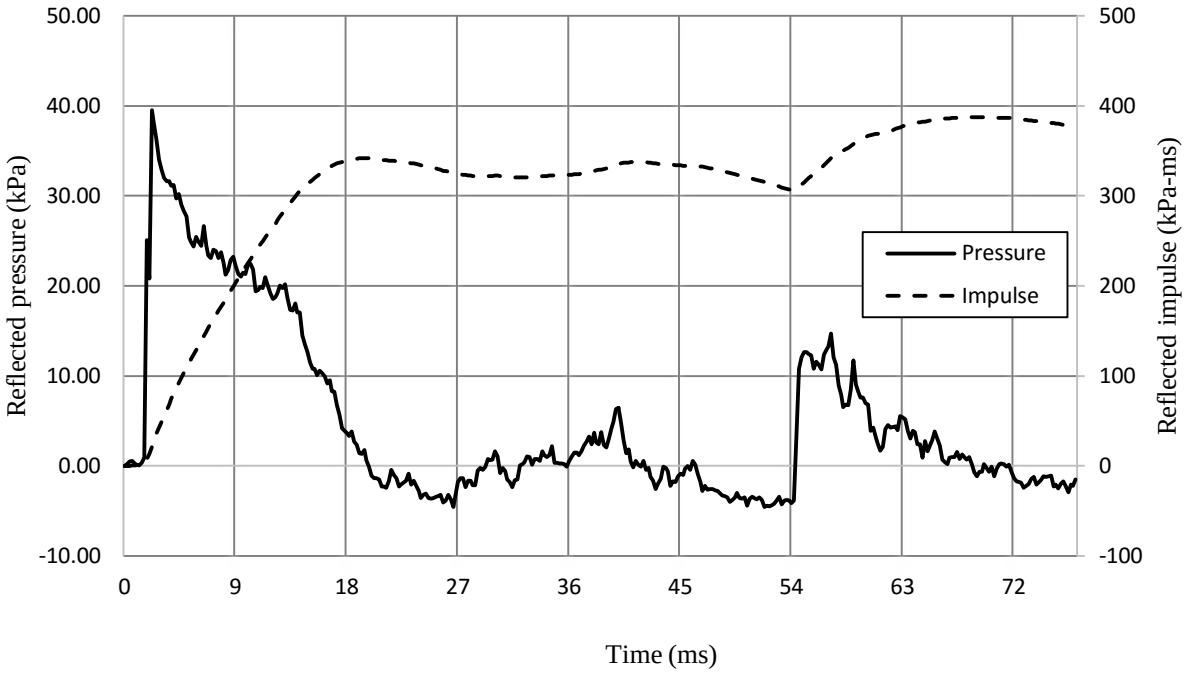

Figure 4.12 : Typical pressure and impulse-time history for dynamically tested stud walls

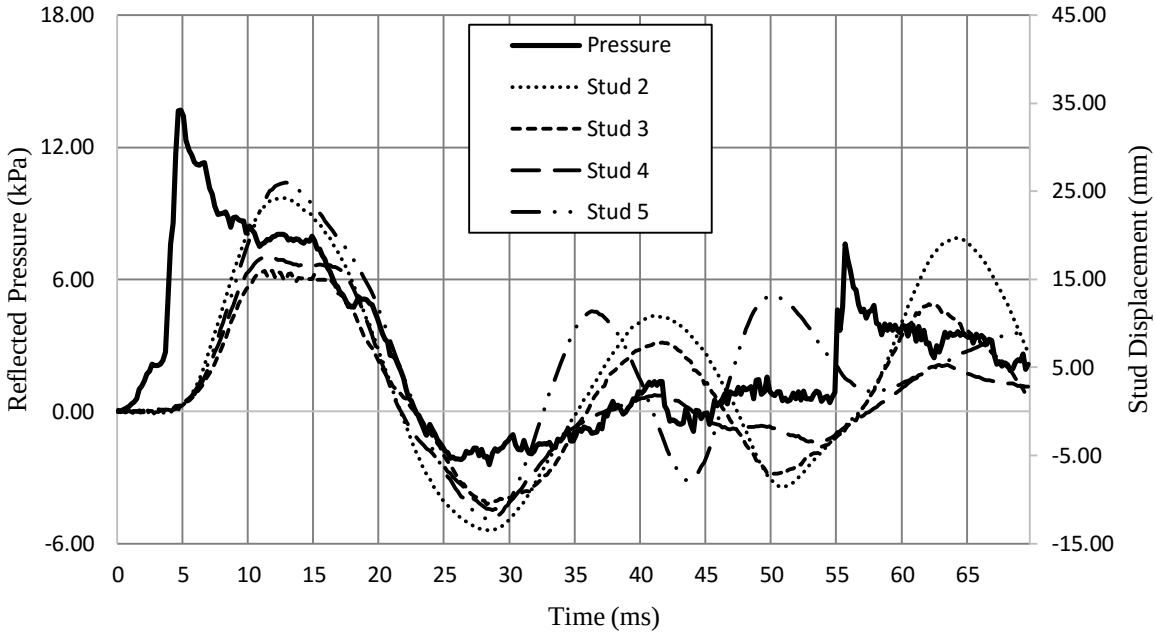

Figure 4.13 : Pressure and displacement-time history for Wall 1 Shot 1

CHAPTER 5 - Analytical Modelling and Results

5.1 General

The analytical modelling methods and results are presented in this chapter. A material predictive model utilizing different combinations of dynamic increase factors (DIFs) from CSA S850 (2012) and established literature (Jacques et al., 2013; Lacroix, 2013) was considered. The effect of partial composite action between the sheathing and stud elements is also investigated. These studies, however, dealt mostly with specimens that were tested and modelled using idealized boundary conditions. The test specimens also consistently had a well-defined failure mode, namely flexural failure of the wall studs in the case of light-frame wood stud walls. In the current study, the introduction of "realistic" boundary conditions requires a model that would permit the inclusion of the effects of rotational restraint due to the boundary connections and the possibility of multiple failure modes in the wall system. Until verified, one cannot simply assume that a SDOF method can be used for light-frame wood walls with boundary connections, and other more sophisticated modelling techniques may be required. The current study investigated the appropriateness of using SDOF modelling due to its simplicity and wide use in blast design.

The modelling computational efforts were carried out through the use of *RCBlast*®, a blast analysis software capable of performing equivalent single degree-of-freedom analysis (Jacques, 2014). Several researchers have reported this software being capable of producing accurate blast response of various types of structural components, including reinforced concrete columns (Burrell, 2012), reinforced concrete slabs (Jacques, 2011), and light-frame wood stud walls (Lacroix, 2013).

5.2 Model description and inputs

For an undamped system, the equation of motion can be written as follows, and solved for displacement:

$$K_{LM} m \ddot{y}(t) + R y(t) = A P_R \left(1 - \frac{t}{t_d}\right) \qquad \text{Equation 5.1}$$

where the terms are the same as those described in section 1.5 of Chapter 1. The following section explains the process of transforming a complex entity (i.e. a light-frame wood stud wall) to a single

mass with a given stiffness. The assumptions and inputs used in the analysis to predict the response of the full-scale stud walls are also stated and discussed.

5.2.1 Geometry and mass

The model is based on the single degree-of-freedom equation of motion, which requires that the entity be lumped into a single mass and attributed a representative stiffness. In this case, the entity which will be subjected to dynamic analysis is a representative T-section, consisting of sheathing, which has a width corresponding to the tributary width of the studs (406 mm) and a wood stud with a clear span equal to that of the shock tube opening (2032 mm). The masses of the representative wall T-sections with OSB, plywood, OSB and plywood, and WWM were determined to be 10.7 kg, 11.9 kg, 17.5 kg, and 15.0 kg, respectively.

5.2.2 Forcing function

Due to the fact that the system is exposed to a blast wave, the forcing function will be that of the reflected pressure over time. A blast forcing function can be described as a short rise in reflected pressure, followed by a relatively linear decline in pressure until the end of the positive phase. It is therefore generally accepted to idealize the forcing function as a triangular pulse load with a peak reflected pressure which is the same as that of the actual peak pressure and a positive phase duration which will yield the same impulse, known as the fictitious positive phase duration. Typical actual and idealized pressure-time histories are shown in Figure 5.1.

To verify whether it is acceptable to use the idealized forcing function, both actual and idealized pressure-time histories were considered in the analysis. For the idealized forcing-function, the peak reflected pressure utilized for dynamic analysis was taken as the actual experimental peak reflected pressure. The positive time duration is that which corresponds to a triangular pressure-time history with the same peak reflected pressure and impulse, in order to maintain a balance of energy between actual and idealized systems. Comparison of the analytical results obtained via the use of the actual pressure-time history versus an idealized pressure-time history showed that an idealized pressure curve could effectively model the response, as seen in Figure 5.2, with negligible differences in terms of predictive results. The loaded area which was used to transform the reflected pressure to a force corresponds to the clear span times the tributary width (i.e. stud spacing), which corresponds to an area of 0.83 m^2.

Two recent studies on wood studs (Jacques et al., 2013) and stud walls (Lacroix & Doudak, 2013) subjected to blast loads utilized SDOF models similar to the one being proposed in the current study. An important difference in the current study is that due to the significance of sheathing tearing, thereby not transferring the load to the studs, a constant loaded area was not always maintained throughout the response of the walls. In cases where premature sheathing tearing occurred, video review and post-test assessments made it feasible to identify when and where the sheathing failed prior to the stud's flexural failure. For those cases (W2-1 and W3-1), the application area was reduced at the time where sheathing tearing was observed from that of a T-section (0.83 m^2) to the loaded area of the stud alone (0.08 m^2). In these tests, two of the four middle studs remained elastic, as significant tearing of the OSB developed.

5.2.4 Load-mass factor

As seen in Equation 5.1, a load-mass factor is required to convert the representative T-section into a lumped mass and spring at the point of displacement of interest, which in this study was at mid-span of the wall studs. All SDOF analysis was conducted through the use of an assumed deflected shape of a simply supported beam subjected to uniformly distributed load. The load-mass factors can be calculated analytically by solving Equations 1.6 to 1.8, presented in Chapter 1. These factors are also readily available in the literature (USACE, 2008; Biggs, 1964). Load-mass factors of 0.78 and 0.66 were utilized throughout all analysis, for the elastic and plastic response regions, respectively. These factors allow for the transformation of the actual specimen to its proper idealized SDOF entity.

5.3 Implementing linear and non-linear stud wall properties into the SDOF model

While a typical SDOF model is often considered linear, various non-linear properties must be taken into account in order to properly model the response of the complex stud wall assembly with reasonable accuracy. Namely, the connections between the sheathing and studs must be modelled as a semi-rigid connection of non-linear nature, due to yielding of the mechanical fasteners and the crushing of the surrounding wood. For the walls that cannot be considered as simply supported, the effects and behaviour of the end conditions must also be taken into account, as they can impact the stiffness and overall capacity of the wall. A summary of all model inputs can be found in Table 5.1.

5.3.1 Partial composite action (PCA)

Sheathing is typically connected to the studs via mechanical fasteners (e.g. steel nails). This creates a semi-rigid interface which has a significant influence on the response of the stud wall. The interface also allows for a system effect to take place, by allowing the uniform load to be distributed to the load-bearing elements by means of their stiffness. This behaviour is non-linear and is often difficult to incorporate into a model without some simplifications being made to the load-displacement relationship. A method developed by McCutcheon (1984), which transforms the semi-rigid section into one that is fully rigid, was utilized in order to model these effects without the loss of significant accuracy. This results in an idealized equivalent section with full composite action that is representative of the actual semi-rigid section.

This relationship was developed from static nail-slip tests, as previously discussed in Chapter 3. Using the experimental interlayer slip stiffness, a modified bending stiffness, which takes into account the partial composite action, was determined by calculating Equations 5.2 to 5.4.

$$EI_{PCA} = EI_w + \frac{(\overline{EA_f})(EA_w)}{\overline{EA_f}+EA_w} h^2 \qquad \text{Equation 5.2}$$

$$\overline{EA_f} = \frac{EA_f}{1+\frac{10EA_f}{SL_f^2}} \qquad \text{Equation 5.3}$$

$$S = \frac{P/\delta}{s} \qquad \text{Equation 5.4}$$

where EI_{PCA} is the bending stiffness taking partial composite section into account, EI_W is the bending stiffness of the web only, h is the distance between the centroid of the web and the flange, $\overline{EA_f}$ is the modified axial stiffness of the flange, EA_W is the axial stiffness of the web only, EA_f is the axial stiffness of the flange only, L_f is the distance between sheathing gaps, and S is the interlayer stiffness, defined as the ratio of the initial nail-slip stiffness over the fastener spacing, *s* (see Figure 5.3). All necessary material properties for inputs in the three equations were obtained from static tests, as described in Chapter 3.

While tri-linear nail-slip curves have shown to accurately model the non-linear behaviour of nail-stud joints (Polensek & Schimel, 1986; Gromala, 1983), many studies have shown that using an equivalent linear-elastic nail-slip secant provides a good representation of the average joint stiffness up to the yield point similar to using non-linear nail-slip curves (Bulleit et al., 2005; Rosowsky et al., 2005; Yu, 2003; Liu & Bulleit, 1995b; Wheat et al., 1983). For verification purposes, both nail-slip curves were used as input into two separate models, following the methodologies laid out by McCutcheon (1984) in order to determine which nail slip representation is more appropriate to use in constructing the resistance curves in the current study.

The secant stiffness was taken from 10 % to 40 % of peak load on the joint nail-slip curve. When using the secant stiffness in determining the resistance curves, the results tended to underpredict the maximum stud displacements by an average of 3 %. This can be explained by the fact that the model omits the stiffness degradation in the response of the T-section to out-of-plane load. As mentioned earlier, the shape of the nail-slip curve is non-linear and basing the PCA calculations on the initial secant stiffness will obviously overestimate the stiffness especially at higher load levels. A benefit of using this method, however, is that the load-sharing effect is inherently taken into account through the use of the modified bending stiffness (Equation 5.2). This ensures that the ultimate resistance of the modelled wall is higher in magnitude than that of the stud alone.

While a tri-linear curve simulates more accurately the nail-slip relationship, the results of the analytical model utilizing the tri-linear curve did not improve the results; on average, the model overpredicted the maximum displacements by 6 %. The method stipulates that at high displacements, the contribution of PCA is nullified and that the resistance is that of the stud alone. No load-sharing factors were implemented in this model, which is proposed to be the explanation for the model to overpredict the displacements. Despite the larger error found in the tri-linear nail-slip model, the author is not able to generally conclude that this model is inferior to the linear secant model based on the results of the current study alone. The error found for both models is relatively small rendering generalization of the finding inconclusive. It should also be noted that the variability in the sheathing-nail-stud joints could affect the analytical results, particularly for plywood T-sections. It is suggested that further work focus on refining the models such that they are capable of capturing both the non-linear nail-slip behaviour as well as load sharing at high force level. For the purpose of the current study, it was deemed adequate to use the nail-slip secant

stiffness, taken from 10 % to 40 % of peak load, in determining the PCA and the resistance curves. Again, this model was chosen solely based on the fact that, on average, it produced better predictions.

For the 2 x 6 in. stud walls with OSB, plywood, and both sheathing combined, the analysis based on partial composite action increased the bending stiffness by 25 %, 32 %, and 38 %, respectively. For the 2 x 8 in. stud walls, an increase of 19 % in bending stiffness was obtained. These results are summarized in Table 5.2. It should be noted that PCA values are highly dependent on the materials used and their respective properties, and therefore cannot be generalized.

5.3.2 Rotational restraint due to the end conditions

The method by which the effects of various types of end connectors were implemented into the SDOF models is based on the equation of deflection for a simply supported beam. Theoretical deflections were calculated using Equation 5.5 (Bulleit et al., 2005).

$$\Delta = \frac{WL^4}{384EI_{PCA}} \frac{(10+B)}{(2+B)} \qquad \text{Equation 5.5}$$

Where W is the uniformly distributed load, L is the clear span, EI_{PCA} is the bending stiffness including partial composite action (PCA) effects, and B is the rotational restraint constant. When B = 0 (i.e. no rotational restraint), the equation becomes the classical deflection equation for simply supported beams. The resistance curves used as input into the analytical model were obtained from static testing and modified for high strain rate effects, partial composite actions, and end restraint (Figure 5.4). Also included in Figure 5.4 is the resistance curve of the pin-ended OSB walls. It can be observed that all three modelled walls with connection retrofits have the same ultimate resistance as the simply supported walls, of 28.53 kN. Also noticeable is the increase in stiffness for the wall detailed with ML24Z connections, stemming from Equation 5.5. Comparison between walls with boundary connections and those with idealized pinned boundary conditions shows that displacement-time histories as well as levels of damage are very similar.

To evaluate the effect of the boundary connections on the wall stiffness, the theoretical displacement (Equation 5.5) was calculated at each time-step using strain data obtained from the

four middle studs and plotted against the experimental displacements. By iteration, the B constant was determined as the value that provided the best fit. The results from the four tested connectors showed that only the ML24Z connector provided partial end-restraint, and a rotational restraint constant of 2.08 was found for this connector. Relative to a pin-ended condition, this value will produce a decrease of approximately 40 % in maximum deflection. Studs connected with either HU28 or LJS26DS were found to behave as simply supported, with no increase in their rotational restraint.

5.4 Resistance curve modelling methodologies

5.4.1 Overview

Utilizing the material properties obtained during the static testing phase as described in Chapter 3, the rotational restraint effects of the end-conditions, and the PCA between the sheathing and studs, various configurations of light-frame wood stud walls could now be modelled as a SDOF system. The resistance curves of the T-sections were modelled by calculating Equations 5.6 to 5.8.

$$R_e = R_u = \frac{8 * M_p}{L} \qquad \text{Equation 5.6}$$

$$M_p = MOR_{EXP.\ AVERAGE} * S_{PCA} * DIF_{MOR} \qquad \text{Equation 5.7}$$

$$K = \frac{384 * MOE_{EXP.AVERAGE} * EI_{PCA}}{L^3} * \frac{(2+B)}{(10+B)} * DIF_{MOE} \qquad \text{Equation 5.8}$$

Where R_e and R_u are the elastic and ultimate resistance, respectively, M_P is the ultimate moment capacity, L is the clear span, $MOR_{EXP.\ AVERAGE}$ is the average MOR for the studs determined from destructive static bending tests, S_{PCA} is the section modulus of the T-section which takes PCA into account, DIF_{MOR} is the strength dynamic increase factor for wood, K is the stiffness, $MOE_{EXP.AVERAGE}$ is the average MOE for the studs determined from non-destructive static bending tests, EI_{PCA} is the bending stiffness which takes PCA into account, B is the rotational restraint constant, and DIF_{MOE} is the stiffness dynamic increase factor for wood.

5.4.2 Dynamic increase factors (DIFs)

Research has shown that the DIF of timber is logarithmically proportional to the strain rate of the applied load (Lacroix, 2013). While there is a relative lack of research regarding the high strain rate effects on wood, there has been good agreement regarding the quantification of the increase on the flexural strength of timber specimens, leading to a DIF for lumber that is approximately 1.4 (Jacques et al., 2013; Lacroix, 2013; CSA, 2012; Nadeau & Bennett, 1982). This DIF would be directly applied to the modulus of rupture (MOR).

The debate is ongoing on whether there is in fact a DIF for the modulus of elasticity (MOE). While recent full-scale testing has found that there is an increase in the MOE of wood elements under blast loads (Lacroix, 2013), other studies were not conclusive, citing large variability in results (Jacques et al., 2013; Liska, 1950). The blast standard currently does not have any value for the DIF on the MOE. However, this again is due to lack of research and conservatism. The DIFs proposed by Lacroix (2013) have shown to model full-scale wood stud wall behaviour with good accuracy (Lacroix & Doudak, 2013). For modelling purposes in the current study, a DIF of 1.4 and 1.18 on the MOR and MOE was used, respectively.

5.4.3 Maximum ductility ratio

Results from the stain measurements provided an indication for when the initial failure and the ultimate failure occurred. Compressive-side strain gauges were vital to verify the time of ultimate failure, due to the post-peak engagement of the compression fibres. Furthermore, video review of each dynamic test was conducted in order to approximately determine the point of ultimate failure. The video camera utilized throughout testing permitted the use of frame-by-frame analysis where one frame represented 2 ms of actual test footage. This method was used to corroborate the information obtained from the strain gauge measurements. In all cases, both methods correlated very well, with some minor discrepancies, due to the 2 ms frame time-step. An average maximum ductility ratio of 2.1 was determined. This value is consistent with the findings presented in Lacroix (2013) and Lacroix and Doudak (2012). More detailed discussion on this topic is presented in Chapter 7.

5.5 Analytical modelling results

The ultimate resistance of a representative T-section was calculated using Equations 5.6 and 5.7, while the initial stiffness was calculated using Equation 5.8. The elastic limit, denoted X_e, was determined by dividing the ultimate resistance by the initial stiffness. A plateau with a cut-off point at a displacement equalling 2.1 times the elastic limit with zero stiffness was integrated into the resistance curve as to represent the yielding which typically occurs in ductile systems.

Figure 5.5 displays the resistance curves for the simply supported walls based on the inputs discussed previously in this chapter. Table 5.3 presents a summary of the maximum displacements and the time-to-maximum displacements for the analytical model, as well as the experimental data. Quantification on the relative accuracy of the model can be found in Table 5.4. Results show that the SDOF model is able to predict the expected response of various stud wall specimens with varying sheathing and end conditions with reasonable accuracy. The model tends to under-predict the maximum displacement on average by 3 %, while it tends to over-predict the time at maximum, on average, by 5 %. Figure 5.6 shows the experimental pressure- and displacement-time histories for W2-1. In this test, two of the four middle studs remained elastic, as significant tearing of the OSB developed. The point at which the tearing occurred has been identified and is indicated in Figure 5.6A on the pressure-time history. Figure 5.6B shows the results of the SDOF analysis of studs that experienced no sheathing tearing and full reflected pressure was therefore assumed. It can be observed that the model is capable of predicting the stud displacement with good accuracy. Figure 5.6C shows the results of an analysis that utilized the identical resistance curve as the analysis in Figure 5.6B, but with a loading function that was adjusted at the point where the sheathing tearing occurred (Figure 5.6A). Here too it can be seen that the model is able to predict the deflection with great accuracy, however, it was not possible to generalize the methodology due to the material variability found in wood and to the limited number of tests where the premature sheathing tearing occurred. This puts some limitations on the use of SDOF analysis techniques for typical light-frame wood structures subjected to pressures that are high enough to cause severe damage in the walls and potential tearing in the sheathing. If such simplified analysis techniques are to be used, the failure mode of the wall has to be well-defined and full transfer of the pressure to the studs needs to be ensured. This can be achieved by, for example, providing thicker sheathing that is capable of such load transfer.

Lastly, the use of SDOF analysis to estimate stud behaviour and wall performance should only be utilized when flexural failure is the expected failure mode. This is achieved by choosing a proper type of connection retrofit (joist-hanger or angle) which allows the stud to deflect freely up until flexural failure, with a design capacity that is close to or above the design dynamic bending capacity of the flexural element. While stud and sheathing failure was easily taken into account in the analytical model, the model has shown to be inadequate in predicting response when connection failure occurs. The reason for this is that the model assumes that flexural failure occurs. For the two walls (Walls 23 and 24) that suffered connection failure (LTS18), Figure 5.7 clearly shows the inability for a simplified SDOF model to capture such behaviour. This modelling limitation can be circumvented by doing either one of the following: using a finite element model, which is able to capture connection failure and the interaction between the connection detail and the failure mode, or a more practical solution would be for the designer to overdesign the connection, thereby forcing the failure to occur in the sheathing or studs; the latter being more efficient and desirable. The results of this study show that some connection damage, in the form of fastener withdrawal or yielding of the connector, is acceptable and will not significantly affect the predicted displacement.

Table 5.1 : Equivalent SDOF model inputs

Input	**Value**
Modulus of elasticity of 2×6 studs, $MOE_{2\times6}$	9270 MPa
Modulus of elasticity of 2×8 studs, $MOE_{2\times8}$	8830 MPa
Modulus of elasticity of OSB, MOE_{OSB}	5020 MPa
Modulus of elasticity of plywood, $MOE_{Plywood}$	4650 MPa
Modulus of rupture of 2×6 studs, $MOR_{2\times6}$	36 MPa
Modulus of rupture of 2×8 studs, $MOR_{2\times8}$	35 MPa
Sheathing span, L_F	2032 mm
Fastener spacing for OSB walls, s_{OSB}	150 mm
Fastener spacing for plywood walls, $s_{Plywood}$	150 mm
Fastener spacing for OSB & plywood walls, $s_{OSB+Plywood}$	300 mm
Interlayer stiffness for OSB walls, S_{OSB}	10.7 MPa
Interlayer stiffness for plywood walls, $S_{Plywood}$	11.7 MPa
Interlayer stiffness for OSB & plywood walls, $S_{OSB+Plywood}$	12.0 MPa
Loaded T-section area, A	0.83 m^2
Mass of OSB wall T-section, m_{OSB}	10.7 kg
Mass of plywood wall T-section, $m_{Plywood}$	11.9 kg
Mass of OSB & plywood wall Tsection, $m_{OSB+Plywood}$	17.5 kg
Mass of OSB wall T-section with catcher system, m_{WWM}	15.0 kg
Rotational restraint constant of ML24Z (Wall 25), B	2.08

Table 5.2 : Partial composite action effect calculation

Sheathing type	**Initial nail-slip stiffness (N/mm)**	**Interlayer stiffness (MPa)**	**Moment of inertia of stud alone (10^6 mm^4)**	**Moment of inertia with PCA (10^6 mm^4)**	**Relative increase in bending stiffness**
OSB	1600	10.7	8.69	10.83	1.25
Plywood	1747	11.7		11.43	1.32
OSB+Plywood	3600	12.0		11.98	1.38

Table 5.3 : Summary of numerical modelling

Test name	**Experimental response**		**SDOF prediction**	
	D_{max} (mm)	**T_{max} (ms)**	**D_{max} (mm)**	**T_{max} (ms)**
Wall 1 Shot 1	16.8	11.2	14.5	11.2
Wall 1 Shot 2	53.1	8.4	54.6	8.8
Wall 2 Shot 1	56.9	9.5	54.9	9.7
Wall 3 Shot 1	50.4	9.9	52.1	10.4
Wall 4 Shot 1	59.5	9.2	54.9	8.8
Wall 5 Shot 1	56.7	9.8	55.1	9.1
Wall 6 Shot 1	52.0	10.3	51.1	9.4
Wall 7 Shot 1	55.0	9.4	53.9	9.9
Wall 8 Shot 1	52.3	10.8	53.9	10.7
Wall 10 Shot 1	51.9	9.5	53.5	11.4
Wall 11 Shot 1	65.8	8.6	53.4	8.1
Wall 12 Shot 1	64.2	9.0	53.8	8.8
Wall 14 Shot 1	35.4	9.6	34.7	10.6
Wall 15 Shot 1	38.4	13.2	27.2	12.9
Wall 20 Shot 1	53.6	16.1	48.1	18.8
Wall 21 Shot 1	42.0	10.5	48.3	13.3
Wall 22 Shot 1	55.5	9.80	49.7	12.1
Wall 25 Shot 1	31.7	10.9	32.6	9.6

Table 5.4 : Summary of experimental-analytical responses

	Number of tests	$\frac{D_{max-SDOF}}{D_{max-EXP.}}$			$\frac{T_{max-SDOF}}{T_{max-EXP.}}$		
		Average	**Standard Dev.**	**COV**	**Average**	**Standard Dev.**	**COV**
All modelled walls	18	0.97	0.10	0.10	1.05	0.11	0.10
OSB walls	11	0.98	0.10	0.10	1.05	0.12	0.11
Plywood walls	4	1.02	0.02	0.02	1.07	0.05	0.05
OSB & plywood walls	3	0.89	0.10	0.11	1.04	0.12	0.11

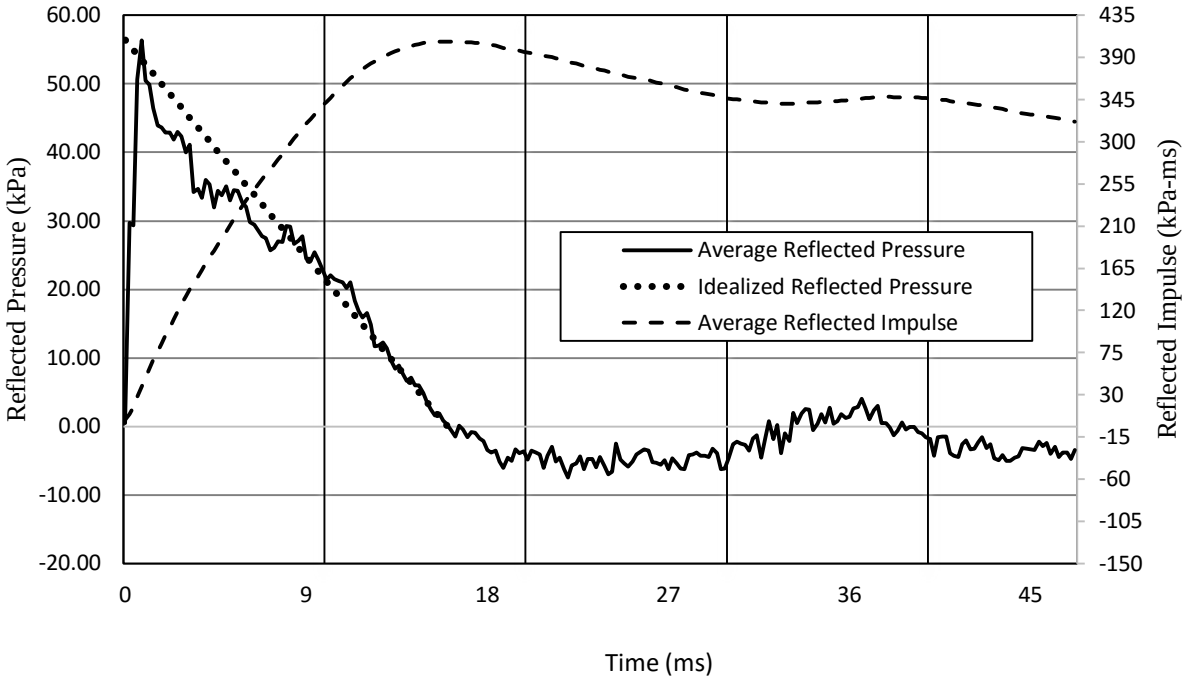

Figure 5.1 : Representation of actual experimental pressure and idealized reflected pressure

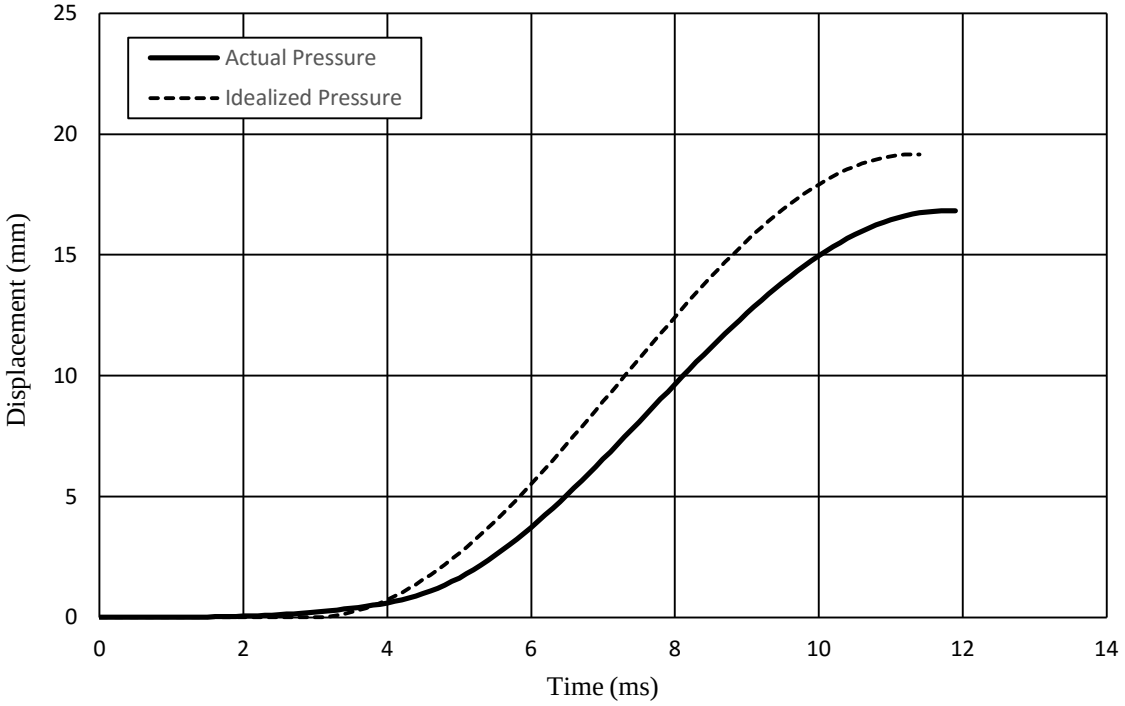

Figure 5.2 : SDOF analysis results for actual pressure versus idealized pressure

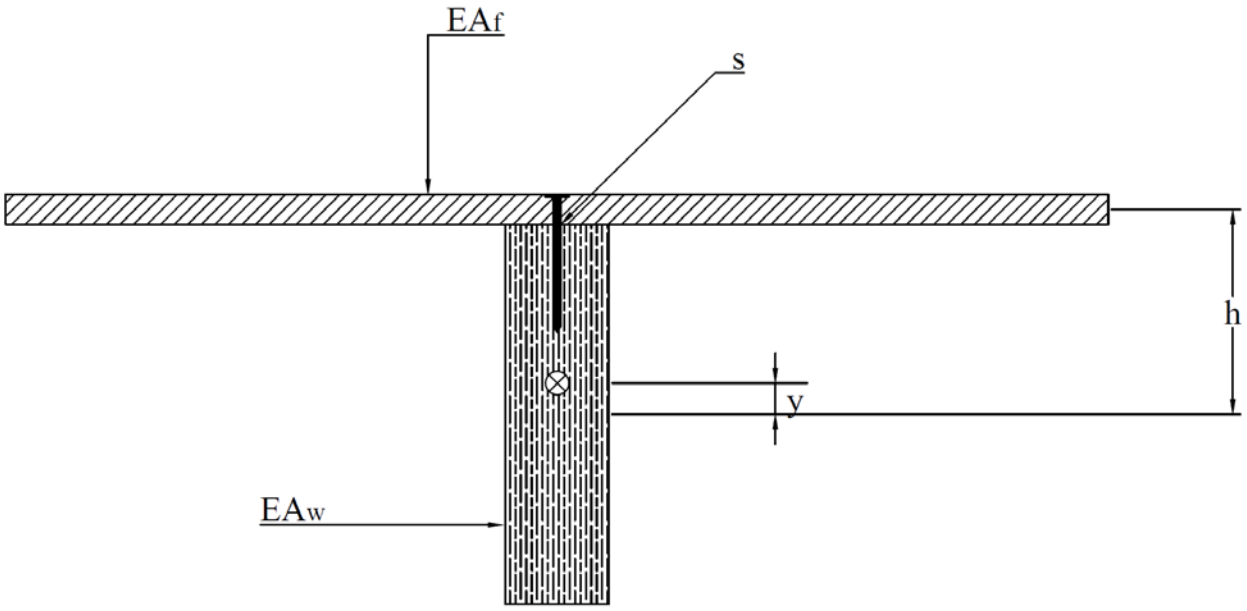

Figure 5.3 : Representative T-section and parameters utilized in PCA computation

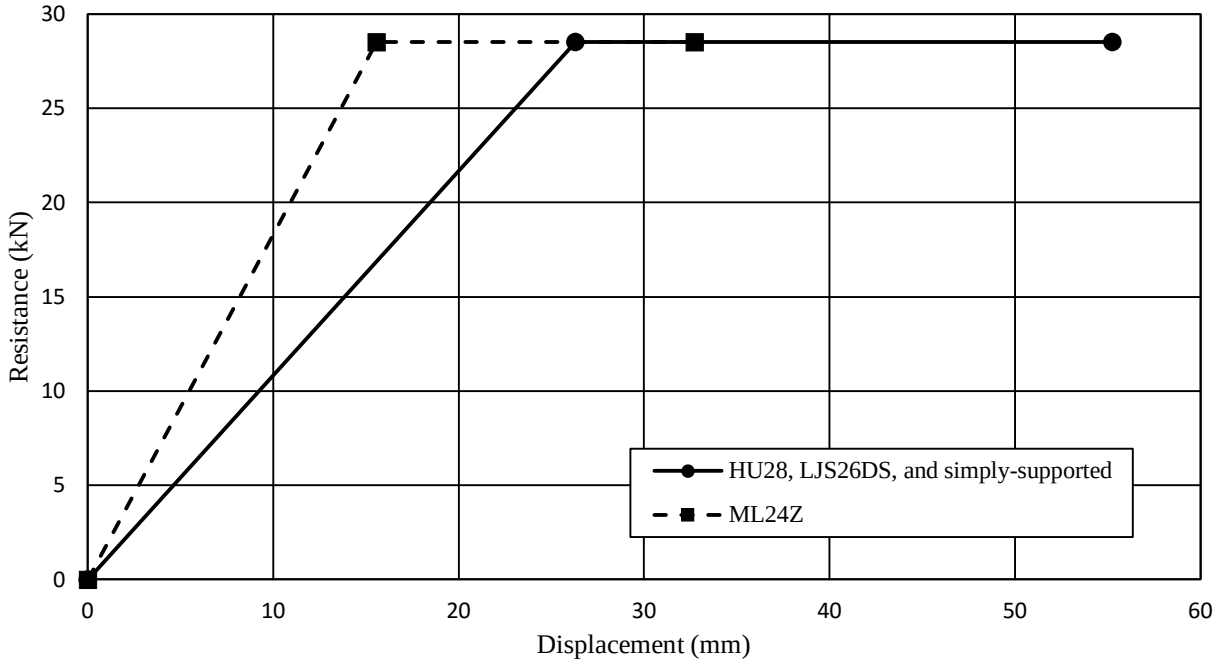

Figure 5.4 : Stiffness increase due to ML24Z connection

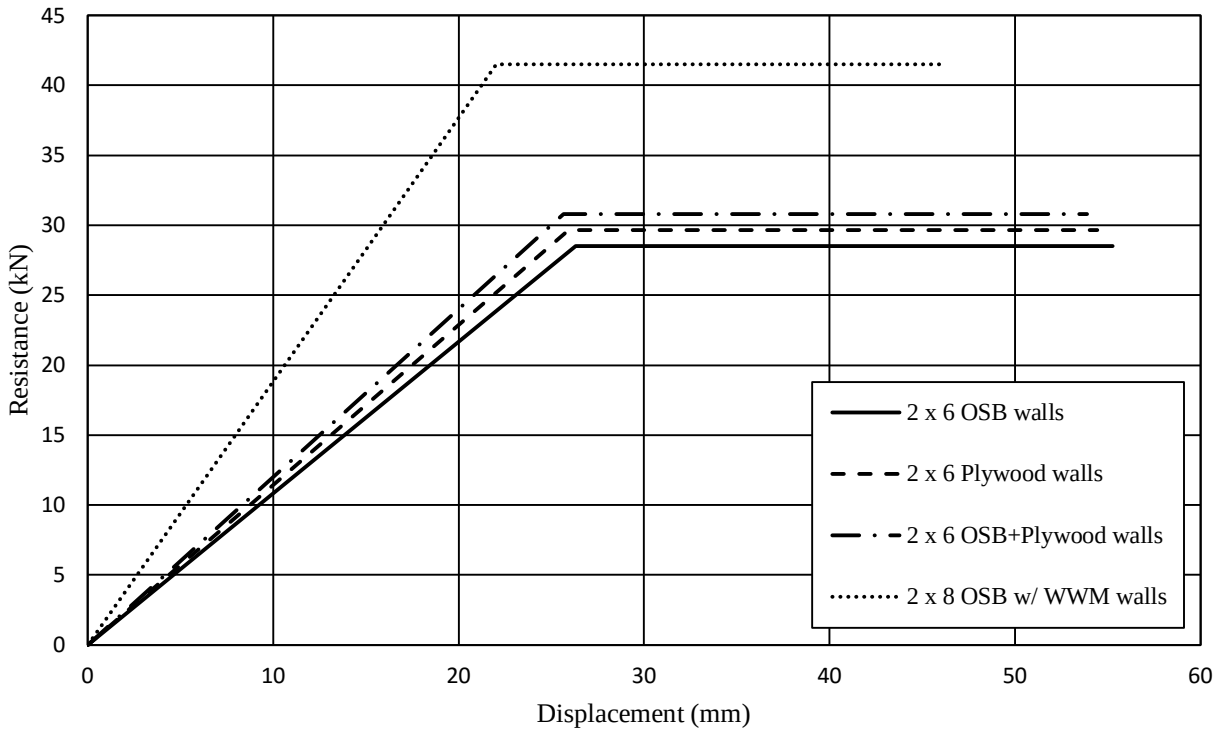

Figure 5.5 : Bi-linear resistance curves for simply supported walls

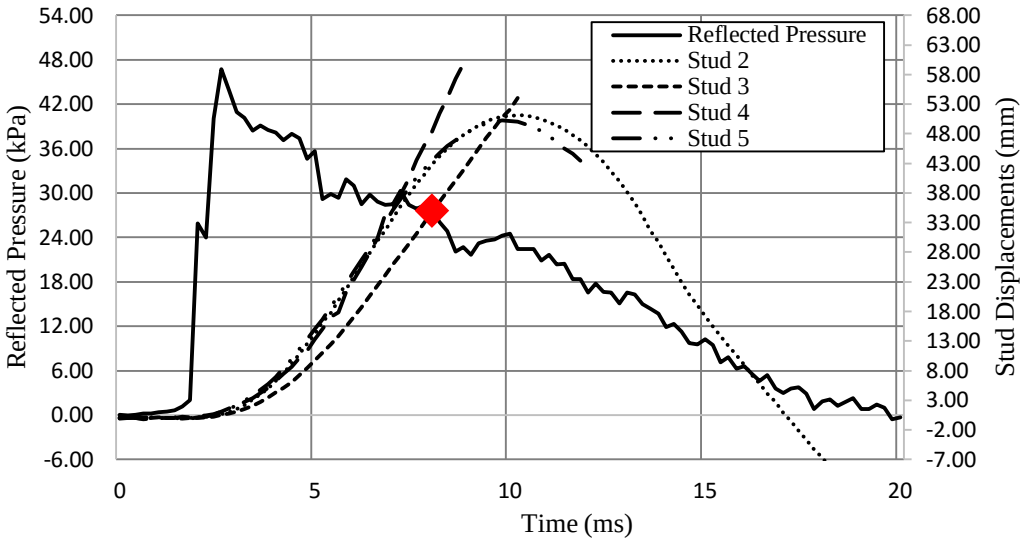

A. Experimental pressure- and displacement-time histories

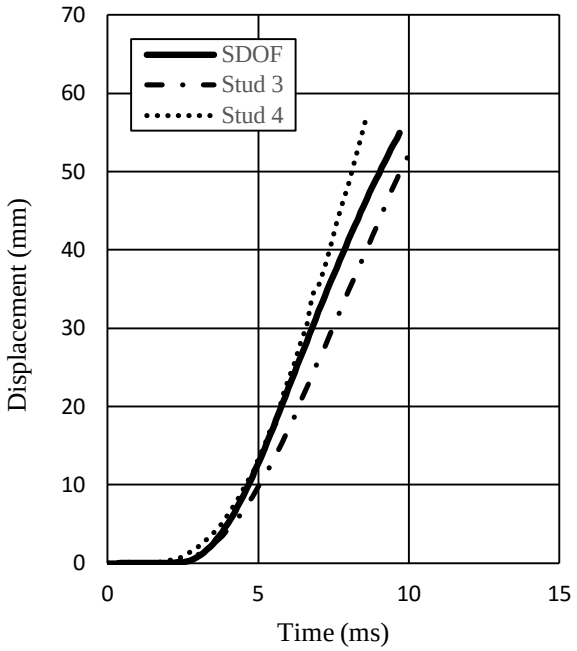

B. Experimental and analytical displacements – no ripping effects

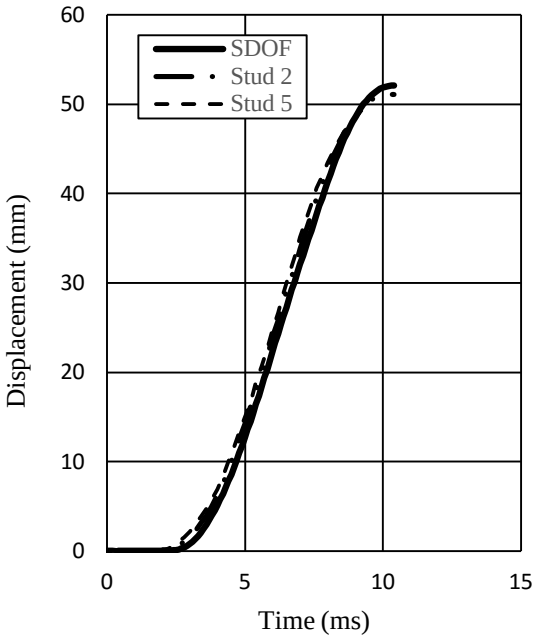

C. Experimental and analytical displacements – with ripping effects

Figure 5.6 : SDOF modelling results for Wall 1 Shot 2

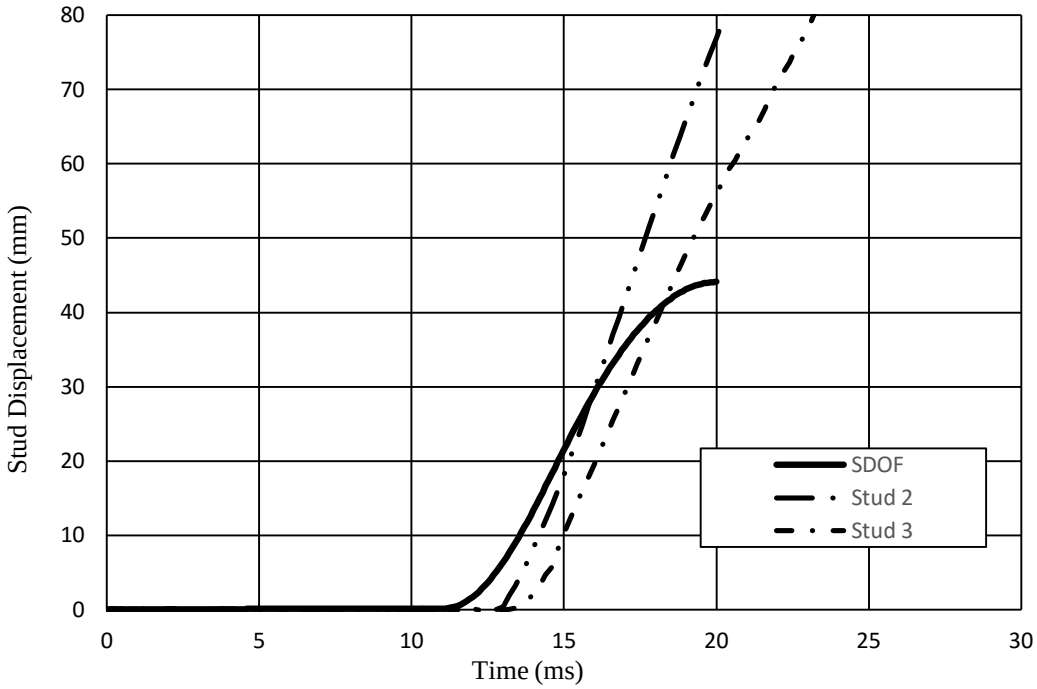

Figure 5.7 : Poor SDOF performance in capturing connection failure of Wall 23

CHAPTER 6 - Discussion

6.1 General

The current study focused on the behaviour of light-frame wood stud walls, especially the sequence of failure of the various components within the wall. Ideally, the wall failure would consist of the wall studs reaching their ultimate capacity, which based on typical stud lengths and dimensions is expected to be a flexural failure. This assumes that the studs are capable of resisting the load without causing harm to the building occupants or leading to progressive collapse of the building. Premature failure may, however, occur if the connections are inadequately designed or if tearing of the sheathing takes place, where the sheathing panels become incapable of transferring the pressure from the blast to the wall studs. Also, failure at the boundary connections is not desirable because it means that the subsystem would fail prematurely and achieve a capacity that is inferior to what can be achieved if the failure occurred in the studs. Losing the sheathing, however, may in some cases be desirable, where it is anticipated that the pressure will otherwise overwhelm the wall, which could lead to harm to occupants or progressive collapse. In such case, limiting debris from the sheathing, while maintaining the axial capacity of the studs, may yield a better design solution. The following discussion addresses the aforementioned possible failure modes through the experimental testing program and analytical prediction of the behaviour.

It is worth mentioning that throughout this study, axial loading and its effect on the response of the stud walls were not investigated nor considered. Although it is recognized by the author that including axial load would have a significant impact on the behaviour of the wall, and that walls will always carry a certain level of axial load (the only exception being a one-storey structure where the roof trusses run parallel to the wall), omitting the effect of axial load was deliberate to establish a baseline for the wall behaviour and allow for future studies to build on findings from the current study. Another reason for omitting the effect of axial load is that it was reasoned that the absence of axial load would yield more conservative results when investigating end connections, since clamping action and friction would have had beneficial effects on the performance.

6.2 Observed failure modes and failure sequence

The first phase of testing focused on the failure modes of the studs and sheathing while eliminating the effect of boundary connections. This was done by providing idealized simply supported end conditions during the experimental testing. Failure modes and sequence of failure had already been investigated for similar wall configurations (Lacroix, 2013), but these tests were limited to low-to-medium pressure levels (producing superficial and moderate damage in the walls). The current study focused therefore on high pressure levels, inducing hazardous and blowout damage levels. Previous tests had reported primarily failure in the wall studs, where the sheathing was capable of transferring the entire load to the studs and where only minor sheathing tearing was observed, the current study reported significantly more sheathing tearing when the wall was exposed to higher pressure. The following describes observed failure modes specific to the studs, sheathing and end connections.

6.2.1 Sheathing

Failure in the wall sheathing panels in this study was based on two sheathing types and thicknesses. More in-depth investigation of the behaviour of wall sheathing is needed before general statements or design provisions can be developed. The complexity stems from the fact that the behaviour of sheathing panels in isolation has not yet been studied. Furthermore, the variability of sheathing layout, orientation, and support conditions may be significant, and therefore, any observation made in this study should be taken within the confines of the experimental setup. Stud spacing, sheathing-to-stud fastener type, size, and spacing, panel thickness, whether blocking is used, etc., can significantly affect the behaviour of the sheathing and thereby the behaviour of the wall as a whole. The attempt in the current study is not to establish effects of construction detailing on the behaviour but rather to investigate whether light sheathing panels with typical sizes and construction detailing are capable of transferring the pressure to the wall studs. In order to be able to choose this sequence of failure, however, more knowledge needs to be acquired about the sheathing behaviour.

Tests on typical wall detailing were conducted to evaluate the behaviour of the sheathing panels under moderate to high pressure and impulse combinations. These walls consisted of 11 mm OSB sheathing, attached to 2 x 6 in. wall studs using 50 mm long nails spaced at 150 mm on center,

with no blocking. When exposed to pressures of approximately 35 kPa and above, the 11 mm OSB proved to be inadequate in transferring the pressure to the walls studs, and significant flying debris was created during those tests, as shown in Figure 6.1A. Failure was observed to mainly be in panel edge tear-through as well as flexural and tearing failure of the sheathing. The former implies that current connection detailing between the sheathing and the studs may be inadequate to transfer the blast load to the main framing members. The latter implies that the capacity and stiffness of the sheathing panels are inadequate for such loading scenario. The deficiencies in the former can be addressed through careful consideration of the connector type, size, spacing and end/edge distances, while the latter's can be addressed through the use of thicker sheathing. Some options (e.g. thicker sheathing, use of screws) were investigated in the current study but an optimization of the wall detailing for blast design is outside the scope of this thesis.

The effect of using thicker and more rigid sheathing (18.5 mm plywood) was investigated under otherwise similar wall construction detailing. None of the plywood walls produced any significant debris stemming from the sheathing panels, and the plywood panels failed in bending at wall mid-height, as shown in Figure 6.1B. This sheathing option proved capable of transferring the pressure to the 2 x 6 in. wall studs, which implies that such sheathing can be used in new constructions or as a retrofit option if exterior access to the walls is feasible.

While the selection of a thicker sheathing shifted the failure from tearing in the sheathing and sheathing debris to flexural failure in the studs, it did not completely prevent potential debris stemming from the studs themselves, as seen in Figure 6.1B. The overall wall capacity as a whole was significantly improved, since full flexural capacity could now be attained and sheathing failure was shifted to a higher pressure-impulse combination. However from a point of view of occupant safety, the flying stud debris could still pose hazardous conditions. This failure is expected, because the sheathing is now capable of transferring the load completely to the stud, however the sheathing and the stud can only move together a small portion of the overall displacement. The low withdrawal capacity of the nails would cause the stud pieces to completely detached from the sheathing and become debris-throw, as can be seen in Figure 6.1. The only reason why the stud pieces from the bottom half of the wall were prevented from detaching from the wall and flying across the lab floor is due to the blue steel bracket, where the displacement measuring devices (LVDTs) were installed.

An attempt was made to improve the withdrawal behaviour of the sheathing-to-stud connection by replacing the nail with a screw fastener, which has significantly larger withdrawal capacity than the nail. Walls 9 – 12 were detailed with screw connections between the sheathing and thicker sheathing. These four specimens showed better overall performance, as the studs were allowed to fail in flexure with no sheathing debris and significantly reduced stud debris. Post-failure investigation showed signs of tension perpendicular to grain or shear failure along a zone which coincided with the presence of the fastener tips. An example of this observation is shown in Figure 6.2. Although not further investigated in this study, it is anticipated that the use of longer screws may further reduce stud debris, since more of the stud cross-section would be held in place by the screws.

Sheathing that is deemed inadequate may also be retrofitted from the interior side of the wall. An attempt at such modification was made using welded wire mesh (WWM), which was attached to the studs while helping the transfer of the pressure from the sheathing to the studs. The WWM grid was secured to the sheathing mainly by the clamping action brought on by the sheathing fasteners, as shown in Figure 6.3A. To ensure that the integrity of the retrofit is maintained throughout response, off-the-shelf steel plates were used to further secure the ends of the WWM to the top and bottom wall plates. The observed failure showed that the WWM allowed for large displacement to occur in the OSB. Even though relatively minor tearing was still observed in the OSB panel, the overall integrity of the sheathing was maintained, as shown in Figure 6.3B.

Nail head pull-through was observed for all OSB-sheathed stud wall specimens, as shown in Figure 6.4. One reason for this may be due to the fact that while similar to typical nails, pneumatically driven nails have a slightly smaller head, which allows for the generation of larger stresses on the top of the sheathing. The author recognizes that this can affect the response of the stud walls at large displacement, however, pull-through of the fastener heads can be assumed to have insignificant effects in the range where partial composite action is effective**.**

6.2.2 Studs

The typical failure mode observed during the static bending tests of the wood studs was flexural failure, with the characteristic fibre tension failure, especially near or at a knot. The static behaviour of wood studs can generally be assumed to be linear-elastic; however, some non-

linearity could be observed in individual stud elements (shown in Figure 6.5A) when crushing of the fibres on the compression side occurred, as seen in Figure 6.5B; this failure is expected when the stud's tensile strength is higher than its compressive strength. When the sheathing was capable of transferring the load to the studs during dynamic testing, all wall studs failed in flexure. However, the mode of flexural failure was "brash", with the majority of the studs failing with a straight "cut-through" its cross-section. Figure 6.6 shows comparison of this brash flexural failure mode versus typical static flexural failure. These differences in static and dynamic failure modes are consistent with other studies on impact loading behaviour of wood specimens (Jansson, 1992; Mindess & Madsen, 1986) and the behaviour of studs under blast loading (Lacroix & Doudak, 2014; Jacques et al., 2013).

When the stud wall is exposed to a static or quasi-static loading, where the load duration is much larger than the natural period of the stud element, the wall distributes the load to the studs based on their stiffness. After the failure of the first stud, the load is redistributed to the other, stronger studs. Under dynamic loading, however, the load duration is so small that the studs tend to reach their maximum deflections approximately all at the same time, which can be corroborated by the results shown in Chapters 4 and 5. An example of such behaviour can be seen in Figure 6.7 for Wall 1 when subjected to a pressure and impulse combinations in the elastic range. The deflections of the four middle studs can be seen to reach their peak in unison, followed by out-of-sync oscillation. This response can be attributed to the sheathing acting as a load-distributor as the inbound pressure pushes against the sheathing. When the pressure wave subsides and the rebound phase begins, the low out-of-plane stiffness of the sheathing and having the nails in withdrawal would typically not be sufficient to maintain this behaviour, and the variability in the stud properties would cause different responses in the individual studs. (Figure 6.7). A second destructive shot consistently yielded similar time-to-maximum displacement for all studs in the wall, as shown in Figure 6.8, which represents the second shot on Wall 1.

6.2.3 Typical boundary connections

Light-frame wood buildings up to three storeys typically fall under the jurisdiction of Part 9 of the National Building Code of Canada (NBCC). The NBCC provides prescriptive connection detailing on how to connect the bottom and top plate of a stud wall to the floors or roofs above or below the wall. Specifically, subsection 9.23.3 of the NBCC deals with fasteners and connection

requirements, all of which are industry standard and have been used for decades. Details on the required nailing for different scenarios can be found in Table 6.1. These design considerations have been developed for gravity loads and wind/earthquake loads, which allow for the lateral load resisting system (LLRS) to become engaged in resisting these loads.

The blast design code (CSA, 2012) states that "connections between structural elements shall be limited to bearing failure in the wood member or connector. The connection shall be designed for forces corresponding to 1.2 times the capacity of the components being considered". This requirement is clearly not accounted for in typical light-frame wood stud walls where no blast design requirements are being considered. For non-seismic applications and according to the prescriptive requirements of Part 9 of the National Building Code of Canada (NRC, 2015), the wall top plate is attached to the floor rim joist by means of toe-nails using 82 mm nails at spacing of 400 mm on-center (o/c). The bottom plate is nailed to the rim joist of the floor below using 82 mm nails at spacing of 400 mm o/c. For braced walls with seismic detailing, these connections are more stringent, with the minimum spacing being reduced to 150 mm (NRC, 2015). Both configurations were tested in the shock tube to investigate whether such typical detailing is sufficient to fully develop the capacity of the stud wall. Wall 17 was tested with both configurations (shot 1 and shot 2), while Wall 18 was tested with seismic detailing only. It should be noted that the current study is not investigating the adequacy of such connections to transfer shear loads along the length of the braced walls (in-plane). The goal here is to investigate whether such detailing, meant for in-plane force transfer are also adequate to transfer pressure applied in the out-of-plane to the wall direction as the case would be in a blast loading scenario.

The results from the walls with prescriptive connection detailing (W17-1, W17-2, and W18-1) clearly showed that they were not adequate to withstand the blast pressure prior to the failure of the studs. Such construction detailing are optimized to resist gravity loads or lateral loads in the in-plane direction of the wall. In the direction parallel to the wall, the toe nails connecting the rim joists to the wall plates are acting in shear, while in the case of loading in the perpendicular to the wall direction, the toe nails would additionally experience withdrawal. The results also show that even with the enhanced nailing to account for seismic detailing (W17-2 and W18-1), the connections, especially at the top plate, were too weak due to the toenails having very low capacity in withdrawal. The tested walls were blown across the laboratory in a rigid body translation, as

shown in Figure 6.9. Failure occurred almost concurrently at the top and bottom plates. Bending in the nails connecting the bottom plate to the blocking was observed, with failure occurring in combination of shear and withdrawal, as shown in Figure 6.10A. Figure 6.10B shows the typical marks left by the nails. The top-plate connection also failed by a combination of shear and nail withdrawal failure, as well as nails tearing through the blocking, as they remained attached to the top-plate, as shown in Figure 6.11. The sequence of failure for Wall 18 was slightly different than that of Wall 17, where failure was initiated at the top plate-to-blocking connection. In this test, the majority of the top-plate connections failed in withdrawal, while the wall slightly rotated and was ejected from the frame. The tilting of the wall caused failure in withdrawal of the bottom-plate connection as well, with little to no yielding occurring in the nails, as shown in Figure 6.12.

The tests on both the non-seismic and the seismic detailing clearly demonstrated the vulnerability of light-frame wood stud walls to the effects of blast loading. It should be noted that light-frame wood structures may have slightly different detailing which could yield better performance. For example, in some cases the sheathing may be constructed so that it extends beyond the top and bottom plates and is attached to the rim joists. This detailing is not common and was therefore not investigated in the current study but it is assumed that this might provide a slightly improved behaviour over the typical connections tested here. The connection performance observed for the prescriptive connections also emphasized the need to design and detail connections in light-frame wood stud walls such that they do not fail before the studs achieving their full capacity.

An attempt to improve on the connection behaviour so that the wall design is in line with the requirements stipulated by the design standard is described next.

6.2.4 Designed wall boundary connections

Four commercially available steel connectors were tested as possible options for connecting the wall to its boundary elements. The selection of the connectors was driven by the design capacity of a single stud element based on the respective design standards (CSA, 2014; 2012). As mentioned earlier, the blast design standard states that connections must be overdesigned to a capacity that is 20 % higher than that of the structural element to which it is connected. This is consistent with guidelines for seismic design, as stipulated by the timber design code (CSA, 2014). In order to evaluate whether the design provision is conservative, adequate, or insufficient for blast

applications, four connections were detailed to have design capacities which are lower, approximately the same, and higher than that of the load-bearing element. The following section presents a description of each connector, their performance, and their effects on wall behaviour. Figure 6.13 shows the fasteners used throughout the testing of various connections. Details of the four connections are summarized in Table 6.2.

6.2.4.1 HU28

The HU28 connector is a standard joist hanger, typically used in wood floors to connect the joists to beams or rim joists. Its use here to connect the stud to the top and bottom plates is atypical but seemed appropriate due to the way it wraps around the stud providing a bearing support and a connection to the bottom plate, as shown in Figure 6.14. This connector had an expected capacity of 14 % lower than the anticipated dynamic reaction, with no increase to account for high strain effects in the connection.

Four #10x1-1/2 in. screws were used to fasten the connector to the stud, while eight #10x2-1/2 in. screws were used to provide connectivity between the plates and the rim joists. 4-5/8 in. (0.22 in. diameter) screws were installed in groups of two (spaced at 406 mm) between studs to connect the bottom plates to the rim-joist. A typical HU28 connector is shown in Figure 6.14A while the actual connection detailing is shown in Figure 6.14B.

The results from tests on Wall 19 and 20, where these connectors were implemented, showed that this connection detail allowed for the studs to reach their ultimate capacity and fail in flexure, as shown in Figure 6.15. However, a significant number of the screws experienced withdrawal failure, and caused damage to the top and bottom plates (Figure 6.16). This could be attributed to the fact that the capacity of this connector was 14 % lower than the dynamic reaction. It is, however, noteworthy to mention that providing a connection between the wall and the top and bottom floors, albeit inadequate from a design perspective, still enhanced the performance of the wall significantly compared to the typical prescriptive detailing. The wall studs were capable of achieving their full ultimate flexural capacity with minor debris stemming from the studs and sheathing panels (Figure 6.15).

6.2.4.2 LJS26DS

Similar to the HU28 connectors, the LJS26DS is also a joist hanger type of connector, but with a larger design capacity of approximately 28 % higher than that of the expected dynamic reaction for the tested wall.

Six #10x1-1/2 in. screws were used to connect the fastener to the stud, while sixteen #10x2-1/2 in. screws were used to provide connectivity between the plates and the rim joists. A 4-5/8 in. (0.22 in. diameter) screw was also between each stud to connect the bottom plates to the rim-joist with spacing of 406 mm. A typical LJS26DS connection is shown in Figure 6.17.

This connector was implemented on Walls 21 and 22. Similar to the case with the HU28 connector, the results showed that the studs were able to rotate at their ends, and deflect until reaching failure in flexure. However, the damage to the bottom and top plates was significantly reduced. Some damage to the stud ends was observed possibly due to the high number of fasteners utilized as well as the short end-distance. However, the observed damage in the LJS26DS connection (Figure 6.18A) was not prevalent throughout the walls, and was significantly less severe than the damage observed in the walls with HU28 connectors (Figure 6.18B). Damage to the top and bottom plates was also reduced when compared to that of the previous connector (see Figure 6.19). A reduction in nail puncture and withdrawal was also observed since the studs were restricted in terms of how far they can deflect post-failure. Due to the shape and overall design approach of the connector, the studs were secured to their bottom/top plates, which meant that large pieces of debris from the studs themselves was prevented.

6.2.4.3 ML24Z

While the previous two connectors are joist hangers, the ML24Z connector is a simple angle plate, with a design capacity approximately 33 % lower than the expected dynamic reaction. This connector was the easiest and quickest to install, and was also the cheapest. Three 1-1/2 in. (1/4 in. diameter) heavy-duty screws were used to connect the angle to the stud, while three 2-1/2 in (1/4 in. diameter) heavy-duty screws were used to provide connectivity between the plates and the rim joists. As with the HU28 detail, 4-5/8 in. (0.22 in. diameter) screws were installed in groups of two (spaced at 406 mm) between studs to connect the bottom plates to the rim-joist. A typical ML24Z connector during installation is shown in Figure 6.20.

While having the lowest capacity amongst all four retrofits, Wall 25 performed reasonably well and all wall studs achieved their ultimate capacity with little damage to the connector. Following a blast load similar to that exerted on the HU28 and LJS26DS walls, the studs of Wall 25 failed in flexure. This is significant since the ML24Z connection detail had a rated capacity of only 67 % of the dynamic reaction, yet it provided the shift in failure mode and maintained the general integrity of the wall. Where the HU28 and LJS26DS connectors were capable of grabbing the end of the stud and keeping the stud in place, the failure of the connection was governed by yielding in the angle and splitting of the studs near the location of the connectors. This created stud debris similar to that observed for walls with plywood and screws. Another significant observation is an apparent increase in rotational stiffness. While the four walls with joist hangers were found to be effectively modelled as simply supported, the ML24Z had a significant effect on the rotational stiffness at the end of each stud, thereby reducing maximum deflections and residual deflections. Signs of yielding in the ML24Z connectors, as well the overall state of the wall after the test are shown in Figure 6.21.

6.2.4.4 LTS18

The LTS18 connector is a twist strap typically used to connect stud walls to roof rafters in order to prevent uplift due to wind forces. This connector was selected because it engages the end of the stud in tension, and could possibly be used as a multi-hazard connector (wind and blast). The capacity of this connection was only approximately 2 % higher than the expected dynamic reaction. It should be noted that when using this connector the assumed load path would be different than that of the other three connectors, as the force flows from the studs, through the strap, and directly to the blocking, bypassing the top and bottom plates.

Thirteen #10x1-1/2 in. screws were used to connect one end of the strap to the side of the stud while twelve screws of the same dimensions were used to provide connectivity between the plates and the rim joists. The load path is drastically different than that of the other three connectors, as the force is assumed to go from the studs, through the strap, and finally to the blocking. The strap bypassed the top and bottom plates, with no fasteners being embedded into them. A typical LTS18 twist strap connector during installation is shown in Figure 6.22A; it can be observed that the sheathing had to be placed following the installation of the connector. The connection detailing is shown in Figure 6.22B.

Walls 23 and 24 were constructed with this type of connector. Surprisingly, the results in both tests showed similar and poor performance, where the failure was either in rupture of the straps or splitting in the stud, as shown in Figure 6.23. These failure mode created very hazardous debris, where the studs and sheathing flew across the lab with high velocities. Alternative placement of the straps such that they are effectively wrapping around the stud ends might have produced better results, since splitting would have been reduced. This alternative was not investigated in the study but is suggested for future investigations.

The test revealed that the type of connection (i.e. joist-hangers, angles, straps, etc.) and their respective geometries greatly affects the overall behaviour of the wall and the amount of damage to the connection and structural elements. In other words, basing the design decision for a connection simply on the connection capacity would not be adequate. As seen with the ML24Z, the connector had a much lower capacity, yet actually improved the response of the wall, when compared to that of the joist-hanger connections, which did not appear to provide any rotational restraint. The findings of the current study clearly show that the design provision for wood structures is too simplistic and connections with performance characteristics that specifically optimize the behaviour of light-frame wood stud walls to blast loading need to be investigated. This will be further discussed in Chapter 7.

6.3 Catcher system

The use of welded wire mesh (WWM) was investigated as a possible catcher system by connecting them to the tension-face of studs with steel staples along the length of the studs at a spacing of 6 in., and securing them to the top and bottom plates with commercially available steel plates (as shown in Figure 6.24). Walls 15 and 16 were designed with larger stud members (2 x 8 in.) than those typically used in light-frame constructions in order to promote a failure in the OSB panels. Results show that a simple application of WWM can effectively capture virtually all debris created by the sheathing. Figure 6.25A shows a specimen after testing, with the debris still inside the wall/shock tube area. A dense Polystyrene foam board was placed 3000 mm away from the wall in order to assess the potential debris hazards. As Figure 6.25B shows, only minor splinter-like pieces of OSB were able to penetrate the panel. Albeit this foam is not similar to human flesh, it provided an indicator that the debris hazard was not severe. By placing the WWM on the interior

side of the wall, this system captures virtually all the debris while allowing for the full axial capacity of the studs to be maintained following a blast. It can be argued, however, that the proposed system allows for the blast pressures to enter the building, which would then injure or kill the occupants. While this concern is reasonable, the use of such catcher system can be justified as the alternative would either be debris throw from the sheathing, or loss of wall capacity which may cause progressive collapse. The implication of using a catcher system such as the one described in this section does not necessarily enhance the performance of the wall system, but rather changes the failure mode.

An injury due to overpressure is known as barotrauma, which is overpressurization or underpressurization of air-filled organs and air-liquid interfaces inside living entities, such as lungs and tympanic membranes (Guy et al., 1998). The tympanic membrane is the most sensitive to change in pressure and is known to rupture in humans at an overpressure of 34.5 kPa (Jensen & Bonding, 1993). This pressure is approximately the lowest pressure at which premature failure in the sheathing occurred and is much lower than the 110 kPa overpressure required to cause damage in lungs, as well as the 200 kPa overpressure known to cause fatalities (Katz et al., 1989). The highest recorded reflected pressure to which the walls with the WWM catcher system were exposed to was 62.5 kPa. The test done with the WWM system was intentionally done with the weakest wall sheathing. The sheathing thickness could be adjusted such that injuries are minimized in the case of a breach. While it may not be desirable to allow such injuries to occur, an argument can be made that it is a preferable alternative in terms of risk and consequence to allow some barotrauma to afflict a fraction of the occupants, rather than to risk progressive collapse, especially if the elements considered are load-bearing.

6.4 Analytical model

The goal of the creation of a constitutive analytical model was to verify the performance of a light-frame wood stud wall design against a far-field blast load. The very nature of this model is based on the material properties of those materials which make up the complex assembly that is a stud wall. In order to conceive a model that is representative and accurate, one must be able to capture the complex interactions between different components and the dynamic effects of the load being applied. This is done through static determination of material properties, as discussed in Chapter

3 and 4, and through the determination of the effect of PCA, rotational restraints, and high strain rate effects. The end goal is to be able to change any parameter of a wood stud wall and still be able to accurately predict the displacements and performance. It is noteworthy to mention that all SDOF modelling analysis was conducted with resistance curves that assume that flexural failure will occur. When sheathing failure did occur, however, the pressure-time history was changed such that the forcing function was only considered up to the point at which the sheathing failed, thereby allowing the pressure wave to pass through the wall. One may make the argument that the stud face is still exposed to pressure, however the loading area is so small (0.08 m^2) that the stud does not receive much load, relative to the magnitude of pressure when the sheathing actually is able to distribute the pressure, which corresponds to a loaded area of 0.83 m^2.

The strength of wood has been found to be logarithmically proportional to the applied strain rate, as discussed in Chapter 2. The current blast design code allows for a capacity DIF of 1.4 for visually graded lumber subjected to high strain rate. Experimentally, one may determine the specific DIF through support reactions, or by iteration with a SDOF model, where one tries to match the displacement-time histories by manipulating the resistance curve accordingly (Lacroix, 2013). In order to do this iteration, it is imperative that the displacement-time histories have the typical "S" shape that is usually found in SDOF systems, in order to match the peak displacement as well as the time-to-peak displacement. In this study, however, the studs exhibited a displacement-time history that typically was not in an "S" shape, making it virtually impossible to find an accurate DIF by iteration. The reason for this is that the walls in question were exposed to pressure-impulse combinations that typically yielded hazardous or blowout damage levels, where the assembly was overwhelmed by the dynamic forces. A DIF of 1.4 on the capacity and 1.18 on the stiffness was chosen based on the established analytical model by Lacroix (2013).

Comparing the analytical and experimental results using a dynamic increase factor on both resistance and stiffness show that the model is capable of predicting the wall behaviour with relatively high level of accuracy. The model is, however, underestimating the maximum response of the studs, as shown in Figure 6.26. A similar model with only a DIF of 1.4 on the stud capacity was investigated, in order to determine the sensitivity of the model to changes of the DIF_{MOE}. This model over-predicted the displacements by a factor similar to that of the model with a DIF on both capacity and stiffness, as shown in Figure 6.27. The dynamic increase factors determined by

Lacroix (2013) were based on stud walls with machine-stress-rated lumber, while the current study uses visually graded No. 2 studs, which is found in typical construction. The fact that the difference between the presence and absence of a dynamic increase factor on the stiffness it yields an average discrepancy of approximately 10 % does not justify any type of sensitivity analysis, or refinement of the factors utilized. For purposes of investigating and predicting behaviour for high damage levels, the proposed model by Lacroix (2013) seems adequate. Since ignoring the dynamic increase factor on the stiffness yielded similar results as those obtained using the model that included an increase on the stiffness, and yielded more conservative results (i.e. more displacement), no further changes are recommended for the blast design standard.

Table 6.1 : Excerpts from Table 9.23.3.4 of NBCC 2010

Construction Detail	**Minimum length of nails (mm)**	**Maximum spacing of nails on center (mm)**
Rim joist, trimmer joist or blocking – supporting walls with required braced wall panels – to sill plate or top wall plate – toe nail	82	150
Bottom wall plate or sole plate to floor joists, rim joists or blocking (exterior walls)	82	400
Bottom wall plate or sole plate – in required braced wall panels – to floor joists, rim joists or blocking (exterior walls)	82	150
Required braced wall panels – in interior walls – to framing above and below	82	150

Table 6.2 : Fastening schedule for various connections

Test ID	Connection	Fastening details		
		Connector-to-stud	**Connector-to-plate/blocking**	**Plate-to-blocking**
W17-1	Nails (non-seismic)	N / A	N / A	82 mm long nails spaced at 400 mm o/c
W17-2 W18-1	Nails (seismic)	N / A	N / A	82 mm long nails spaced at 150 mm o/c
W19-1 W20-1	HU28 joist hangers	Four 1-1/2 in. #10 screws	Eight 2-1/2 in. #10 screws	4-5/8 in. (0.22 in. diameter) screws installed in groups of two spaced at 406 mm
W21-1 W22-1	LJS26DS joist hangers	Six 1-1/2 in. #10 screws	Sixteen 2-1/2 in. #10 screws	4-5/8 in. (0.22 in. diameter) screws spaced at 400 mm o/c
W23-1 W24-1	LTS18 hurricane twist straps	Thirteen 1-1/2 in. #10 screws	Twelve 1-1/2 in. #10 screws	N / A
W25-1	ML24Z steel angles	Three 1-1/2 in. (1/4 in. diameter) heavy-duty screws	Three 2-1/2 in (1/4 in. diameter) heavy-duty screws	4-5/8 in. (0.22 in. diameter) screws installed in groups of two spaced at 400 mm o/c

A. OSB wall with noticeable sheathing failure

B. Plywood wall with failed studs missing from specimen

Figure 6.1 : Typical wall damage after blast testing

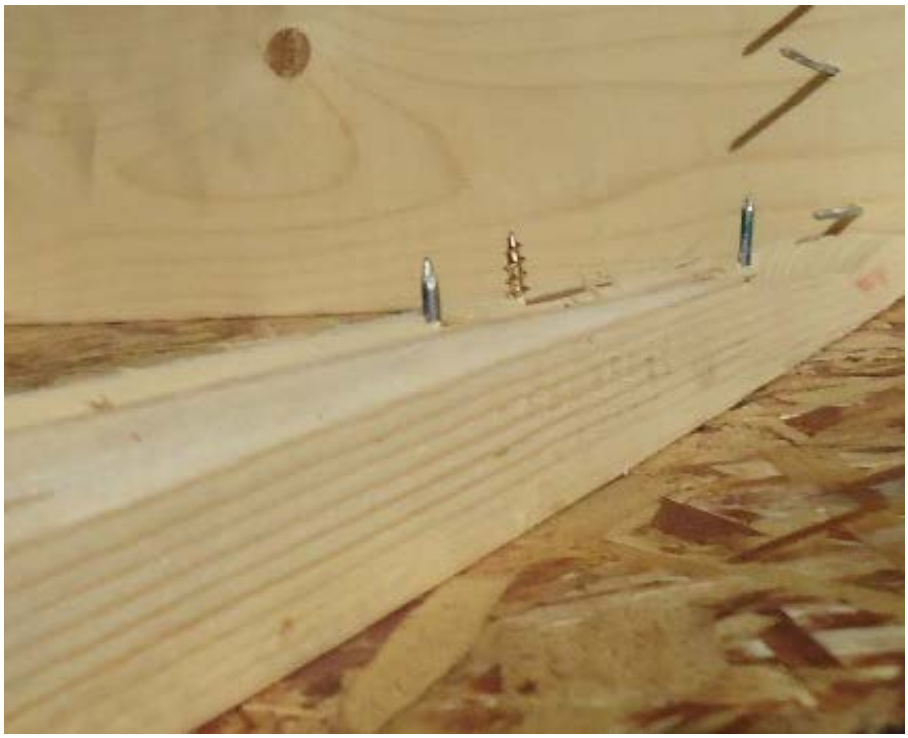

Figure 6.2 : Failure line with presence of nail and screw tips

A. WWM clamped by OSB

B. Wall with reinforced OSB sheathing

Figure 6.3 : Application of WWM as sheathing reinforcement

A. Nail head pull-through

B. Nail withdrawal and screw head pull-through

Figure 6.4 : Observed head pull-through and withdrawal of sheathing-to-stud fasteners

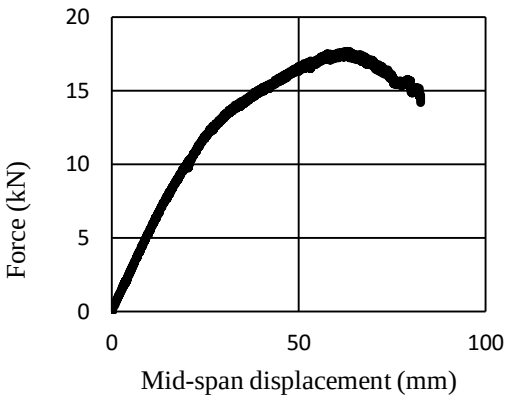

A. Load-displacement relationship B. Crushing of wood fibres and tension failure

Figure 6.5 : Failure behaviour of specimen with strong tension face

A. Typical static failure mode B. Typical dynamic failure mode

Figure 6.6 : Comparison between observed static and dynamic flexural failure modes

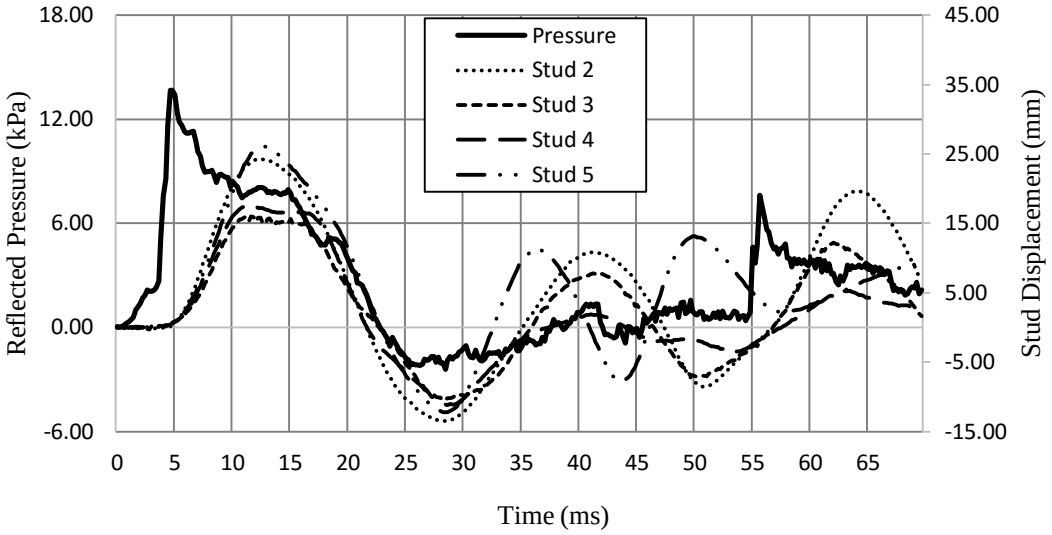

Figure 6.7 : Pressure- and displacement-time histories for Wall 1 Shot 1

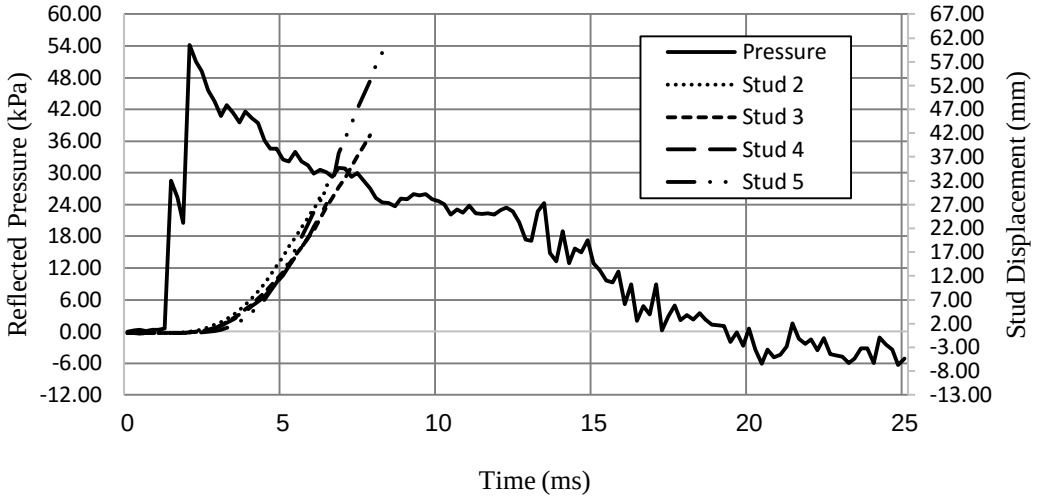

Figure 6.8 : Pressure- and displacement-time histories for Wall 1 Shot 2

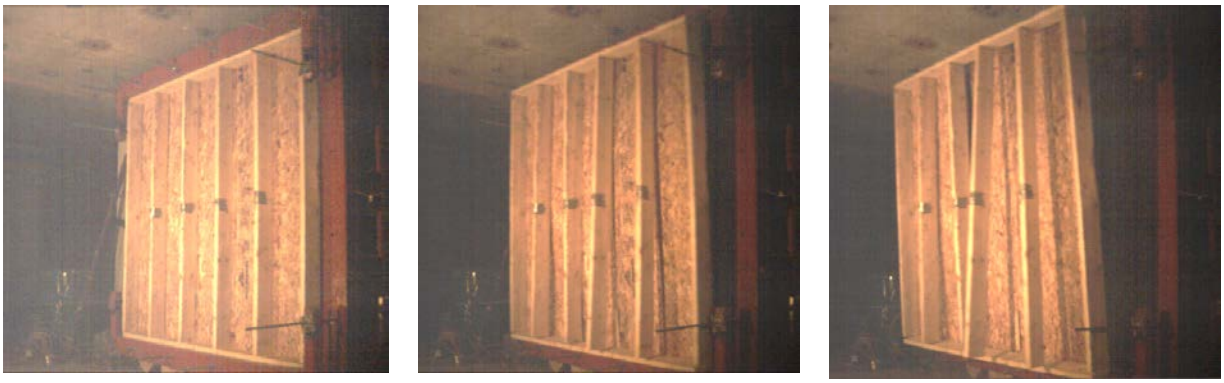

A. Arrival of shock wave

B. Post-connection failure

C. Specimen dislodged from test setup

Figure 6.9 : Time-lapse of typical connection failure

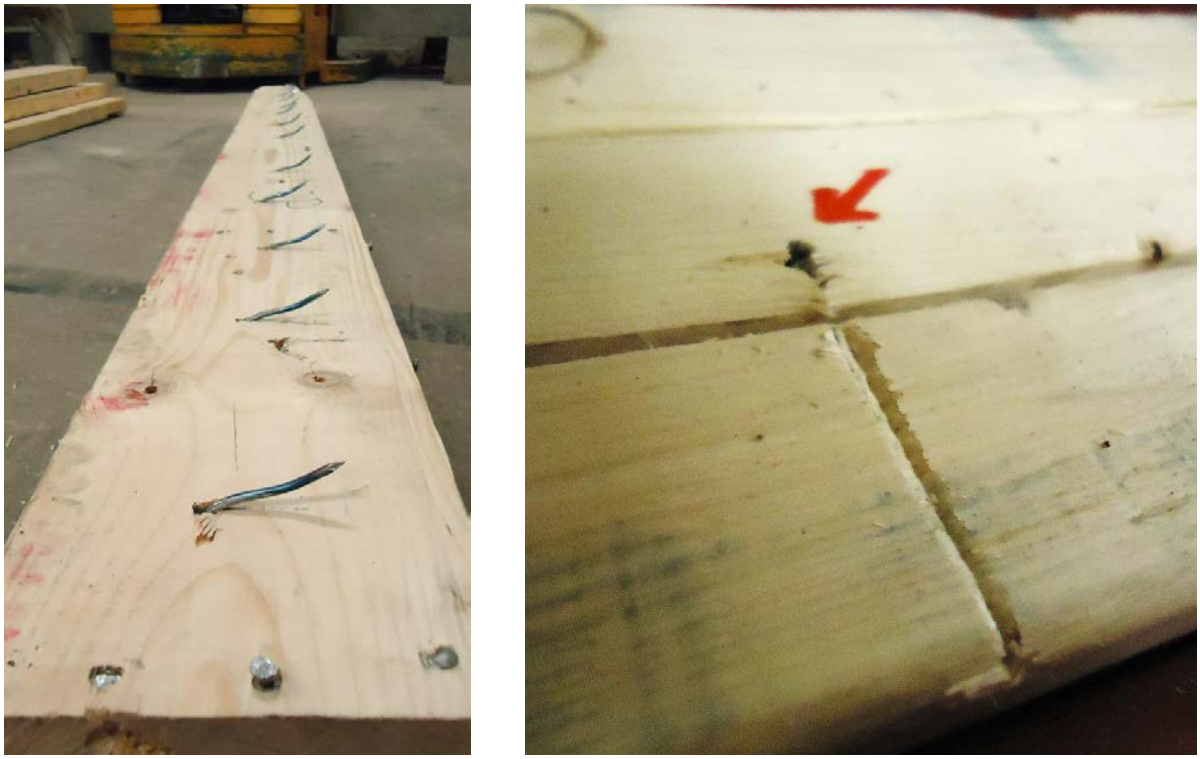

A. Yielding of nails at bottom-plate connection

B. Nail-withdrawal zone with drag marks on bottom blocking

Figure 6.10 : Observed bottom plate nail failure mode

A. Nail-withdrawal failure at top blocking

B. Nail puncture failure at top plate

Figure 6.11 : Observed top plate nail failure mode

Figure 6.12 : Nail-withdrawal failure at bottom plate for Wall 18 Shot 1

***(Left-to-right: #10x1.5in, #10x2.5in, 0.25x4.5in, 0.25x2.5in, 0.254x1.5in, 0.22x4 5/8in)**

Figure 6.13 : Fasteners used in retrofitted connections

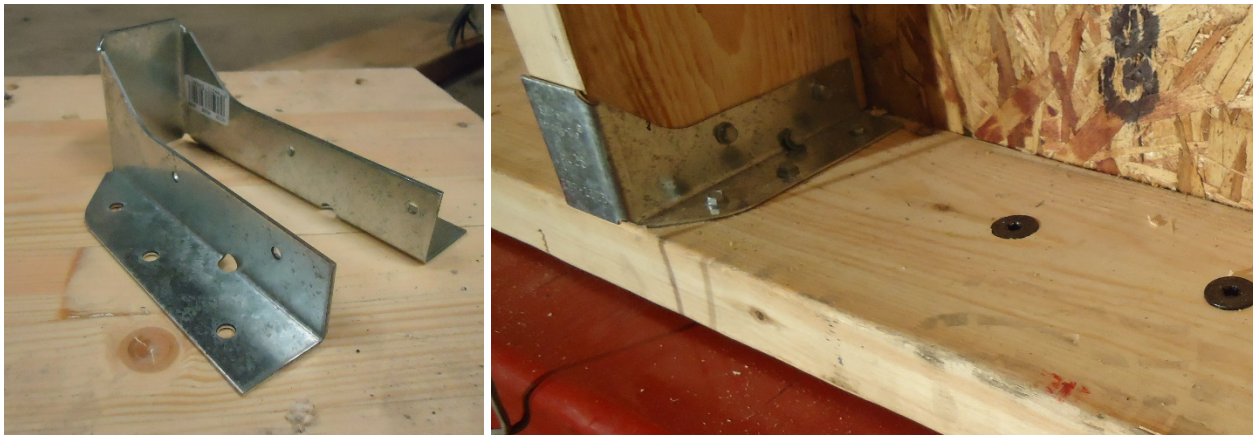

A. HU28 connector B. HU28 connection detail

Figure 6.14 : HU28 details

Figure 6.15 : Wall 20 detailed with HU28 connectors

Figure 6.16 : Typical connection damage for HU28 connections

Figure 6.17 : LJS26DS connection detail

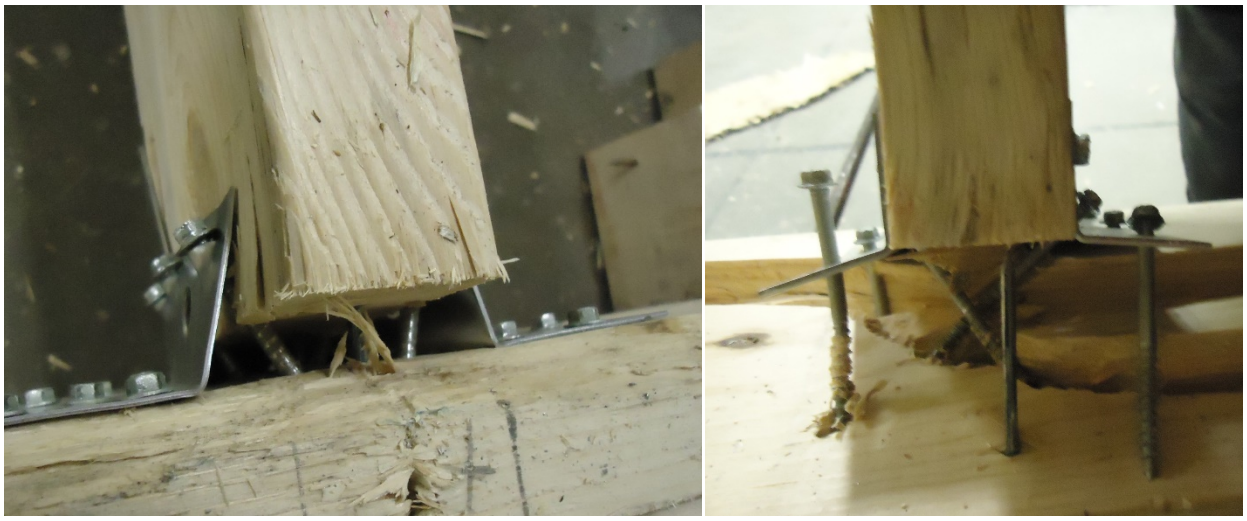

A. LJS26DS connection damage B. HU28 connection damage

Figure 6.18 : Damage comparison between HU28 and LJS26DS

Figure 6.19 : Damage in top plate in wall with LJS26DS

Figure 6.20 : Installation process of ML24Z connection

A. Wall 25

B. Yielding of ML24Z

Figure 6.21 : Observed effects of ML24Z connection

A. Installation of LTS18

B. LTS18 connection

Figure 6.22 : LTS18 detailing

A. Splitting failure

B. Combined rupture/splitting failure

Figure 6.23 : Observed failure modes for LTS18 walls

Figure 6.24 : Top-plate connection for WWM

A. Control of sheathing debris

B. Splinters embedded in Polystyrene panel

Figure 6.25 : Performance of WWM as a catcher system

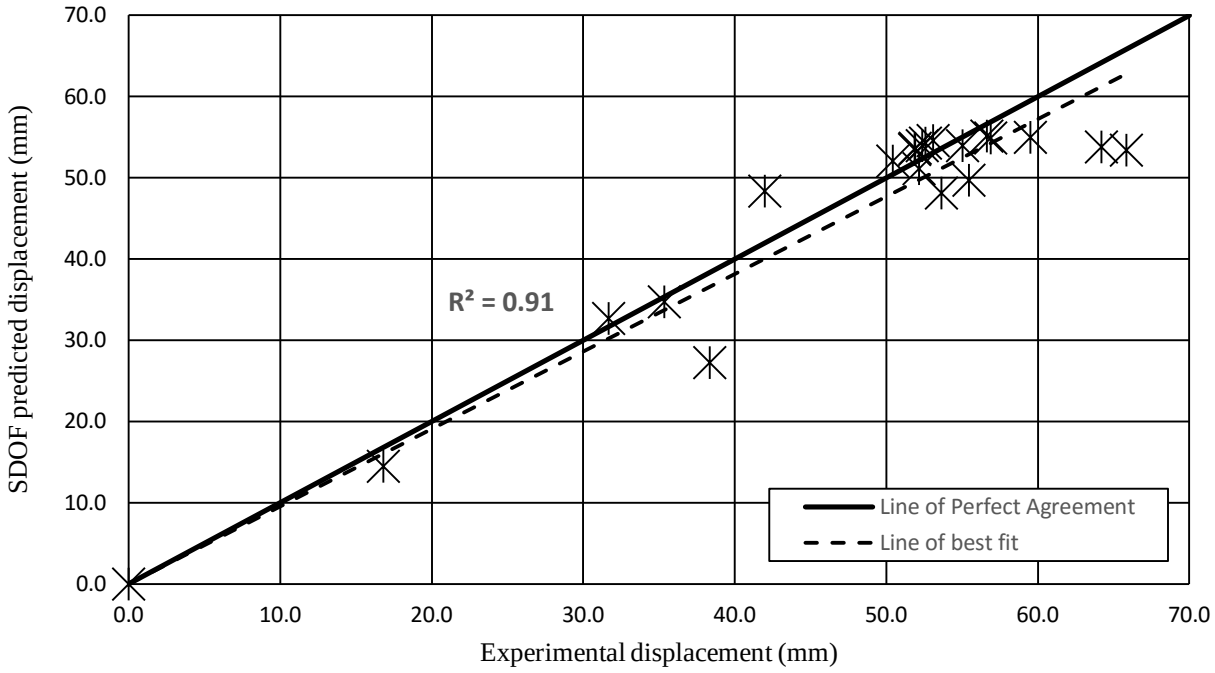

Figure 6.26 : SDOF and experimental displacement comparison

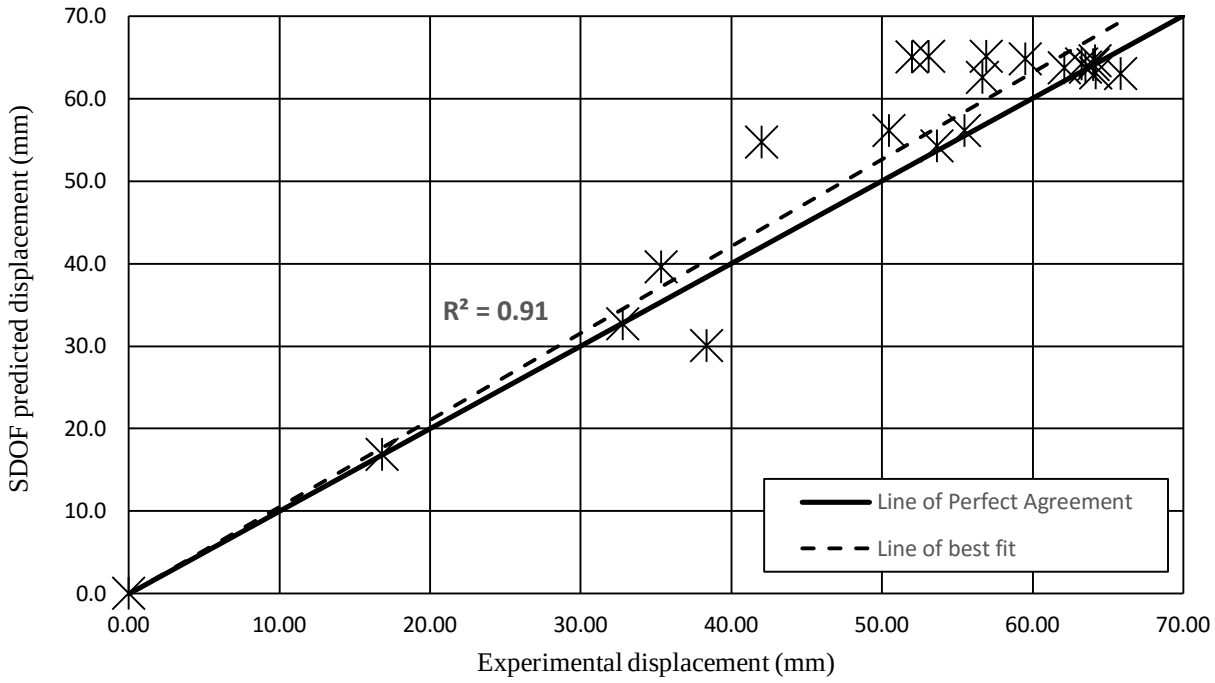

Figure 6.27 : Effects of no DIF_{MOE} on SDOF prediction

CHAPTER 7 - Code Considerations

7.1 General

The main objective of CSA S850 (2012) is to prevent human casualties and allow designers and owners to assess potential damage to the structure by providing tools to determine whether the target damage level is met. Major emphasis is put on the mitigation of progressive collapse, to allow for emergency evacuation of the occupants following a blast loading event (CSA, 2012). Similar to earthquake design, some inelastic deformations are accepted following a blast loading event. Limiting the damage level to structural components, minimizing flying debris, and most importantly, preventing progressive collapse are the chief objectives. Therefore, the performance requirements and levels of protection (LOP), along with associated component damage level, have been developed, as seen in Table 7.1. A "blowout" damage level is unacceptable when designing for a blast threat; however, it is still quantified in order to be able to evaluate a structure's performance following a blast event, as shown in Table 7.2. Clearly, damage descriptions such as "component has not failed, but it has significant permanent deflections causing it to be unrepairable" and "component has some permanent deflection. It is generally repairable" are not applicable to wood structural elements. There is therefore a need to develop more appropriate damage level descriptions that are more suitable, and that can be used for light-frame wood stud walls. In such complex systems consisting of components that are known to have variability in their stiffnesses and strengths, the damage of one component (e.g. stud) may not accurately reflect the subsystem (wall) or overall building damage. This chapter evaluates certain design guidelines presented in CSA S850 (2012) and determines, based on the findings of the current study, as well as the findings of two previous studies (Lacroix, 2013; Lacroix & Doudak, 2012), if they are appropriate or require revision. Presented in this chapter is a detailed assessment of the behaviour of thirty-three full-scale light-frame wood stud walls subjected to a total of forty-eight shots of simulated blast loading.

7.2 Ductility ratio

Conventional thinking about wood is that it is a brittle material, which in principle, is correct for certain failure modes, such as tension and shear. However, wood is ductile in compression and for failure modes such as flexure, both tension and compression stresses are experienced in the

material. Furthermore, light-frame wood stud walls consist of ribbed plates acting together in partial composite action through metallic fasteners (usually nails) joining the sheathing panels to the framing members. The slip in these joints, caused by the wall bending, provides some ductility in the wall system (e.g. Lacroix, 2013; Liu & Bulleit, 1995a, 1995b; McCutcheon, 1986). One noticeable aspect of these systems is their ability to share the load through a distribution which is based on the studs' stiffness, as well as load redistribution when individual elements such as studs or nails experience different levels of damage. Due to this complex behaviour, one cannot simply base the design of the wall on the failure of the weakest stud and therefore a more comprehensive approach at the system level needs to be considered. Several proposed approaches for static design based on system-level analysis currently exists in literature, varying from system failures based on the failure of the weakest member (Folz & Foschi, 1989), which have been shown to be too conservative, to multiple-member failure (Liu & Bulleit, 1995a, 1995b; Gromala, 1983). Research by Liu and Bulleit (1995b) has shown, through reliability and sensitivity analyses, that a system failure criteria is highly dependent on whether the systems are brittle or non-brittle, and is a function of its post-yield properties (i.e. plastic properties, post-yield resistance, and ultimate deflection limit).

Currently, the blast design standards (CSA, 2012; ASCE, 2011; USADD, 2008) use ductility ratios of 1, 2, 3, and 4 which correlate to response limits B1, B2, B3, and B4, respectively, for light-frame wood stud walls in flexure (see Table 7.2). These blast provisions for wood structures are based on limited data obtained primarily through live-explosive testing conducted by Marchand (2002). While no systematic approach for damage evaluation of light-frame wood structures exists, the test data available in the literature was reviewed by Oswald (2005) and an overall damage assessment was proposed based on the limited available information in form of damage photos and pressure-impulse combinations. In-situ properties of the structural members were not available and therefore published data was used to obtain the strength and stiffness of the specimens in order to conduct the assessment (Oswald, 2005). Although the specific damage descriptors were not explicitly defined in Oswald's study, it is assumed that the maximum ductility ratio of 4 was chosen because this limit defined the most severe damage observed during the assessment. A "blow-out" region is notoriously difficult to estimate, because if there is a lack of

data points representing the onset of collapse or ultimate failure, the limit is likely to be overestimated.

As discussed in Chapter 5 of this thesis, the current study determined that a maximum ductility ratio of 2.1 was appropriate based on strain data measurements and observation made from video review of the tests. Also, static test data previously performed by Lacroix (2013) confirms this observation. As shown in Figure 7.1, the force-displacement relationship of a statically loaded typical full-scale wall is plotted with ductility ratios up to 4. The graph clearly shows that the actual static behaviour was limited to ductility ratios of slightly higher than 2. These findings are consistent with those reported in other published studies on statically loaded floor and wall assemblies (Bulleit et al. 2005; Liu & Bulleit, 1995b; Gromala; 1983). These findings suggest that the assumption used in the design codes overestimates the ductility ratios for light-frame wood stud walls, and that using a maximum ductility of 2 is more appropriate and safer for blast design. This finding is crucial when ductility ratios and damage levels are being assessed for the walls tested dynamically. The code guidelines and the proposed ratios will be further evaluated analytically in a subsequent section of this chapter.

7.3 Proposed damage level assessment

The proposed assessment in this study is based on the assumption that limited failure of individual studs does not constitute complete failure in the wall system and that the number as well as the distribution of failed studs have different impacts on the overall wall performance. Therefore, both the severity as well as the extent of damage is evaluated. Component damage levels based on observed behaviour of light-frame wood stud walls subjected to blast loading were established using experimental results as well as published literature. Data such as the pressure-, displacement- and strain-time histories from the current study and past studies (Lacroix & Doudak, 2013; 2012) were agglomerated and evaluated. The proposed evaluation criteria, shown in Table 7.3, were developed based on the overall performance of the wall system and its estimated post-blast axial residual capacity. Typically, the lowest damage level corresponds to that of no observable damage on the structural elements. Due to the strength and stiffness variability between studs, a loading of relatively low magnitude may potentially cause cracking in the weakest studs. As mentioned in the introduction section, even though this is a permanent damage, it has little to no impact on the

axial capacity of the wall or the structure as a whole, and therefore, the proposed descriptor for "superficial damage" allows for limited splitting in an individual stud. Figure 7.2A shows an example of what the authors have characterized as "superficial" damage, where one stud experienced minor cracks on the tension face while the other studs did not experience any damage. This clearly does not meet the intent of the current damage level description in the blast design codes (CSA, 2012; ASCE, 2011), where a superficial damage level entails "no visible permanent damage". Since the wall (and the "failed" stud) has no permanent deflection, the "moderate" and "heavy" damage description from Table 7.2 would also not apply. If the assessment was made based on the failure of a single stud (weakest member within the wall subsystem) then the description for "hazardous" damage, defined as "Component has failed with no significant velocities", would apply to this wall. This was deemed as too conservative, and it reiterates the need for different and more appropriate descriptors specifically developed for light-frame wood stud walls. It is assumed here that the inherited variability in wood, which may lead to a stud with inferior capacity to experience some damage, should not mean that the level of damage of the entire wall is characterized for a higher damage level.

During the documentation of observed damage in the experimental phase, it was deemed very difficult to differentiate between moderate and heavy damage. For practical reasons, a merging of these two damage regions is proposed for the purpose of assessing wood stud walls. The proposed wording for the moderate-heavy range is based on observed wall failure being more appropriately defined by failure of two adjacent studs or any three studs. This is based on the assumption that overall wall failure is unlikely to occur when two adjacent studs or any three studs have completely failed in the wall system (Liu & Bulleit, 1995b). Although the current study is based on the damage assessment of walls with six studs only, Liu and Bulleit (1995b) showed, through reliability analyses, that similar limit-state failure criteria could be applicable to walls with up to 32 members. Figure 7.2B shows a representative example of the moderate-heavy damage.

The proposed "hazardous" damage is defined by the failure of three or more adjacent studs where debris has no significant velocity. At this damage level it is assumed that the wall segment would be at the onset of structural collapse. Finally, the blowout region is described by the structural component being overwhelmed by the load and where the debris have significant velocities. Figure 7.2C shows a representative observed damage level for what has been characterized as "blowout".

The damage assessment of light-frame wood stud walls described above has been summarized in Table 7.3 in a format that resembles that currently found in the blast design codes.

In order to evaluate whether the proposed damage description and ductility ratios are consistent with the applied pressure and impulse imparted on the walls, analysis using SDOF is used as described in the next section.

7.4 Response limits and normalized pressure-impulse (P-I) diagrams

A common method to describe the performance characteristics for a range of blast loading for a specific type of element and failure mode is through the use of P-I diagrams. The different curves in a P-I diagram indicate different damage levels or levels of protection (i.e. iso-damage curves). These can be derived obtained using a SDOF analysis method, obtained from experimental results, or from an actual blast events. While useful, its main drawback is that if not normalized, P-I diagrams cannot be generalized and can only be used to assess the behaviour of structural elements of identical properties, geometries, loading and end conditions. To expand the applicability of P-I diagrams to a broader range of specimens, normalized pressure-impulse combinations can be used to directly compare results of similar specimens with different geometry geometries and properties. The specimen stiffness, resistance, mass, and loaded-area are all taken into account and each data point is normalized by removing the direct effects of each of these properties. Curve fitting factors that take into account the effects of the negative phase of the blast wave are also available in the literature (USACE, 2008; Oswald, 2005).

Scaled P-I diagrams contain non-dimensional scaled peak blast pressure (P_{bar}) and scaled positive blast impulse (I_{bar}) terms, which are obtained by dividing the pressure and impulse by the component properties using the conservation of energy principle (Dragos & Wu, 2013; Krauthammer et al., 2008; USACE, 2008; Oswald, 2005). Rather than describing a deflection limit, the scaled P-I diagram reflects a non-dimensional response criterion, which is often described as a ductility ratio or support rotation. For wood, the common approach to relate the response limits to damage levels is through the use of the ductility ratio, μ, which consists of the ultimate deflection, x_{max}, divided by the elastic deflection of the system, x_e.

The difference between the static deformed shape and the first mode approximations is insignificant for blast loading, thus allowing the use of the static shape, which is more convenient (USADD, 2008). Most importantly, the time-scale between the real and equivalent systems is not altered; therefore, at any instance during the displacement-time history, the displacement of the equivalent system is equal to that of the real structure at the equivalent ordinate. Equations (2) and (3) describe the non-dimensional response criterion of ductility ratio.

$$P_{bar} = \frac{P_R}{R_u} \qquad \text{Equation 7.1}$$

$$I_{bar} = \frac{I_R}{R_u}\sqrt{\frac{K}{K_{LM}m}} \qquad \text{Equation 7.2}$$

Where P_R is the reflected peak positive pressure, R_u is the ultimate flexural resistance of the component obtained from static testing and modified for strain rate effects, I_R is the reflected impulse associated with the positive phase, K is the stiffness of the system, K_{LM} is the load-mass factor, and m is the mass of the system. By scaling the pressure and impulse combinations, it is possible to include walls with different properties and geometries into the same P-I diagram.

The test data of eighteen of the twenty-five specimens from the current study, as well as the test data from Lacroix (2013) and Lacroix & Doudak (2012), were scaled using Equations 7.1 and 7.2. The scaled data is presented in Table 7.4, which includes the evaluation of all the test results based on the proposed damage level description. Figure 7.3 shows the agglomerated test points plotted with the response limits specified in the current provisions of the Canadian blast design standard (CSA, 2012). It is clearly shown that data points characterized as “superficial” and “moderate-heavy” fit reasonably well within the regions proposed by the code, however, damage regions for “hazardous” and “blowout” are non-conservative. The need to reduce the ductility ratio corresponding to response limit B3 and B4 is apparent when comparing the fit between the data points and the respective response limits.

Based on the observed damage levels obtained from the three experimental studies, the author proposes the use of only four damage regions, separated by three response limits, denoted B1, B2, and B3, corresponding based onto ductility ratios of 1, 1.5, and 2, respectively (see Table 7.3).

Figure 7.4 shows the same data as in Figure 7.3 but with the proposed damage regions. It can be observed that test walls characterized as “blowout” fit well within the proposed blowout region, located to the right of the iso-curve corresponding to response limit B3 (i.e. $\mu = 2$) for ductility ratio of 2 and above. The damage region corresponding to “hazardous” can be seen to be relatively small, because it is often difficult to attain flexural failure of several load-bearing elements without any hazardous debris. This observation may imply that for all practical purposes and given the uncertainty associated with defining damage in the hazardous region, only three regions, namely superficial, moderate/heavy/hazardous, and blowout, may be adequate to describe the behaviour of light-frame wood stud walls. More data points are needed in the hazardous region before such recommendations can be made. The “superficial” region has not been changed, since it is based on the elastic limits.

Table 7.1 : CSA S850 level of protection (LOP) and component damage levels

Level of Protection	Primary component damage level	Secondary component damage level
Very Low (VL)	Heavy	Hazardous
Low (L)	Moderate	Heavy
Medium (M)	Superficial	Moderate
High (H)	Superficial	Superficial

Table 7.2 : CSA S850 damage level descriptors and response limits

Component damage level	Component damage level descriptions	Response limits
Superficial	Component has no visible permanent damage	Response less than B1
Moderate	Component has some permanent deflection. It is generally repairable, if necessary, although replacement may be more economical and aesthetic	Response between B1 and B2
Heavy	Component has not failed, but it has significant permanent deflections causing it to be unrepairable	Response between B2 and B3
Hazardous failure	Component has failed with no significant velocities	Response between B3 and B4
Blowout	Component is overwhelmed by blast loading causing debris with significant velocities	Response greater than B4

Table 7.3 : Proposed damage level descriptors and response limits

Component damage level	**Component damage level descriptions**	**Response limits**
Superficial	-No more than one stud with cracks extending to 50% of the stud depth. No debris.	Response less than B1
Moderate-heavy	-No more than two adjacent or three non-adjacent studs with cracks extending to 50% or more of the stud depth.	Response between B1 and B2
Hazardous failure	-Three or more adjacent stud failure with cracks extending to 50% or more of the stud depth. Debris is limited to small sized pieces of sheathing and/or stud fragments that have detached from the structural system with no significant velocities.	Response between B2 and B3
Blowout	-Sheathing overwhelmed, and sheathing debris detached from the structure with significant velocities. Studs may or may not be damaged -Majority of studs failed. Complete loss of axial capacity. Debris with significant velocities created.	Response greater than B3

Table 7.4 : Agglomeration of normalized dynamic test results

Test name	P_{bar}	I_{bar}	Damage level	Test name	P_{bar}	I_{bar}	Damage level
W1-1	0.40	1.46	Superficial	B4-2	1.20	1.53	Moderate-heavy
W1-2	1.57	4.63	Blowout	B5-1	0.90	1.51	Superficial
W2-1	1.35	4.02	Blowout	C1-1‡	N/A	N/A	Superficial
W3-1	1.46	4.24	Blowout	C1-2	0.74	3.00	Moderate-heavy
W4-1	1.63	4.62	Blowout	C2-1	0.88	3.12	Moderate-heavy
W5-1	1.34	4.56	Blowout	C3-1	0.25	0.20	Superficial
W6-1	1.32	4.65	Blowout	C3-2	1.32	1.38	Moderate-heavy
W7-1	1.34	4.61	Blowout	C4-1	0.15	0.57	Superficial
W8-1	1.39	4.94	Blowout	C4-2	0.65	2.10	Superficial
W10-1	1.33	4.16	Blowout	C4-3	0.95	3.13	Moderate-heavy
W11-1	1.75	5.39	Blowout	C5-1	0.25	1.45	Superficial
W12-1	1.90	5.65	Blowout	C5-2	0.66	3.76	Superficial
W13-1	1.26	4.97	Blowout	C6-1	0.25	1.04	Superficial
W14-1	1.02	4.20	Hazardous	C6-2	0.72	2.92	Superficial
W19-1	1.28	4.39	Blowout	C6-3	0.75	3.32	Moderate-heavy
W20-1	1.08	3.87	Blowout	C7-1	0.25	1.76	Superficial
W21-1	1.14	3.88	Blowout	C7-2	0.79	6.33	Moderate-heavy
W22-1	1.17	4.13	Blowout	C8-1	0.27	0.23	Superficial
W25-1	1.13	5.56	Blowout	C8-2	1.54	1.60	Moderate-heavy
B1-1†	0.70	1.03	Superficial	C9-1	0.24	0.92	Superficial
B2-1	1.13	1.46	Moderate-heavy	C9-2	0.92	3.67	Moderate-heavy
B3-1	0.63	0.90	Superficial	C10-1	0.29	1.12	Superficial
B3-2	0.68	1.00	Superficial	C10-2	0.71	2.11	Superficial
B4-1	0.61	0.76	Superficial	C10-3	0.89	3.25	Moderate-heavy

† *B1-1 to B5-1*: Lacroix & Doudak (2012)
‡ *C1-1 to C10-3*: Lacroix (2013)

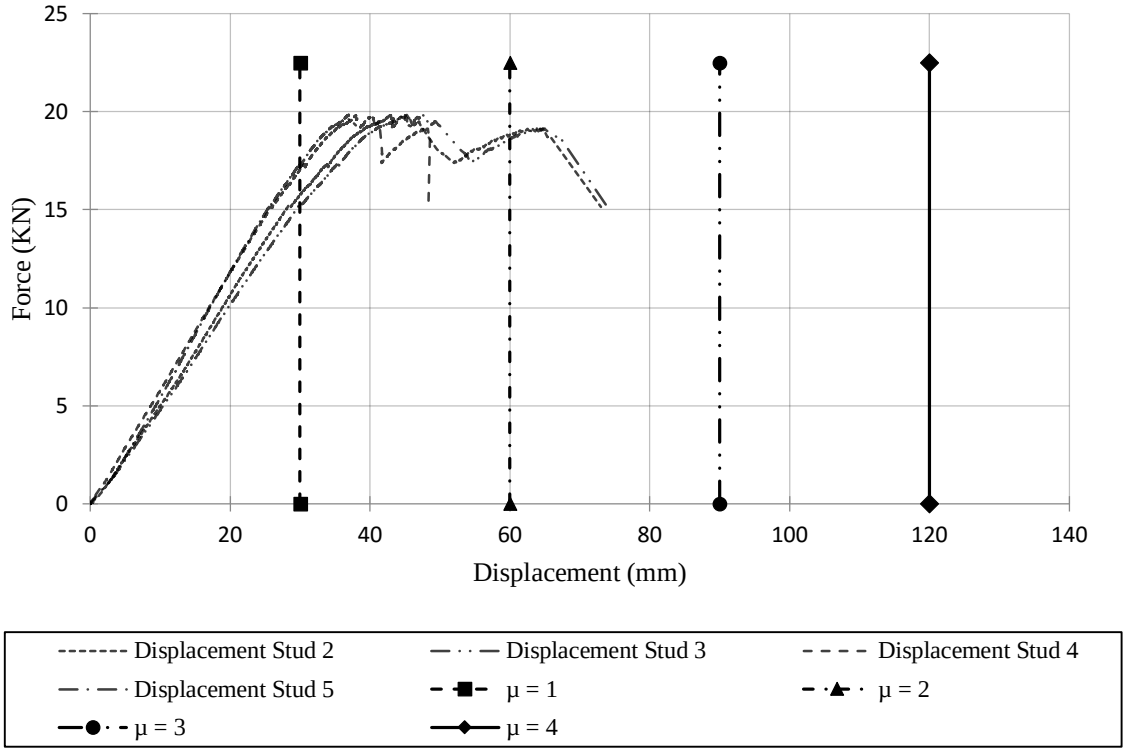

Figure 7.1 : Static full-scale wall load-displacement relationship (Lacroix, 2013)

A. Superficial B. Moderate-Heavy C. Blowout

Figure 7.2 : Representative damage level

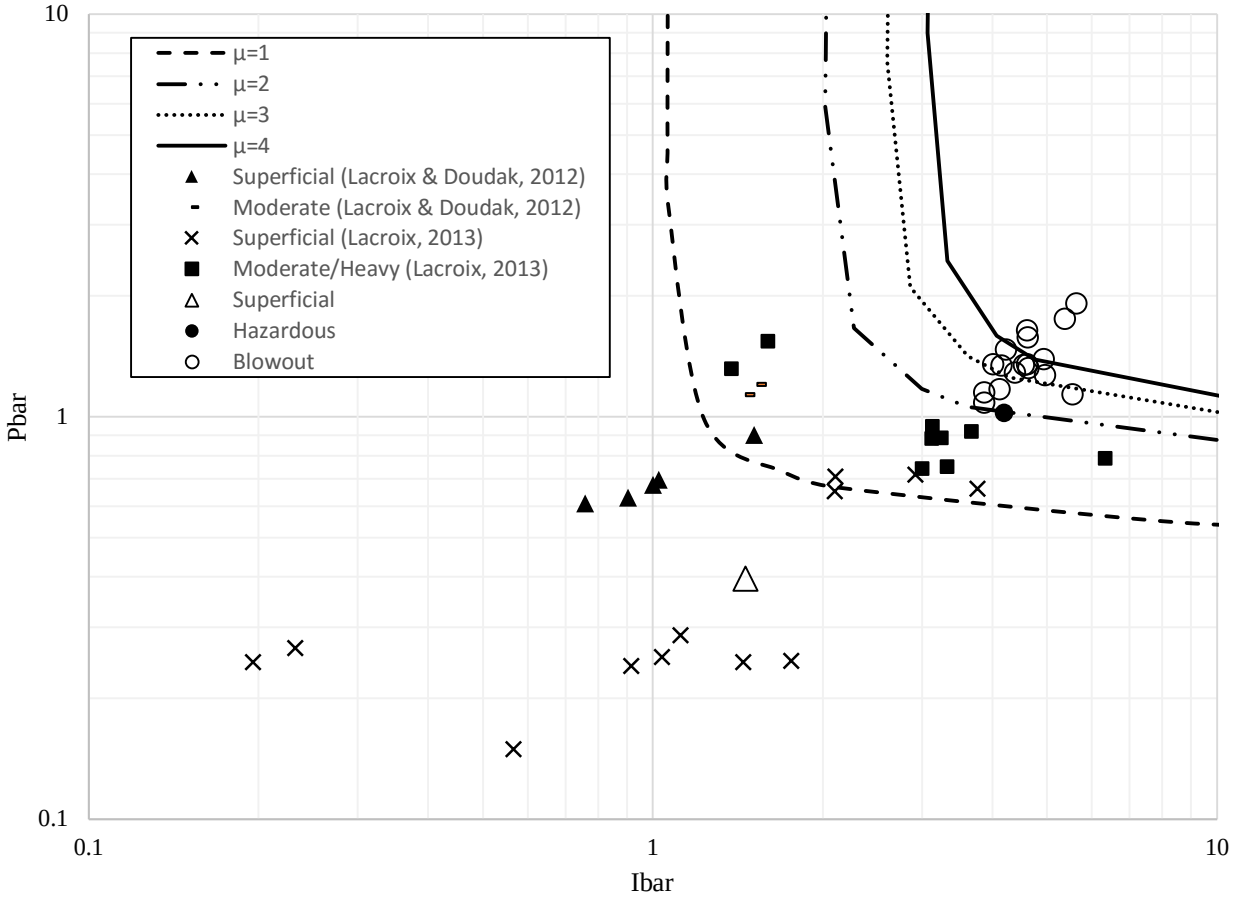

Figure 7.3 : Pressure-impulse diagram using CSA S850 response limits and ductility ratios

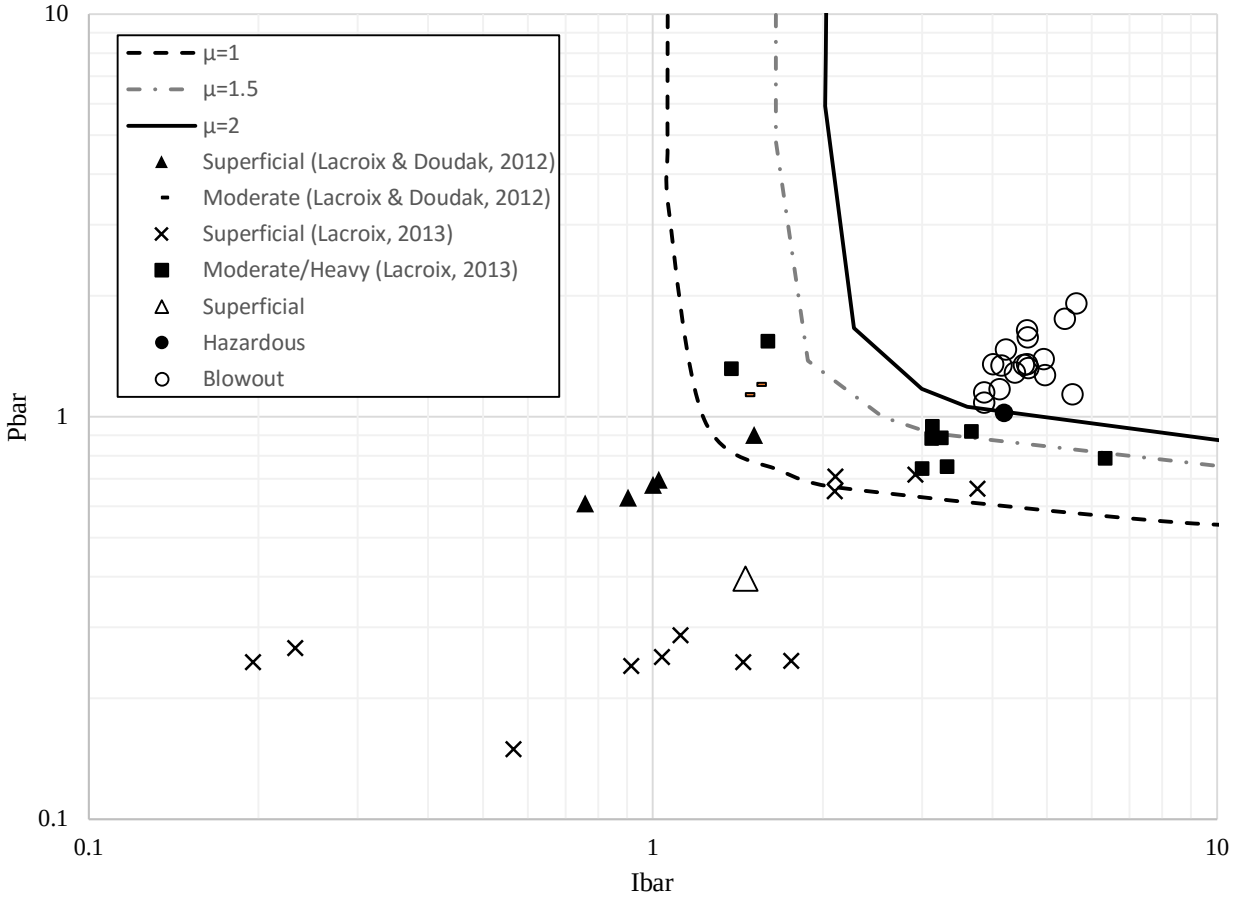

Figure 7.4 : Pressure-impulse diagram with proposed damage regions and response limits

CHAPTER 8 - Conclusions and Recommendations

8.1 General

The current study primarily dealt with assessing the flexural behaviour of light-frame wood stud walls when subjected to blast loads. However, the main focus was to establish the sequence of failure, which required separate investigations on three different failure modes: flexural failure of the load-bearing elements, ripping failure of the sheathing, and failure of the boundary connections. Strain rates between $1.92E^{-1}$ to $9.05E^{-1}$ were generated using a shock tube. Throughout these tests, considerations for debris hazards and possible mitigation techniques and retrofits were also considered, such as for stud and sheathing debris. The following chapter summarizes the main findings and conclusions of the current study and will attempt to lay out the possible future research work.

8.2 Conclusions

- Differences in failure modes were observed between the static and dynamic testing, where the mode of flexural failure in the dynamic tests was “brash”, with the majority of the studs failing with a straight “cut-through” its cross-section. A small portion of the studs showed signs of compressive-side bowing and major splintering of the tension fibres.
- Tests on light-frame wood stud walls with typical construction detailing and exposed to high blast pressure showed that 11 mm (7/16 in.) OSB sheathing panels tend to fail prematurely at pressures higher than approximately 35 kPa.
- The use of thicker sheathing shifts the failures to the studs, while concurrently decreasing the amount of sheathing debris. The amount of stud debris was found to be easily controlled through the use of screws as fasteners between the sheathing and the studs.
- An investigation of the use of welded wire mesh (WWM) as a reinforcement of the sheathing or as a catcher system showed promising results. The pressure in the reinforced sheathing panels was completely transferred to the studs. In the case of using the WWM as a catcher system, it was found that the stud’s residual axial capacity was maintained while the catcher system was used successfully to capture all the sheathing debris.
- Typical nailed connection detailing, even those detailed for high seismic regions, did not possess adequate capacity to maintain connectivity to the floors prior to the wall studs

reaching their full capacity. Premature failure of the stud wall assembly was observed and hazardous debris was generated.

- Connector types that had adequate capacity according to the blast design code and that provided bearing support for the wall studs performed well and seemed to have adequate capacity to allow the studs to fail before the connections.
- An angle connector with design capacity less than that required by the code provisions provided adequate performance. Splitting in the studs was observed but this type of connector provided partial rotational restraint at the stud end, which reduced the deflection and damage.
- From the two previous findings, it can be concluded that basing the connection design solely on the capacity may not be adequate. Additional considerations regarding the connection type and detailing should also be considered.
- A single degree-of-freedom material-predictive model, which utilizes the material properties of each individual component, was successfully validated using the experimental test results. The model was found to accurately predict the behaviour of the wall studs in cases where sheathing tearing was observed.
- The current dynamic increase factor of 1.4 on the material strength has been found to be adequate and conservative for blast and correlates well with the experimental results. A dynamic increase factor of 1.18 on the stiffness, which was determined by Lacroix (2013), also correlated well with experimental data, however the predicted results were not conservative.
- The current response limits specified in the CSA S850 (2012) overestimate the ductility capabilities of light-frame wood assemblies. Strain-time profiles along with video review show that walls will typically exhibit some ductility up until a ductility ratio of approximately 2, where blowout occurs.
- The description of the performance criteria in the CSA S850 (2012) for wood structures are not representative. The current study outlines some proposed descriptors and the author recommends that the redundancy and nature of lumber are taken into account for damage level assessment of light-frame wood stud walls.

8.3 Recommendations for future work

Based on the work that has been done in the current study, the following areas and topics have been identified for future work and possible research topics:

- Typical wood stud walls are load-bearing walls; the effects of axial load on the response of the studs and connections were not investigated in the study. The introduction of axial loading might play a significant role in how light-frame wood structures behave when subjected to a blast load.
- The effects of additional components which are typically found in buildings with stud walls, such as insulation and gypsum wallboard (GWB) was not taken into consideration in the current study. The added mass and stiffness provided by the gypsum panel could potentially affect the wall performance, due to the relatively high stiffness/low-capacity of the GWB, as well in terms of potential debris hazards.
- While it has been determined that the studs do in fact exhibit high strain rate effects (i.e. increase in capacity), it is not well known whether any increase would be experienced in the connections at the top and bottom plates. A study that would investigate the possible increase in connection capacity due to high strain effects could potentially contribute to the guidelines for connection design in the Canadian Blast Standard (CSA, 2012).
- A rudimentary approach was utilized during the investigation of a possible catcher system, through the use of WWM. Other more advanced methods, such as the application of spray-on coatings of elastomers, such as polyurethane, could yield similar or better results in terms of debris mitigation.

REFERENCES

ASTM. (2006). ASTM D1037 - *Evaluating Properties of Wood-Base Fiber and Particle Panel Materials*. West Conshohocken, PA: American Society for Testing and Materials.

ASTM. (2009). ASTM D198 - *Static Tests of Lumber in Structural Sizes*. West Conshohocken, PA: American Society for Testing and Materials.

ASTM. (2010). ASTM D2915 - *Sampling and Data-Analysis for Structural Wood and Wood-Based Products*. West Conshohocken, PA: American Society for Testing and Materials.

ASTM. (2012). ASTM D1761 - *Standard Test Methods for Mechanical Fasteners in Wood*. West Conshohocken, PA: American Society for Testing and Materials.

AWC. (2014). *National Design Specification for Wood Construction*. Leesburg, VA: American Wood Council.

Barrett, J., & Lau, W. (1994). *Canadian lumber properties*. Ottawa: Canadian Wood Council.

Biggs, M. (1964). *Introduction to structural dynamics*. New York, NY: McGraw-Hill.

Bogosian, D., & Avanessian, H. D. (2004). Blunt Trauma from Blast-Induced Building Debris. 31st Explosives Safety Seminar. San Antonio, TX.

Bulleit, W., Pang, W.C., & Rosowsky, D. (2005). *Modeling Wood Walls Subjected to Combined Transverse and Axial Loads*. Journal of Structural Engineering - ASCE, 781-793.

Burrell, R. (2012). *Performance of steel fibre reinforced concrete columns under shock tube induced shock wave loading*. Ottawa, ON: University of Ottawa.

Canadian Wood Council. (2010). *Wood Design Manual*. Ottawa, ON: Canadian Wood Council.

CEN. (2008). *Eurocode 5: Design of timber structures*. Brussels, BE: Comité Européen de Normalisation.

Cormie, D., Mays, G., & Smith, P. (2009). *Blast effects on buildings*. Reston, VA: Thomas Telford.

CSA. (2012). *CSA S850 - Design and assessment of buildings subjected to blast loads*. Mississauga: Canadian Standards Association Group.

CSA. (2014). *CSA O86 - Engineering design in wood*. Mississauga: Canadian Standards Association.

DHS. (2011). *FEMA-426 - Reference Manual to Mitigate Potential Terrorist Attacks Against Buildings*. Washingston D.C: U.S. Department of Homeland Security.

Dragos, J., & Wu, C. (2013). *A new general approach to derive normalised pressure impulse curves*. International Journal of Impact Engineering, 62, 1-12.

Dusenberry, D. (2010). *Handbook for blast-resistant design of buildings*. Hoboken, NJ: J. Wiley.

Folz, B., & Foschi, R. (1989). *Reliability-based design of wood structural systems*. Journal of Structural Engineering, 115(7), 1660-1680.

Government of BC. (2009). *Bill 9 - Wood First Act*. Retrieved from Legislative Session: 1st Session, 39th Parliament: https://www.leg.bc.ca/39th1st/1st_read/gov09-1.html.

Government of Ontario. (2014). *Ontario Building Code*. Retrieved from CodeNews Issue 232 - Amendments to Ontario's Building Code Allowing Mid-Rise Wood Frame Buildings: http://www.mah.gov.on.ca/Page10816.aspx.

Gromala, D. S. (1983). *Light-Frame Wall Systems: Performance and Predictability*. Madison, WI: United States Department of Agriculture.

Guy, R. J., Glover, M. A., & Cripps, N. P. (1998). *The pathophysiology of primary blast injury and its implications for treatment. Part I: the thorax.* Journal of the Royal Naval Medical Service, 79-86.

Jacques, E. (2011). *Blast Retrofit of Reinforced Concrete Walls and Slabs*. Ottawa, ON: University of Ottawa.

Jacques, E. (2014). *RCBlast* (Version. 0.5.1) [Computer program]. Retrieved 2014, from www.rcblast.ca.

Jacques, E., Lloyd, A., Braimah, A., Saatcioglu, M., Doudak, G., & Abdelalim, O. (2013). *Influence of high strain-rates on the dynamic flexural material properties of spruce-pine-fir wood studs*. Canadian Journal of Civil Engineering, 9.

Jansson, B. (1992). *Impact Loading of Timber Beams*. Vancouver, BC: University of British Columbia.

Jensen, J. H., & Bonding, P. (1993). *Experimental pressure induced rupture of the tympanic membrane in man*. Acta Otolaryngol, 62-70.

Johnson, W. (1986). *Historical and Present-Day References Concerning Impact on Wood*. International Journal of Impact Engineering, 4(3).

Katz, E., Ofek, B., Adler, J., Abramowitz, H. B., & Krausz, M. M. (1989). *Primary blast injury after a bomb explosion in a civilian bus.* Ann Surg, 484-488.

Krauthammer, T. (2008). *Modern Protective Structures*. Boca Raton, FL: CRC Press.

Krauthammer, T., Astarlioglu, S., Blasko, J., Soh, T.B., & Ng, P.H. (2008). *Pressure-impulse diagrams for the behavior assessment of structural components*. International Journal of Impact Engineering, 35(8), 771-783.

Lacroix, D. (2013). *Behaviour of light-frame wood stud walls subjected to blast loading*. Ottawa: University of Ottawa.

Lacroix, D., & Doudak, G. (2012). *Behaviour of typical light-frame wood stud walls subjected to blast loading*. World Conference on Timber Engineering: Strength and Serviceability - Extreme Events. Auckland, New-Zealand.

Lacroix, D., & Doudak, G. (2013). *Modelling the Behaviour of Light-Frame Wood Stud Walls Subjected to Blast Loading*. 3rd Specialty Conference on Material Engineering & Applied Mechanics (pp. 1-10). Montreal, QC: CSCE.

Lacroix, D., & Doudak, G. (2014). *Investigation of Dynamic Increase Factors in Light-Frame Wood Stud Walls Subjected to Out-of-Plane Blast Loading*. Journal of Structural Engineering, ASCE, 1-10.

Lacroix, D., & Doudak, G. (2015). *Experimental and Analytical Evaluation of the Flexural Capacity of Light-Frame Wood Stud Walls Under Blast Loading - An Assessment of the Canadian Blast Design Standard Provisions*. 11th International Conference on Shock & Impact Loads on Structures (pp. 213 - 221). Ottawa, ON: C-I Premier Conference Organisation.

Lacroix, D., Doudak, G., & El-Domiaty, K. (2013). *Retrofit Options for Light-Frame Wood Stud Walls Subjected to Blast Loading*. Journal of Structural Engineering, ASCE, 1-8.

Liska, J. (1950). *Effect of Rapid Loading on the Compressive and Flexural Strength of Wood*. Madison, WI: United States Department of Agriculture.

Liu, W., & Bulleit, W. (1995a). *Approximate reliability analysis of wood structural systems*. Journal of Structural Safety, 17(2), 59-78.

Liu, W., & Bulleit, W. (1995b). *Overload behavior of sheathed lumber systems*. Journal of Structural Engineering, 121(7), 1110-1118.

Lloyd, A. (2010). *Performance of Reinforced Concrete Columns Under Shock Tube Induced Shock Wave Loading*. Ottawa, ON: University of Ottawa.

Lloyd, A., & Jacques, E. (2011). *Innovative and Cost Effective Blast Strengthening of Wood Framed Structures*. Ottawa, ON: University of Ottawa.

Marchand, K.A. (2002). *BAIT, BASS & RODS Testing Results*. USAF Protection Battlelab, The Technical Support Working Group, Defense Threat Reduction Agency.

Mamlouk, M., & Zaniewski, J. (2011). *Materials for Civil and Construction Engineers*. Upper Saddle River, NJ: Prentice Hall.

McCutcheon, W. (1977). *Method for predicting the stiffness of wood-joist floor systems with partial composite action*. Madison, WI: US Department of Agriculture.

McCutcheon, W. (1984). *Deflections of Uniformly Loaded Floors - A Beam-Spring analogy*. Madison, WI: United States Department of Agriculture.

McCutcheon, W. (1986). *Stiffness of Framing Members with Partial Composite Action*. Journal of Structural Engineering, 112(7), 1623-1637.

Mindess, S., & Madsen, B. (1986). *The fracture of wood under impact loading*. Journal of Materials and Structures, 19(1), 49-53.

Muñoz, W., Salenikovich, A., Mohammad, M., & Quenneville, P. (2008). *Determination of Yield Point and Ductility of Timber Assemblies: In Search for a Harmonised Approach*.

Nadeau, J., & Bennett, R. (1982). *An explanation for the rate-of-loading and duration-of-load effects in wood in terms of fracture mechanics*. Journal of Materials Science, 2831-2840.

NRC. (2015). *National Building Code of Canada*. Ottawa: National Research Council of Canada.

Office of the Deputy Prime Minister. (2004). *Disproportionate Collapse, The Building Regulations 2000*.

Oswald, C.J. (2005). *Component Explosive Damage Assessment Workbook (CEDAW) Methodology Manual V1.0. BakerRisk Project No. 02-0752-001*, Protective Design Center, US Army Corps of Engineers (Omaha District), San Antonio, TX.

Parlin, N. (2010). *Behavior of FRP-Coated Wood Panels under Dynamic Loading*. Orono, Maine: University of Maine.

Polensek, A., & Schimel, B. (1986). *Rotational restraint of wood-stud wall supports*. Journal of Structural Engineering, 1247-1262.

Polensek, A., & Schimel, B. (1991). *Dynamic Properties of Light-Frame Wood Subsystems*. ASCE Volume 117, 1079-1095.

Polensek, A., Atherton, G., Corder, S., & Jenkins, J. (1972). *Reponses of Nailed Wood-Joist Floors to Static Loads.* Forest Products Journal, 52-64.

Rosowsky, D. V., Yu, G., & Bulleit, W. M. (2005). *Reliability of Light-Frame Wall Systems Subject to Combined Axial and Transverse Loads.* Journal of Structural Engineering, 1444-1455.

Sorensen, A., & McGill, W. (2011). *What to look for in the aftermath of an explosion? A review of blast scene damage observables.* Engineering Failure Analysis, 836-846.

Spencer, R. (1978). *Rate of Loading Effect in Bending for Douglas-Fir Lumber.* 1st International Conference on Wood Fracture. Banff, Alberta.

Sukontasukkul, P., Lam, F., & Mindess, S. (2000). *Fracture of parallel strand lumber (PSL) under impact loading.* Materials and Structures, 445-449.

Syron, W. (2010). *Strain rate-dependent behavior of laminated strand lumber.* Orono, Maine: University of Maine.

USACE. (2008). *Methodology Manual for the Single-Degree-of-Freedom Blast Effects Design Spreadsheets (SBEDS).* Washington D.C: U.S Army Corps of Engineers.

USADD. (2008). *Unified Facilities Criteria (UFC) 03-340-02 - Structures to Resist the Effects of Accidental Explosions.* Washington, D.C: United States of America Department of Defense.

USADD. (2009). *Unified Facilities Criteria (UFC) 4-023-03 - Design of Buildings to Resist Progressive Collapse.* Washington D.C: United States of America Department of Defense.

USAF. (2006). *Vehicle Bomb Mitigation Guide.* Lackland AFB, Texas: United States Air Force.

Wheat, D. L., Vanderbilt, D., & Goodman, J. R. (1983). *Wood Floors with Nonlinear Nail Stiffness.* Journal of Structural Engineering, 1290-1302.

Yasumura, M., & Kawai, N. (1998). *Estimating seismic performance of wood-framed structures.* Proceedings of 1998 I.W.E.C., (pp. 564-571). Switzerland.

Yu, G. (2003). *Load Sharing and System Factors for Light-Frame Wall Systems.* Corvallis, OR: Oregon State University.

APPENDIX A - Dynamic Test Results

Wall 1 Test Summary

Test name: Wall_1_Shot_1 **Test date:** 27/6/2014

Driver length: 2745 mm **Driver pressure:** 68.9 kPa

Wall mass: 64.86 kg

Test specimen properties:

- 6-38 mm x 140 mm No. 2 studs @ 406.4 mm o/c
- Nails, 50 mm x 2.87 mm @ 150 mm o/c (field and edge)
- 2108 mm total length of wall
- 2032 mm long studs
- 2032 mm clear span
- 11 mm OSB

Average maximum reflected pressure: 13.7 kPa **Average max. deflection of wall studs:** 20.94 mm

Average maximum reflected impulse: 140.0 kPa-ms **Average time to max. deflection:** 11.1 ms

Positive phase duration: 17.8 ms **Quantified wall damage level:** Superficial

Table A1.1 : Stud data from Wall 1 Shot 1

Stud number	Stud reference ID	Maximum mid-span displacement	Time to Maximum	Debris projection	Stud damage level
		mm	ms	mm	
1	S237	-	-	No debris	Superficial
2	S160	24.21	11.4	No debris	Superficial
3	S174	16.01	10.2	No debris	Superficial
4	S181	17.58	10.8	No debris	Superficial
5	S187	25.96	12.0	No debris	Superficial
6	S238	-	-	No debris	Superficial

Comments:

No damage to studs or sheathing was observed. Small nail withdrawal on stud 5 was observed, but was mostly reversed on rebound, when the nails were brought back to their initial positions. Studs time/displacement history are in sync up until maximum where they then behave differently. No debris was observed. Displacement readings on studs 2 and 5 are questionable since damage to the connection between the LVDTs and the studs was observed.

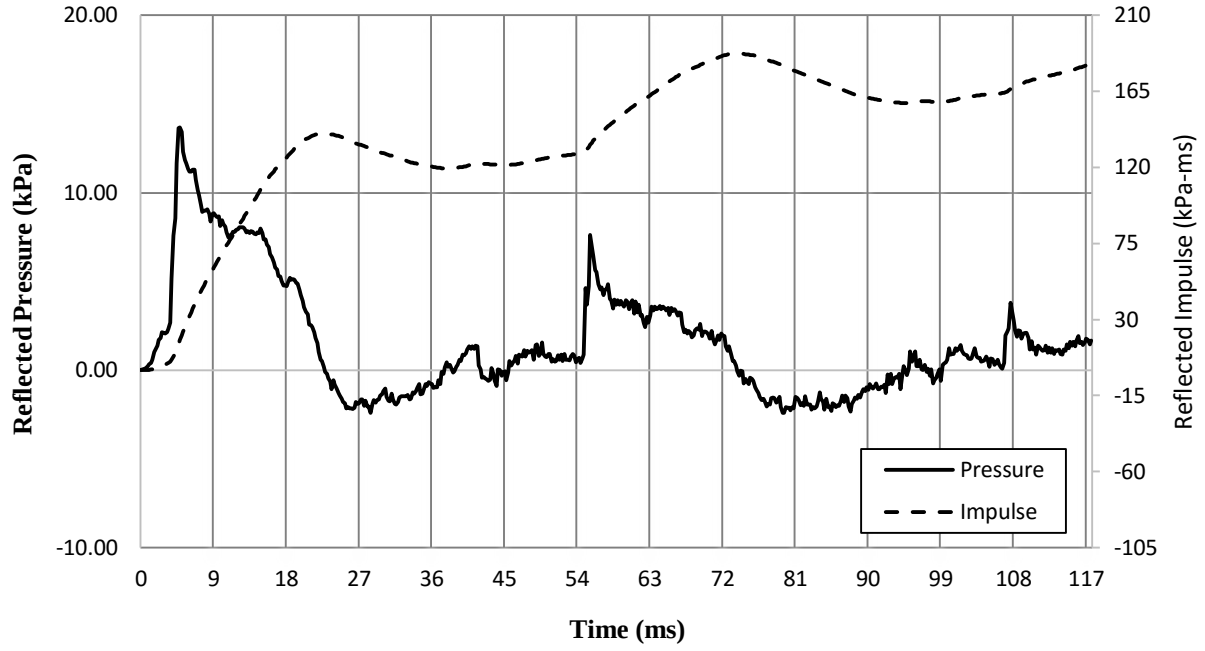

Figure A1.1 : Reflected pressure and impulse time histories for Wall 1 Shot 1

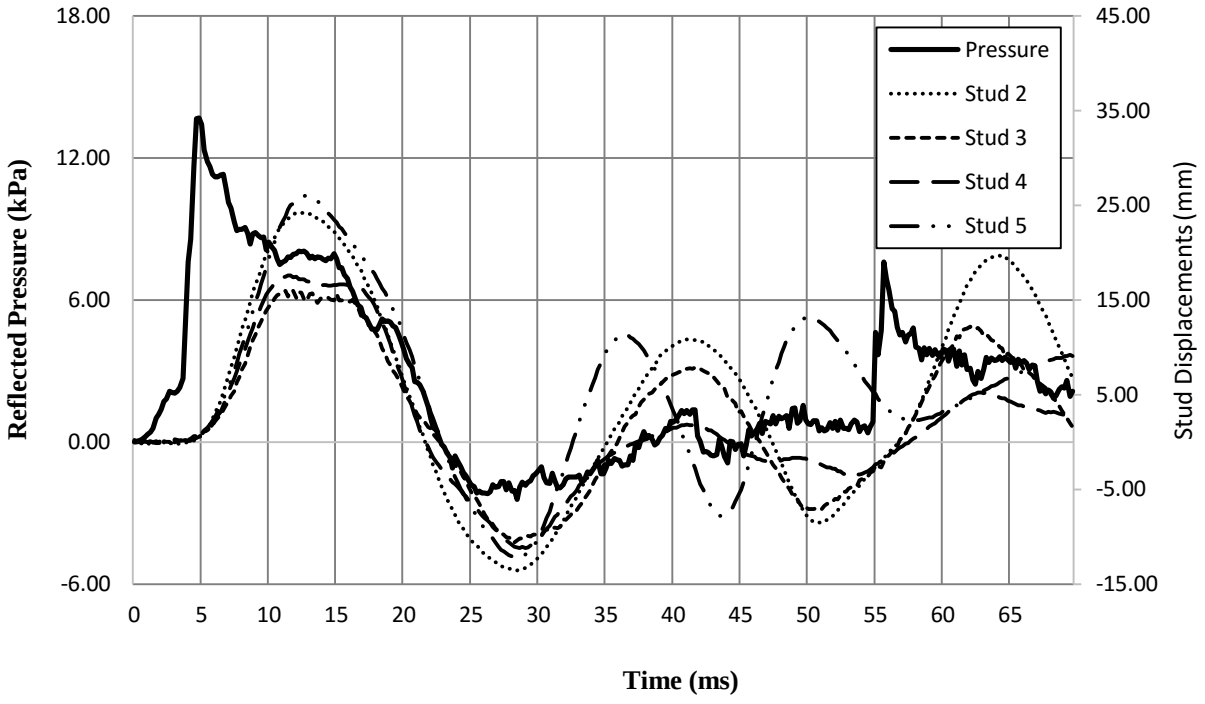

Figure A1.2 : Reflected pressure and displacement time histories for Wall 1 Shot 1

Test date: 27/6/2014

Test name: Wall_1_Shot_2

Driver length: 2745 mm

Driver pressure: 296.5 kPa

Wall mass: 64.86 kg

Test specimen properties:

- 6-38 mm x 140 mm No. 2 studs @ 406.4 mm o/c
- Nails, 50 mm x 2.87 mm @ 150 mm o/c (field and edge)
- 2108 mm total length of wall
- 2032 mm long studs
- 2032 mm clear span
- 11 mm OSB

Average maximum reflected pressure: 54.2 kPa

Average max. deflection of wall studs: 53.08 mm

Average maximum reflected impulse: 408.1 kPa-ms

Average time to max. deflection: 7.2 ms

Positive phase duration: 17.2 ms

Quantified wall damage level: Blowout

Table A1.2 : Stud data from Wall 1 Shot 2

Stud number	Stud reference ID	Maximum mid-span displacement	Time to Maximum	Debris projection	Stud damage level
		mm	ms	mm	
1	S237	-	-	No debris	Failed
2	S160	48.39	6.8	5000	Failed
3	S174	65.72	8.8	3000	Failed
4	S181	39.33	6.2	No debris	Failed
5	S187	58.88	7.0	No debris	Failed
6	S238	-	-	No debris	Cracked

Comments:

Stud 1 failed brashly at mid-span with splitting occurring in both halves. Stud 2 and 3 failed brashly with their top-halves being ejected from the wall. Stud 4 also failed brashly but its top-half remained attached to the top-plate. Splitting was also observed in both halves for Stud 4. Stud 5 experienced flexural failure near its bottom third point and did not create any debris. Stud 6 did not directly fail but lost a good portion of its effective cross-section due to spalling occurring near its mid-span.

Two of the six studs produced hazardous debris, with ejection length varying from 3000 to 5000 mm. Approximately 50% of the sheathing was ripped and blown out of the wall, which created sheathing debris. Nail withdrawal and pull-out was observed on all studs. There was significant warping in both plates due to uneven rotation in the studs. This is however due to the fact that the pressure wave is in fact not uniform when striking the wall. Two LVDTs perforated the sheathing due to extreme wall displacement.

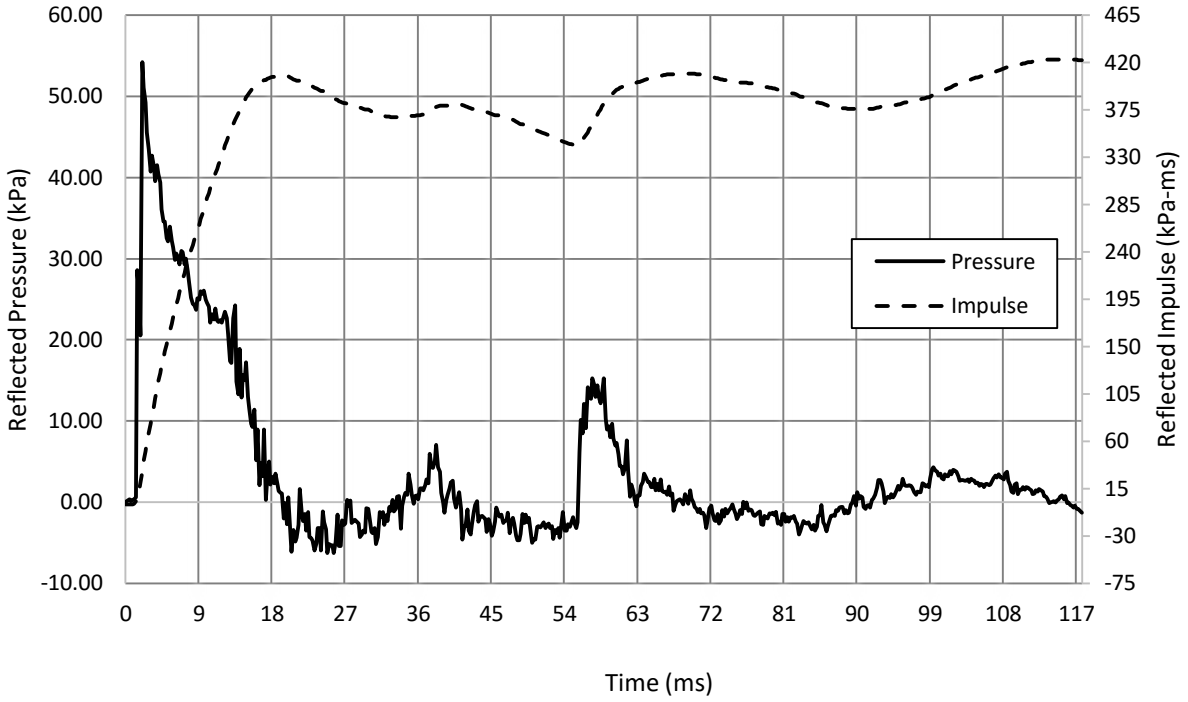

Figure A1.3 : Reflected pressure and impulse time histories for Wall 1 Shot 2

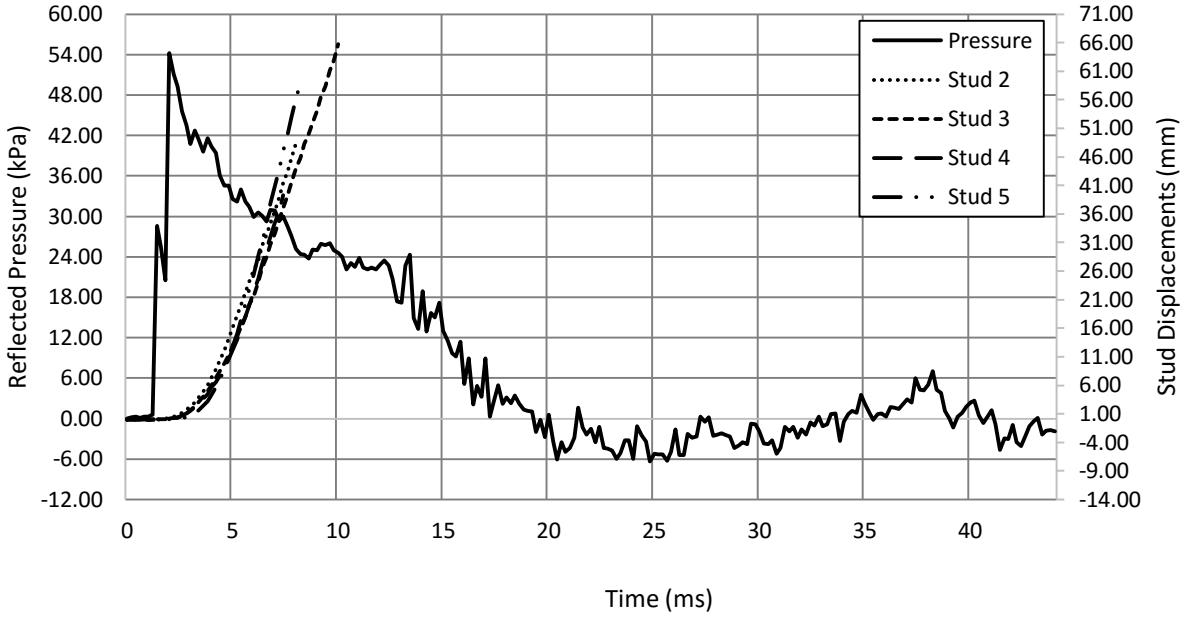

Figure A1.4 : Reflected pressure and displacement time histories for Wall 1 Shot 2

a) t = 0 ms

b) t = 6 ms

c) t = 12 ms

d) t = 20 ms

Figure A1.5 : Evolution of damage with time for Wall 1 Shot 2

a) Front view

b) Oblique view

c) Nail withdrawal and head pull-through

Figure A1.6 : Damage of Wall 1 after shot 2

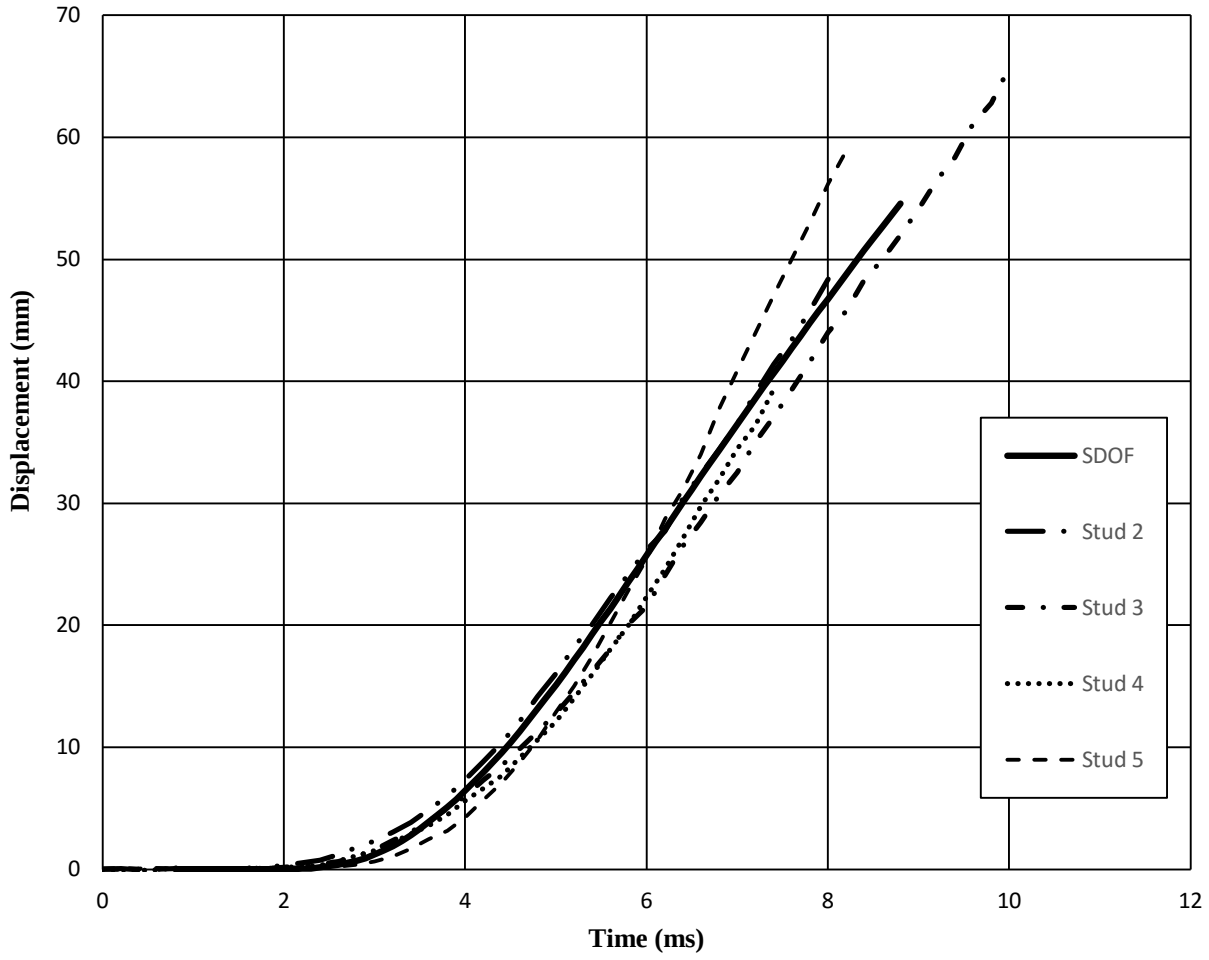

Figure A1.7 : SDOF prediction for Wall 1 Shot 2

Wall 2 Test Summary

Test name: Wall_2_Shot_1 **Test date:** 27/6/2014

Driver length: 2745 mm **Driver pressure:** 275.8 kPa

Wall mass: 70.00 kg

Test specimen properties:

- 6-38 mm x 140 mm No. 2 studs @ 406.4 mm o/c
- Nails, 50 mm x 2.87 mm @ 150 mm o/c (field and edge)
- 2108 mm total length of wall
- 2032 mm long studs
- 2032 mm clear span
- 11 mm OSB

Average maximum reflected pressure: 46.7 kPa **Average max. deflection of wall studs:** 53.67 mm

Average maximum reflected impulse: 354.5 kPa-ms **Average time to max. deflection:** 8.7 ms

Positive phase duration: 17.0 ms **Quantified wall damage level:** Blowout

Table A2.1 : Stud data from Wall 2 Shot 1

Stud number	Stud reference ID	Maximum mid-span displacement	Time to Maximum	Debris projection	Stud damage level
		mm	ms	mm	
1	S171	-	-	No debris	Superficial
2	S152	51.10	9.4	No debris	Superficial
3	S97	54.04	9.2	1000	Failed
4	S203	59.77	7.8	1000	Failed
5	S252	49.77	8.4	No debris	Superficial
6	S142	-	-	No debris	Failed

Comments:

Stud 1, while undamaged, was disconnected at the bottom plate due to general plate rotation (from the other studs bending). Stud 2 remained elastic and did not suffer any damage. This is due to the rupture of the nearby sheathing which did not fully distribute the applied load to that stud. Stud 3 failed at mid-span in a brash fashion and had its top half thrown vertically towards the lab ceiling. The debris was therefore not ejected very far. Stud 4 failed similarly to Stud 3. Stud 5 remained elastic and did not show any signs of damage. Minor crushing of wood was detected near the ends of the studs that remained elastic. Stud 6 failed had moderate flexural damage at mid-span. Approximately 60% of the sheathing was blown out of the wall with the remaining portions being located around Stud 3 and Stud 4 (which permitted them to be loaded until failure). Nail withdrawal was observed on most studs. Major sheathing debris was observed. There was no significant hazard from stud debris since the only debris produced was directed vertically upwards (due to the attachment to the top plate). This test displays that OSB carries a chance of not being able to effectively distribute the airwave to the studs due to it ripping prematurely.

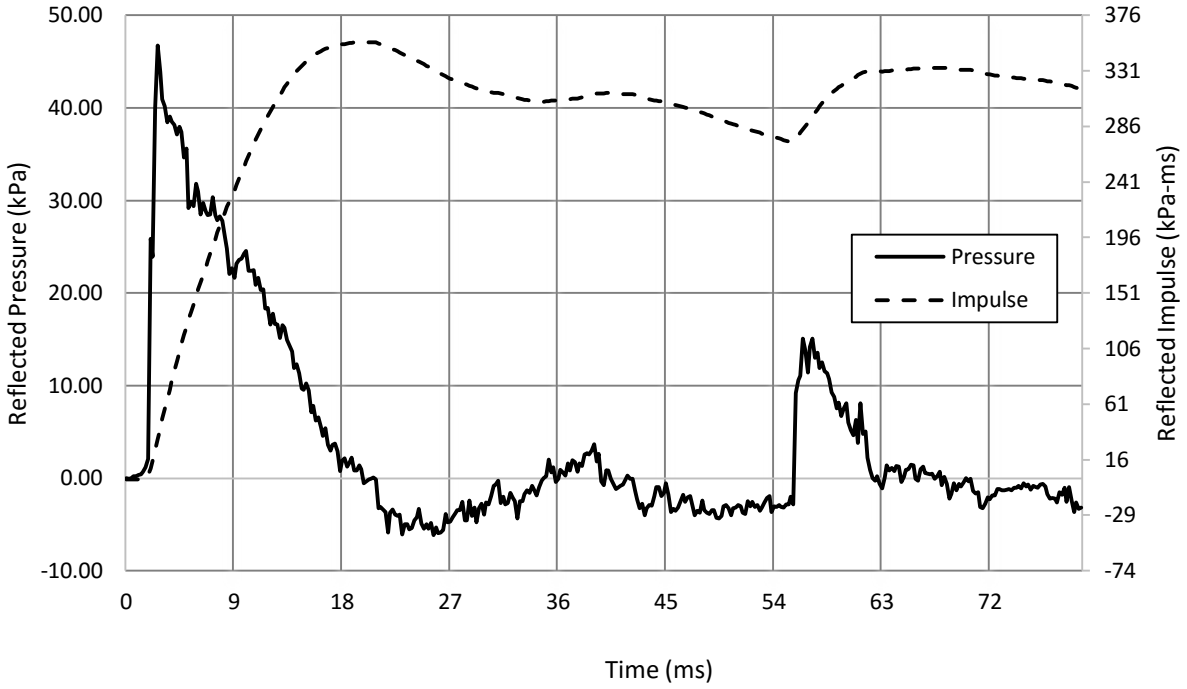

Figure A2.1 : Reflected pressure and impulse time histories for Wall 2 Shot 1

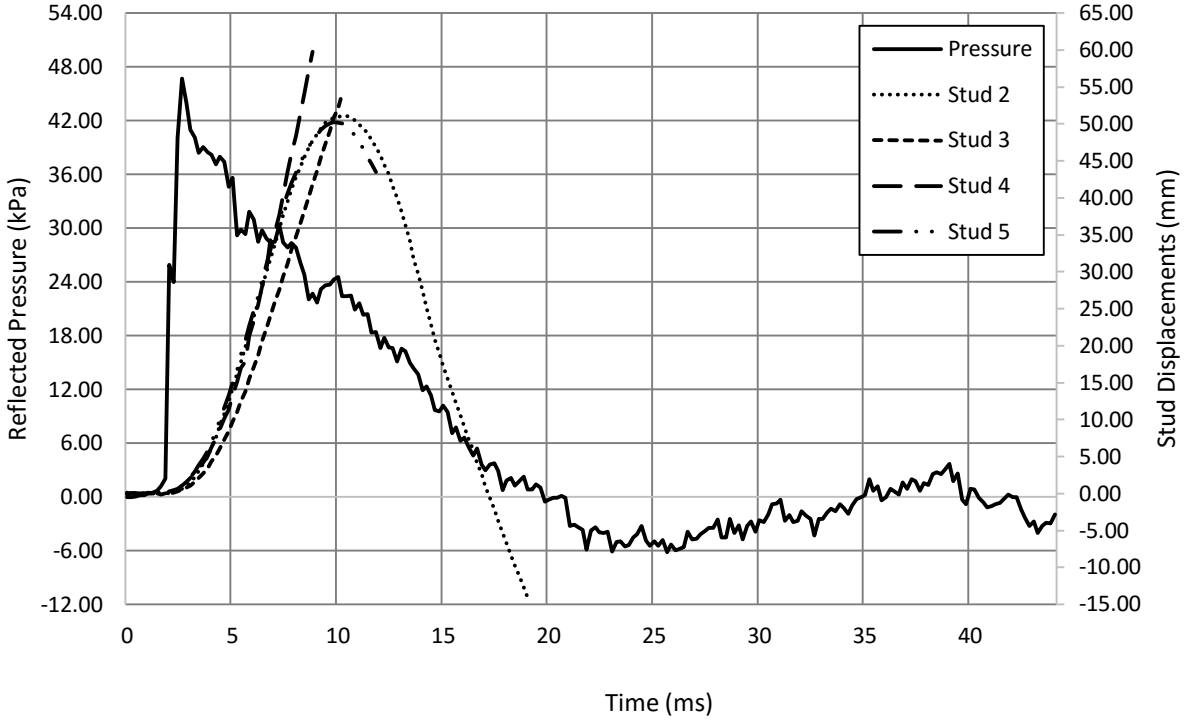

Figure A2.2 : Reflected pressure and displacement time histories for Wall 2 Shot 1

a) t = 0 ms

b) t = 8 ms

c) t = 12 ms

d) t = 24 ms

Figure A2.3 : Evolution of damage with time for Wall 2 Shot 1

a) Front view

b) Brash failure of stud 4

c) Oblique view

Figure A2.4 : Damage of Wall 2 after shot 1

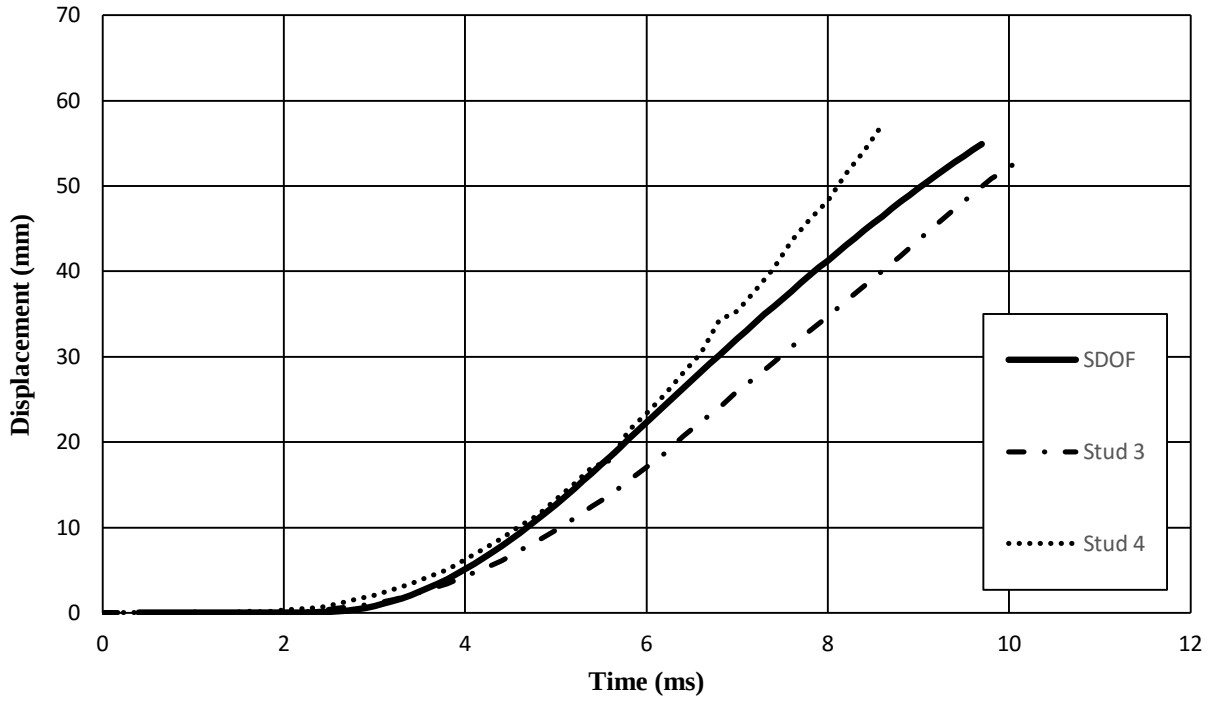

Figure A2.5 : SDOF prediction for Stud 3 and 4 of Wall 2 Shot 1

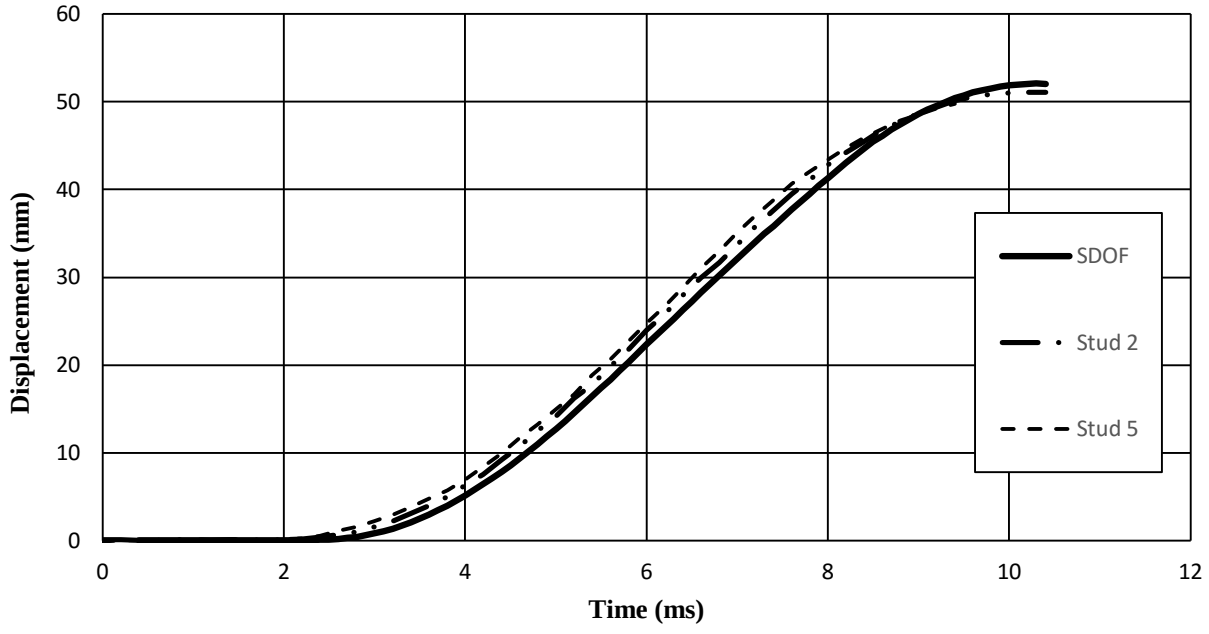

Figure A2.6 : SDOF prediction for Stud 2 and 5 of Wall 2 Shot 1

Wall 3 Test Summary

Test name: Wall_3_Shot_1 **Test date:** 2/7/2014

Driver length: 2745 mm **Driver pressure:** 306.8 kPa

Wall mass: 69.70 kg

Test specimen properties:

- 6-38 mm x 140 mm No. 2 studs @ 406.4 mm o/c
- Nails, 50 mm x 2.87 mm @ 150 mm o/c (field and edge)
- 2108 mm total length of wall
- 2032 mm long studs
- 2032 mm clear span
- 11 mm OSB

Average maximum reflected pressure: 50.5 kPa **Average max. deflection of wall studs:** 58.08 mm

Average maximum reflected impulse: 373.5 kPa-ms **Average time to max. deflection:** 8.3 ms

Positive phase duration: 15.0 ms **Quantified wall damage level:** Blowout

Table A3.1 : Stud data from Wall 3 Shot 1

Stud number	Stud reference ID	Maximum mid-span displacement	Time to Maximum	Debris projection	Stud damage level
		mm	ms	mm	
1	S89	-	-	No debris	Superficial
2	S163	52.09	8.4	No debris	Superficial
3	S83	62.88	9.4	No debris	Failed
4	S233	56.14	6.6	2500	Failed
5	S226	61.20	8.8	No debris	Failed
6	S255	-	-	No debris	Superficial

Comments:

Stud 1 was not damaged but presence of nail withdrawal was observed. Stud 2 remained elastic and did not suffer any damage. This is due to the rupture of the nearby sheathing which did not fully distribute the applied load to that stud. Nail withdrawal was observed on Stud 2, as well as minor crushing of wood near the end points (due to plate rotation). Stud 3 failed suffered flexural failure at mid-span but the two halves remained connected to the wall. Stud 4 failed in a brash fashion and had its top half ejected from the wall. Splitting was observed in the piece that was ejected. Large pieces of sheathing was found to still be attached to Stud 4. Stud 5 showed signs of moderate flexural damage at its mid-span. No presence of damage on Stud 6.

A large portion of the sheathing was blown out of the wall with the remaining portions being located around Stud 3 and Stud 4 (which permitted them to be loaded until failure). Nail withdrawal was observed on most studs. Significant sheathing debris was observed. Stud 4 produced flying debris up to a distance of approximately 2500 mm. This test displays that OSB carries a chance of not being able to effectively distribute the airwave to the studs due to it ripping prematurely.

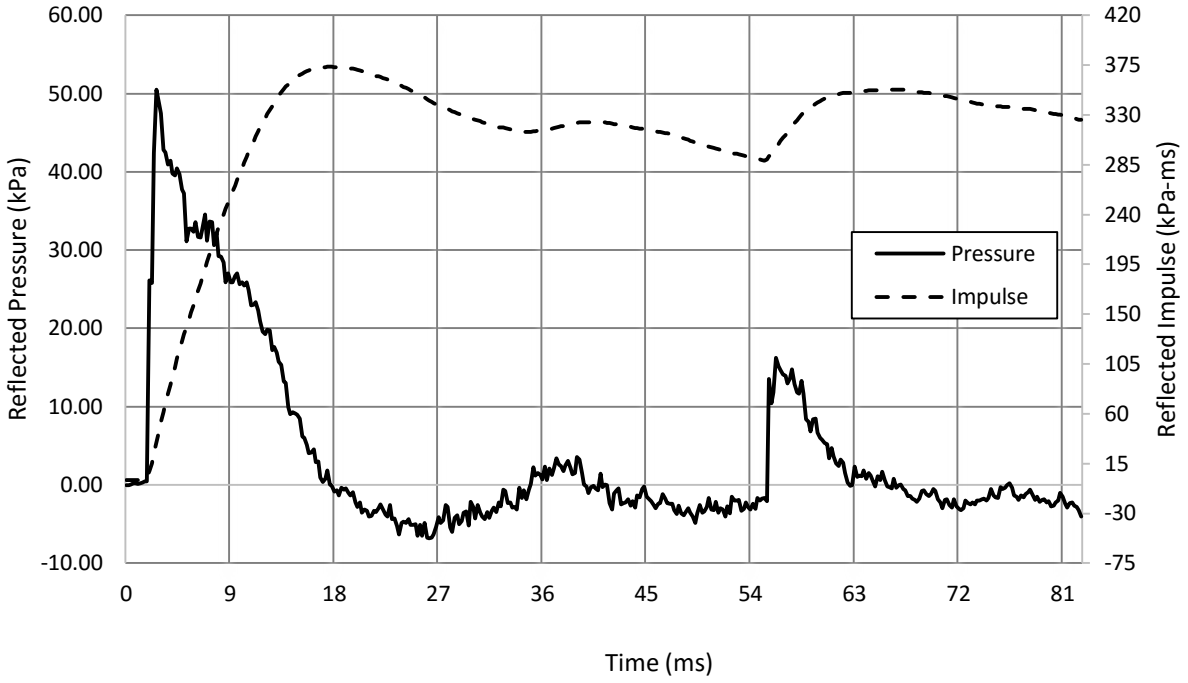

Figure A3.1 : Reflected pressure and impulse time histories for Wall 3 Shot 1

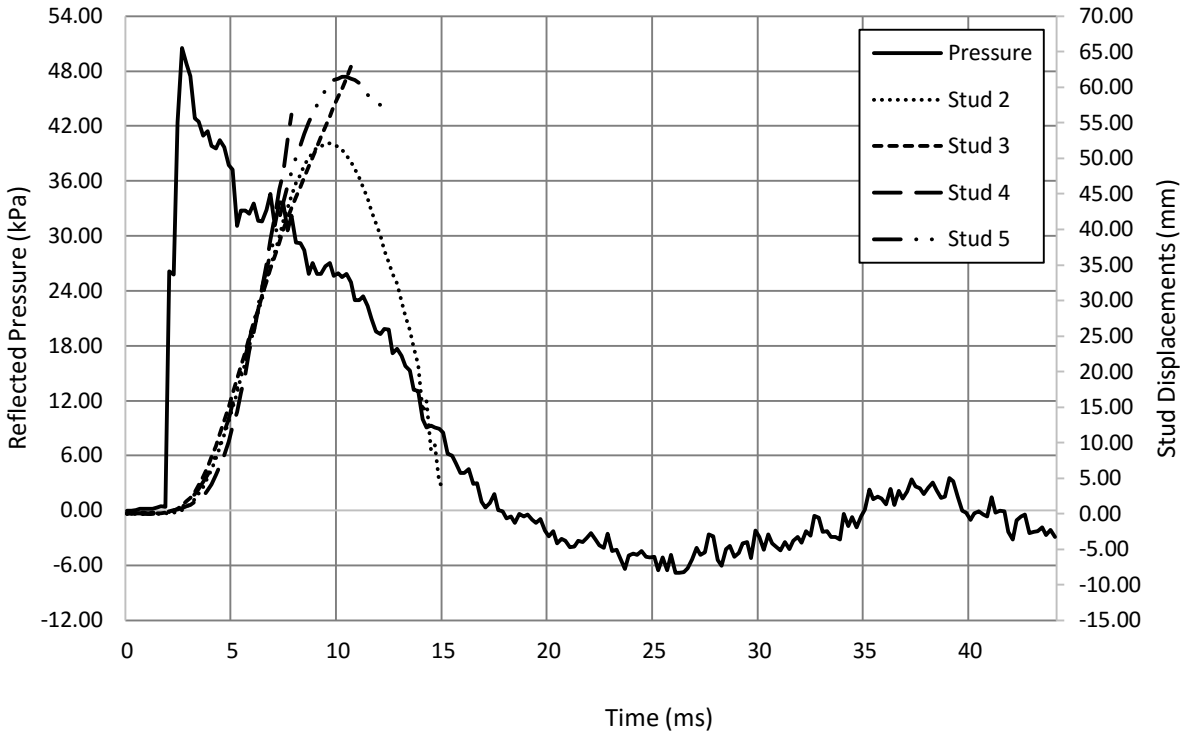

Figure A3.2 : Reflected pressure and displacement time histories for Wall 3 Shot 1

a) t = 0 ms

b) t = 6 ms

c) t = 10 ms

d) t = 18 ms

Figure A3.3 : Evolution of damage with time for Wall 3 Shot 1

a) Front view

b) Oblique view

c) Wall debris

Figure A3.4 : Damage of Wall 3 after shot 1

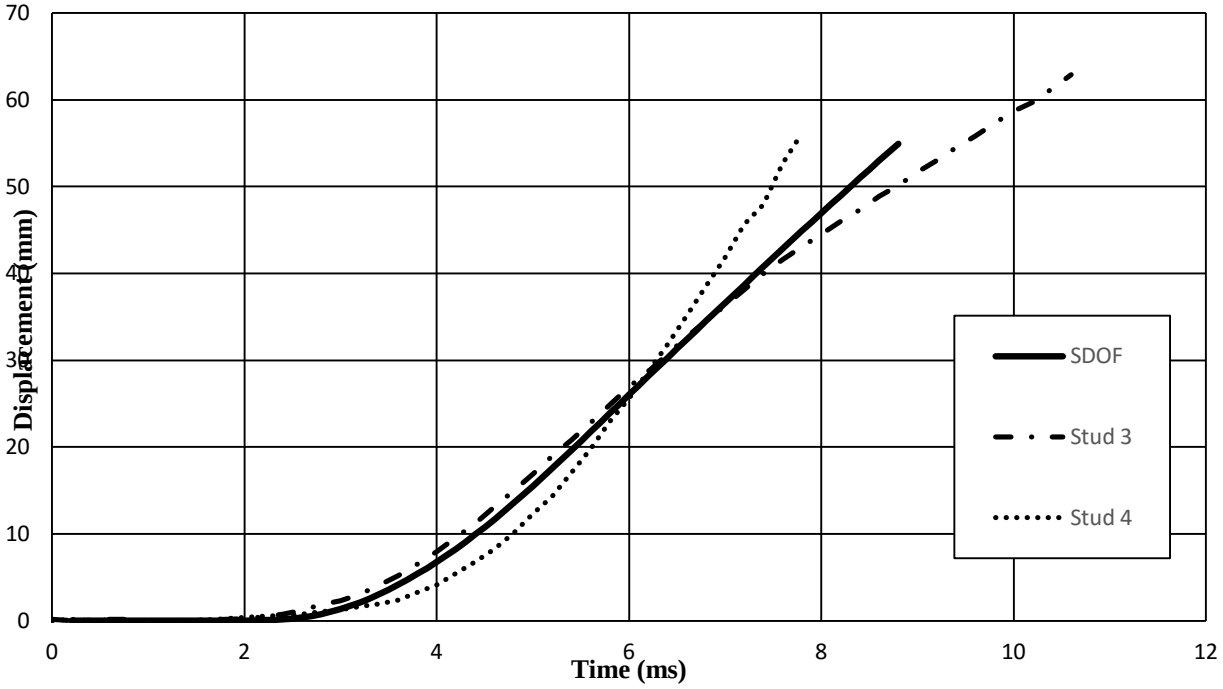

Figure A3.5 : SDOF prediction for Stud 3 and 4 of Wall 3 Shot 1

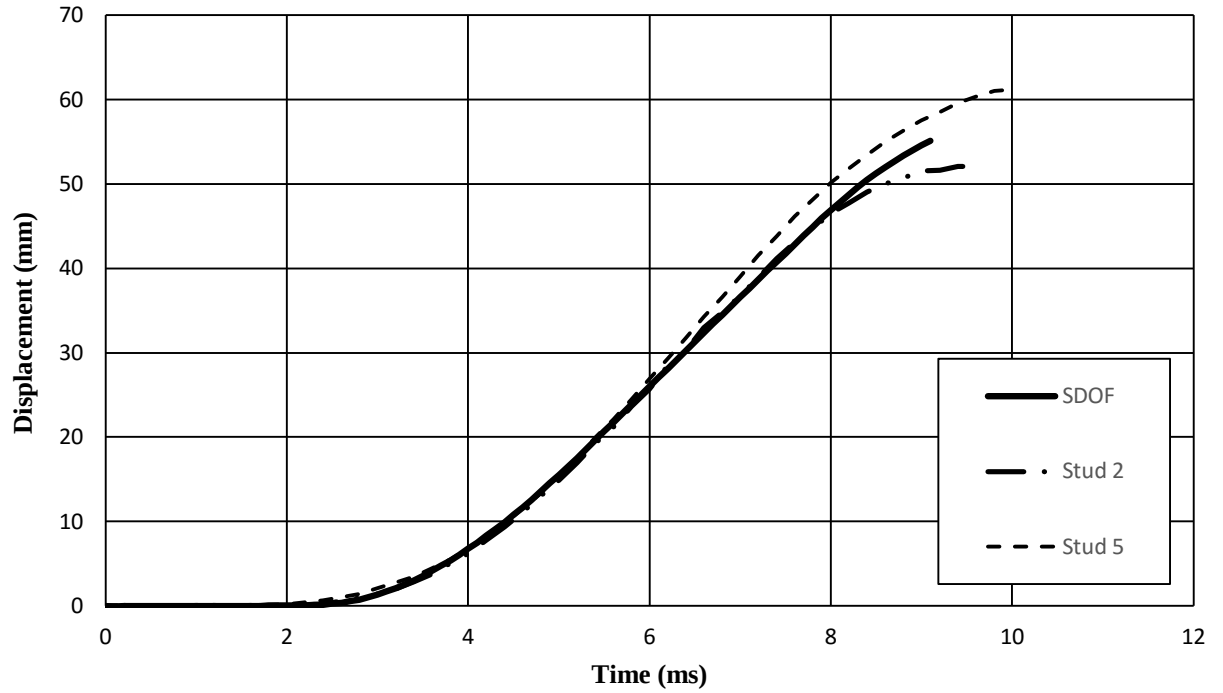

Figure A3.6 : SDOF prediction for Stud 2 and 5 of Wall 3 Shot 1

Wall 4 Test Summary

Test name: Wall_4_Shot_1 **Test date:** 11/7/2014

Driver length: 2745 mm **Driver pressure:** 310.3 kPa

Wall mass: 66.24 kg

Test specimen properties:

- 6-38 mm x 140 mm No. 2 studs @ 406.4 mm o/c
- Nails, 50 mm x 2.87 mm @ 150 mm o/c (field and edge)
- 2108 mm total length of wall
- 2032 mm long studs
- 2032 mm clear span
- 11 mm OSB

Average maximum reflected pressure: 56.4 kPa **Average max. deflection of wall studs:** 52.17 mm

Average maximum reflected impulse: 407.0 kPa-ms **Average time to max. deflection:** 8.1 ms

Positive phase duration: 15.2 ms **Quantified wall damage level:** Blowout

Table A4.1 : Stud data from Wall 4 Shot 1

Stud number	Stud reference ID	Maximum mid-span displacement	Time to Maximum	Debris projection	Stud damage level
		mm	ms	mm	
1	S240	-	-	No debris	Cracking
2	S177	-	-	6250	Failed
3	S153	53.06	9.0	4500	Failed
4	S210	50.51	8.0	No debris	Failed
5	S232	52.95	7.2	1000	Failed
6	S218	-	-	No debris	Cracking

Comments:

Stud 1 and 6, the two end studs, were subjected to some kind of torsion about their longitudinal axis. While they did not show signs of flexural failure, their boundary conditions with the plates were compromised. Stud 2 failed at mid-span with the top half being ejected. Nail puncture observed. Stud 3 failed at mid-span in a brash fashion and was completely blown out of the wall. Stud 4 had flexural damage at its extreme fibre and was deemed to have failed. The reason for this is that the sheathing did not withstand enough pressure for the stud to have received the same amount of force as the other studs. Stud 5 failed brashly and had its top half ejected.

Majority of sheathing was blown out of the wall with only small top and bottom pieces still connected to the wall. Stud 4 did not completely receive full loading due to early failure of the sheathing. Nail withdrawal was observed on most studs. Major sheathing debris was observed. Three of the six studs produced hazardous debris, with projection lengths varying from 1000 mm to 6250 mm (the debris of Stud 2 struck the lab wall). These lengths are conservatives since the LVDT support bracket came into contact with some of the flying debris. The LVDT for Stud 2 did not record properly and therefore no displacement data for that stud was obtained.

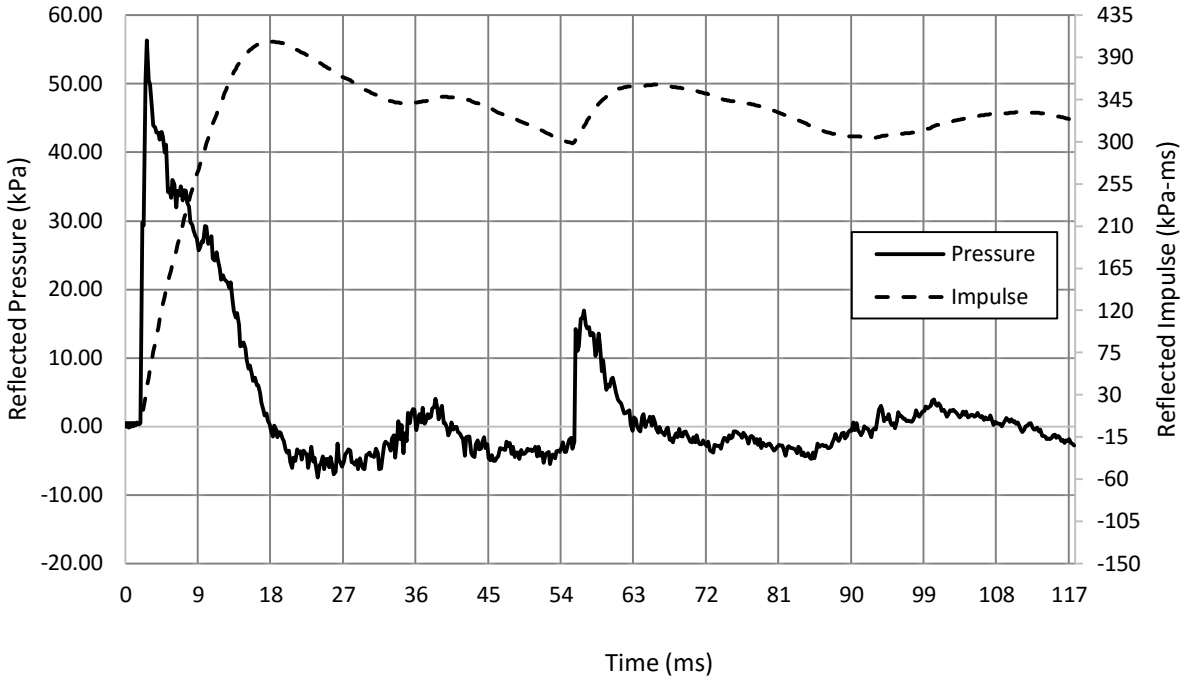

Figure A4.1 : Reflected pressure and impulse time histories for Wall 4 Shot 1

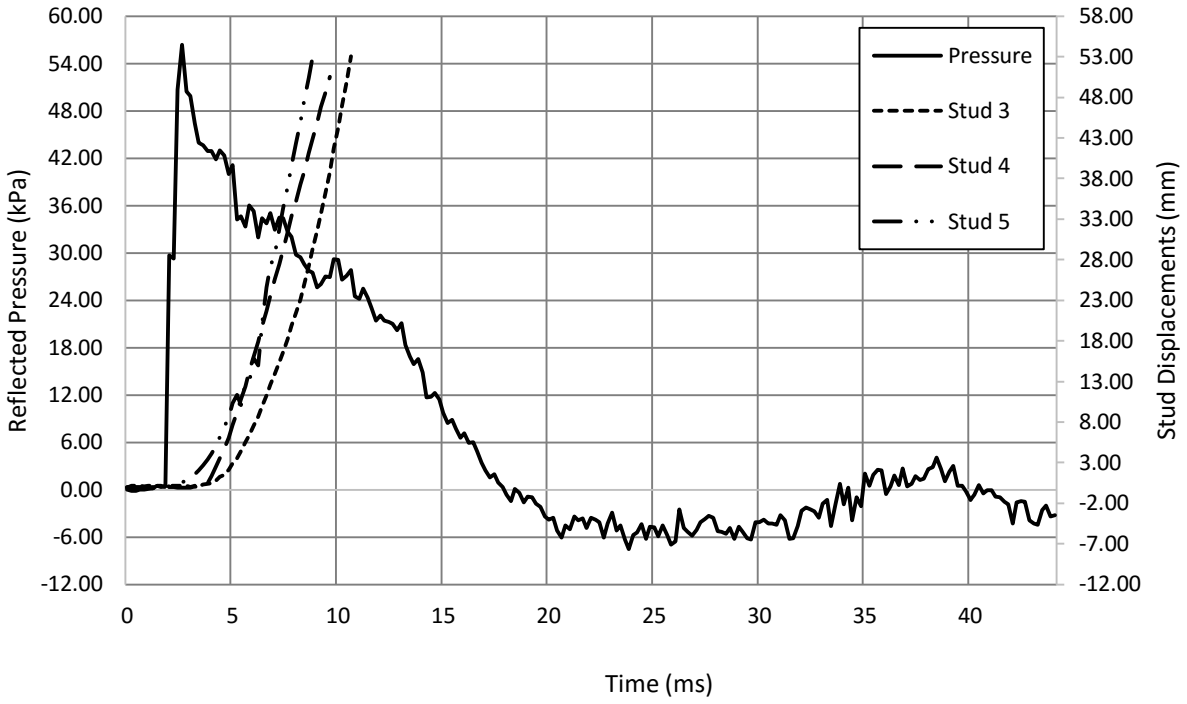

Figure A4.2 : Reflected pressure and displacement time histories for Wall 4 Shot 1

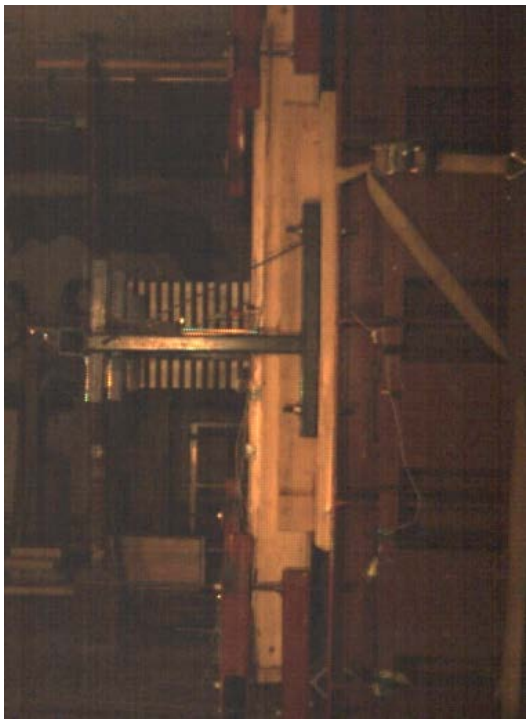

a) t = 0 ms

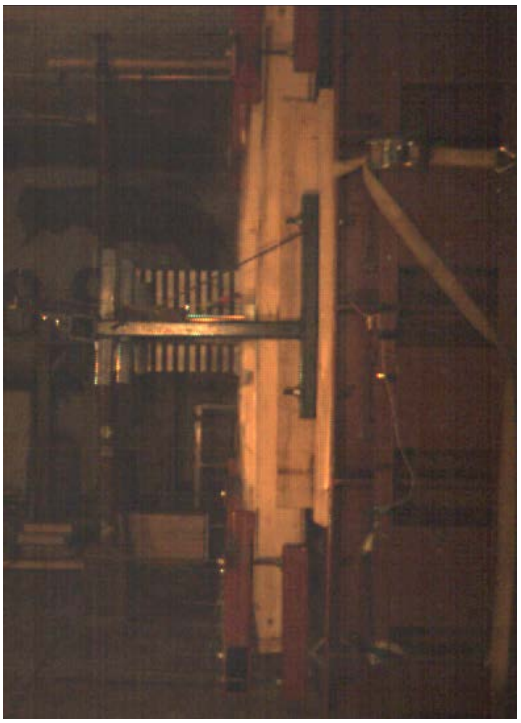

b) t = 6 ms

c) t = 12 ms

d) t = 24 ms

Figure A4.3 : Evolution of damage with time for Wall 4 Shot 1

a) Front view

b) Brash failure of Stud 5

c) Wall debris

Figure A4.4 : Damage of Wall 4 after shot 1

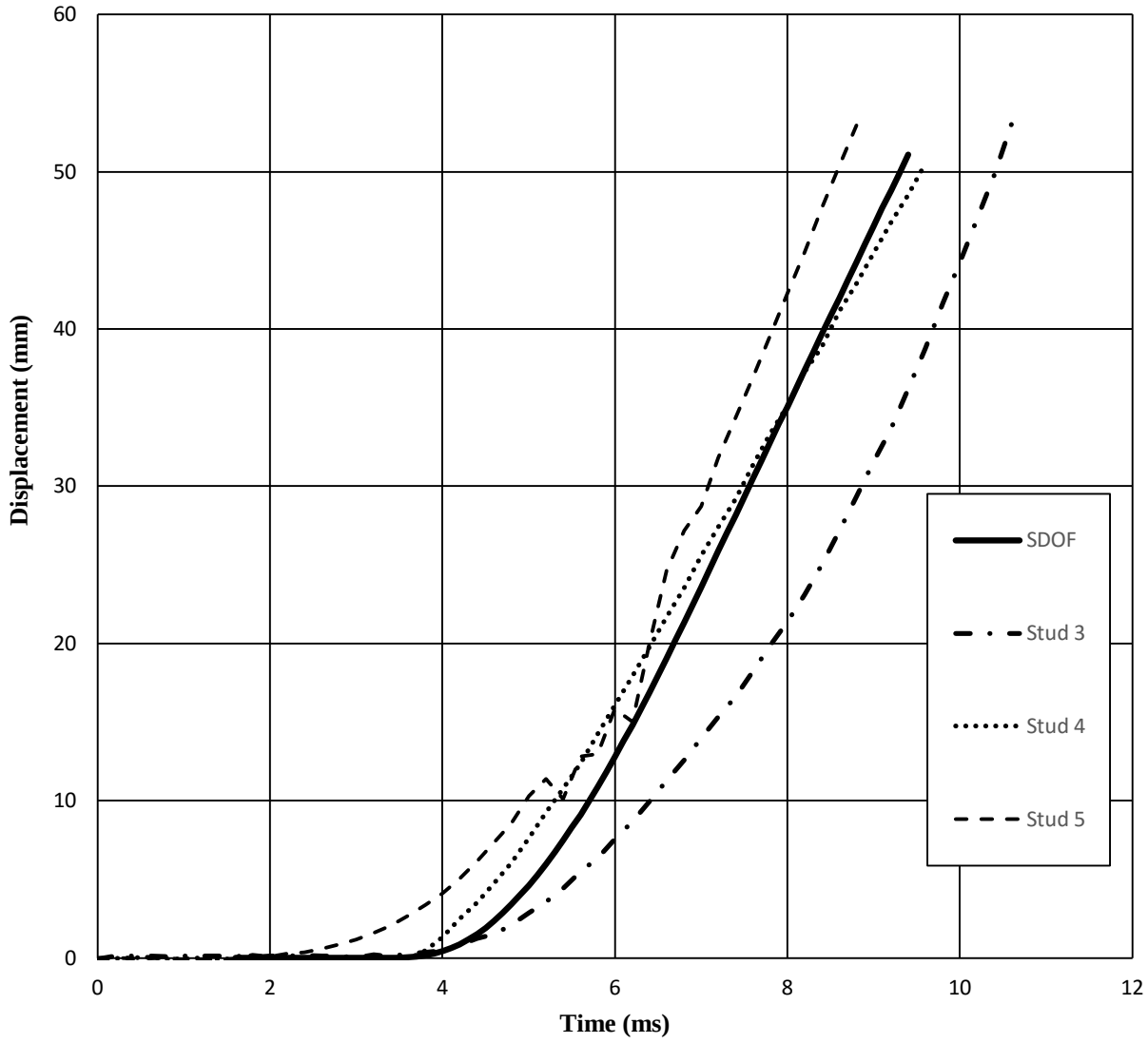

Figure A4.5 : SDOF prediction for Wall 4 Shot 1

Wall 5 Test Summary

Test name: Wall_5_Shot_1 **Test date:** 17/7/2014

Driver length: 2745 mm **Driver pressure:** 275.8 kPa

Wall mass: 73.44 kg

Test specimen properties:

- 6-38 mm x 140 mm No. 2 studs @ 406.4 mm o/c
- Nails, 50 mm x 2.87 mm @ 150 mm o/c (field and edge)
- 2108 mm total length of wall
- 2032 mm long studs
- 2032 mm clear span
- 18.5 mm plywood

Average maximum reflected pressure: 48.1 kPa **Average max. deflection of wall studs:** 55.04 mm

Average maximum reflected impulse: 428.95 kPa-ms **Average time to max. deflection:** 8.2 ms

Positive phase duration: 19.8 ms **Quantified wall damage level:** Blowout

Table A5.1 : Stud data from Wall 5 Shot 1

Stud number	Stud reference ID	Maximum mid-span displacement	Time to Maximum	Debris projection	Stud damage level
		mm	ms	mm	
1	S213	-	-	300	Failed
2	S204	55.04	8.2	4200	Failed
3	S111	-	-	350	Failed
4	S207	-	-	2500	Failed
5	S144	-	-	No debris	Failed
6	S224	-	-	No debris	Superficial

Comments:

Stud 1 failed at mid-span with the top section being projected. Stud 2 failed at mid-span with the bottom half being projected and the top half splitting down its center. Stud 3 failed in a brash fashion and was completely projected from the wall. Stud 4 failed in a brash fashion at mid-span with its top half being projected. Stud 5 failed at the top third section

The smaller sheathing piece experienced flexural failure at mid-span, coinciding with the failure line of Stud 1, 2, and 3. No rebound was observed in the smaller piece. The larger sheathing piece experienced rebound and very little local damage at Stud 3 (sheathing joint).

No sheathing debris was observed. Four of the six studs produced hazardous debris, with projection lengths varying from 300 mm to 4200 mm. These lengths are conservatives since the LVDT support bracket came into contact with most of the flying debris. Nail withdrawal was observed. The LVDTs for Stud 3, 4, and Stud 5 did not record properly and therefore no displacement data for these studs were obtained.

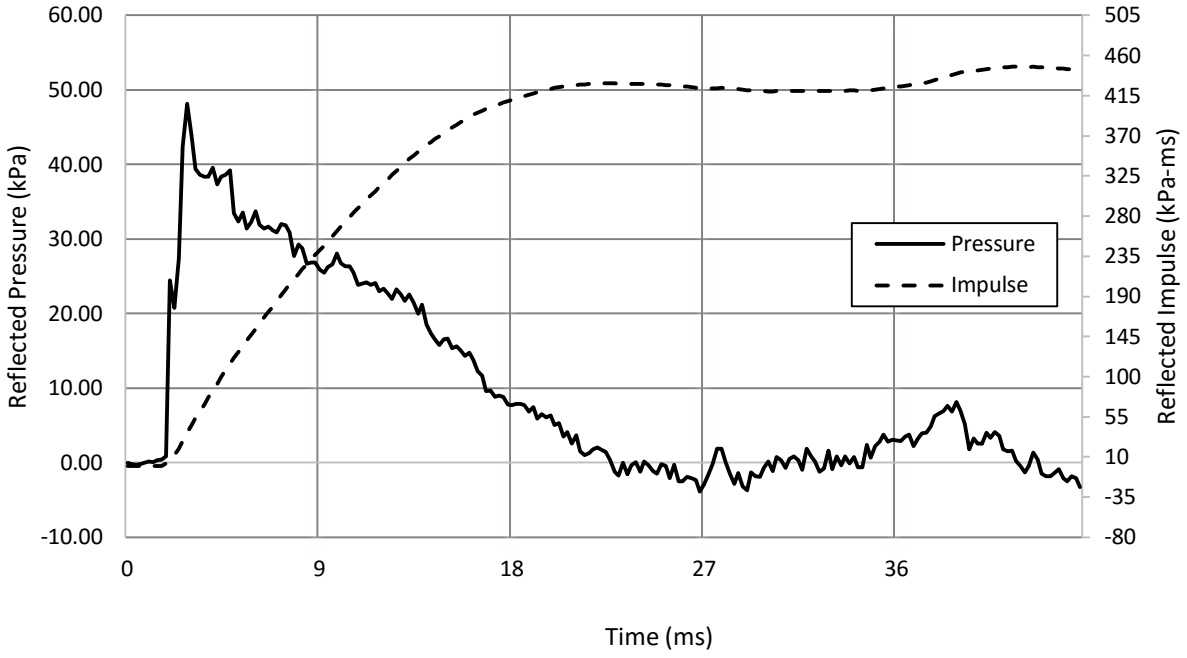

Figure A5.1 : Reflected pressure and impulse time histories for Wall 5 Shot 1

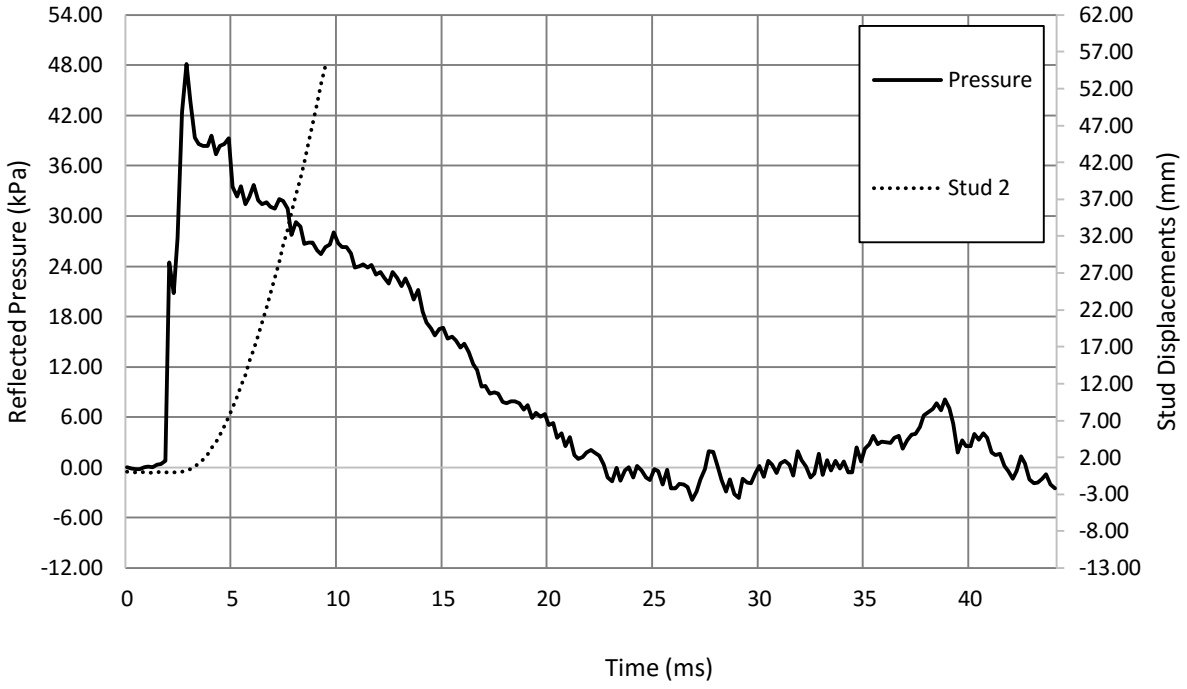

Figure A5.2 : Reflected pressure and displacement time histories for Wall 5 Shot 1

a) t = 0 ms

b) t = 8 ms

c) t = 14 ms

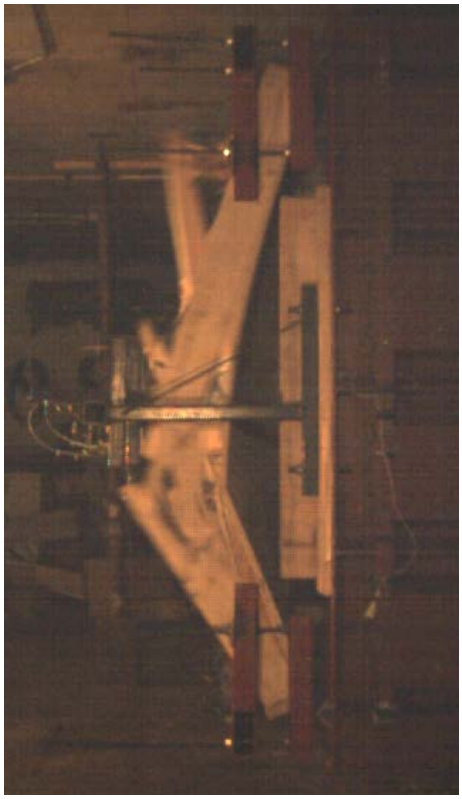

d) t = 22 ms

Figure A5.3 : Evolution of damage with time for Wall 5 Shot 1

a) Front view

b) Side view

c) Damage to plywood panel

d) Nail head pull-through

Figure A5.4 : Damage of Wall 5 after shot 1

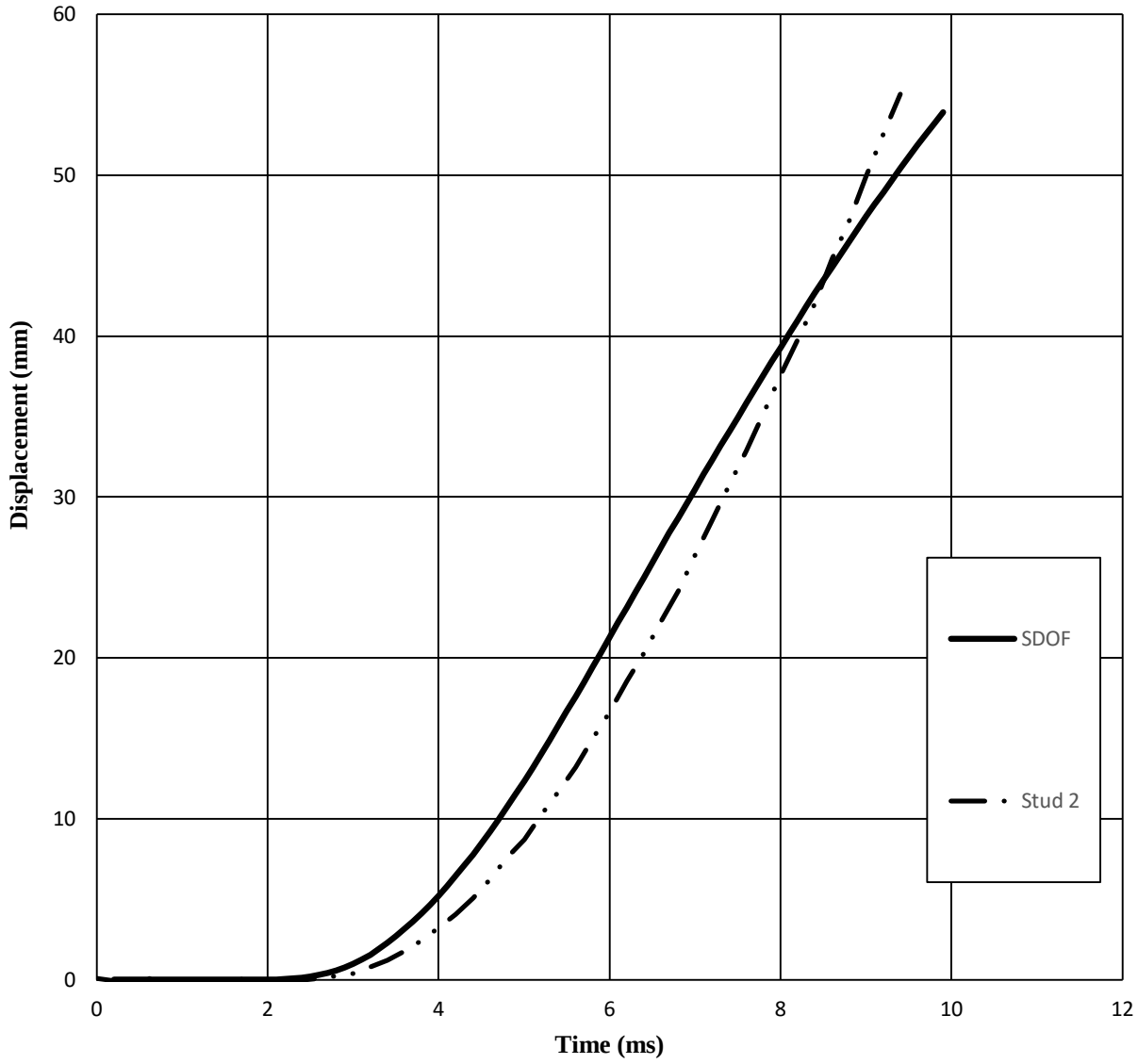

Figure A5.5 : SDOF prediction for Wall 5 Shot 1

Wall 6 Test Summary

Test name: Wall_6_Shot_1 **Test date:** 17/7/2014

Driver length: 2745 mm **Driver pressure:** 282.7 kPa

Wall mass: 71.30 kg

Test specimen properties:

- 6-38 mm x 140 mm No. 2 studs @ 406.4 mm o/c
- Nails, 50 mm x 2.87 mm @ 150 mm o/c (field and edge)
- 2108 mm total length of wall
- 2032 mm long studs
- 2032 mm clear span
- 18.5 mm plywood

Average maximum reflected pressure: 47.3 kPa **Average max. deflection of wall studs:** 52.35 mm

Average maximum reflected impulse: 437.23 kPa-ms **Average time to max. deflection:** 9.4 ms

Positive phase duration: 19.4 ms **Quantified wall damage level:** Blowout

Table A6.1 : Stud data from Wall 6 Shot 1

Stud number	Stud reference ID	Maximum mid-span displacement	Time to Maximum	Debris projection	Stud damage level
		mm	ms	mm	
1	S221	-	-	No debris	Failed
2	S208	-	-	1500	Failed
3	S200	-	-	No debris	Failed
4	S209	52.70	8.8	1000	Failed
5	S222	52.00	10.0	No debris	Failed
6	S170	-	-	1100	Failed

Comments:

Stud 1 failed at mid-span with no debris being projected. Stud 2 failed at mid-span with the top half being projected. Clear view of the wood fibres at the flexural failure site. Stud 3 failed in a brash fashion with splitting occurring in both halves. Stud 4 failed in a brash fashion with no debris. Clear view of wood fibres at failure site .Stud 5 failed at mid-span with splitting occurring in both halves towards the ends. Stud 6 failed in a brash fashion.

A major sheathing rip was present throughout the wall, right below mid-span. This failure line corresponds with the location of failure occurring in the studs. Small localized rips were also observed through the sheathing. The sheathing joint had a significant gap, approximately 50 mm wide.

No sheathing debris was observed. Three of the six studs produced hazardous debris, with projection lengths varying from 1000 mm to 1500 mm. These lengths are conservatives since the LVDT support bracket came into contact with most of the flying debris. Significant nail withdrawal was observed on most studs. The LVDTs for Stud 2 and Stud 3 did not record properly and therefore no displacement data for these studs were obtained.

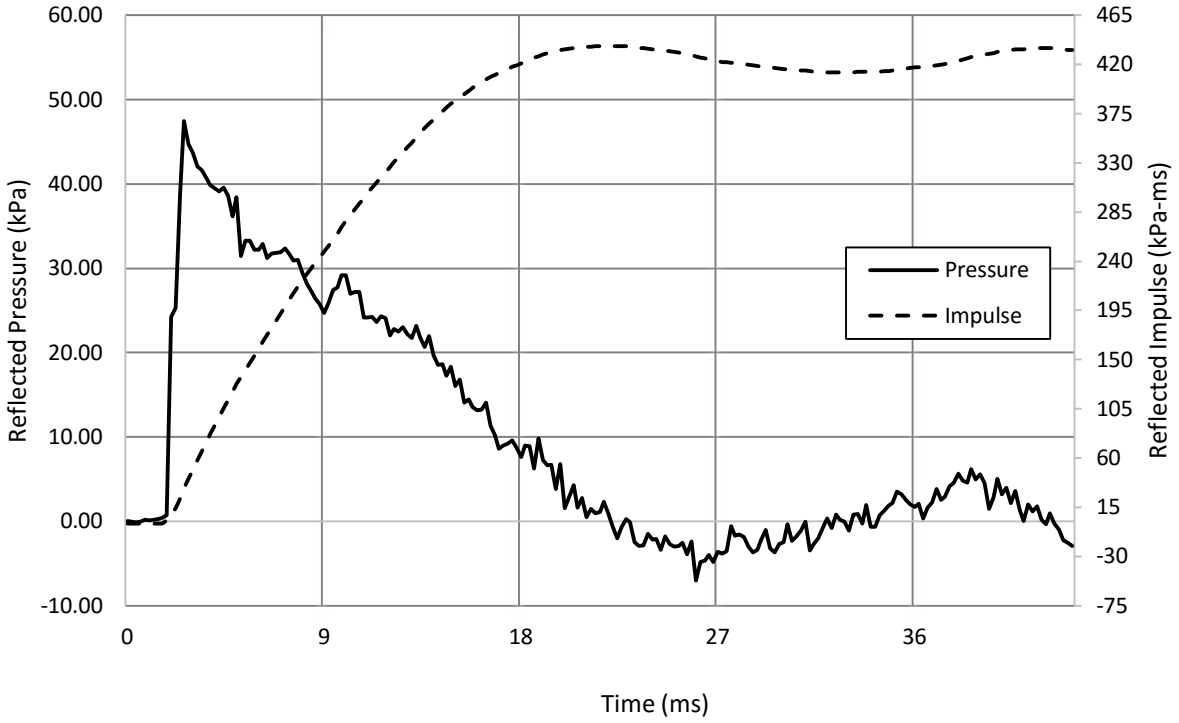

Figure A6.1 : Reflected pressure and impulse time histories for Wall 6 Shot 1

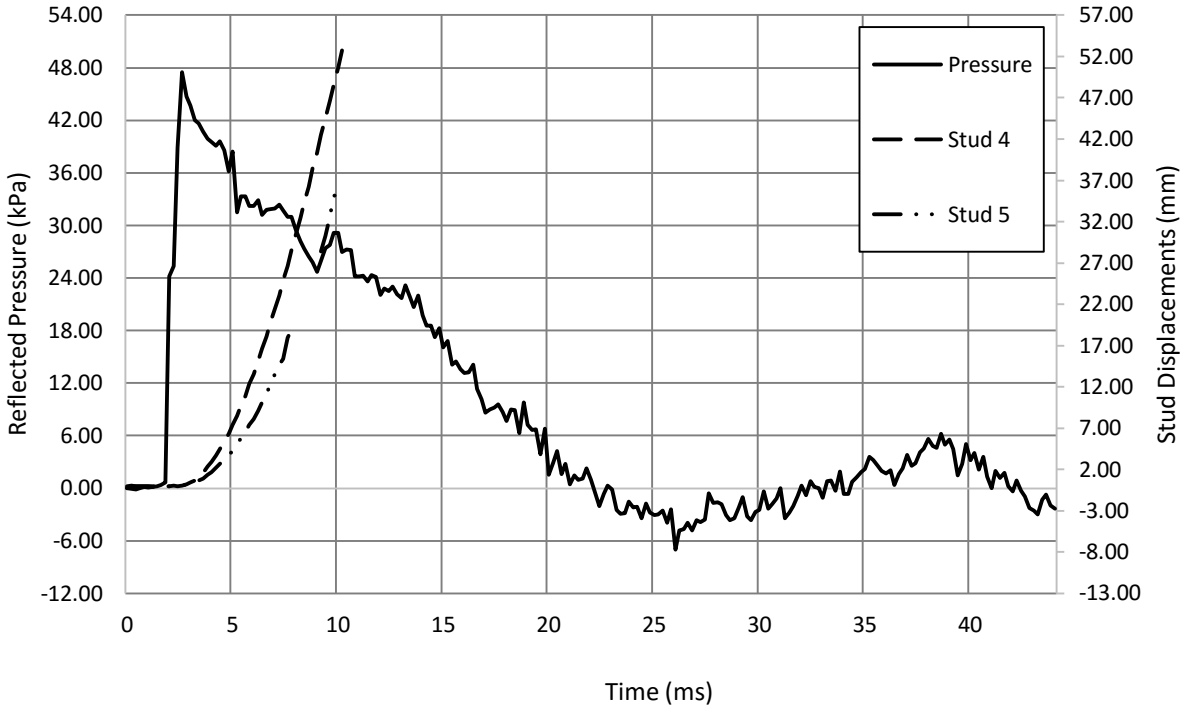

Figure A6.2 : Reflected pressure and displacement time histories for Wall 6 Shot 1

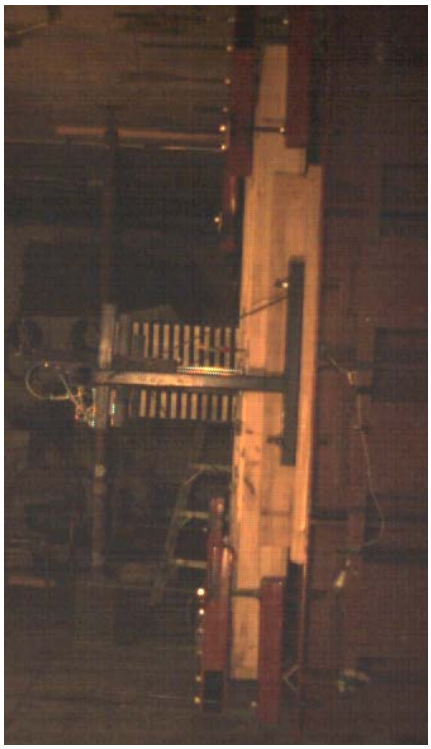

a) t = 0 ms

b) t = 8 ms

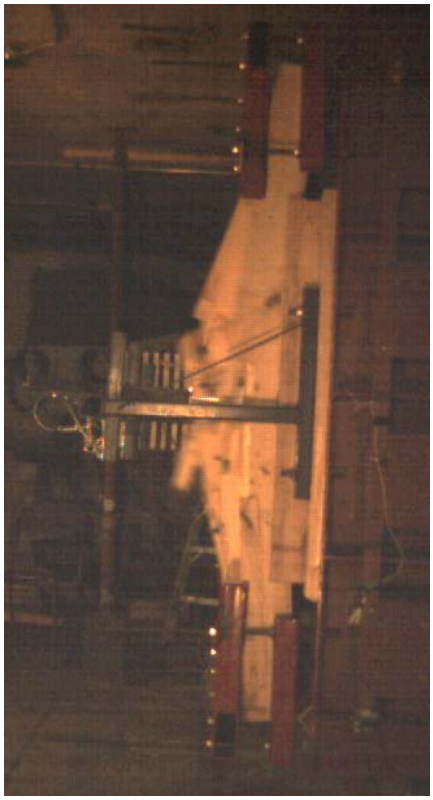

c) t = 14 ms

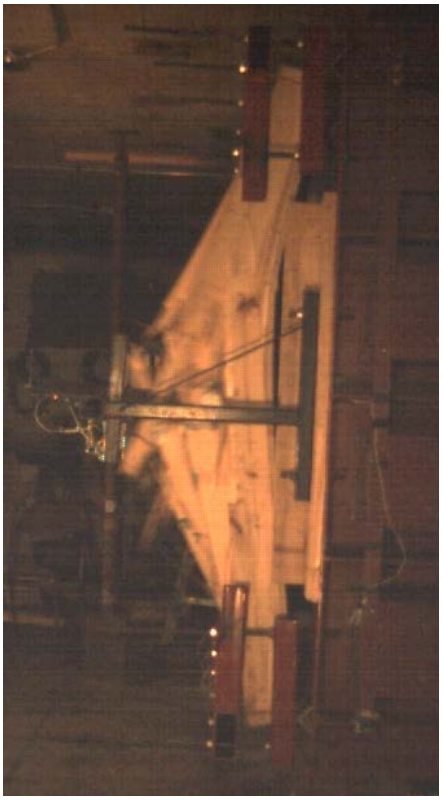

d) t = 22 ms

Figure A6.3 : Evolution of damage with time for Wall 6 Shot 1

a) Front view

b) Oblique view

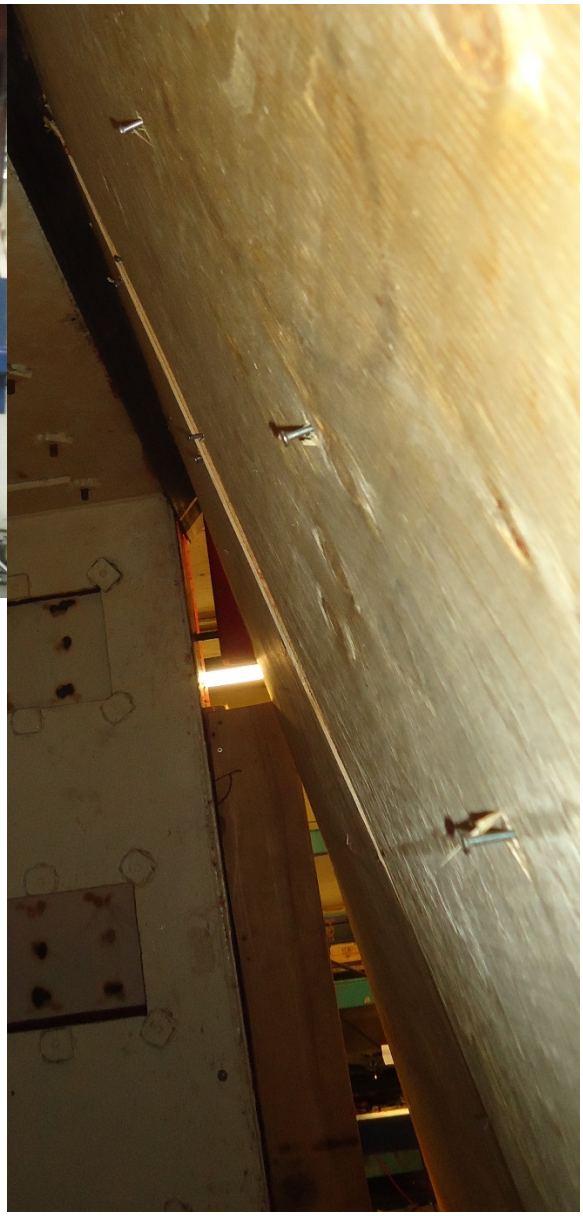

c) Nail withdrawal

Figure A6.4 : Damage of Wall 6 after shot 1

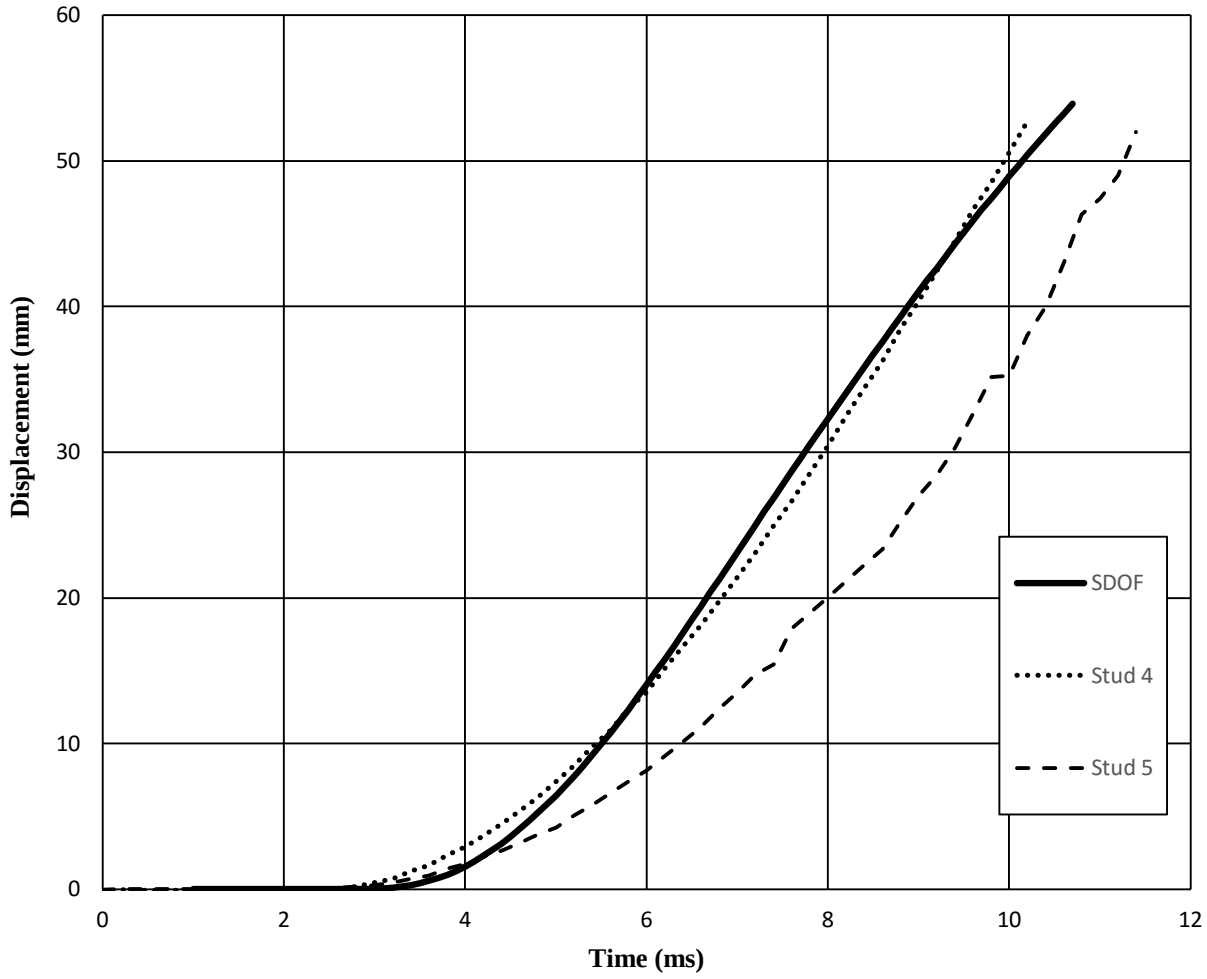

Figure A6.5 : SDOF prediction for Wall 6 Shot 1

Wall 7 Test Summary

Test name: Wall_7_Shot_1 **Test date:** 18/7/2014

Driver length: 2745 mm **Driver pressure:** 282.7 kPa

Wall mass: 72.00 kg

Test specimen properties:

- 6-38 mm x 140 mm No. 2 studs @ 406.4 mm o/c
- Nails, 50 mm x 2.87 mm @ 150 mm o/c (field and edge)
- 2108 mm total length of wall
- 2032 mm long studs
- 2032 mm clear span
- 18.5 mm plywood

Average maximum reflected pressure: 48.3 kPa **Average max. deflection of wall studs:** 52.60 mm

Average maximum reflected impulse: 434.19 kPa-ms **Average time to max. deflection:** 8.4 ms

Positive phase duration: 19.6 ms **Quantified wall damage level:** Blowout

Table A7.1 : Stud data from Wall 7 Shot 1

Stud number	Stud reference ID	Maximum mid-span displacement	Time to Maximum	Debris projection	Stud damage level
		mm	ms	mm	
1	S154	-	-	1500	Failed
2	S227	53.06	8.0	2000	Failed
3	S191	52.14	8.8	2000	Failed
4	S162	-	-	4000	Failed
5	S214	-	-	3000	Failed
6	S189	-	-	No debris	Failed

Comments:

Stud 1 failed at mid-span with the top-half being projected and with splitting occurring in both halves. Stud 2 failed at mid-span with the top half being projected. Stud 3 failed near its mid-span with the top-half being projected. Stud 4 failed in a brash fashion with its top half being projected and observable splitting in both halves. Stud 5 failed in a brash fashion with the top-half being split and projected. Stud 6 failed at mid-span with no projected debris. The stud failure line is relatively clear.

A major sheathing rip was present throughout the wall, near mid-span. This failure line corresponds with the location of failure occurring in the studs. Large discontinuity in the sheathing rip at the location of Stud 5. Overall severe sheathing failure.

No sheathing debris was observed. Five of the six studs produced hazardous debris, with projection lengths varying from 1500 mm to 4000 mm. These lengths are conservatives since the LVDT support bracket came into contact with some of the flying debris. Significant nail withdrawal was observed on most studs. The LVDTs for Stud 4 and Stud 5 did not record properly and therefore no displacement data for these studs were obtained.

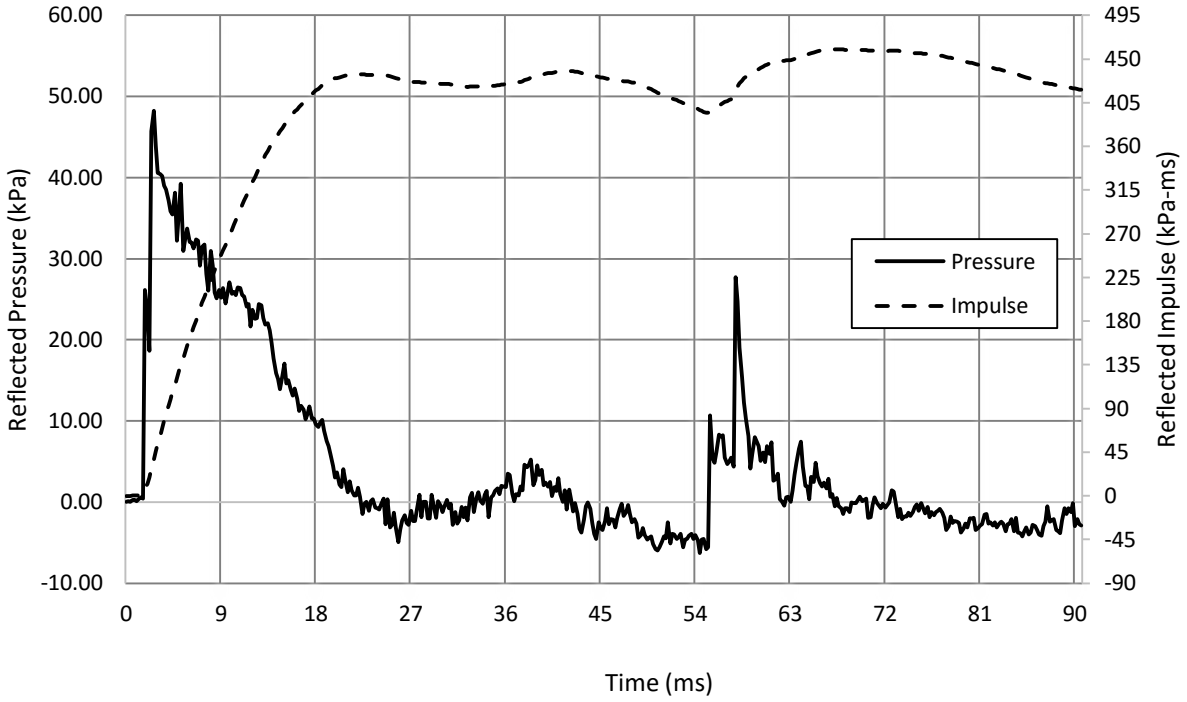

Figure A7.1 : Reflected pressure and impulse time histories for Wall 7 Shot 1

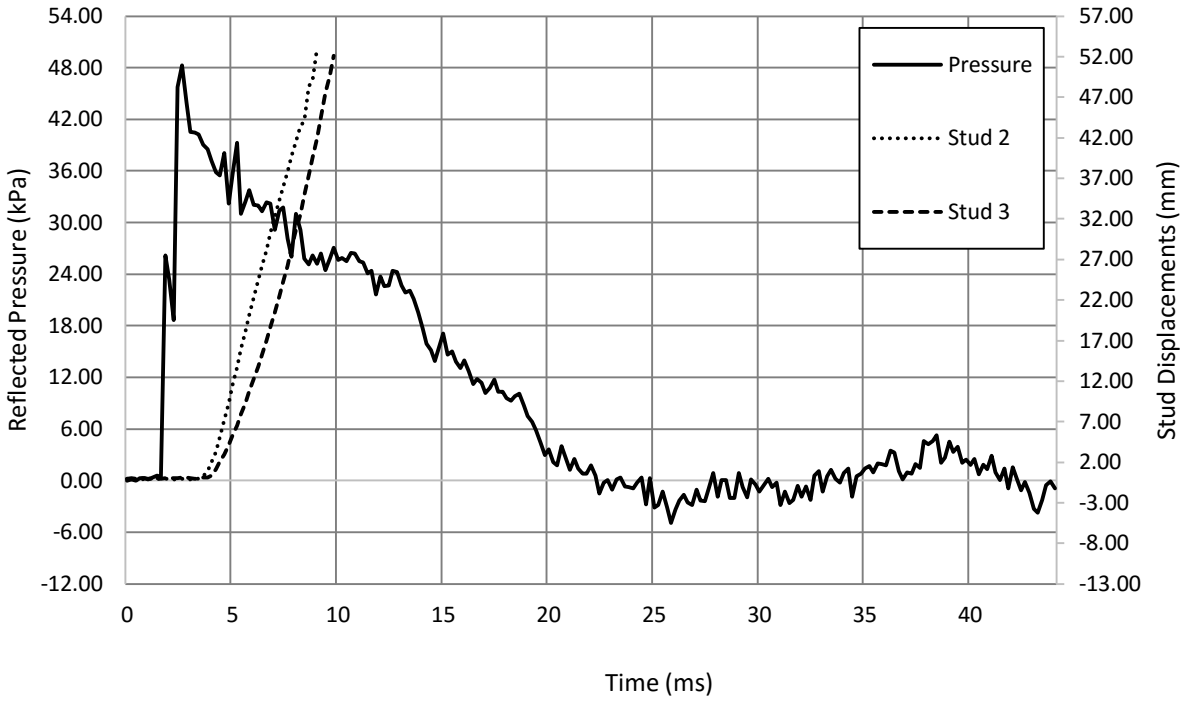

Figure A7.2 : Reflected pressure and displacement time histories for Wall 7 Shot 1

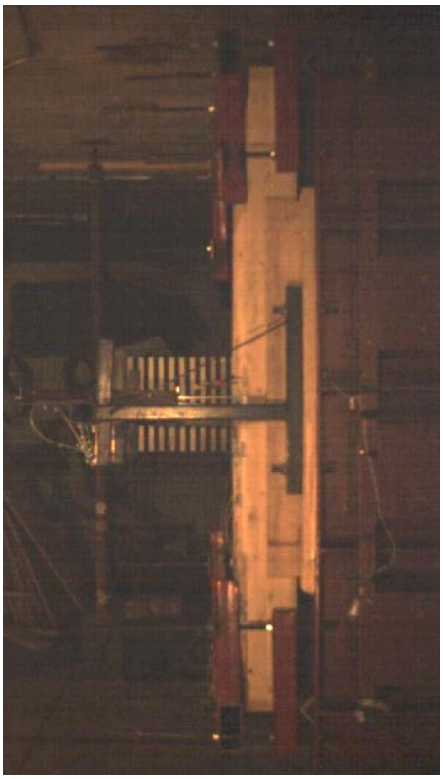

a) t = 0 ms

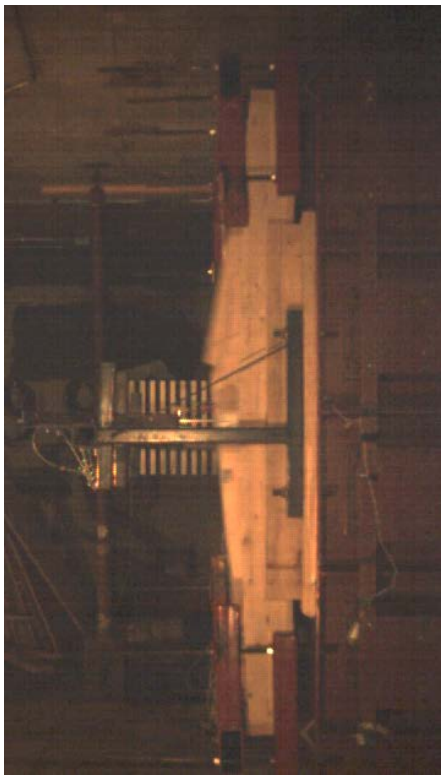

b) t = 6 ms

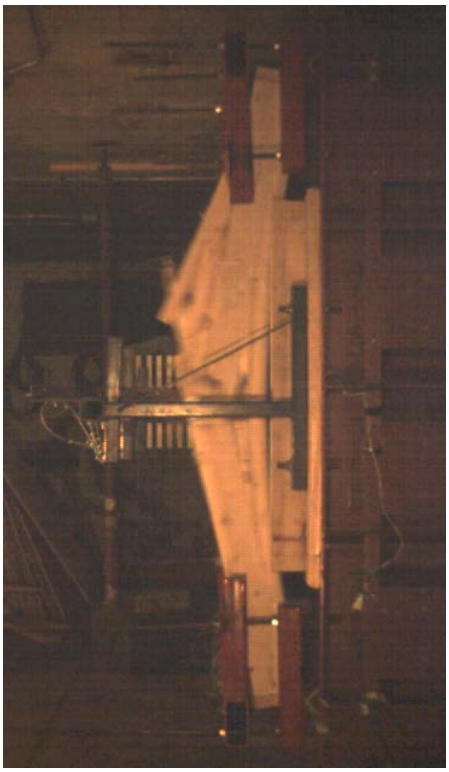

c) t = 14 ms

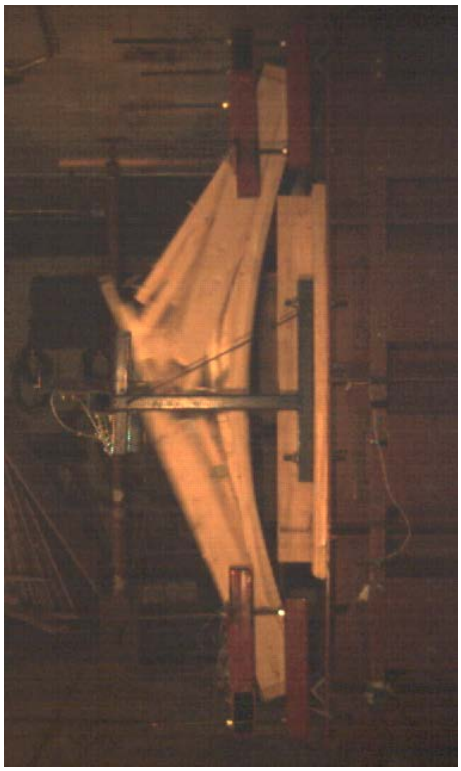

d) t = 22 ms

Figure A7.3 : Evolution of damage with time for Wall 7 Shot 1

a) Front view

b) Damage to sheathing and exposed nails

c) Side view

Figure A7.4 : Damage of Wall 7 after shot 1

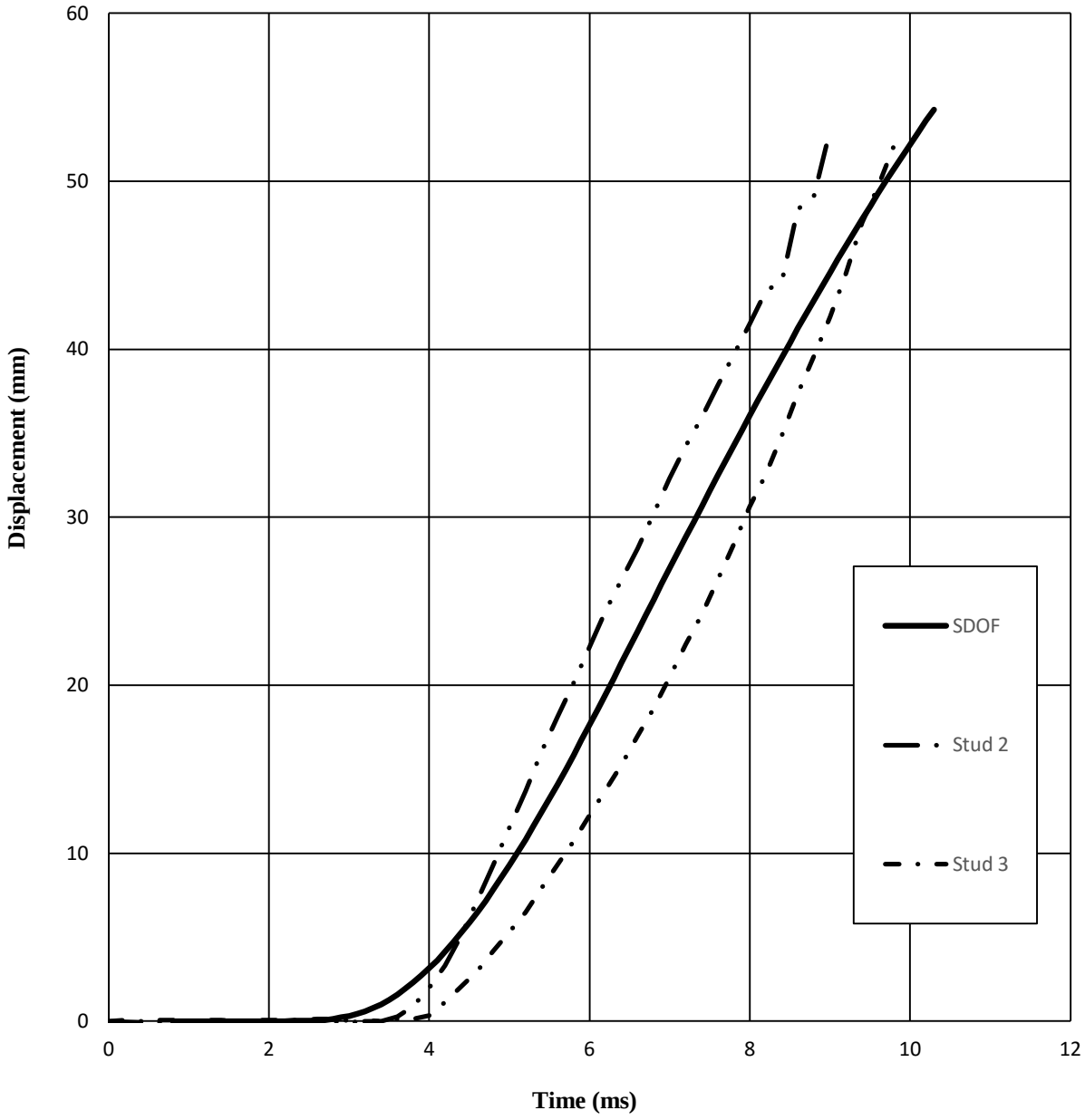

Figure A7.5 : SDOF prediction for Wall 7 Shot 1

Wall 8 Test Summary

Test name: Wall_8_Shot_1 **Test date:** 15/7/2014

Driver length: 2745 mm **Driver pressure:** 290.3 kPa

Wall mass: 71.56 kg

Test specimen properties:

- 6-38 mm x 140 mm No. 2 studs @ 406.4 mm o/c
- Nails, 50 mm x 2.87 mm @ 150 mm o/c (field and edge)
- 2108 mm total length of wall
- 2032 mm long studs
- 2032 mm clear span
- 18.5 mm plywood

Average maximum reflected pressure: 49.8 kPa **Average max. deflection of wall studs:**51.90 mm

Average maximum reflected impulse: 465.21 kPa-ms **Average time to max. deflection:** 6.9 ms

Positive phase duration: 19.6 ms **Quantified wall damage level:** Blowout

Table A8.1 : Stud data from Wall 8 Shot 1

Stud number	Stud reference ID	Maximum mid-span displacement	Time to Maximum	Debris projection	Stud damage level
		mm	ms	mm	
1	S86	-	-	No debris	Major cracking
2	S172	53.89	7.2	2000	Failed
3	S228	-	-	>4000	Failed
4	S241	49.92	6.6	No debris	Failed
5	S158	-	-	No debris	Failed
6	S219	-	-	300	Failed

Comments:

Stud 1 had cracking near a large knot and had very little rotation. Nail withdrawal was observed at the top plate. Sheathing was still connected thoroughly. Stud 2 failed at mid-span with the top half being projected and some splitting occurring near the failure site. Stud 3 was fully projected from the wall with the top half having some splitting. All sheathing nails punctured through and were attached to the stud. Stud 4 failed in a brash fashion at mid-span with splitting occurring in the top half. Stud 5 suffered heavy nail pull-out at both end plates. Stud 6 failed at mid-span and projected only a small amount of debris. Splitting occurred in both halves.

Presence of a large rip throughout the wall at mid-span, with the larger of the two sheathing pieces having suffered the greatest amount of damage. There was significant amounts of delamination of the plywood near Stud 6.

No sheathing debris was observed. Three of the six studs produced hazardous debris, with projection lengths varying from 300 mm to over 4000 mm (the debris of Stud 3 struck the lab wall). These lengths are conservatives since the LVDT support bracket came into contact with some of the flying debris. Significant nail withdrawal was observed on all studs. The LVDTs for Stud 3 and Stud 5 did not record properly and therefore no displacement data for these studs were obtained.

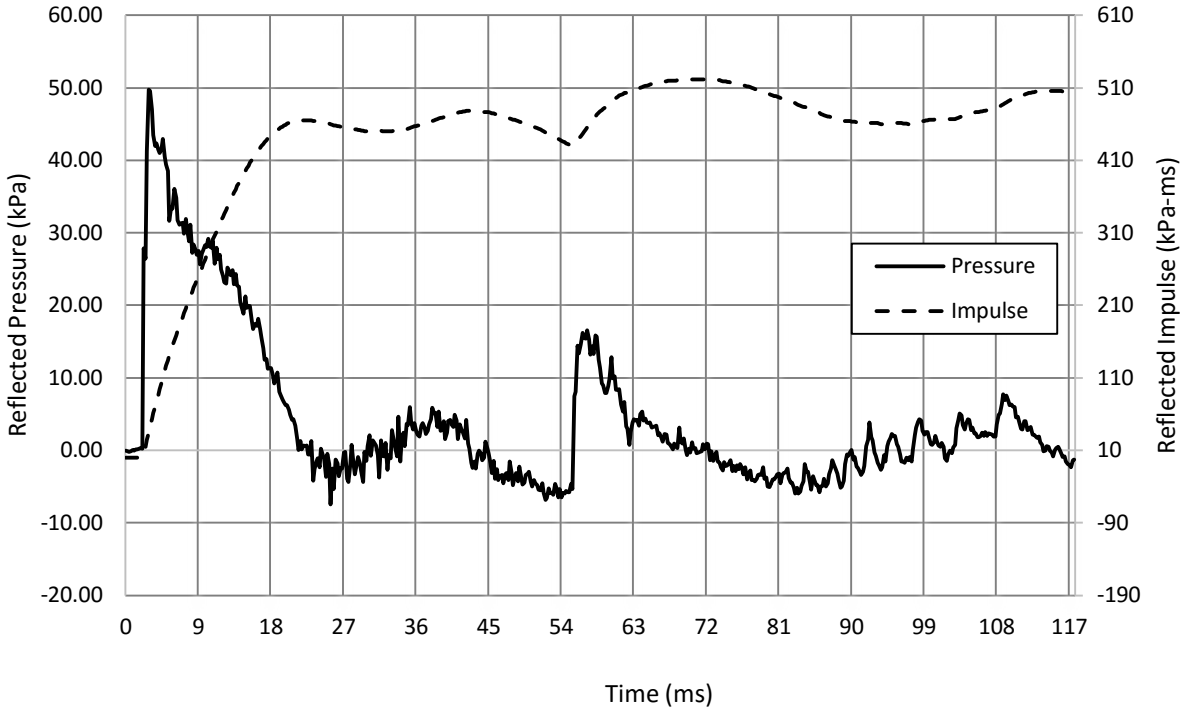

Figure A8.1 : Reflected pressure and impulse time histories for Wall 8 Shot 1

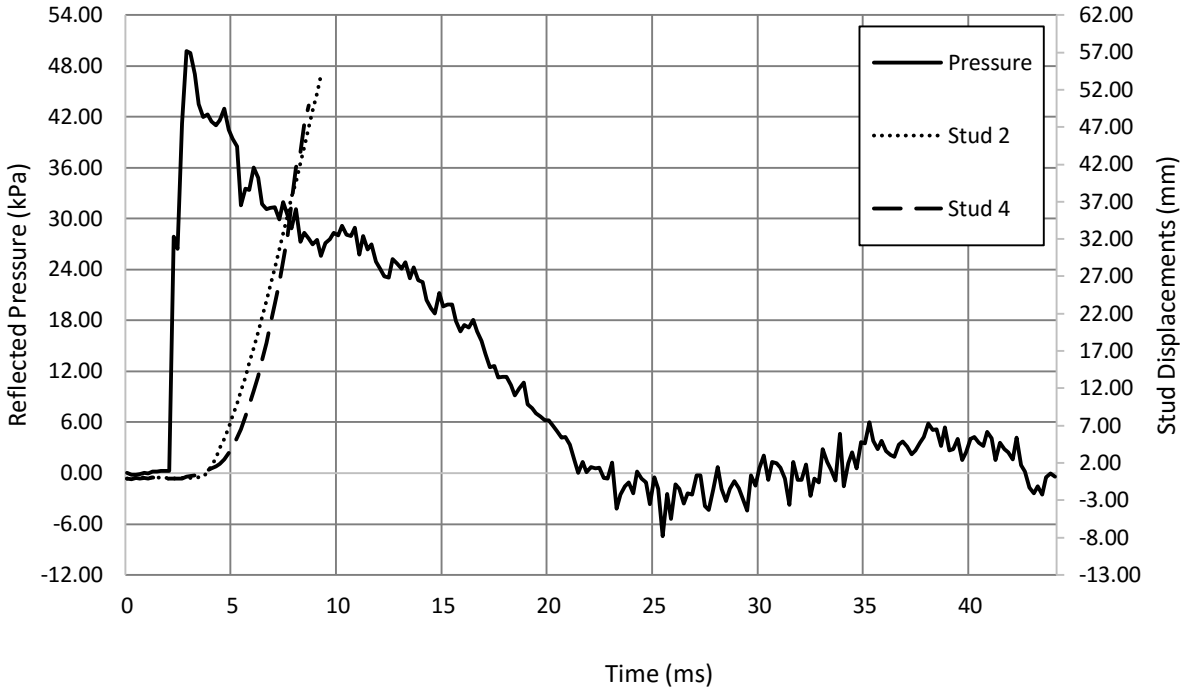

Figure A8.2 : Reflected pressure and displacement time histories for Wall 8 Shot 1

a) t = 0 ms

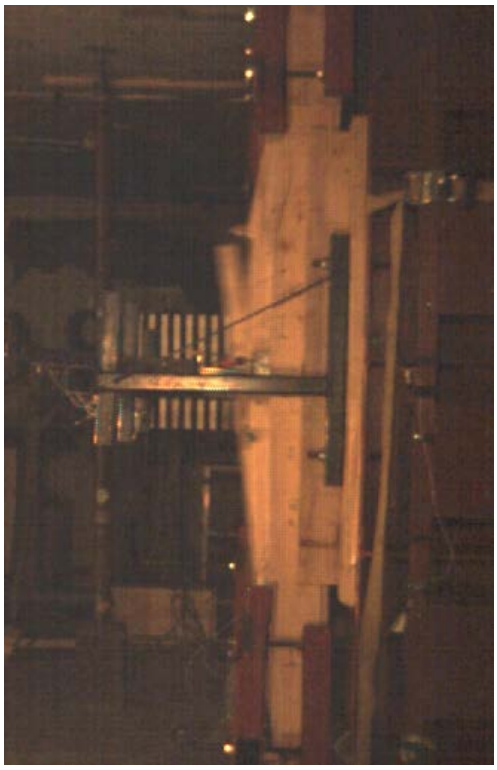

b) t = 8 ms

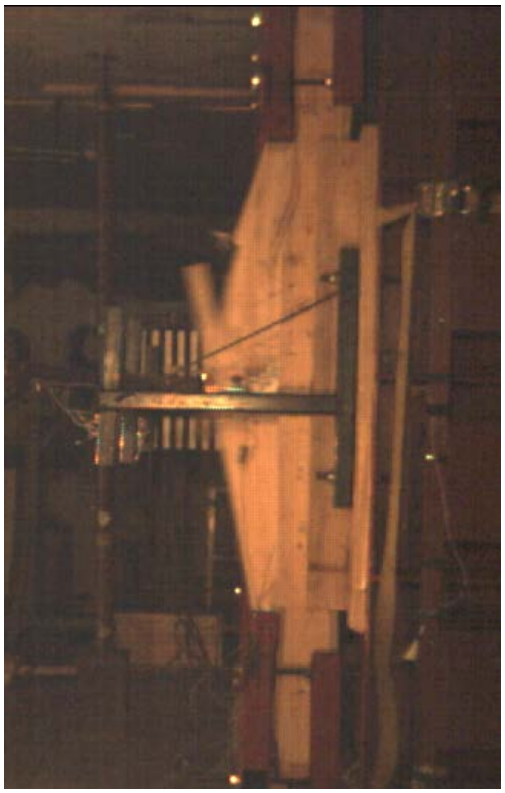

c) t = 12 ms

d) t = 20 ms

Figure A8.3 : Evolution of damage with time for Wall 8 Shot 1

a) Oblique view

b) Damage to sheathing and exposed nails

c) Side view

Figure A8.4 : Damage of Wall 8 after shot 1

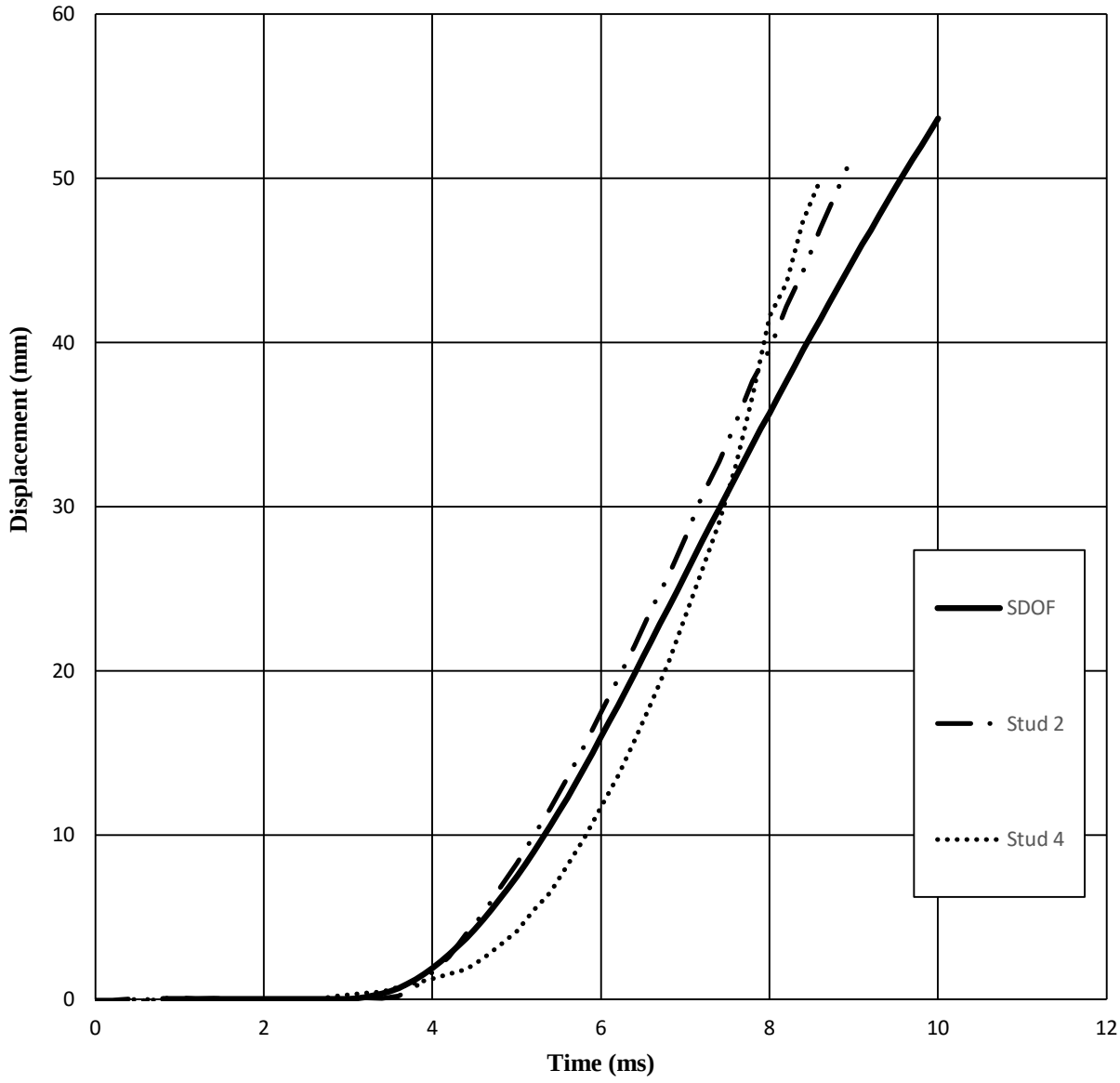

Figure A8.5 : SDOF prediction for Wall 8 Shot 1

Wall 9 Test Summary

Test name: Wall_9_Shot_1 **Test date:** 10/7/2014

Driver length: 2745 mm **Driver pressure:** 310.3 kPa

Wall mass: 106.22 kg

Test specimen properties:

- 6-38 mm x 140 mm No. 2 studs @ 406.4 mm o/c
- Nails, 50 mm x 2.87 mm @ 150 mm o/c (field and edge) – OSB sheet
- Screws, 76 mm x 4.2 mm @ 300 mm o/c (field and edge) – Plywood sheet
- 2108 mm total length of wall
- 2032 mm long studs
- 2032 mm clear span
- 18.5 mm plywood atop 11 mm OSB

Average maximum reflected pressure: No data **Average max. deflection of wall studs:** No data

Average maximum reflected impulse: No data **Average time to max. deflection:** No data

Positive phase duration: No data **Quantified wall damage level:** Blowout

Table A9.1 : Stud data from Wall 9 Shot 1

Stud number	Stud reference ID	Maximum mid-span displacement	Time to Maximum	Debris projection	Stud damage level
		mm	ms	mm	
1	S90	-	-	No debris	No damage
2	S106	-	-	No debris	Failed
3	S257	-	-	No debris	Failed
4	S93	-	-	1000	Failed
5	S141	-	-	No debris	Failed
6	S212	-	-	1000	Failed

Comments:

Stud 1 suffered no damage. Full withdrawal of the top plate nails occurred due to the overall rotation of the top plate and the lack of pressure distribution on Stud 1. Stud 2 failed at mid-span with splitting occurring in the top half. Stud 3 failed in a brash fashion with small amounts of splitting occurring in the bottom half. Full withdrawal of the top plate nails occurred due to the overall rotation of the top plate and the lack of pressure distribution on Stud 3. Stud 4 failed in a brash fashion at mid-span with splitting occurring in the top half as well as the top half being ejected. Stud 5 failed at its flexural fibre with splitting occurring in both halves. Stud 6 failed at mid-span with splitting occurring in the top half. The split portion was ejected.

Presence of a large rip in the OSB sheet in the larger of the two OSB sheets. The plywood layer was barely damaged.

Little sheathing debris was observed. Two of the six studs produced debris, with an ejection of 1000 mm. Significant nail and screw withdrawal was observed on most studs. The data acquisition system did not function properly and data was not recorded.

a) Oblique view

b) Failure of stud 2 caused by fastener tips

c) Damage to OSB panel

Figure A9.1 : Damage of Wall 8 after shot 1

Wall 10 Test Summary

Test name: Wall_10_Shot_1 **Test date:** 19/7/2014

Driver length: 2745 mm **Driver pressure:** 326.1 kPa

Wall mass: 102.05 kg

Test specimen properties:

- 6-38 mm x 140 mm No. 2 studs @ 406.4 mm o/c
- Nails, 50 mm x 2.87 mm @ 150 mm o/c (field and edge) – OSB sheet
- Screws, 76 mm x 4.2 mm @ 300 mm o/c (field and edge) – Plywood sheet
- 2108 mm total length of wall
- 2032 mm long studs
- 2032 mm clear span
- 18.5 mm plywood atop 11 mm OSB

Average maximum reflected pressure: 49.7 kPa **Average max. deflection of wall studs:** 51.86 mm

Average maximum reflected impulse: 480.8 kPa-ms **Average time to max. deflection:** 8.9 ms

Positive phase duration: 19.6 ms **Quantified wall damage level:** Blowout

Table A10.1 : Stud data from Wall 10 Shot 1

Stud number	Stud reference ID	Maximum mid-span displacement	Time to Maximum	Debris projection	Stud damage level
		mm	ms	mm	
1	S155	-	-	No debris	Failed
2	S169	52.40	9.0	No debris	Failed
3	S176	51.39	8.4	No debris	Failed
4	S159	52.59	9.4	No debris	Failed
5	S140	51.06	8.6	No debris	Failed
6	S82	-	-	No debris	Failed

Comments:

Stud 1 failed with a large split occurring from its top third point all the way to its bottom end. Stud 2, 3, and 4 failed brashly with a significant splitting occurring. Massive amounts of nail puncturing was observed. A large knot was present at the failure site of Stud 4. Stud 5 experienced flexural failure with some splitting occurring and propagating towards its top end. Stud 6 had a very defined brash failure at mid-span.

Little to no debris was produced. This is due to the extra sheet of plywood which reinforced the load-distribution system as to not cause it to rip, versus OSB acting alone. The studs were restricted from being ejected due to the screws and their relatively high pull-out strength. A large rip in the sheathing was observed at mid-span, corresponding with the zone of failure of all the studs. The OSB was overall more damaged than the plywood sheet.

Possibility of the LVDTs colliding with the wall might have had an effect on residual and/or maximum deflection.

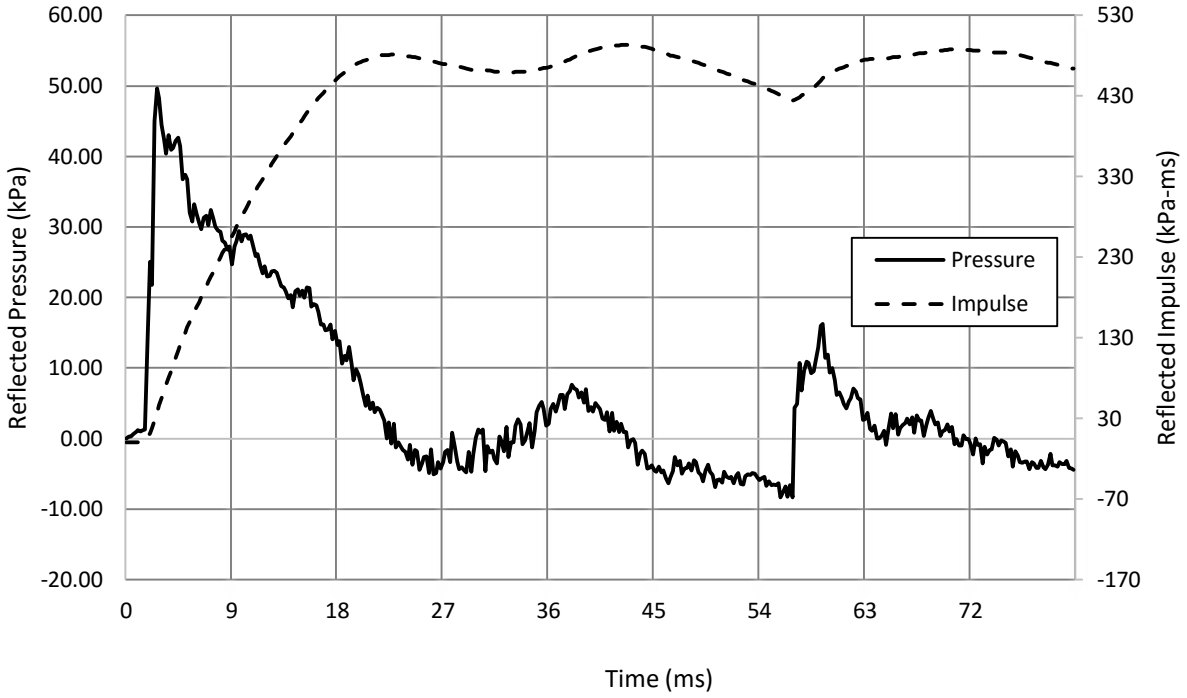

Figure A10.1 : Reflected pressure and impulse time histories for Wall 10 Shot 1

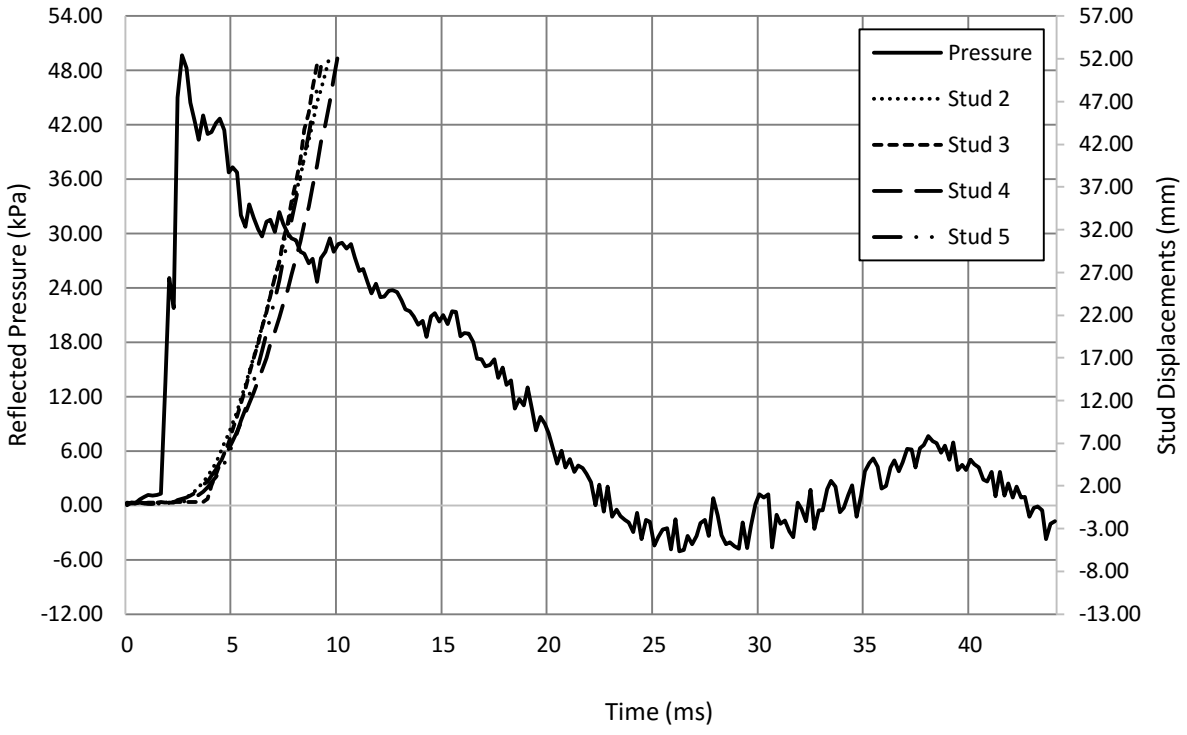

Figure A10.2 : Reflected pressure and displacement time histories for Wall 10 Shot 1

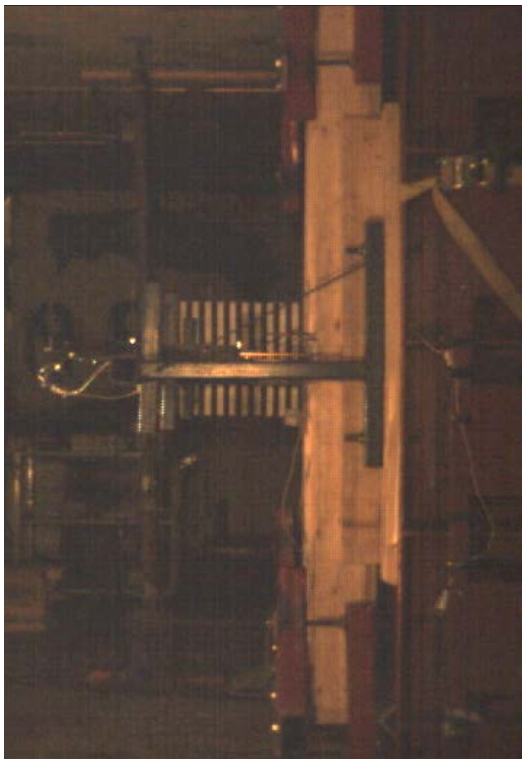

a) t = 0 ms

b) t = 8 ms

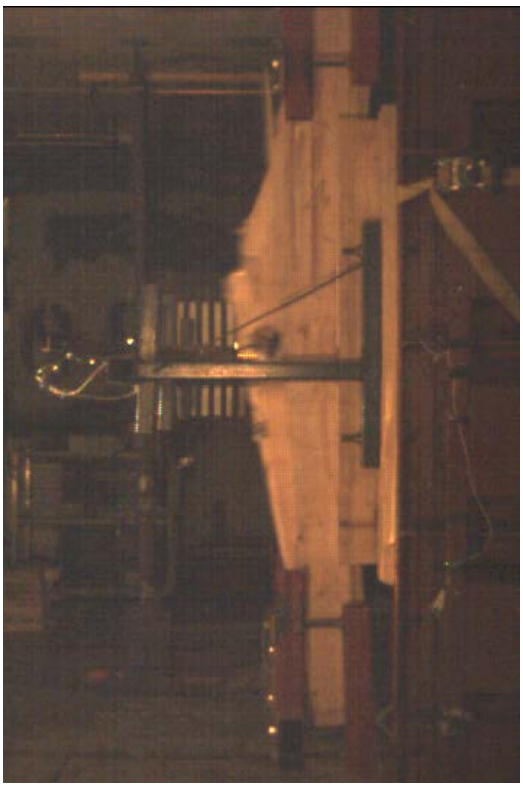

c) t = 14 ms

d) t = 24 ms

Figure A10.3 : Evolution of damage with time for Wall 10 Shot 1

a) Oblique view

b) Nail and screw head pull-through

c) Side view

Figure A10.4 : Damage of Wall 10 after shot 1

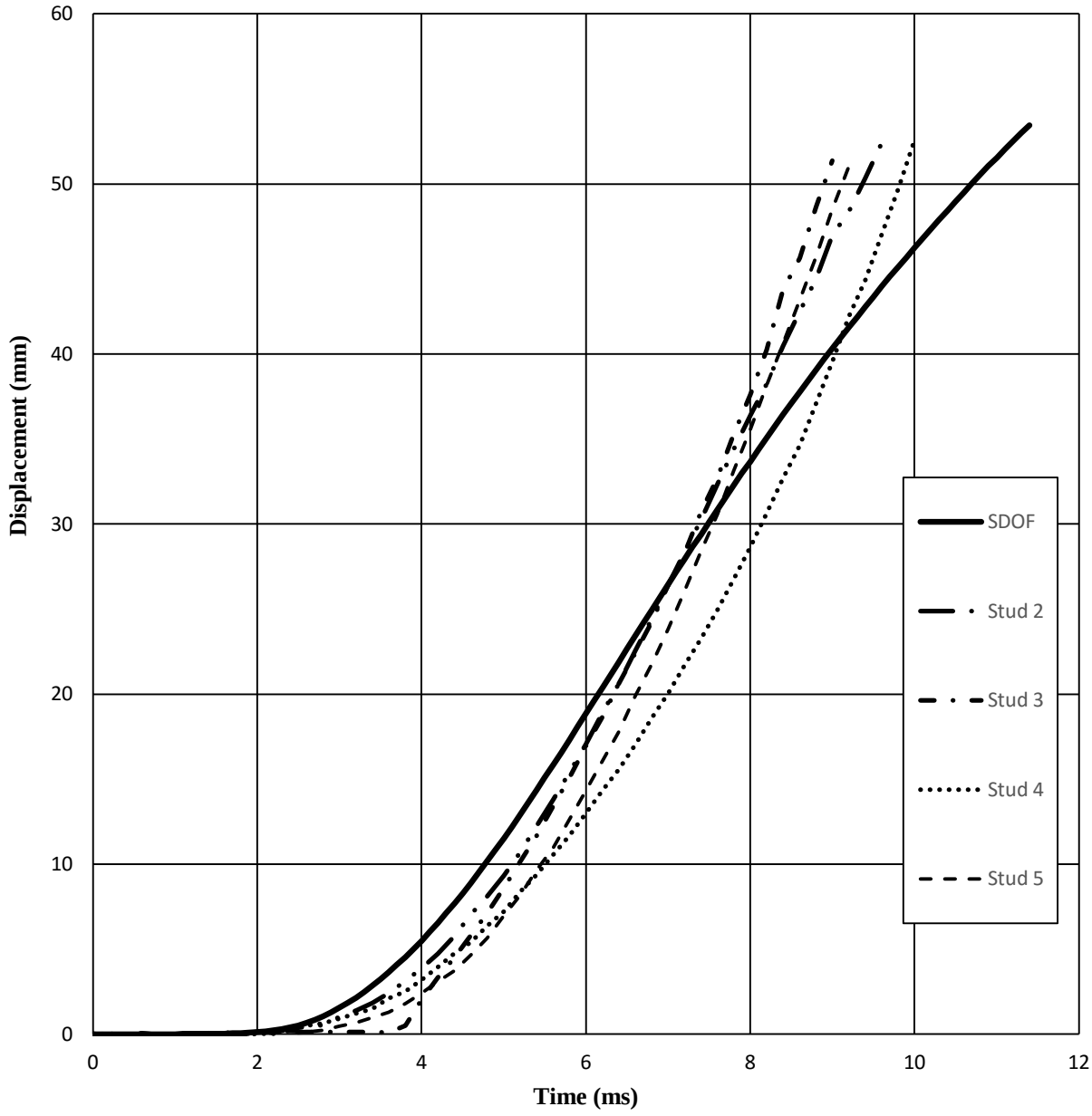

Figure A10.5 : SDOF prediction for Wall 10 Shot 1

Wall 11 Test Summary

Test name: Wall_11_Shot_1 **Test date:** 3/7/2014

Driver length: 2745 mm **Driver pressure:** 407.5 kPa

Wall mass: 101.78 kg

Test specimen properties:

- 6-38 mm x 140 mm No. 2 studs @ 406.4 mm o/c
- Nails, 50 mm x 2.87 mm @ 150 mm o/c (field and edge) – OSB sheet
- Screws, 76 mm x 4.2 mm @ 300 mm o/c (field and edge) – Plywood sheet
- 2108 mm total length of wall
- 2032 mm long studs
- 2032 mm clear span
- 18.5 mm plywood atop 11 mm OSB

Average maximum reflected pressure: 65.1 kPa **Average max. deflection of wall studs:** 65.84 mm

Average maximum reflected impulse: 623.0 kPa-ms **Average time to max. deflection:** 7.8 ms

Positive phase duration: 20.6 ms **Quantified wall damage level:** Blowout

Table A11.1 : Stud data from Wall 11 Shot 1

Stud number	Stud reference ID	Maximum mid-span displacement	Time to Maximum	Debris projection	Stud damage level
		mm	ms	mm	
1	S239	-	-	1000	Failed
2	236	64.09	7.0	1500	Failed
3	S242	62.05	7.4	No debris	Failed
4	S249	61.62	8.2	2900	Failed
5	S123	75.62	8.4	No debris	Failed
6	S220	-	-	No debris	Failed

Comments:

Stud 1 and 2 both failed at mid-span. Both had a large split from mid-span to their bottom end which caused debris to be ejected. Stud 3 failed brashly at its top-third point. Presence of large centre splitting was present in its top portion. Stud 4 failed brashly and had both top and bottom halves experiencing splitting, where the bottom half produced flying debris. The debris nearly destroyed strain-gauge equipment by almost ripping it out of the system. Stud 5 failed in brash fashion with significant amount of splitting occurring in both halves. Stud 6 failed in flexure with splitting occurring in its bottom half.

Three of the six studs produced hazardous debris. Stud 1 and 2 only produced minimal debris, caused mostly by splitting, while Stud 4 produced a large piece of debris (half of a full-size stud) being ejected to a distance of 2900 mm. Most of the studs were restricted from being ejected due to the screws and their relatively high pull-out strength. When splitting occurred, it naturally occurred along the path of least resistance, i.e.: where the screws and nails protruded. Naturally, this caused those pieces not to be attached to the wall system anymore. A large rip in the sheathing was observed at mid-span, corresponding with the zone of failure of all the studs. The OSB was overall more damaged than the plywood sheet. The wall smashed into the LVDTs and this might have had an effect on residual and maximum deflection.

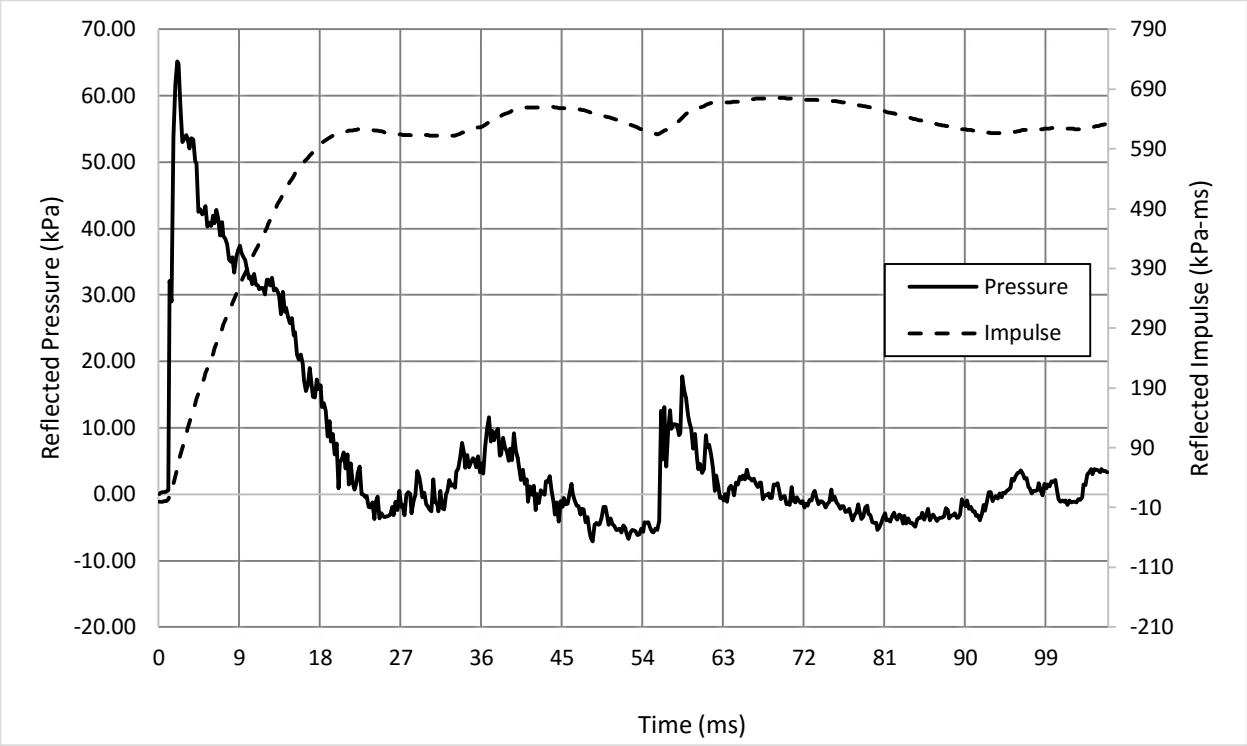

Figure A11.1 : Reflected pressure and impulse time histories for Wall 11 Shot 1

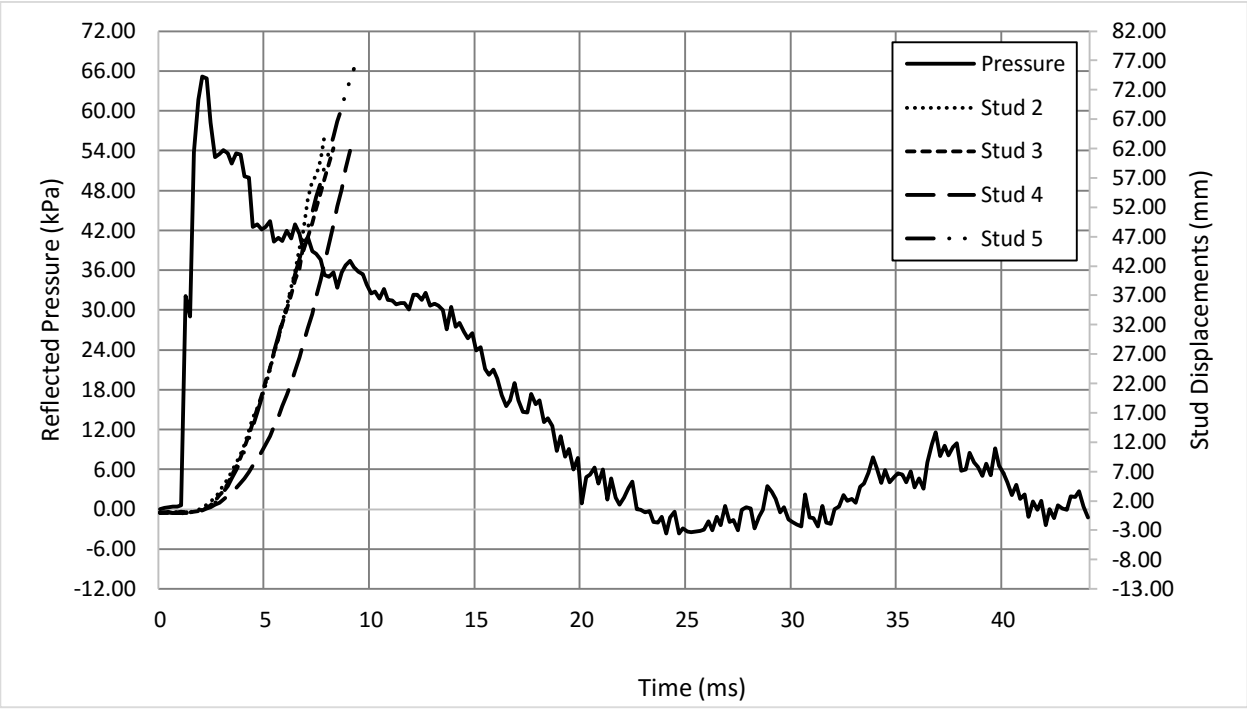

Figure A11.2 : Reflected pressure and displacement time histories for Wall 11 Shot 1

a) t = 0 ms b) t = 6 ms

c) t = 12 ms d) t = 20 ms

Figure A11.3 : Evolution of damage with time for Wall 11 Shot 1

a) Front view

b) Exposed fasteners at Stud 1

c) Side view

Figure A11.4 : Damage of Wall 11 after shot 1

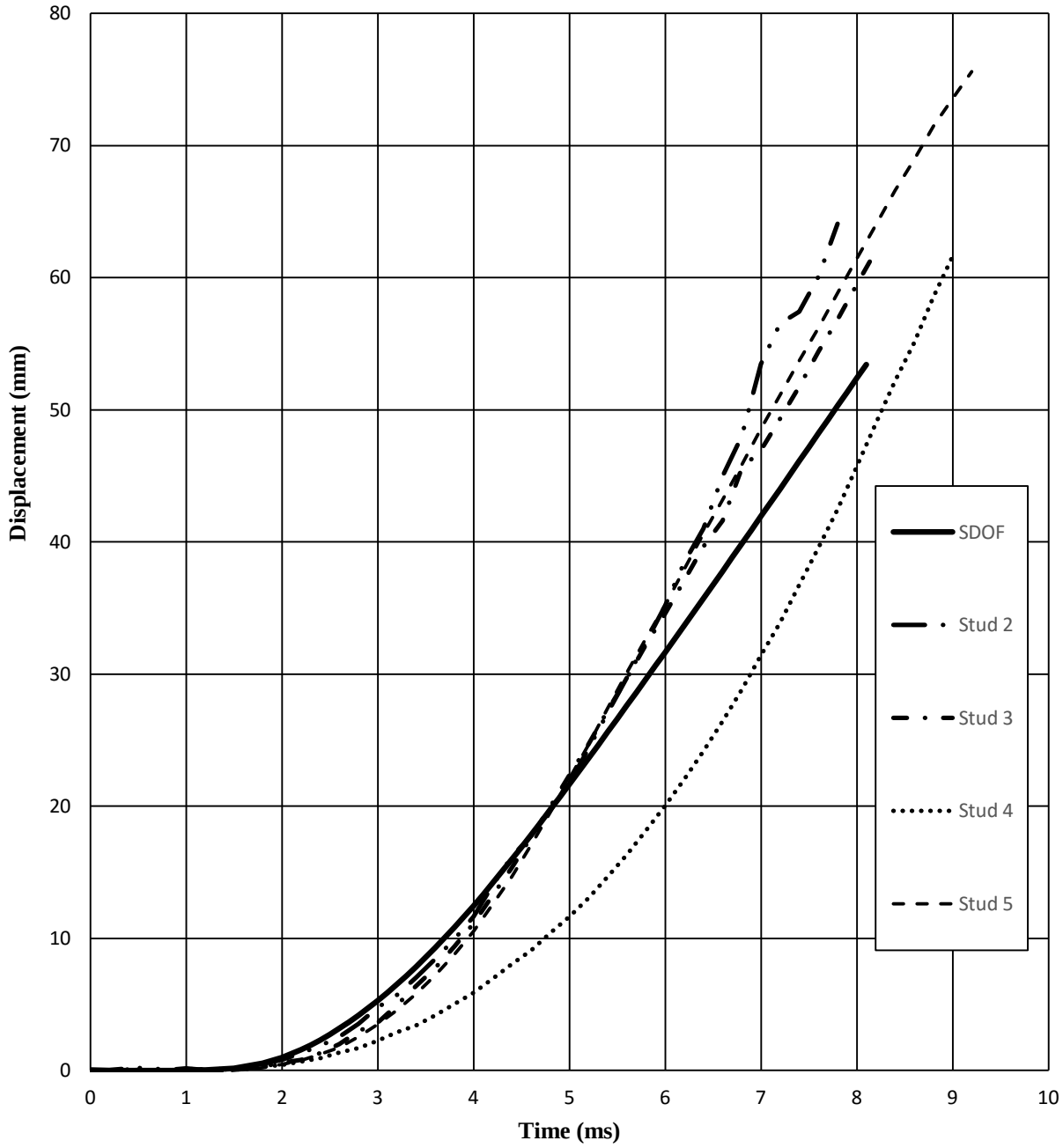

Figure A11.5 : SDOF prediction for Wall 11 Shot 1

Wall 12 Test Summary

Test name: Wall_12_Shot_1 **Test date:** 4/7/2014

Driver length: 2745 mm **Driver pressure:** 447.5 kPa

Wall mass: 98.16 kg

Test specimen properties:

- 6-38 mm x 140 mm No. 2 studs @ 406.4 mm o/c
- Nails, 50 mm x 2.87 mm @ 150 mm o/c (field and edge) – OSB sheet
- Screws, 76 mm x 4.2 mm @ 300 mm o/c (field and edge) – Plywood sheet
- 2108 mm total length of wall
- 2032 mm long studs
- 2032 mm clear span
- 18.5 mm plywood atop 11 mm OSB

Average maximum reflected pressure: 70.9 kPa **Average max. deflection of wall studs:** 64.17 mm

Average maximum reflected impulse: 654.1 kPa-ms **Average time to max. deflection:** 8.0 ms

Positive phase duration: 21.4 ms **Quantified wall damage level:** Blowout

Table A12.1 : Stud data from Wall 12 Shot 1

Stud number	Stud reference ID	Maximum mid-span displacement	Time to Maximum	Debris projection	Stud damage level
		mm	ms	mm	
1	S103	-	-	2000	Failed
2	S145	71.14	8.8	1000	Failed
3	S184	54.00	7.6	1000	Failed
4	S88	67.37	7.6	3200	Failed
5	S234	-	-	2500	Failed
6	S206	-	-	4000	Failed

Comments:

All 6 studs failed in similar fashion and produced debris. Average residual deflection was majorly significant, which meant that the wall was unable to stay in its supports and started to fold down on itself after the test was completed. Presence of connector tips in failure areas (path of least resistance). Most studs failed in a brash fashion, with a near "clean-cut" through its mid-span. Significant amounts of nail withdrawal and puncture was observed on all six studs.

Large rip in sheathing at mid-span, with the OSB losing most of its integrity; only the plywood, at this point, is actually holding the wall together. Puncture of LVDTs through the sheathing. Extreme residual deflection. The LVDT for stud 5 was damaged and did not record any data.

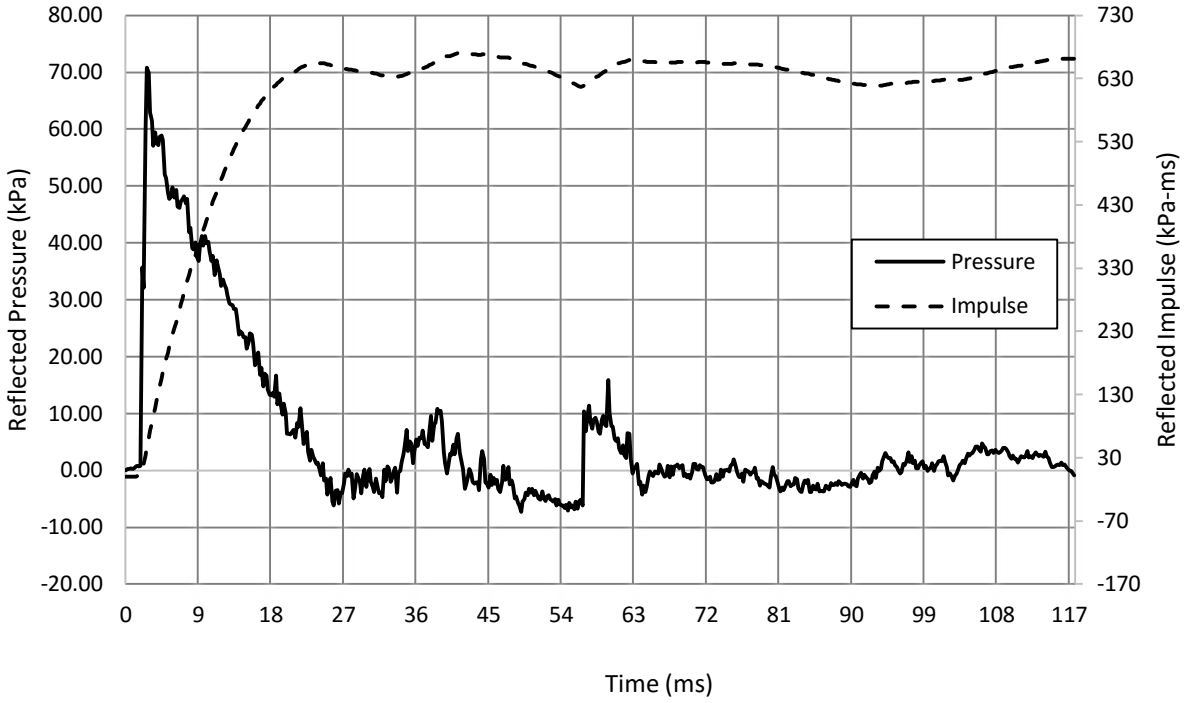

Figure A12.1 : Reflected pressure and impulse time histories for Wall 12 Shot 1

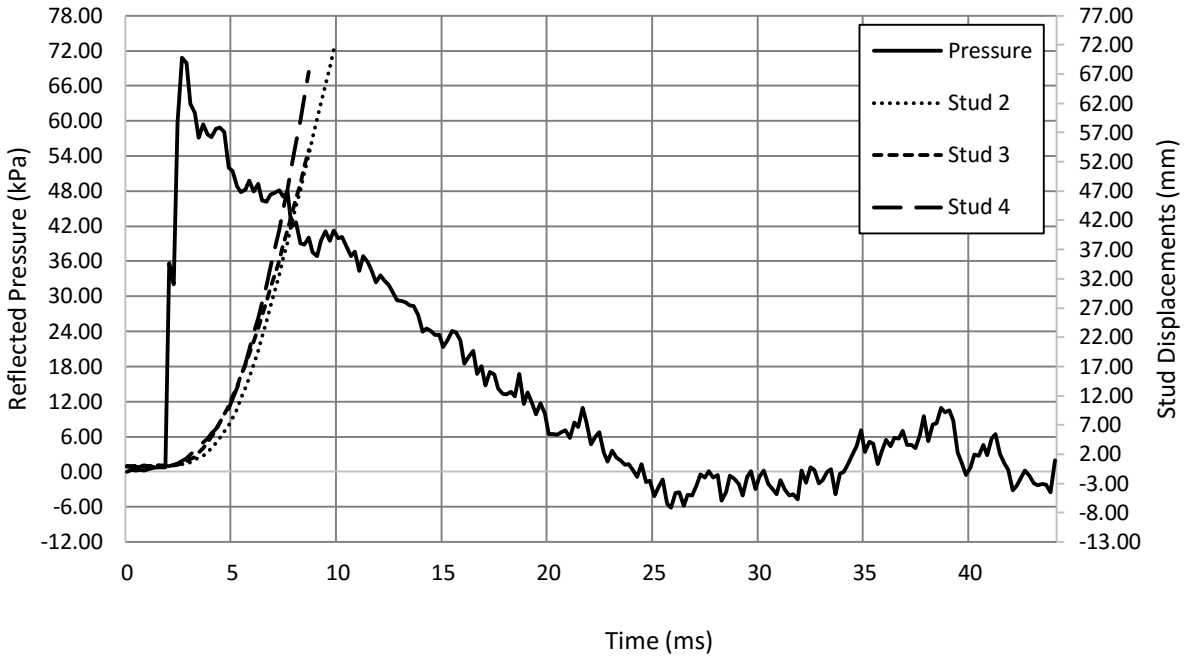

Figure A12.2 : Reflected pressure and displacement time histories for Wall 12 Shot 1

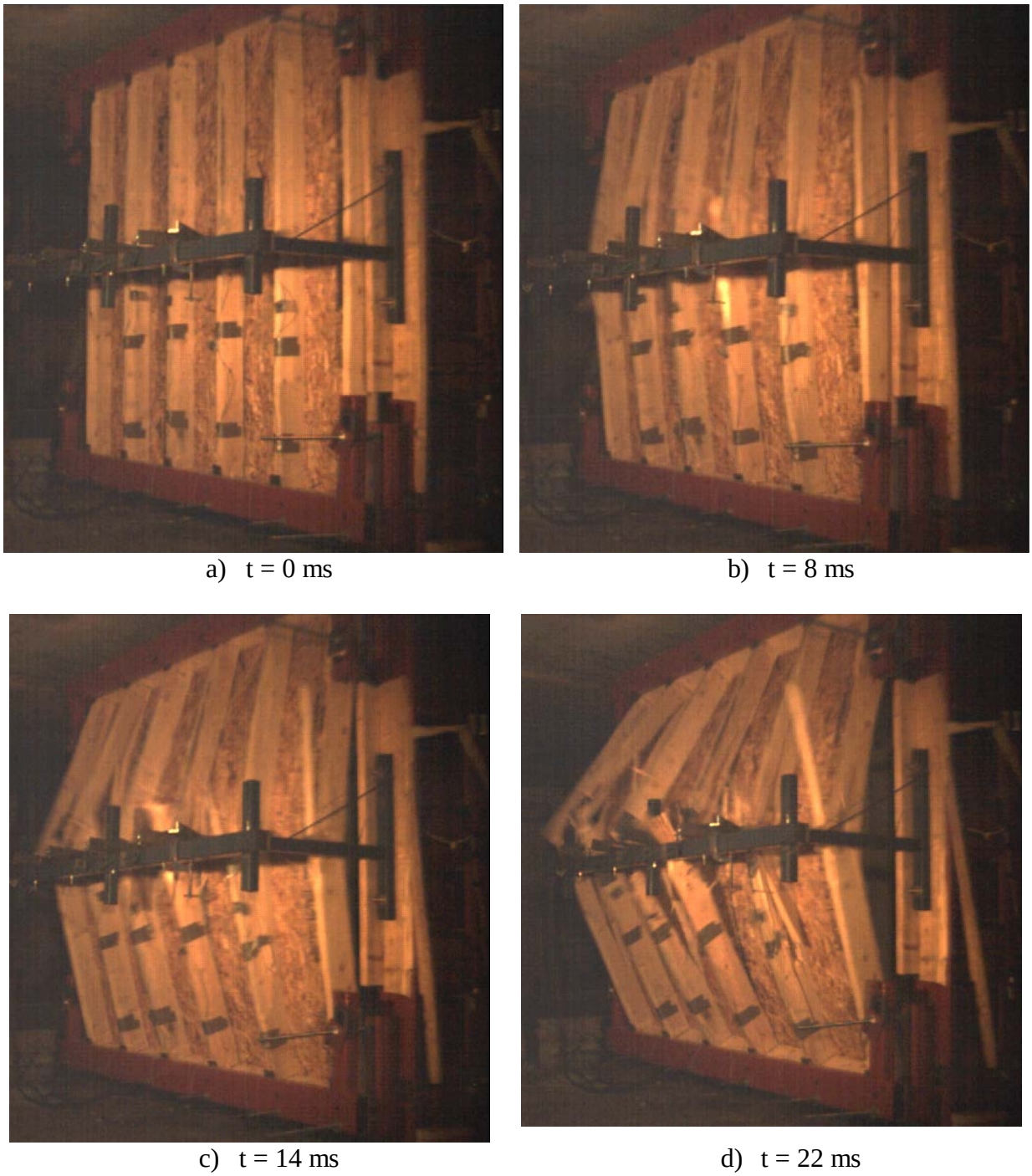

a) t = 0 ms

b) t = 8 ms

c) t = 14 ms

d) t = 22 ms

Figure A12.3 : Evolution of damage with time for Wall 12 Shot 1

a) Oblique view

b) Exposed fastener tips along failure zone of Stud 5

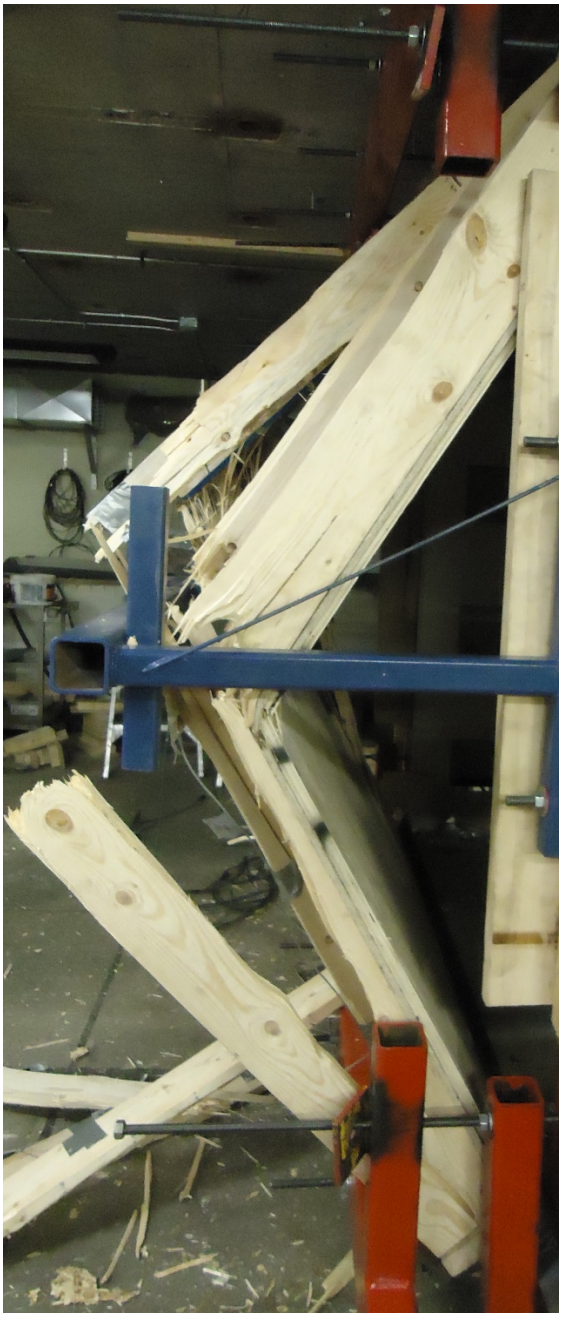

c) Side view

Figure A12.4 : Damage of Wall 12 after shot 1

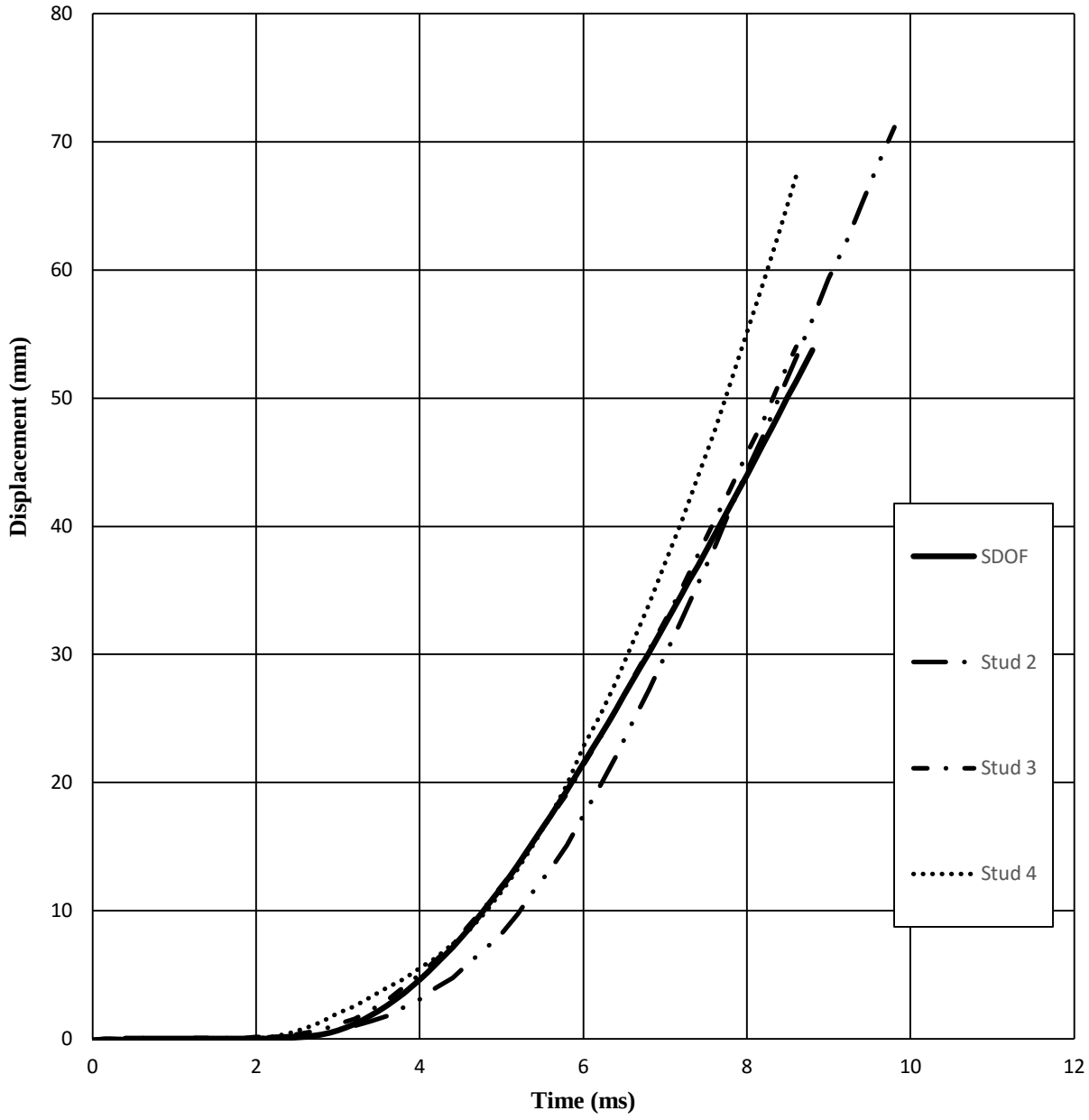

Figure A12.5 : SDOF prediction for Wall 12 Shot 1

Wall 13 Test Summary

Test name: Wall_13_Shot_1 **Test date:** 17/8/2014

Driver length: 2745 mm **Driver pressure:** 434.4 kPa

Wall mass: 92.80 kg

Test specimen properties:

- 6-38 mm x 184 mm No. 2 studs @ 406.4 mm o/c
- Nails, 50 mm x 2.87 mm @ 150 mm o/c (field and edge)
- 2108 mm total length of wall
- 2032 mm long studs
- 2032 mm clear span
- 11 mm OSB
- Welded wire fabric (152 x 152 mm gaps, 11.1 mm^2 thick) placed in-between studs and OSB

Average maximum reflected pressure: 63.4 kPa **Average max. deflection of wall studs:** No data

Average maximum reflected impulse: 571.7 kPa-ms **Average time to max. deflection:** 8.00 ms

Positive phase duration: 22.0 ms **Quantified wall damage level:** Blowout

Table A13.1 : Stud data from Wall 13 Shot 1

Stud number	Stud reference ID	Maximum mid-span displacement	Time to Maximum	Debris projection	Stud damage level
		mm	ms	mm	
1	S8-10	-	-	No debris	Superficial
2	S8-13	-	-	1500	Superficial
3	S8-1	-	7.4	5000	Failed
4	S8-4	-	8.6	No debris	Failed
5	S8-11	-	-	5500	Failed
6	S8-12	-	-	No debris	Superficial

Comments:

Torsion was applied to Stud 1 and 6 due to the OSB not ripping and the relatively high reflected pressure being applied to the wall. Only one side of these two studs received loading, therefore creating a moment about their longitudinal axis. Failure at these studs were at the top and bottom of the stud. Stud 2 was completely ejected from the wall but the stud itself was not damaged. The technique by which the WWM was attached to the wall frame (by hooking it to the underside of both top and bottom plates) created additional plate rotation, which explains why the toe-nails failed to provide support. Stud 3 failed in brash fashion with splitting occurring throughout the member, and was ejected from the wall. Stud 4 experienced flexural failure, as well as failure at the top toe-nail, again due to excessive plate rotation. Stud 5 experienced brash failure and was ejected across the lab room.

Massive amount of rips in sheathing, however no debris was due to the OSB. Three of the six studs produced hazardous debris. The deflected shape and behaviour of the WWM resembles that of a simply supported beam/one-way slab. Small disconnection of the WWM atop Stud 6, not significant to results.

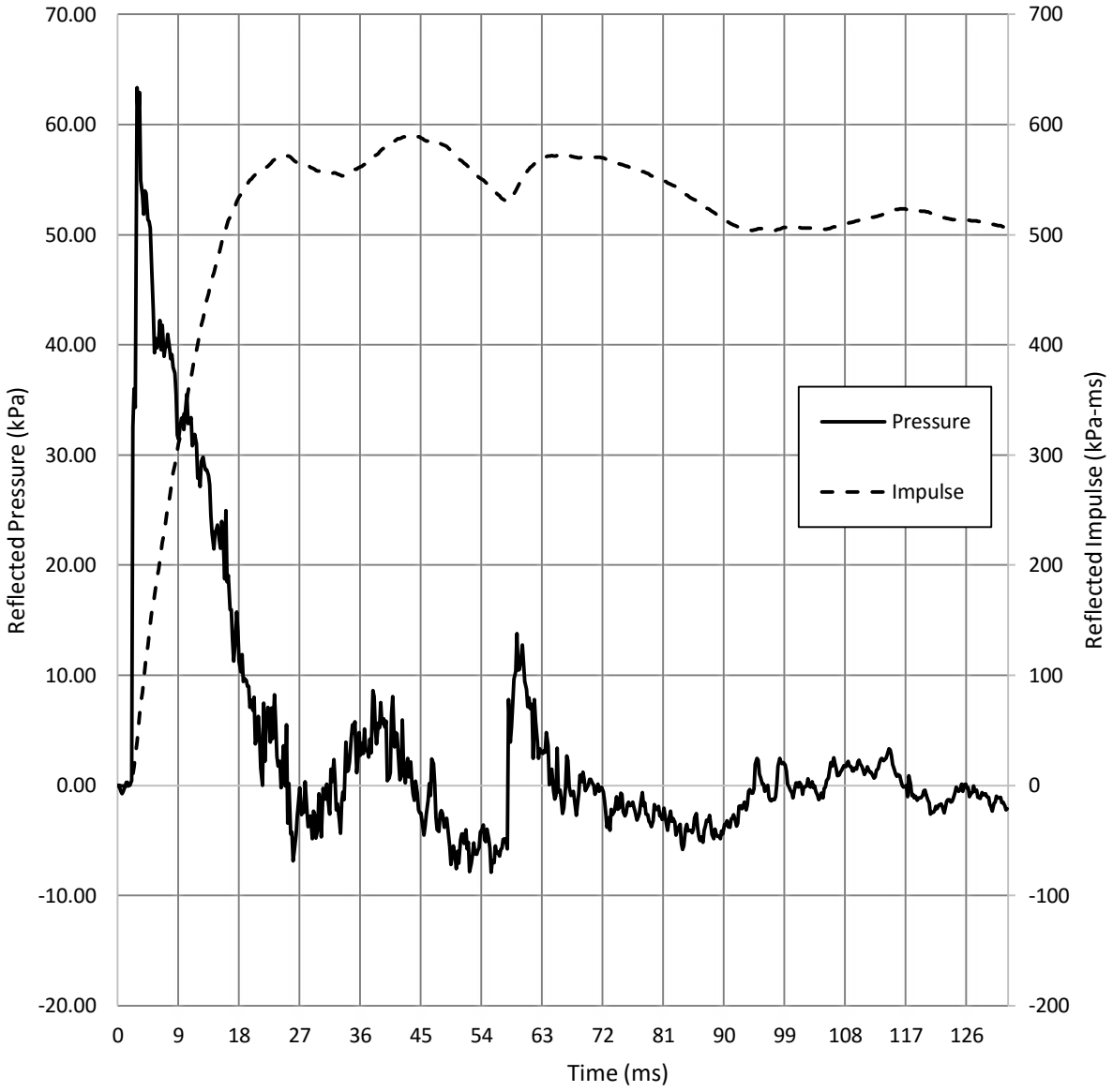

Figure A13.1 : Reflected pressure and impulse time histories for Wall 13 Shot 1

a) t = 0 ms

b) t = 8 ms

c) t = 12 ms

d) t = 20 ms

Figure A13.2 : Evolution of damage with time for Wall 13 Shot 1

a) Front view

b) Damage to OSB and WWM

c) Wall debris

Figure A13.3 : Damage of Wall 13 after shot 1

Wall 14 Test Summary

Test name: Wall_14_Shot_1 **Test date:** 14/8/2014

Driver length: 2745 mm **Driver pressure:** 303.4 kPa

Wall mass: 92.90 kg

Test specimen properties:

- 6-38 mm x 184 mm No. 2 studs @ 406.4 mm o/c
- Nails, 50 mm x 2.87 mm @ 150 mm o/c (field and edge)
- 2108 mm total length of wall
- 2032 mm long studs
- 2032 mm clear span
- 11 mm OSB
- Welded wire fabric (152 x 152 mm gaps, 11.1 mm^2 thick) placed in-between studs and OSB

Average maximum reflected pressure: 51.2 kPa **Average max. deflection of wall studs:** 35.36 mm

Average maximum reflected impulse: 482.8 kPa-ms **Average time to max. deflection:** 7.5 ms

Positive phase duration: 21.4 ms **Quantified wall damage level:** Hazardous

Table A14.1 : Stud data from Wall 14 Shot 1

Stud number	Stud reference ID	Maximum mid-span displacement	Time to Maximum	Debris projection	Stud damage level
		mm	ms	mm	
1	S8-34	-	-	1500	Failed
2	S8-37	29.04	7.0	1200	Failed
3	S8-17	41.68	8.0	1500	Failed
4	S8-20	-	-	No debris	Cracked
5	S8-36	-	-	No debris	Superficial
6	S8-23	-	-	No debris	Superficial

Comments:

Stud 1 failed brashly at mid-span with the bottom-half being ejected and with splitting occurring in both halves. Stud 2 also failed brashly at mid-span with the top half being projected. Stud 3 failed at its mid-span with the bottom-half being ejected and splitting occurring in the top half. Stud 4 had a major crack develop in a lamination on the tension side running from the top end all the way down to the other. This was considered as failure. Stud 5 and 6 did not suffer any apparent damage.

Large vertical sheathing rips in both panels found in between studs. Large residual deflections. Large gap at sheathing joint along Stud 3. Some damage to the bottom plate near Stud 1 and Stud 2.

No significant sheathing debris was observed. Three of the six studs produced hazardous debris, with ejection lengths varying from 1200 mm to 1500 mm. These lengths are conservatives since the LVDT support bracket came into contact with some of the flying debris. Significant nail withdrawal was observed on Stud 1-3. The WWM by itself yielded/deflected but did not suffer any apparent damage. Reinforcement brought by the WWM permitted effective pressure distribution to the studs. While the WWM was deformed, it did not suffer any significant damage.

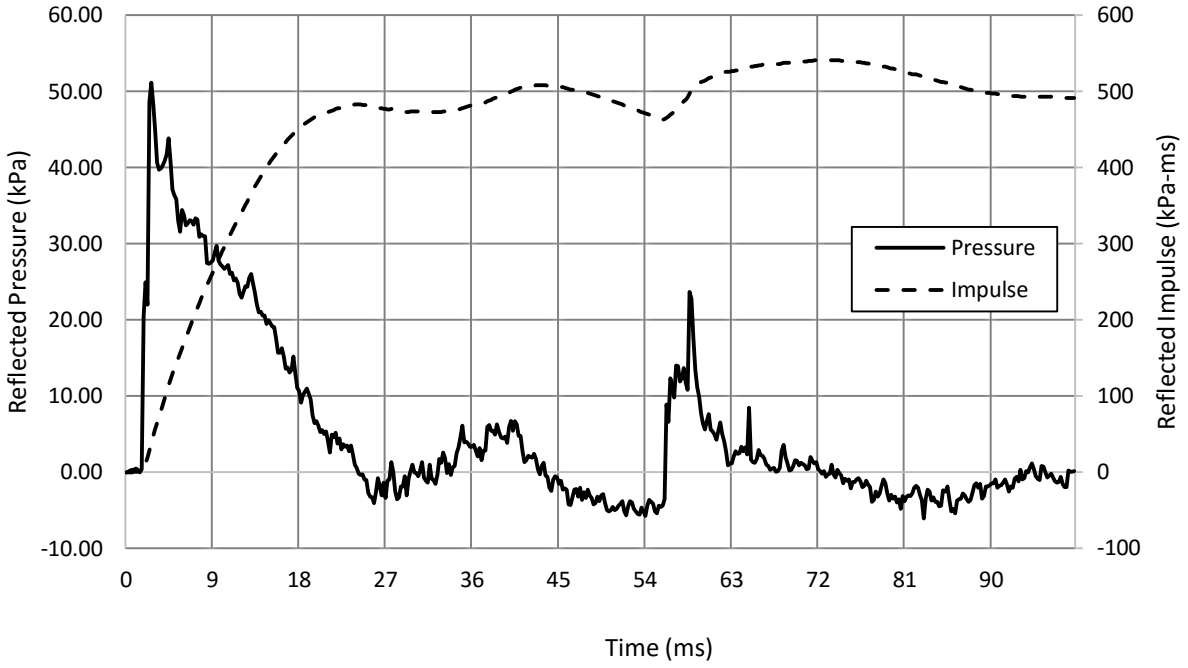

Figure A14.1 : Reflected pressure and impulse time histories for Wall 14 Shot 1

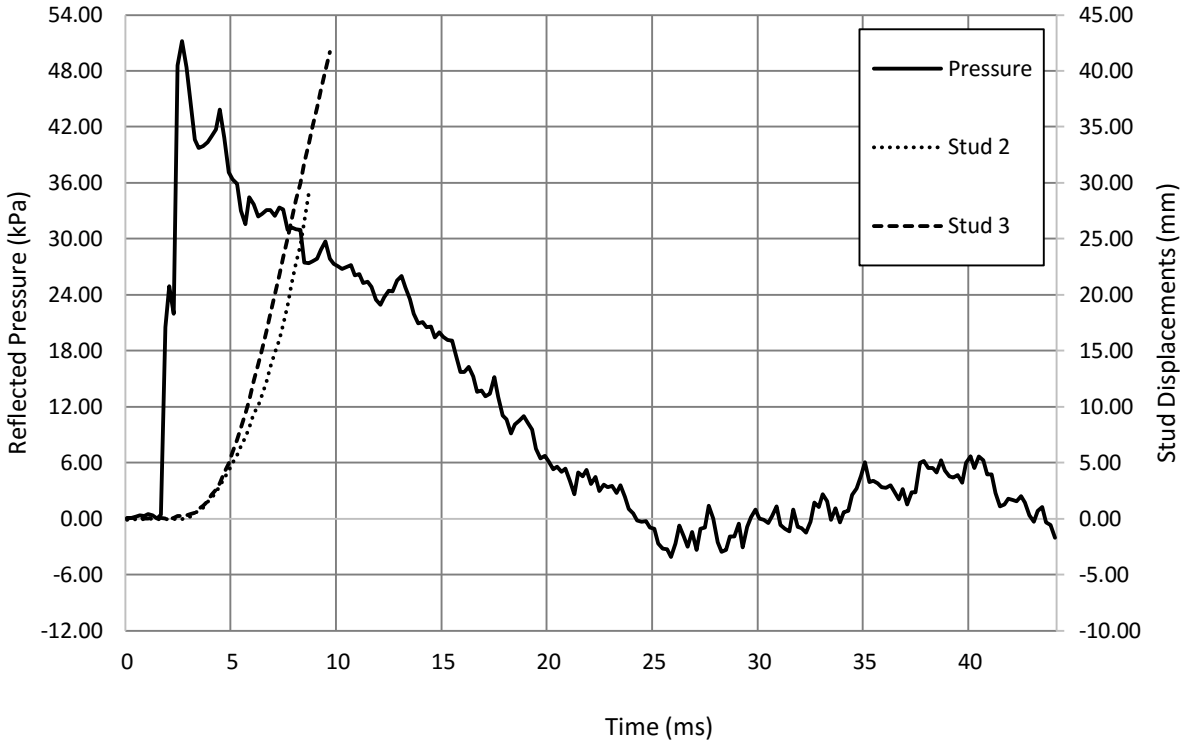

Figure A14.2 : Reflected pressure and displacement time histories for Wall 14 Shot 1

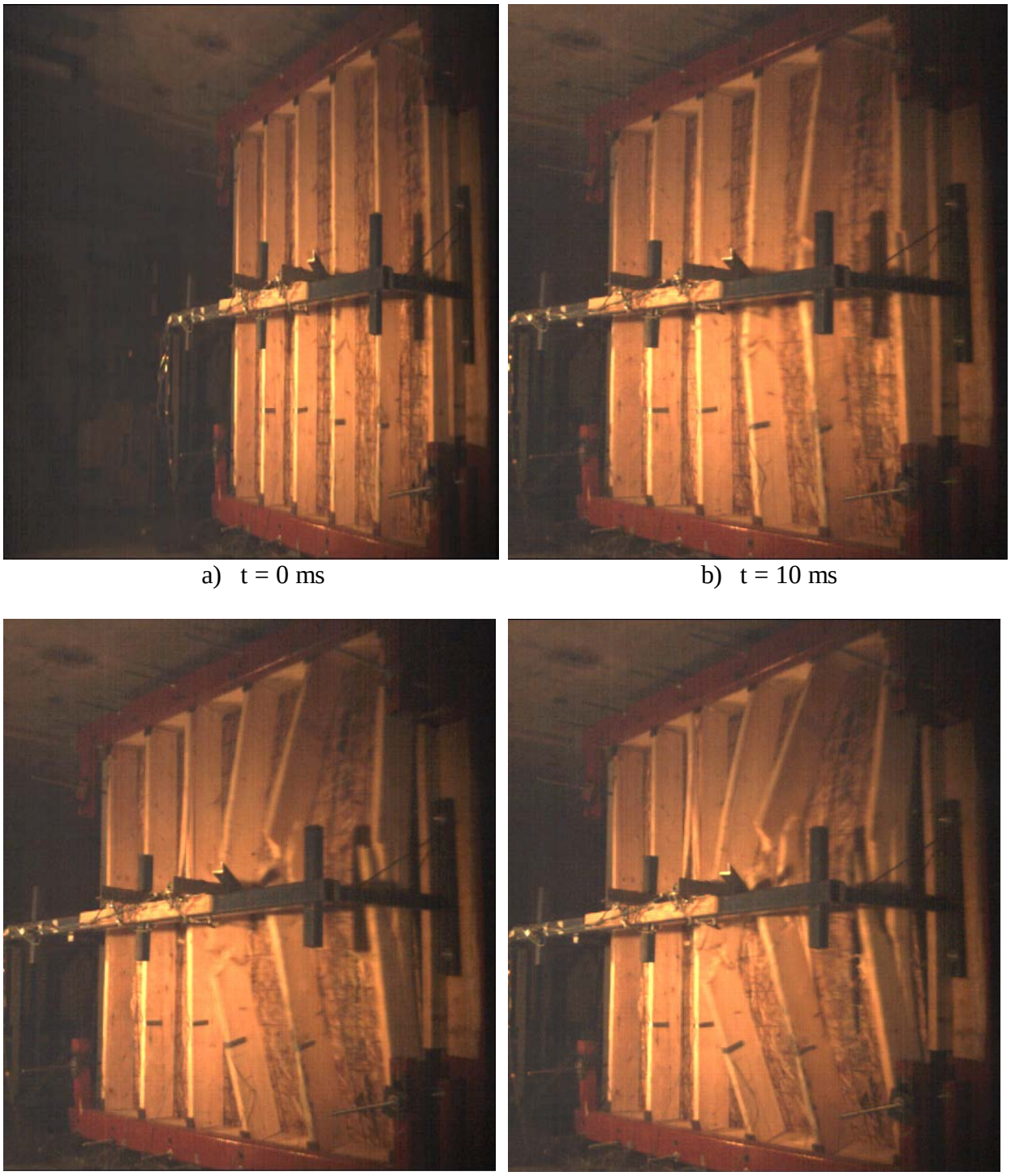

a) t = 0 ms b) t = 10 ms

c) t = 16 ms d) t = 20 ms

Figure A14.3 : Evolution of damage with time for Wall 14 Shot 1

a) Oblique view

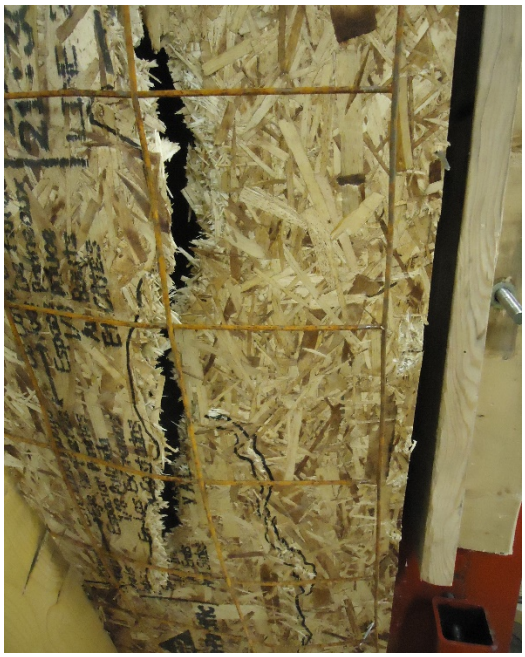

b) Damage to OSB

c) Superficial damage to Stud 4

Figure A14.4 : Damage of Wall 14 after shot 1

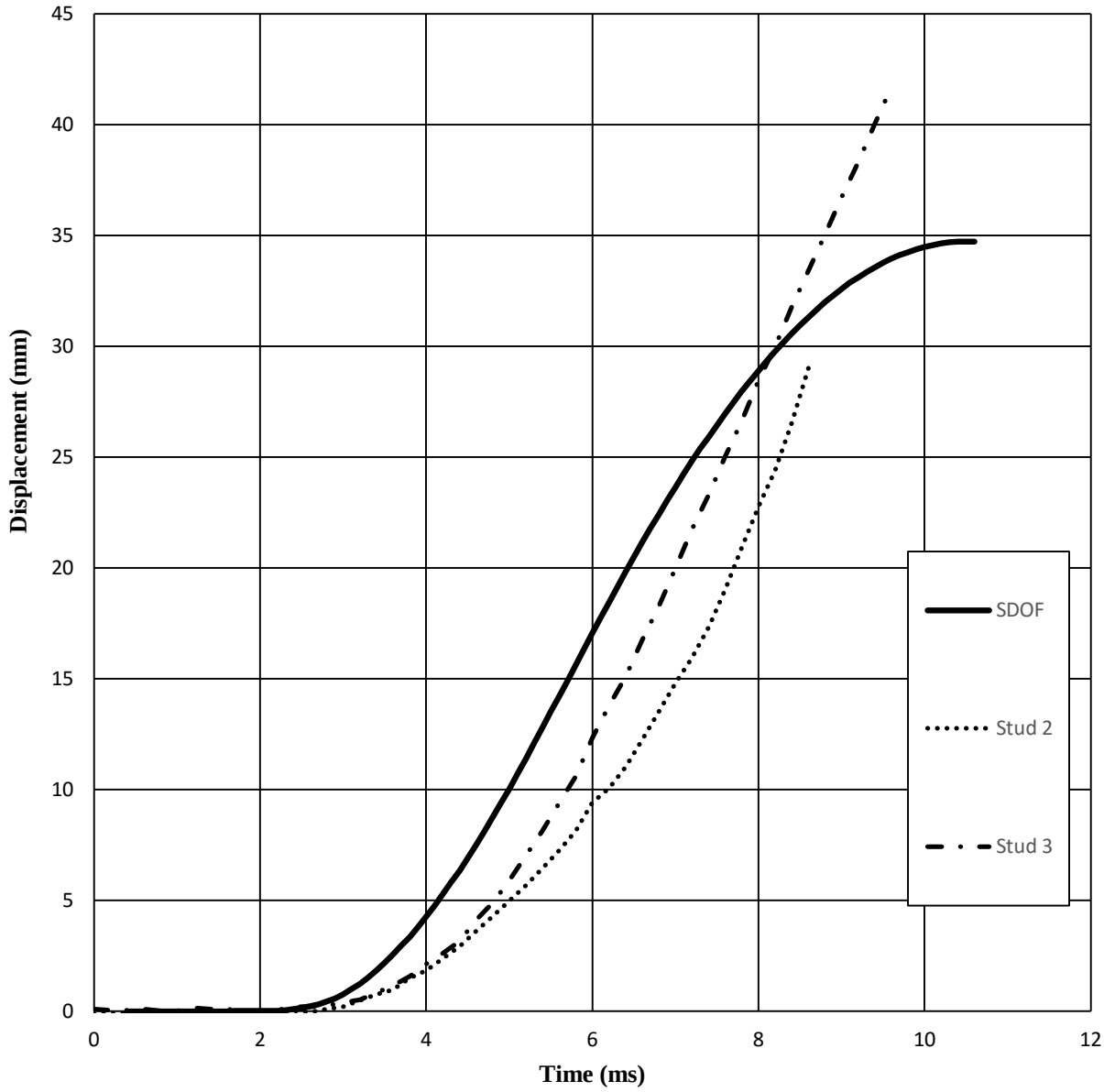

Figure A14.5 : SDOF prediction for Wall 14 Shot 1

Wall 15 Test Summary

Test name: Wall_15_Shot_1 **Test date:** 14/8/2014

Driver length: 2745 mm **Driver pressure:** 297.9 kPa

Wall mass: 95.36 kg

Test specimen properties:

- 6-38 mm x 184 mm No. 2 studs @ 406.4 mm o/c
- Nails, 50 mm x 2.87 mm @ 150 mm o/c (field and edge)
- 2108 mm total length of wall
- 2032 mm long studs
- 2032 mm clear span
- 11 mm OSB
- Welded wire fabric (152 x 152 mm gaps, 11.1 mm^2 thick) placed on the tension face of wall studs

Average maximum reflected pressure: 47.6 kPa **Average max. deflection of wall studs:** 38.36 mm

Average maximum reflected impulse: 397.9 kPa-ms **Average time to max. deflection:** 8.1 ms

Positive phase duration: 15.2 ms **Quantified wall damage level:** Moderate

Table A15.1 : Stud data from Wall 15 Shot 1

Stud number	Stud reference ID	Maximum mid-span displacement	Time to Maximum	Debris projection	Stud damage level
		mm	ms	mm	
1	S8-15	-	-	No debris	Superficial
2	S8-14	38.36	7.6	No debris	Superficial
3	S8-3	-	-	No debris	Failed
4	S8-5	-	9.6	No debris	Superficial
5	S8-7	-	7.0	No debris	Superficial
6	S8-27	-	-	No debris	Superficial

Comments:

Stud 3 was significantly cracked following the shot, henceforth the stud was considered to have failed. The remaining studs remained elastic and did not suffer any visual damage. The OSB panels were very heavily damaged, with almost no significant area still attached to the inside stud face. The WWM was effectively in catching all sheathing debris and maintain the integrity of the stud wall. Very little debris was created by the shot, with the largest piece being approximately 100 mm. Small steel anchors utilized to attach the field area of the WWM to the studs were thrown and created additional debris. Further testing will neglect the use of these.

The WWM by itself yielded/deflected but did not suffer any apparent damage. No nail withdrawal was observed since most of the sheathing was blown off before this phenomenon could occur. Required repairs to the stud wall would include new sheathing panels and a new Stud 3. The LVDT for Stud 3 was damaged during the test and did not record any data.

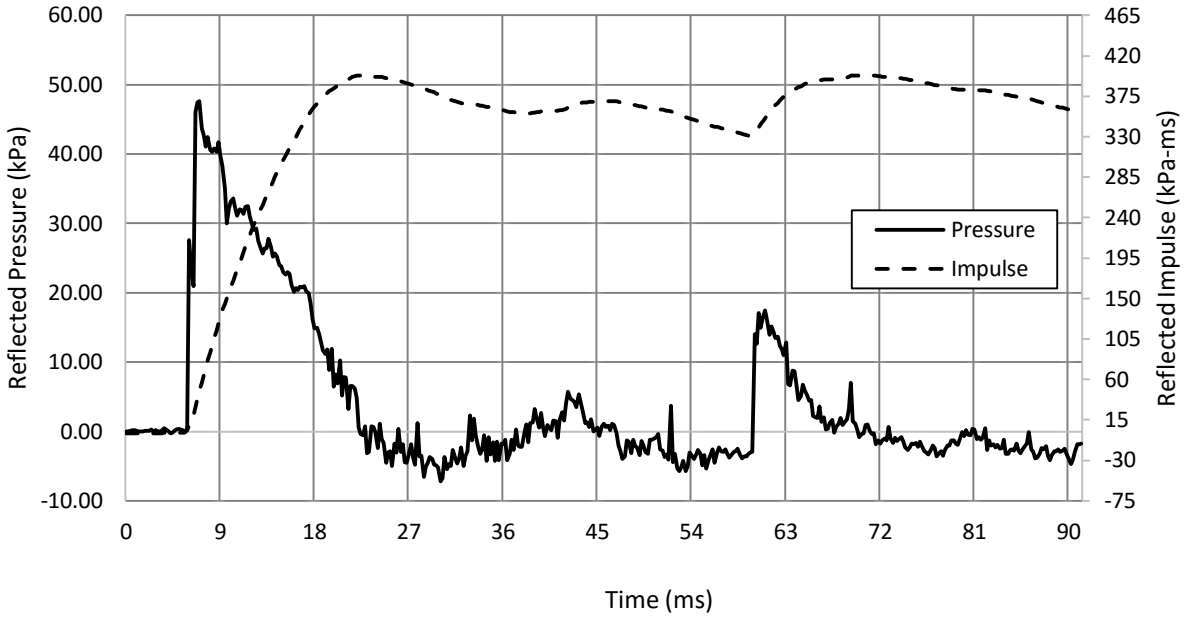

Figure A15.1 : Reflected pressure and impulse time histories for Wall 15 Shot 1

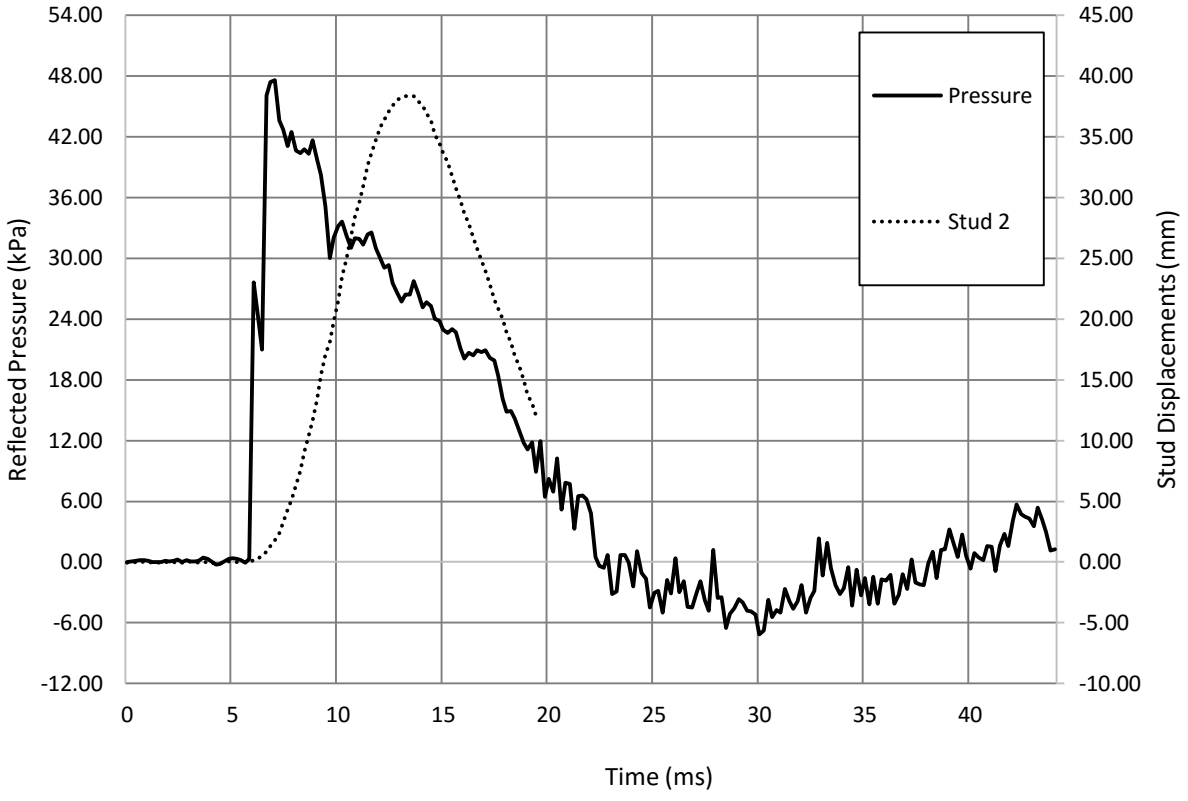

Figure A15.2 : Reflected pressure and displacement time histories for Wall 15 Shot 1

a) t = 0 ms

b) t = 10 ms

c) t = 16 ms

d) t = 30 ms

Figure A15.3 : Evolution of damage with time for Wall 15 Shot 1

a) Front view

b) Lack of noticeable debris

c) Failed Stud 3

Figure A15.4 : Damage of Wall 15 after shot 1

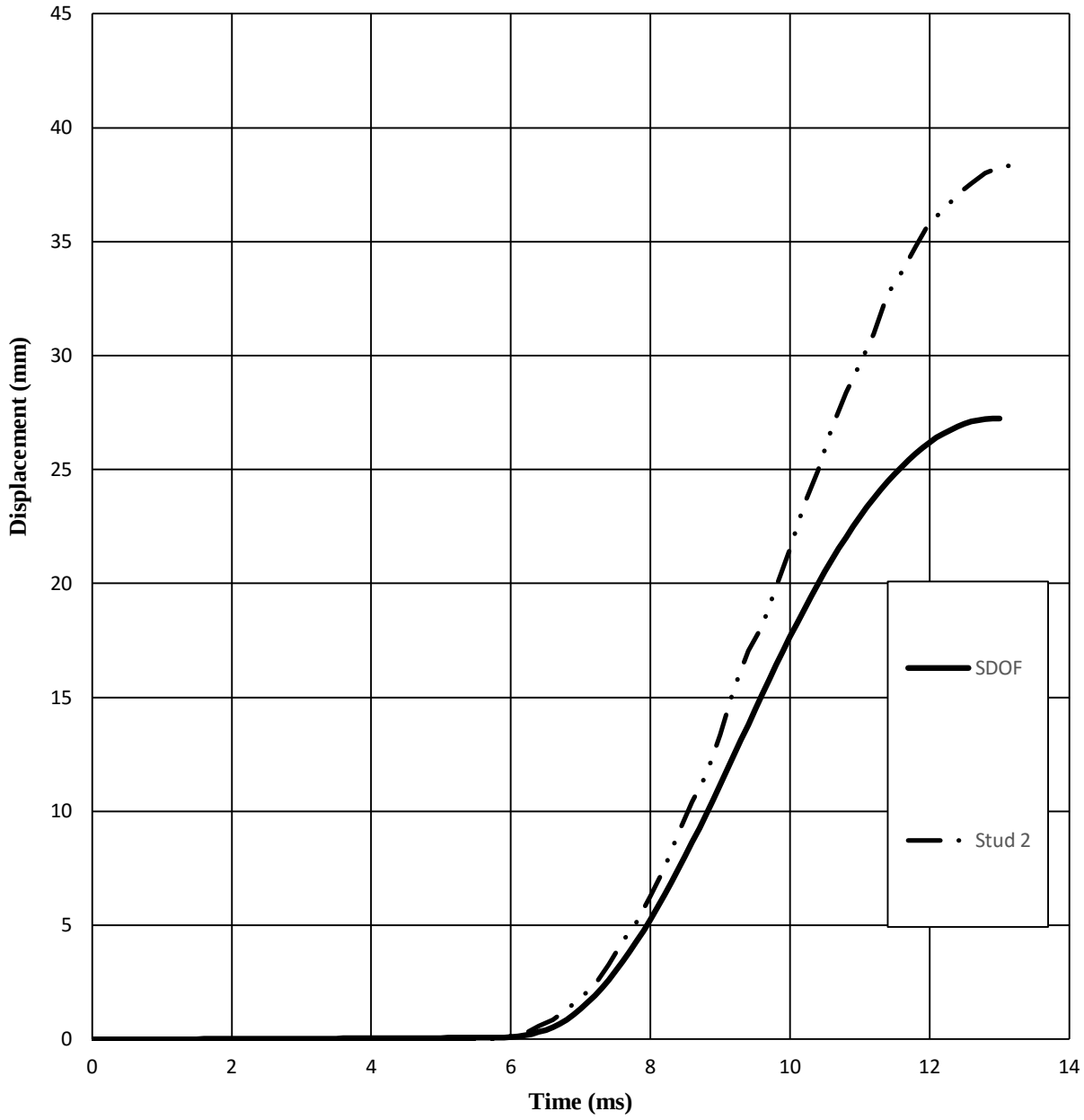

Figure A15.5 : SDOF prediction for Wall 15 Shot 1

Wall 16 Test Summary

Test name: Wall_16_Shot_1 **Test date:** 17/8/2014

Driver length: 2745 mm **Driver pressure:** 413.7 kPa

Wall mass: 96.04 kg

Test specimen properties:

- 6-38 mm x 184 mm No. 2 studs @ 406.4 mm o/c
- Nails, 50 mm x 2.87 mm @ 150 mm o/c (field and edge)
- 2108 mm total length of wall
- 2032 mm long studs
- 2032 mm clear span
- 11 mm OSB
- Welded wire fabric (152 x 152 mm gaps, 11.1 mm^2 thick) placed on the tension face of wall studs

Average maximum reflected pressure: 62.5 kPa **Average max. deflection of wall studs:** No data

Average maximum reflected impulse: 437.1 kPa-ms **Average time to max. deflection:** 7.0 ms

Positive phase duration: 14.0 ms **Quantified wall damage level:** Superficial

Table A16.1 : Stud data from Wall 16 Shot 1

Stud number	Stud reference ID	Maximum mid-span displacement	Time to Maximum	Debris projection	Stud damage level
		mm	ms	mm	
1	S8-25	-	-	No debris	Superficial
2	S8-9	-	8.0	No debris	Superficial
3	S8-32	-	6.4	No debris	Superficial
4	S8-21	-	6.8	No debris	Superficial
5	S8-19	-	6.8	No debris	Superficial
6	S8-26	-	-	No debris	Superficial

Comments:

None of the stud had apparent damage. All of the sheathing was blown off from the shot but was caught by the catcher system. The WWM was no longer connected to the outside face of the stud but remained connected to the wall via top and bottom plate connectors. No damage to the WWM apart from bending and deformation due to stud deflection and sheathing debris. Large residual deflections to the WWM.

Some bottom and top plate rotation was observed due to the grab-and-pull effect of the WWM which is connected to the top and bottom plate.

No significant sheathing debris was observed. Largest sheathing debris measured approximately 150 mm. The WWM by itself yielded/deflected but did not suffer any apparent damage. The catcher system effectively caught all debris that would otherwise injure occupants.

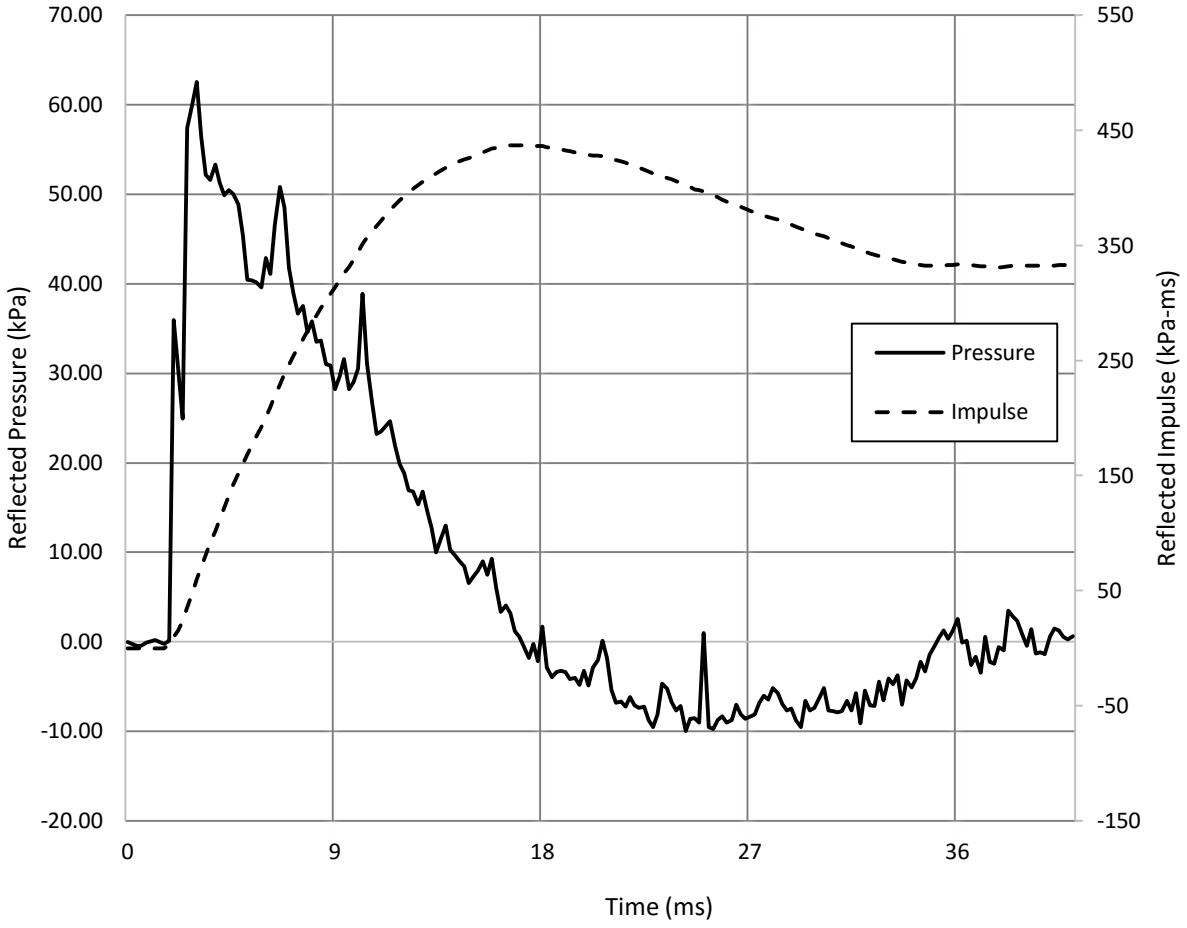

Figure A16.1 : Reflected pressure and impulse time histories for Wall 16 Shot 1

a) t = 0 ms

b) t = 8 ms

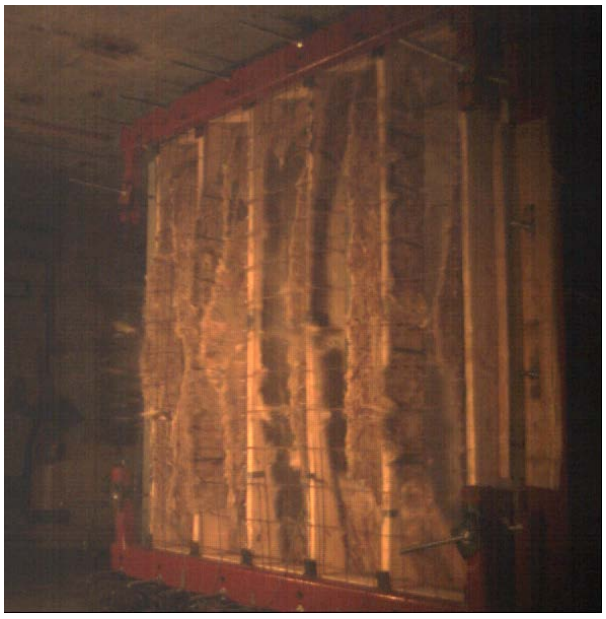

c) t = 12 ms

d) t = 20 ms

Figure A16.2 : Evolution of damage with time for Wall 16 Shot 1

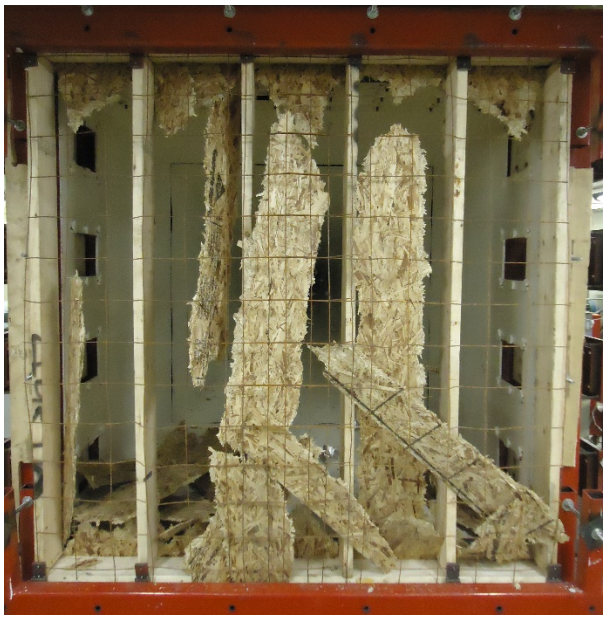

a) Front view

b) Oblique view

c) Lack of noticeable debris

Figure A16.3 : Damage of Wall 16 after shot 1

Wall 17 Test Summary

Test name: Wall_17_Shot_1 **Test date:** 30/7/2014

Driver length: 2745 mm **Driver pressure:** 71.7 kPa

Wall mass: 68.46 kg

Test specimen properties:

- 6-38 mm x 140 mm No. 2 studs @ 406.4 mm o/c
- Nails, 50 mm x 2.87 mm @ 150 mm o/c (field and edge)
- 2108 mm total length of wall
- 2032 mm long studs
- 2032 mm clear span
- 11 mm OSB
- 12-82 mm x 2.87mm nails @ 400 mm o/c connecting top and bottom plates to blocking

Average maximum reflected pressure: 13.9 kPa **Average max. deflection of wall studs:** No data

Average maximum reflected impulse: 139.2 kPa-ms **Average time to connection failure:** 10.0 ms

Positive phase duration: 16.6 ms **Quantified wall damage level:** Blowout

Table A17.1 : Stud data from Wall 17 Shot 1

Stud number	Stud reference ID	Maximum mid-span displacement	Time to Maximum	Debris projection	Stud damage level
		mm	ms	mm	
1	S-76	-	-	No debris	Superficial
2	S-105	-	10.2	No debris	Superficial
3	S-231	-	9.6	No debris	Superficial
4	S-75	-	10.0	No debris	Superficial
5	S-122	-	10.0	No debris	Superficial
6	S-81	-	-	No debris	Superficial

Comments:

None of the stud had apparent damage. The connections to the blocking failed at a relatively low pressure. Nail withdrawal and puncture was observed at the sheathing joint along Stud 3, along the top plate, and along Stud 5 and Stud 6. The HSS holding the top blocking clamped the sheathing and prevented the wall from fully sliding out of the shock tube. Connection failure was still evident.

All 6 top plate toe nail fasteners were pulled out. 4 bottom connector nails were pulled out while the remaining 2 were partially still embedded into the blocking. Dragging marks of the yielded nails along the blockings was observed. Review of the test video shows that the top plate toe nails failed before the bottom plate ones, which is expected since toe nails have lower capacity than normal perpendicularly driven nails.

No deflection readings were measured since blowout was expected.

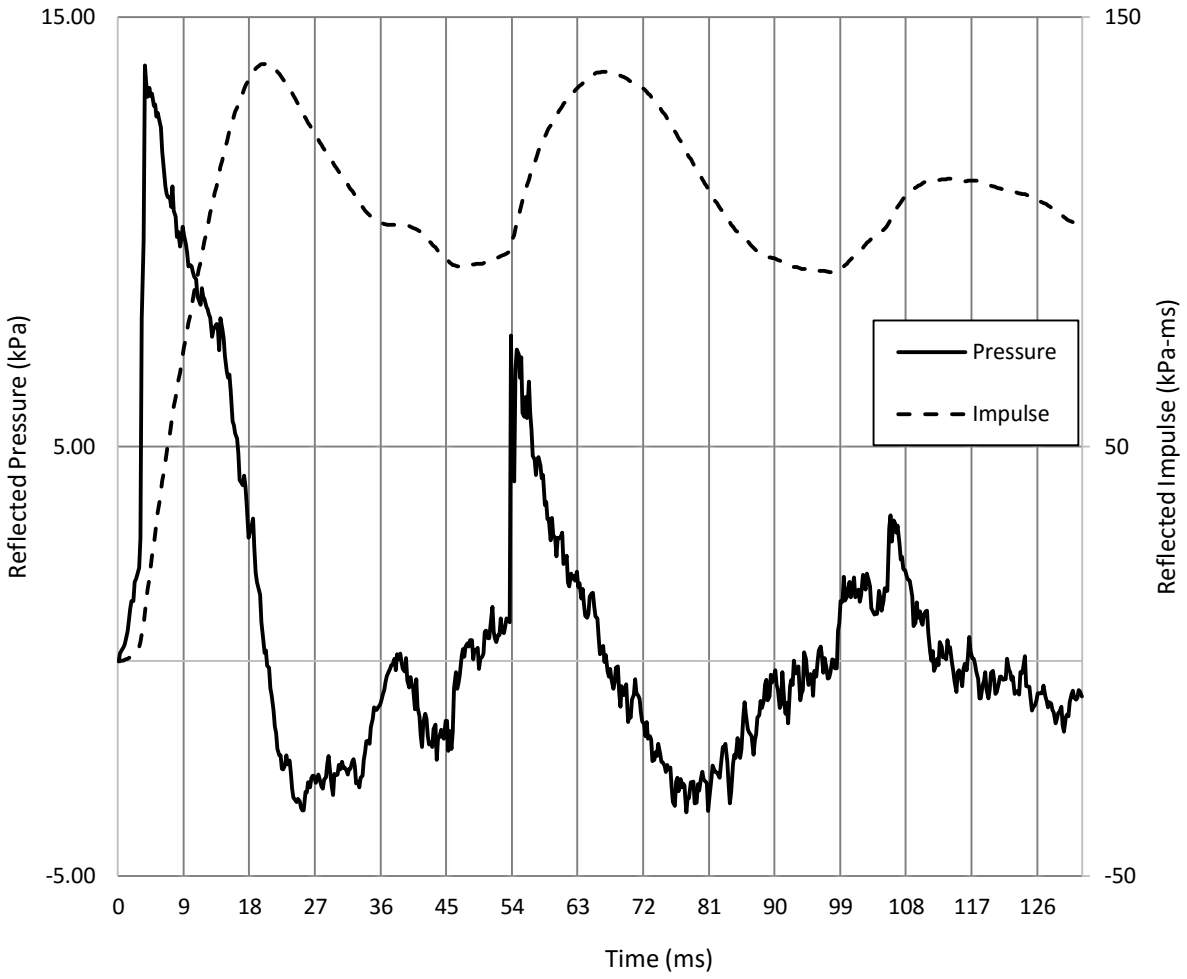

Figure A17.1 : Reflected pressure and impulse time histories for Wall 17 Shot 1

a) t = 0 ms

b) t = 6 ms

c) t = 12 ms

d) t = 40 ms

Figure A17.2 : Evolution of connection failure with time for Wall 17 Shot 1

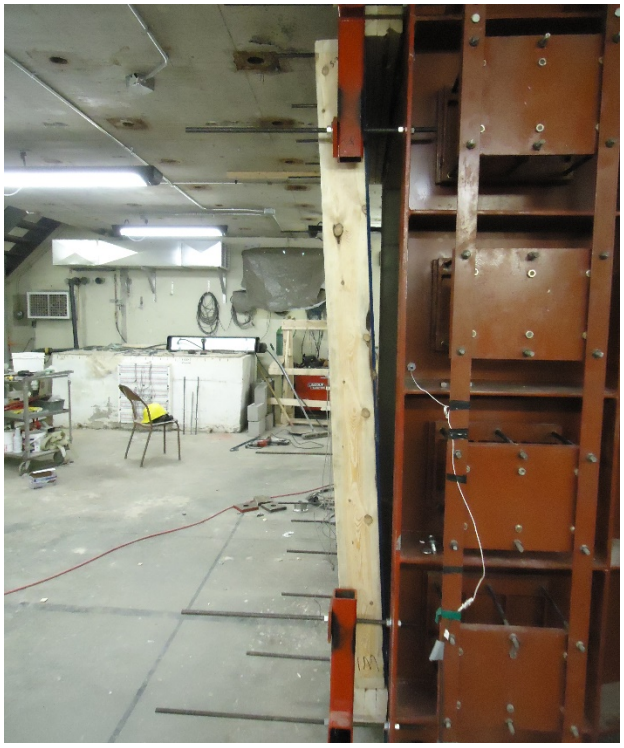

a) Side view

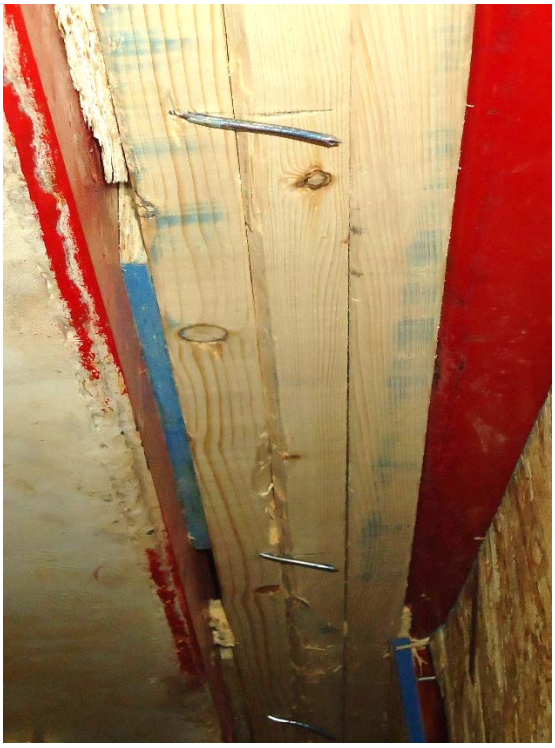

b) Nail yielding and withdrawal at top blocking

c) Nail yielding and withdrawal at bottom plate

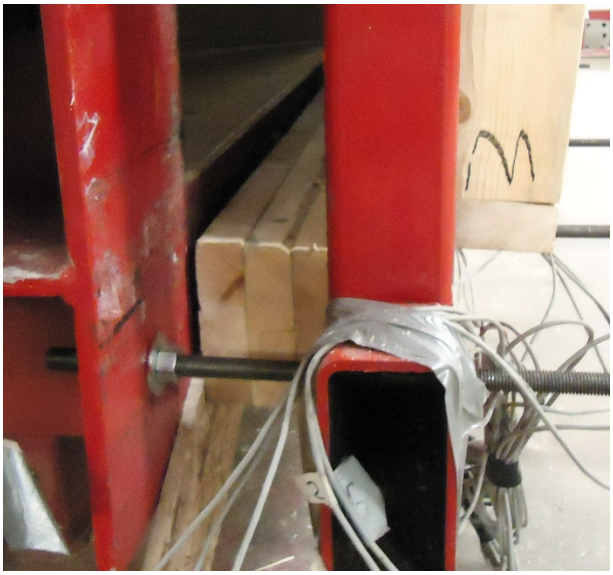

d) Lateral displacement due to bottom connection failure

Figure A17.3 : Damage of Wall 17 after shot 1

Test name: Wall_17_Shot_2 **Test date:** 30/7/2014

Driver length: 2745 mm **Driver pressure:** 214.4 kPa

Wall mass: 68.46 kg

Test specimen properties:

- 6-38 mm x 140 mm No. 2 studs @ 406.4 mm o/c
- Nails, 50 mm x 2.87 mm @ 150 mm o/c (field and edge)
- 2108 mm total length of wall
- 2032 mm long studs
- 2032 mm clear span
- 11 mm OSB
- 28-82 mm x 2.87mm nails @ 150 mm o/c connecting top and bottom plates to blocking

Average maximum reflected pressure: 41.4 kPa **Average max. deflection of wall studs:** No data

Average maximum reflected impulse: 302.5 kPa-ms **Average time to connection failure:** 7.0 ms

Positive phase duration: 16.0 ms **Quantified wall damage level:** Blowout

Table A17.2 : Stud data from Wall 17 Shot 2

Stud number	Stud reference ID	Maximum mid-span displacement	Time to Maximum	Debris projection	Stud damage level
		mm	ms	mm	
1	S-76	-	-	5500	Superficial
2	S-105	-	6.6	5500	Superficial
3	S-231	-	6.0	5500	Superficial
4	S-75	-	9.6	5500	Superficial
5	S-122	-	7.0	5500	Superficial
6	S-81	-	-	5500	Superficial

Comments:

None of the stud had apparent damage. The connections failed and the wall was propelled across the laboratory room, where it then hit the laboratory wall and was disassembled into individual components. Six of the fourteen top plate toe nail fasteners, located between Stud 2 to Stud 4, were pulled out from the blocking, while the rest remained in the blocking. All 14 bottom connector nails remained in the blocking. All nails yielded significantly. Dragging marks of the yielded nails along the blockings was observed. Sheathing remained overall undamaged.

No deflection readings were measured since full blowout was expected. Review of the test video shows that the top plate toe nails failed before the bottom plate ones, which is expected since toe nails have lower capacity than normal perpendicularly driven nails.

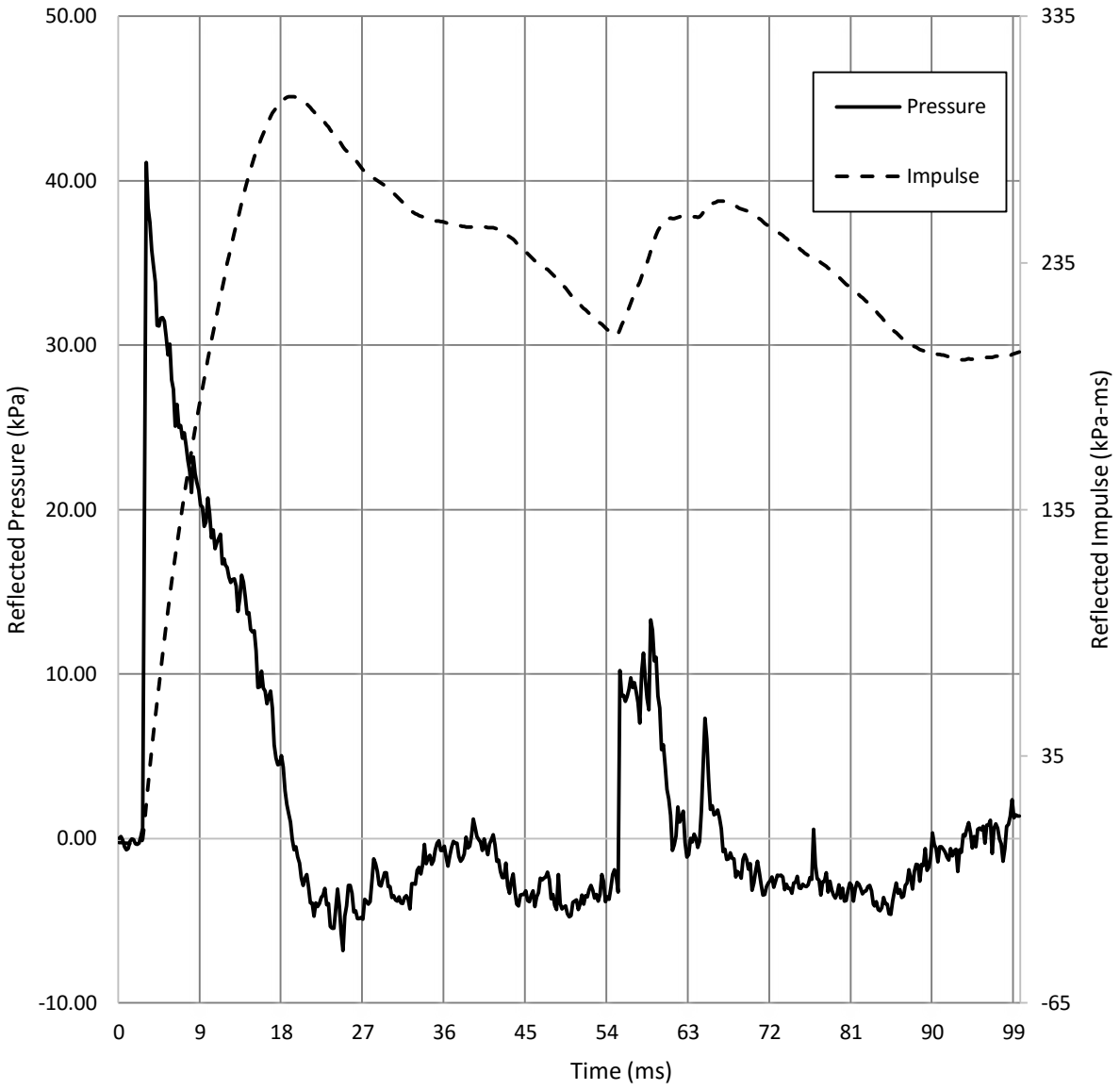

Figure A17.4 : Reflected pressure and impulse time histories for Wall 17 Shot 2

a) t = 0 ms

b) t = 10 ms

c) t = 20 ms

d) t = 40 ms

Figure A17.5 : Evolution of connection failure with time for Wall 17 Shot 2

a) Decomposed specimen

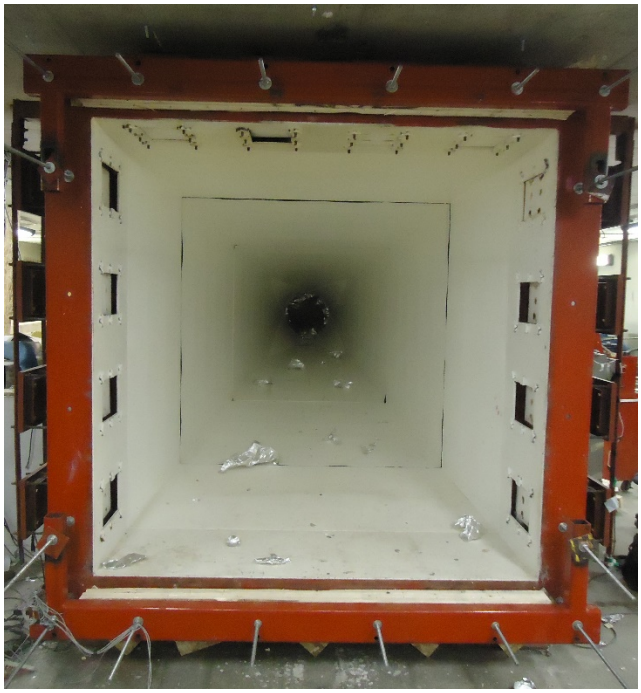

b) Front view

c) Nail yielding and withdrawal at bottom plate

d) Nail yielding and head pull-through at top plate

Figure A17.6 : Damage of Wall 17 after shot 2

Wall 18 Test Summary

Test name: Wall_18_Shot_1 **Test date:** 31/7/2014

Driver length: 2745 mm **Driver pressure:** 137.9 kPa

Wall mass: 68.66 kg

Test specimen properties:

- 6-38 mm x 140 mm No. 2 studs @ 406.4 mm o/c
- Nails, 50 mm x 2.87 mm @ 150 mm o/c (field and edge)
- 2108 mm total length of wall
- 2032 mm long studs
- 2032 mm clear span
- 11 mm OSB
- 28-82 mm x 2.87mm nails @ 150 mm o/c connecting top and bottom plates to blocking

Average maximum reflected pressure: 29.3 kPa **Average max. deflection of wall studs:** No data

Average maximum reflected impulse: 234.6 kPa-ms **Average time to connection failure:** 8.9 ms

Positive phase duration: 17.4 ms **Quantified wall damage level:** Blowout

Table A18.1 : Stud data from Wall 18 Shot 1

Stud number	Stud reference ID	Maximum mid-span displacement	Time to Maximum	Debris projection	Stud damage level
		mm	ms	mm	
1	S-92	-	-	5500	Superficial
2	S-205	-	10.8	5500	Superficial
3	S-217	-	7.6	5500	Superficial
4	S-199	-	8.7	5500	Superficial
5	S-202	-	8.4	5500	Superficial
6	S-77	-	-	4500	Superficial

Comments:

None of the stud had apparent damage. The connections failed and the wall was propelled across the laboratory room, where it then hit the laboratory wall and was disassembled into individual components. Stud 6 remained attached to the bottom plate. One of the fourteen top plate toe nail fasteners, located near Stud 2, was pulled out from the blocking, while the rest remained in the blocking. All 14 bottom connector nails remained in the blocking. All nails yielded significantly. Dragging marks of the yielded nails along the blockings was observed. Sheathing remained undamaged. Some stud-to-plate nails are visibly present without any yielding having occurred.

No deflection readings were measured since full blowout was expected. Review of the test video shows that the top plate toe nails failed before the bottom plate ones, which is expected since toe nails have lower capacity than normal perpendicularly driven nails.

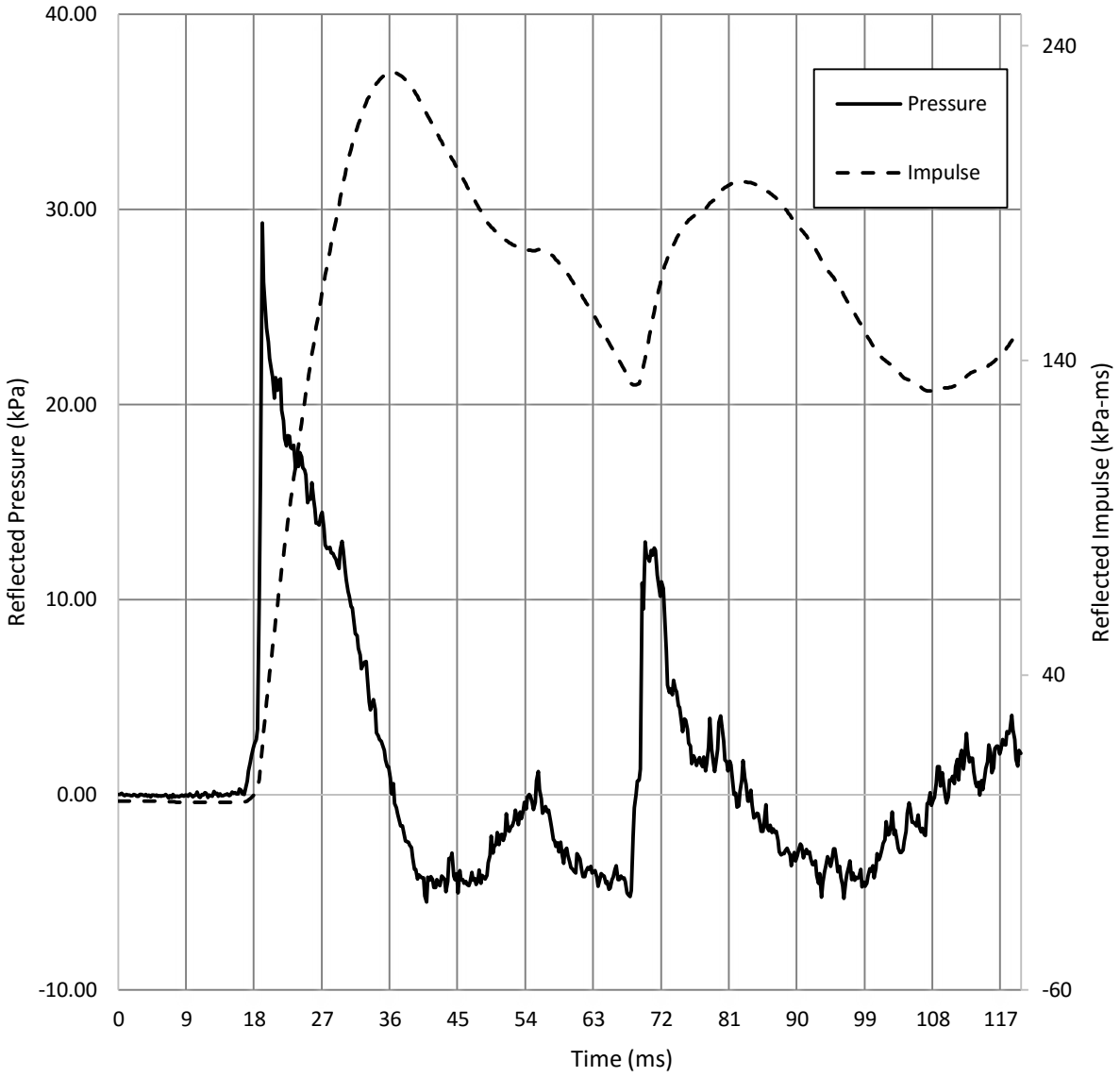

Figure A18.1 : Reflected pressure and impulse time histories for Wall 18 Shot 1

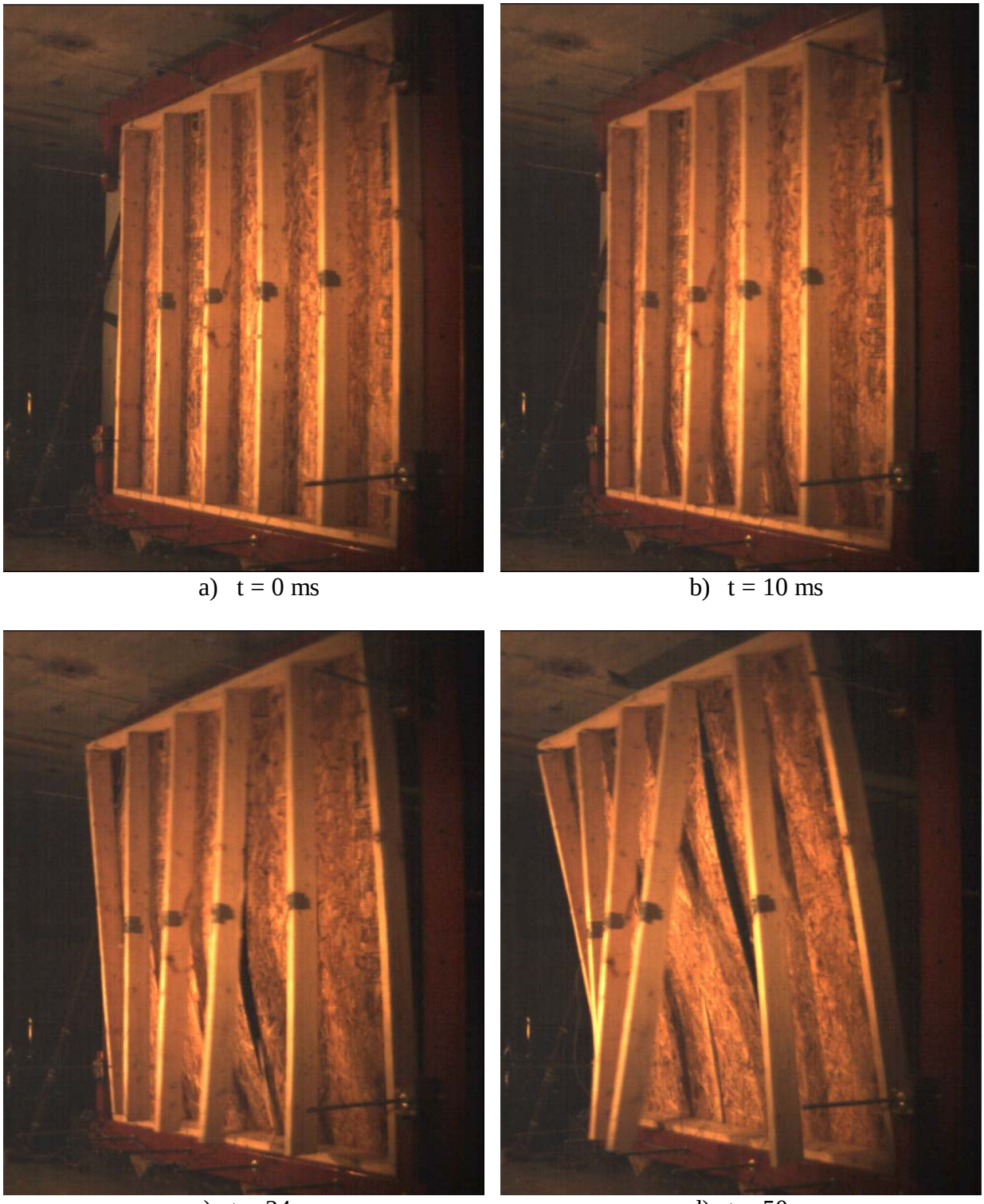

a) t = 0 ms

b) t = 10 ms

c) t = 24 ms

d) t = 50 ms

Figure A18.2 : Evolution of connection failure with time for Wall 18 Shot 1

a) Oblique view

b) Decomposed specimen

c) Nail withdrawal at bottom plate

Figure A18.3 : Damage of Wall 18 after shot 1

Wall 19 Test Summary

Test name: Wall_19_Shot_1 **Test date:** 1/8/2014

Driver length: 2745 mm **Driver pressure:** 241.3 kPa

Wall mass: 73.24 kg

Test specimen properties:

- 6-38 mm x 140 mm No. 2 studs @ 406.4 mm o/c
- Nails, 50 mm x 2.87 mm @ 150 mm o/c (field and edge)
- 2108 mm total length of wall
- 2032 mm long studs
- 2032 mm clear span
- 11 mm OSB
- 12 Simpson Strong-Tie® HU28 joist hanger-type connectors used to connect wall to blocking

Average maximum reflected pressure: 44.3 kPa **Average max. deflection of wall studs:** No data

Average maximum reflected impulse: 387.3 kPa-ms **Average time to max. deflection:** 5.0 ms

Positive phase duration: 19.8 ms **Quantified wall damage level:** Blowout

Table A19.1 : Stud data from Wall 19 Shot 1

Stud number	Stud reference ID	Maximum mid-span displacement	Time to Maximum	Debris projection	Stud damage level
		mm	ms	mm	
1	S-79	-	-	No debris	Superficial
2	S-115	-	4.0	2000	Failed
3	S-117	-	7.4	No debris	Failed
4	S-104	-	4.4	5500	Failed
5	S-84	-	4.2	No debris	Failed
6	S-107	-	-	No debris	Superficial

Comments:

The four center studs failed in brash fashion at mid-span. Stud 1 had no visual damage, while the surrounding sheathing was completely blown off. The sheathing around Stud 2 was also completely blown off. The sheathing near Stud 4 was sucked-in or fell into the shock tube. Significant amount of cracking and splitting was observed in the bottom plates near Stud 2, Stud 3, Stud 5, and Stud 6. Top plate damage observed near Stud 1, Stud 2, and Stud 6. Overall large rotation occurring at the plates, with the HU28 screws being pulled out from the plates. Review of the video shows that the HU28 effectively maintained the connection between the studs and the plates, and reduced residual deflection. Wall conditions behaved similar to that of pin-pin.

No deflection readings were measured since connector behaviour was unknown. Large amounts of sheathing was blown off, with some significant debris created. Majority of blown sheathing remained on the shock tube side, and most fell back into the shock tube after the shot. Two of the studs created very hazardous debris, ranging from a range of 2000 mm to 5500 mm. Minor connector yielding observed at Stud 2.

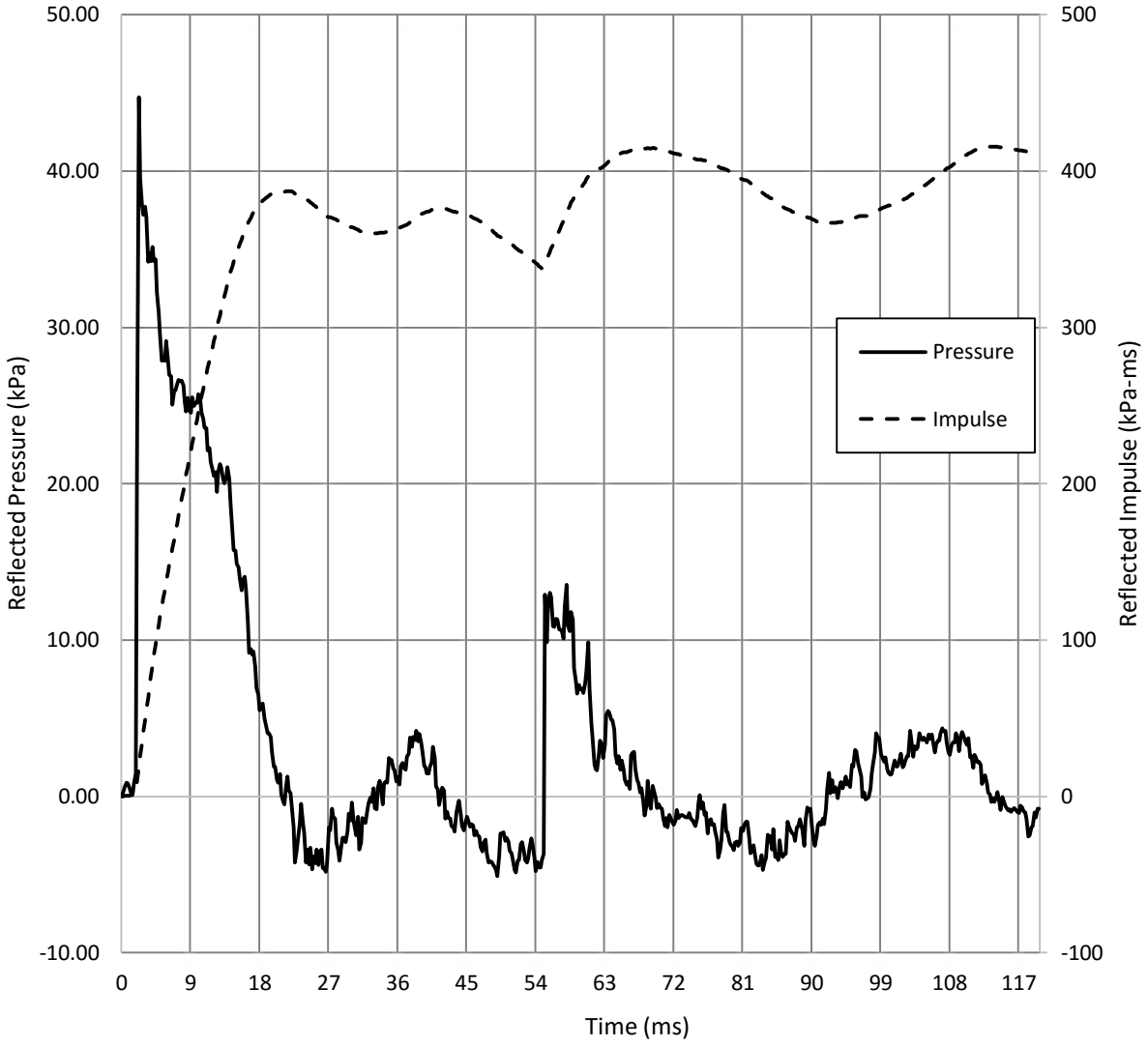

Figure A19.1 : Reflected pressure and impulse time histories for Wall 19 Shot 1

a) t = 0 ms

b) t = 8 ms

c) t = 14 ms

d) t = 22 ms

Figure A19.2 : Evolution of damage with time for Wall 19 Shot 1

a) Oblique view

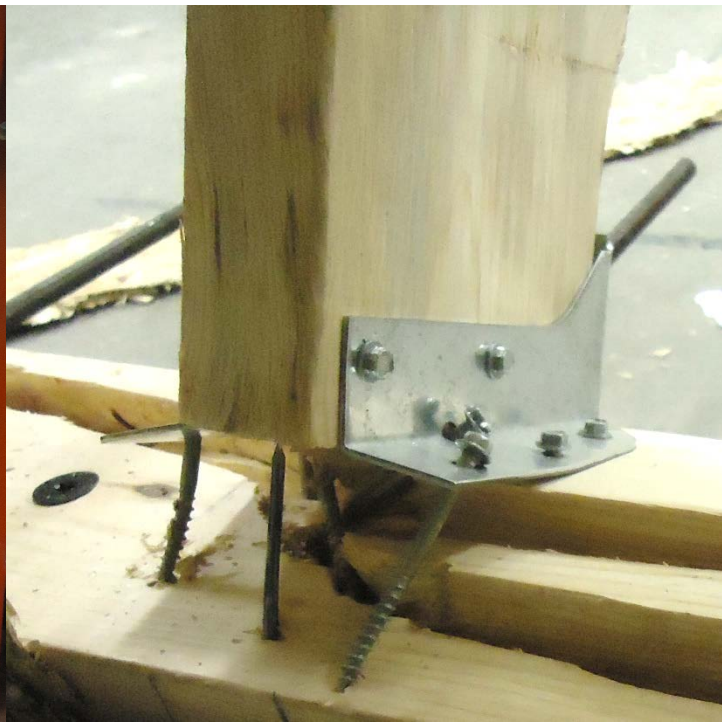

b) HU28 fastener withdrawal

c) Damage to top plate between Stud 1 and 2

Figure A19.3 : Damage of Wall 19 after shot 1

Wall 20 Test Summary

Test name: Wall_20_Shot_1 **Test date:** 4/8/2014

Driver length: 2745 mm **Driver pressure:** 206.8 kPa

Wall mass: 73.54 kg

Test specimen properties:

- 6-38 mm x 140 mm No. 2 studs @ 406.4 mm o/c
- Nails, 50 mm x 2.87 mm @ 150 mm o/c (field and edge)
- 2108 mm total length of wall
- 2032 mm long studs
- 2032 mm clear span
- 11 mm OSB
- 12 Simpson Strong-Tie® HU28 joist hanger-type connectors used to connect wall to blocking

Average maximum reflected pressure: 37.3 kPa **Average max. deflection of wall studs:** 53.63 mm

Average maximum reflected impulse: 341.5 kPa-ms **Average time to max. deflection:** 8.7 ms

Positive phase duration: 18.4 ms **Quantified wall damage level:** Blowout

Table A20.1 : Stud data from Wall 20 Shot 1

Stud number	Stud reference ID	Maximum mid-span displacement	Time to Maximum	Debris projection	Stud damage level
		mm	ms	mm	
1	S-99	-	-	No debris	Superficial
2	S-108	55.56	8.0	No debris	Failed
3	S-96	51.71	9.4	No debris	Failed
4	S-114	-	-	No debris	Failed
5	S-113	-	-	No debris	Failed
6	S-100	-	-	No debris	Superficial

Comments:

The four center studs failed in brash fashion at mid-span. Stud 1 had no visual damage, while a major portion of the surrounding sheathing was completely blown off. A large OSB piece near Stud 1 was ejected to a distance of 2000 mm. Large rips in the sheathing near the failure site of Stud 2 and 3, with a small chunk missing near Stud 2 which was ejected to a distance of 750 mm. Large gap at the sheathing joint running along Stud 3. Large vertical sheathing rip between Stud 5 and 6. The sheathing near Stud 4 was sucked-in or fell into the shock tube. Significant amount of cracking and splitting was observed in the bottom plates near Stud 3. Significant cracking and splitting along the top-plate. Overall large rotation occurring at the plates, with the HU28 screws being pulled out from the plates. Review of the video shows that the HU28 effectively maintained the connection between the studs and the plates during the shot and reduced residual deflection. Wall conditions behaved similarly to that of pin-pin.

Not as much sheathing debris produced compared to the other wall with HU28 connectors. Reason for this is the lower pressure.. No stud debris was created, partially due to the connectivity between the studs and the wall plates. No damage observed in the connectors, besides minor screw withdrawal.

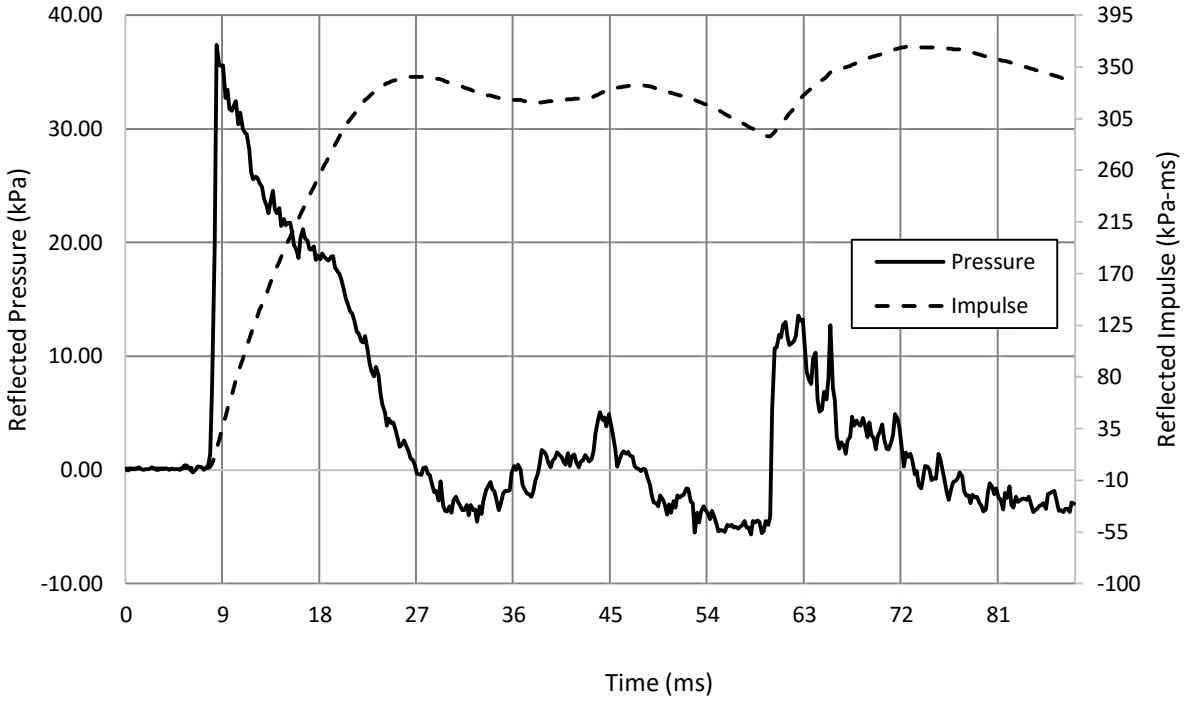

Figure A20.1 : Reflected pressure and impulse time histories for Wall 20 Shot 1

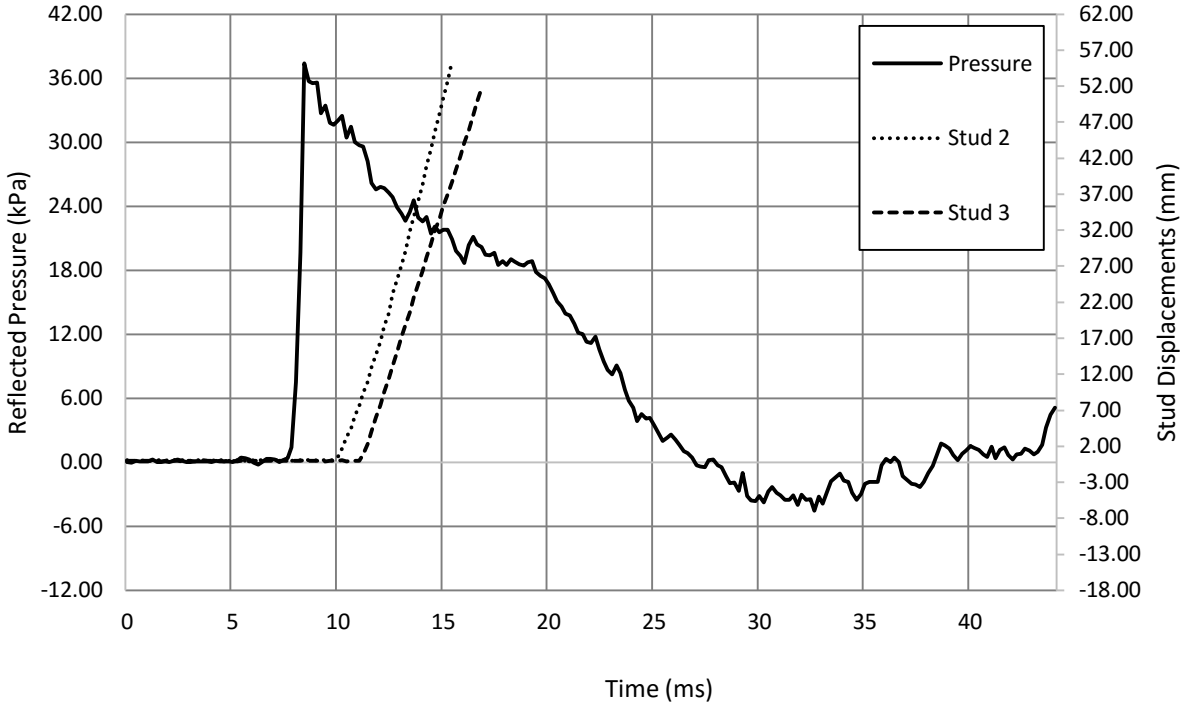

Figure A20.2 : Reflected pressure and displacement time histories for Wall 20 Shot 1

a) t = 0 ms

b) t = 10 ms

c) t = 16 ms

d) t = 22 ms

Figure A20.3 : Evolution of damage with time for Wall 20 Shot 1

a) Front view

b) Inside view

c) Damage to top plate

d) HU28 fastener withdrawal

Figure A20.4 : Damage of Wall 20 after shot 1

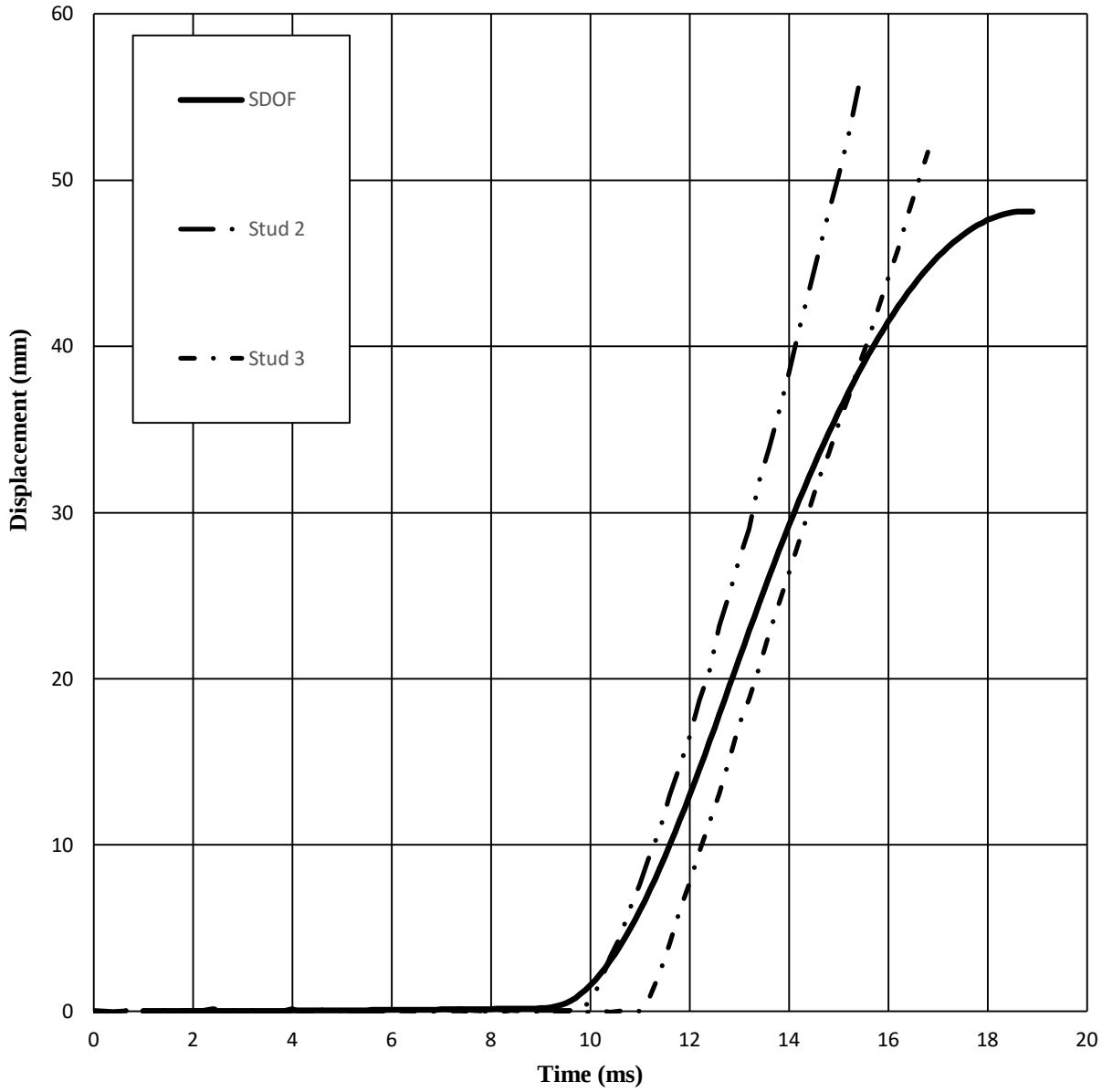

Figure A20.5 : SDOF prediction for Wall 20 Shot 1

Wall 21 Test Summary

Test name: Wall_21_Shot_1 **Test date:** 4/8/2014

Driver length: 2745 mm **Driver pressure:** 213.7 kPa

Wall mass: 69.76 kg

Test specimen properties:

- 6-38 mm x 140 mm No. 2 studs @ 406.4 mm o/c
- Nails, 50 mm x 2.87 mm @ 150 mm o/c (field and edge)
- 2108 mm total length of wall
- 2032 mm long studs
- 2032 mm clear span
- 11 mm OSB
- 12 Simpson Strong-Tie® LJS26DS joist hanger-type connectors used to connect wall to blocking

Average maximum reflected pressure: 39.5 kPa **Average max. deflection of wall studs:** 42.00 mm

Average maximum reflected impulse: 342.2 kPa-ms **Average time to max. deflection:** 9.3 ms

Positive phase duration: 17.4 ms **Quantified wall damage level:** Blowout

Table A21.1 : Stud data from Wall 21 Shot 1

Stud number	Stud reference ID	Maximum mid-span displacement	Time to Maximum	Debris projection	Stud damage level
		mm	ms	mm	
1	S-85	-	-	No debris	Superficial
2	S-94	33.79	8.8	No debris	Failed
3	S-110	50.20	9.8	No debris	Failed
4	S-91	-	-	5500	Failed
5	S-119	-	-	No debris	Failed
6	S-101	-	-	No debris	Superficial

Comments:

The four center studs failed in brash fashion at mid-span. Stud 1 had no visual damage. Large section of sheathing between Stud 1 and Stud 2 was blown off to a distance of 2000 mm. Large rips in the sheathing near the failure site of Stud 2, 3, and 4. Sheathing joint still intact. Large vertical sheathing rip between Stud 5 and 6. Significant amount of cracking and splitting was observed in the bottom plates near Stud 1 3, 5, and 6. Significant cracking and splitting along the top-plate at Stud 1. Overall smaller rotation occurring at the plates when comparing the HU28 videos to that of this test. Review of the video shows that the LJS26DS effectively maintained the connection between the studs and the plates during the shot and reduced residual deflection as well as rotation of the wall plates.

Only stud debris created was a small section of the tension fibre of Stud 4 which was ejected to the end of the laboratory. No damage observed in the connectors. Connector screw withdrawal observed at the bottom plate of Stud 2, but nothing significant.

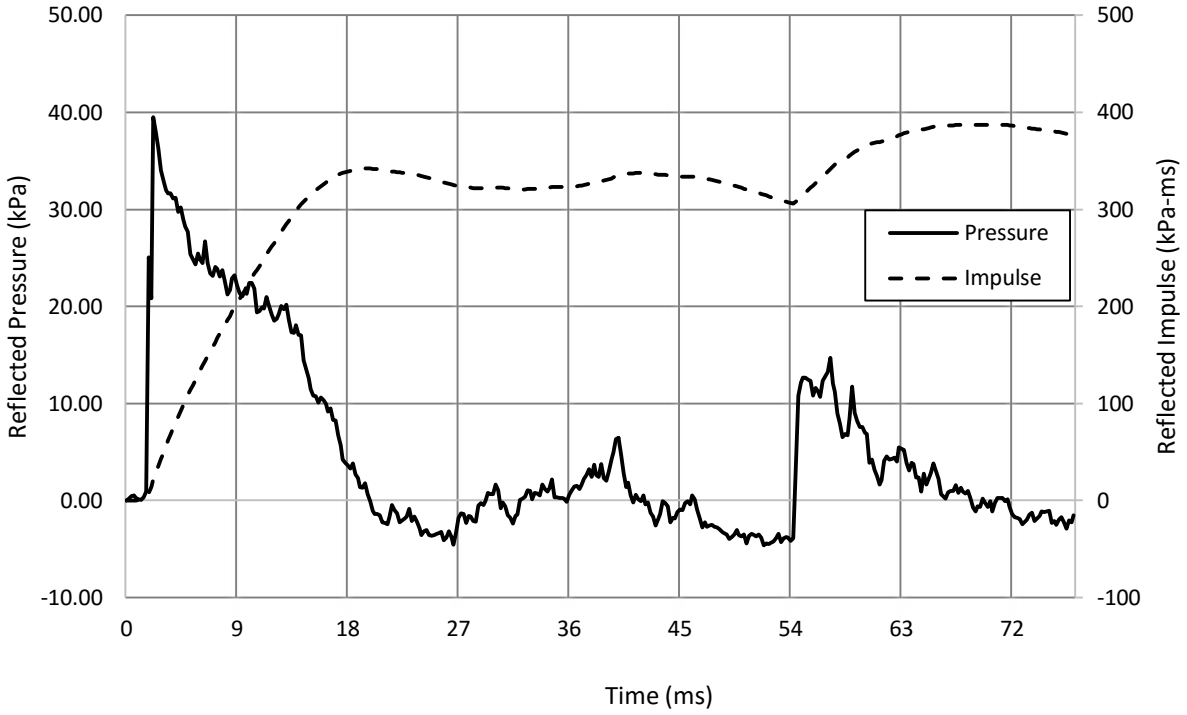

Figure A21.1 : Reflected pressure and impulse time histories for Wall 21 Shot 1

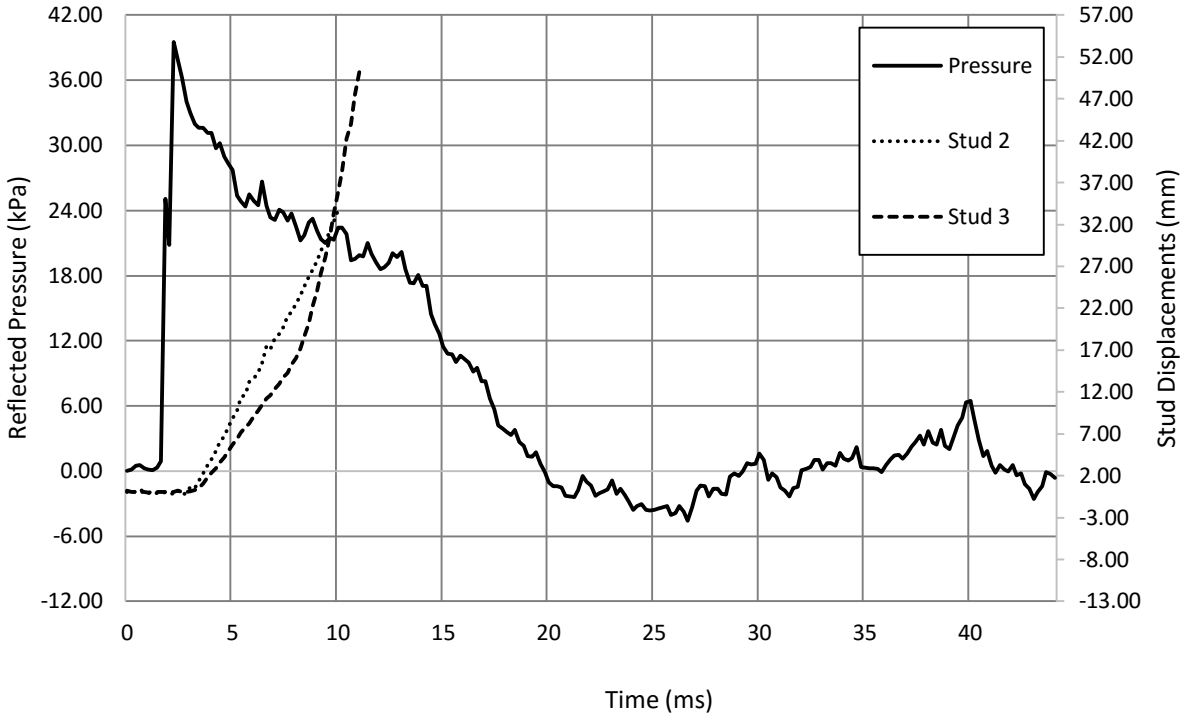

Figure A21.2 : Reflected pressure and displacement time histories for Wall 21 Shot 1

a) t = 0 ms b) t = 6 ms

c) t = 12 ms d) t = 22 ms

Figure A21.3 : Evolution of damage with time for Wall 21 Shot 1

a) Oblique view

b) Inside view

c) Damage to bottom plate

d) Slight LJS26DS fastener withdrawal

Figure A21.4 : Damage of Wall 21 after shot 1

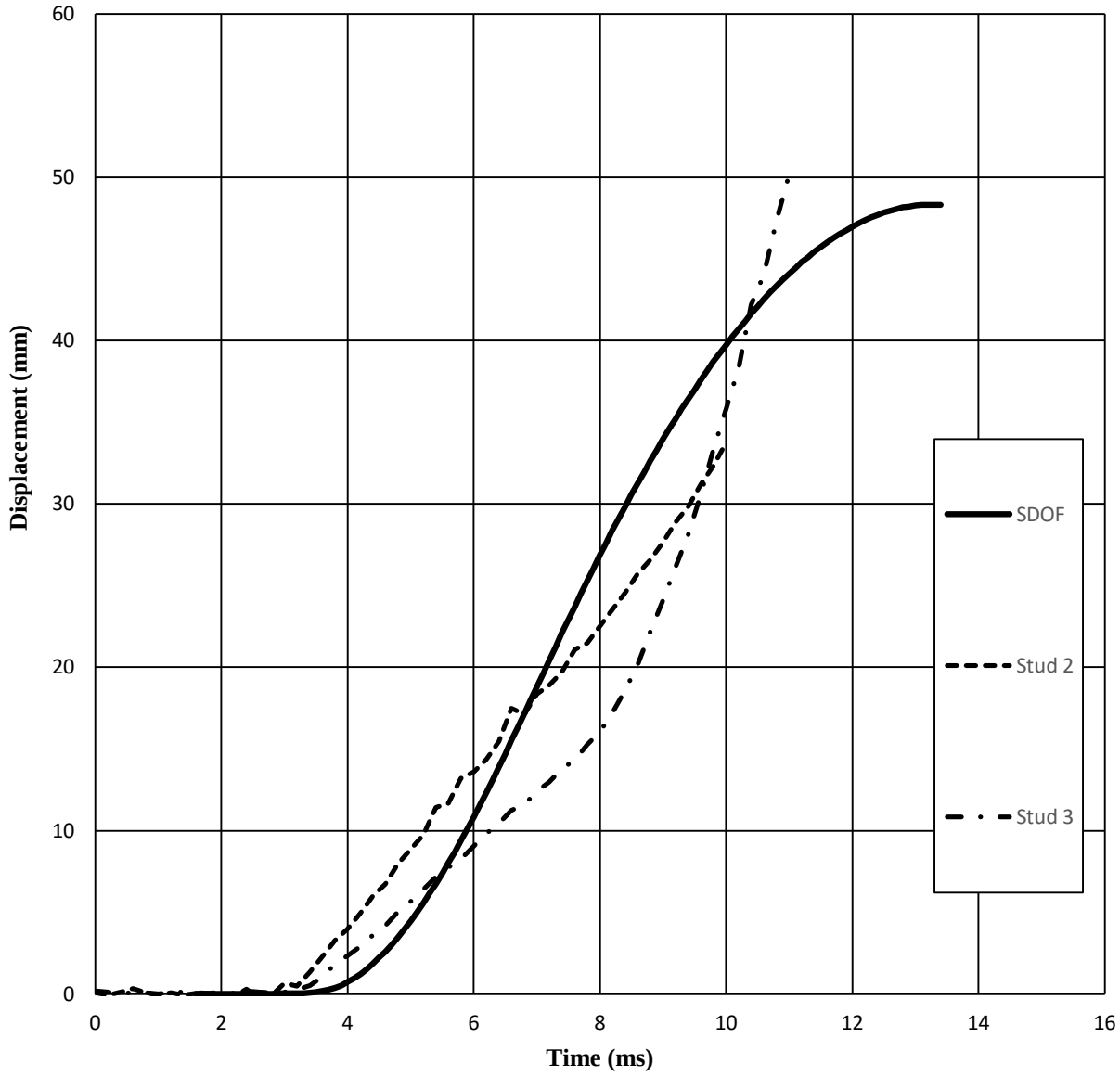

Figure A21.5 : SDOF prediction for Wall 21 Shot 1

Wall 22 Test Summary

Test name: Wall_22_Shot_1 **Test date:** 5/8/2014

Driver length: 2745 mm **Driver pressure:** 215.1 kPa

Wall mass: 71.78 kg

Test specimen properties:

- 6-38 mm x 140 mm No. 2 studs @ 406.4 mm o/c
- Nails, 50 mm x 2.87 mm @ 150 mm o/c (field and edge)
- 2108 mm total length of wall
- 2032 mm long studs
- 2032 mm clear span
- 11 mm OSB
- 12 Simpson Strong-Tie® LJS26DS joist hanger-type connectors used to connect wall to blocking

Average maximum reflected pressure: 40.3 kPa **Average max. deflection of wall studs:** 55.47 mm

Average maximum reflected impulse: 364.4 kPa-ms **Average time to max. deflection:** 8.2 ms

Positive phase duration: 18.8 ms **Quantified wall damage level:** Blowout?

Table A22.1 : Stud data from Wall 22 Shot 1

Stud number	Stud reference ID	Maximum mid-span displacement	Time to Maximum	Debris projection	Stud damage level
		mm	ms	mm	
1	S-87	-	-	No debris	Superficial
2	S-102	53.53	8.0	No debris	Failed
3	S-98	57.40	8.4	No debris	Failed
4	S-121	-	-	No debris	Failed
5	S-109	-	-	No debris	Failed
6	S-95	-	-	No debris	Superficial

Comments:

The four center studs failed in brash fashion at mid-span. Stud 1 and 6 had no visual damage. Large section of sheathing between Stud 1 and Stud 2 was blown off to a distance of 3000 mm. Large rips in the sheathing near the failure site of Stud 2, 3, 4, and 5. Sheathing joint partially intact, small gap present. Large vertical sheathing rip between Stud 1 and Stud 2, as well as between Stud 5 and 6. Significant amount of cracking and splitting was observed in the bottom plates near Stud 1 2, 5, and 6. Significant cracking and splitting in the top plate at Stud 5 and 6. Overall smaller rotation occurring at the plates when comparing the HU28 videos to that of this test. Review of the video shows that the LJS26DS effectively maintained the connection between the studs and the plates during the shot and reduced residual deflection as well as rotation of the wall plates.

No significant stud debris was created throughout the test. Minor connector screw withdrawal observed at Stud 4 and Stud 5, at both the top and bottom plate. Nail withdrawal and puncture was observed along Stud 2, 3, and 4.

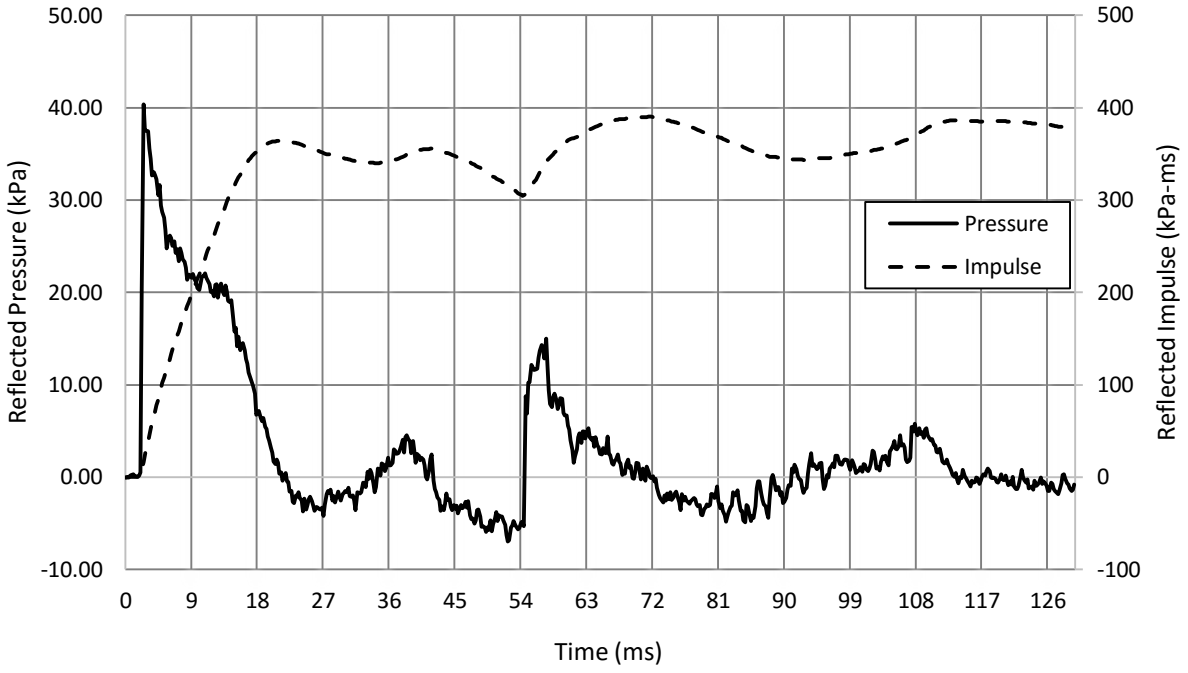

Figure A22.1 : Reflected pressure and impulse time histories for Wall 22 Shot 1

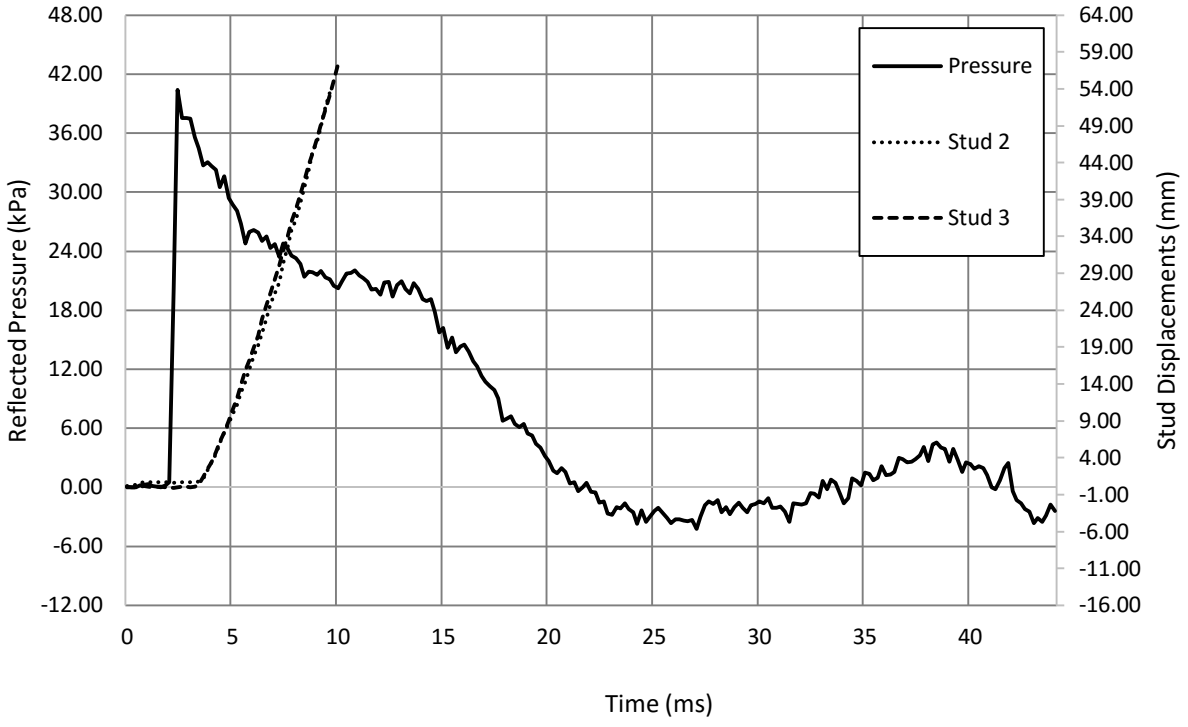

Figure A22.2 : Reflected pressure and displacement time histories for Wall 22 Shot 1

a) t = 0 ms

b) t = 10 ms

c) t = 16 ms

d) t = 24 ms

Figure A22.3 : Evolution of damage with time for Wall 22 Shot 1

a) Oblique view

b) Side view

c) Stud 4 failure mode

d) Slight LJS26DS fastener withdrawal

Figure A22.4 : Damage of Wall 22 after shot 1

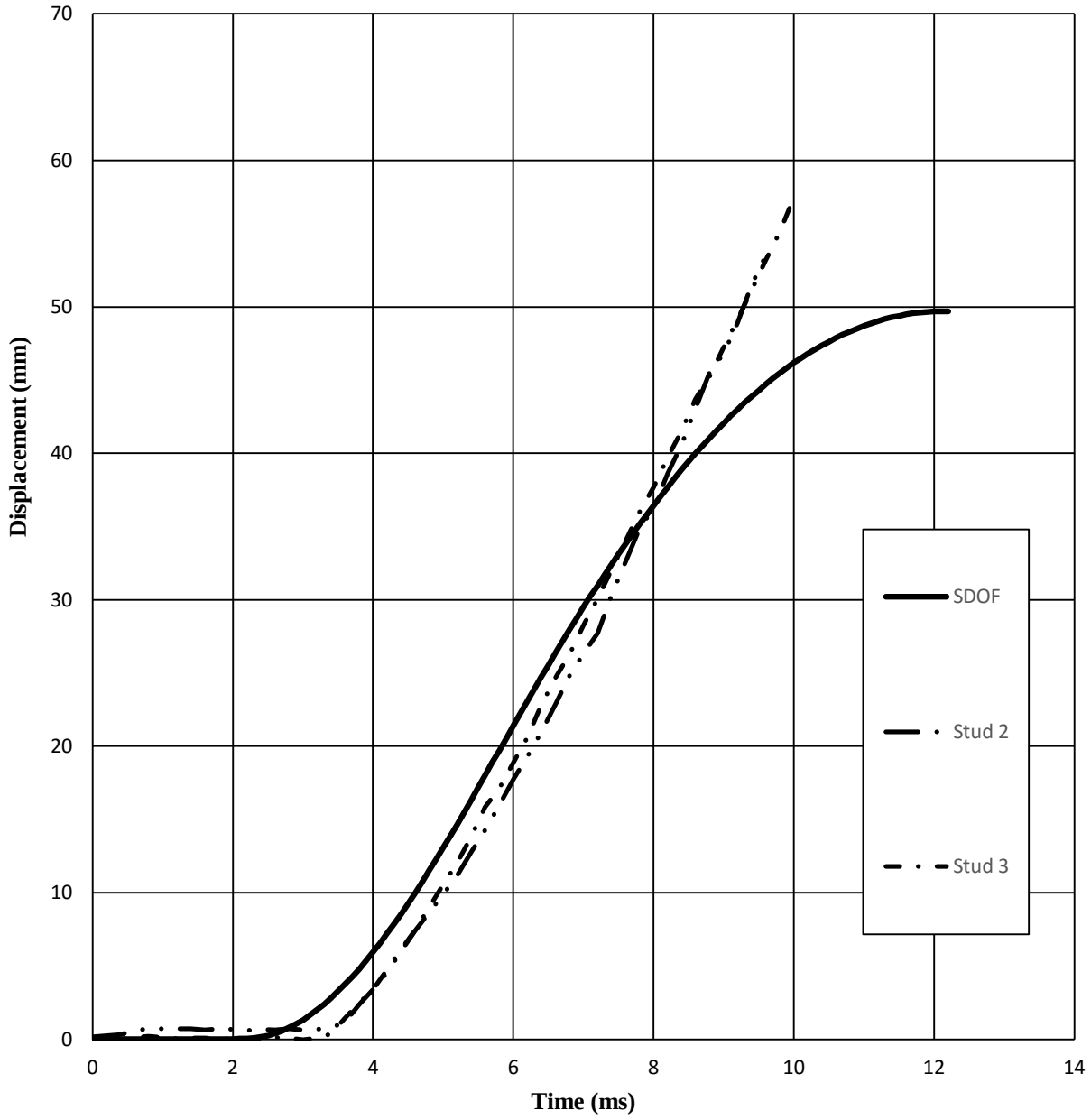

Figure A22.5 : SDOF prediction for Wall 22 Shot 1

Wall 23 Test Summary

Test name: Wall_23_Shot_1 **Test date:** 2/8/2014

Driver length: 2745 mm **Driver pressure:** 210.3 kPa

Wall mass: 70.80 kg

Test specimen properties:

- 6-38 mm x 140 mm No. 2 studs @ 406.4 mm o/c
- Nails, 50 mm x 2.87 mm @ 150 mm o/c (field and edge)
- 2108 mm total length of wall
- 2032 mm long studs
- 2032 mm clear span
- 11 mm OSB
- 12 Simpson Strong-Tie® LTS18 hurricane tie-down-type connectors used to connect wall to blocking

Average maximum reflected pressure: 42.1 kPa **Average max. deflection of wall studs:** 20.54 mm

Average maximum reflected impulse: 328.9 kPa-ms **Average time to max. deflection:** 6.8 ms

Positive phase duration: 18.0 ms **Quantified wall damage level:** Blowout

Table A23.1 : Stud data from Wall 23 Shot 1

Stud number	Stud reference ID	Maximum mid-span displacement	Time to Maximum	Debris projection	Stud damage level
		mm	ms	mm	
1	S-139	-	-	No debris	Cracking
2	S-136	19.84	7.0	No debris	Cracking
3	S-182	21.24	5.4	5500	Failed
4	S-150	-	8.4	5500	Failed
5	S-211	-	6.4	300	Failed
6	S-78	-	-	No debris	Cracking

Comments:

Connection failure occurred at Stud 1, at both top and bottom ends. Twisting of the stud was observed due to the asymmetrical nature of the connector. Some ripping in the sheathing located near the top right corner. Stud 2 was ejected from the wall, only connector by the top connector. Damage occurred at the bottom end due to splitting near the connection site. Top connector also caused some damage on the top end of the stud. Stud 3 was ejected from the wall due to splitting at the top connection site. Most likely the stud hitting the LVDT bracket caused the stud to fail. Rips in sheathing observed. Stud 4 was also ejected from the wall in the same fashion as Stud 3. Again, the connectors caused splitting failure/damage at the ends of the studs. Rupture of the top connector observed. Stud 5 was ejected from the wall due to rupture of the top connector and splitting occurring at the bottom of the stud. Stud 6 was twisted due to the asymmetrical nature of the connector, and suffered similar end damage/splitting as other studs. Large piece of missing sheathing in between Stud 5 and 6.

Significant stud debris was created by Stud 3, 4, and 5, all due to the failure of the connector or connector site (splitting). Nail withdrawal and puncture was observed along Stud 2, 3, 4, and 5. The LVDT on Stud 2 was damaged in the shot and did not record displacement data. Typical failure at the end regions occurred where the connector screws penetrated the stud. Some pieces of ruptured connectors were still attached to the studs where rupture occurred. Twisting was present in all six studs.

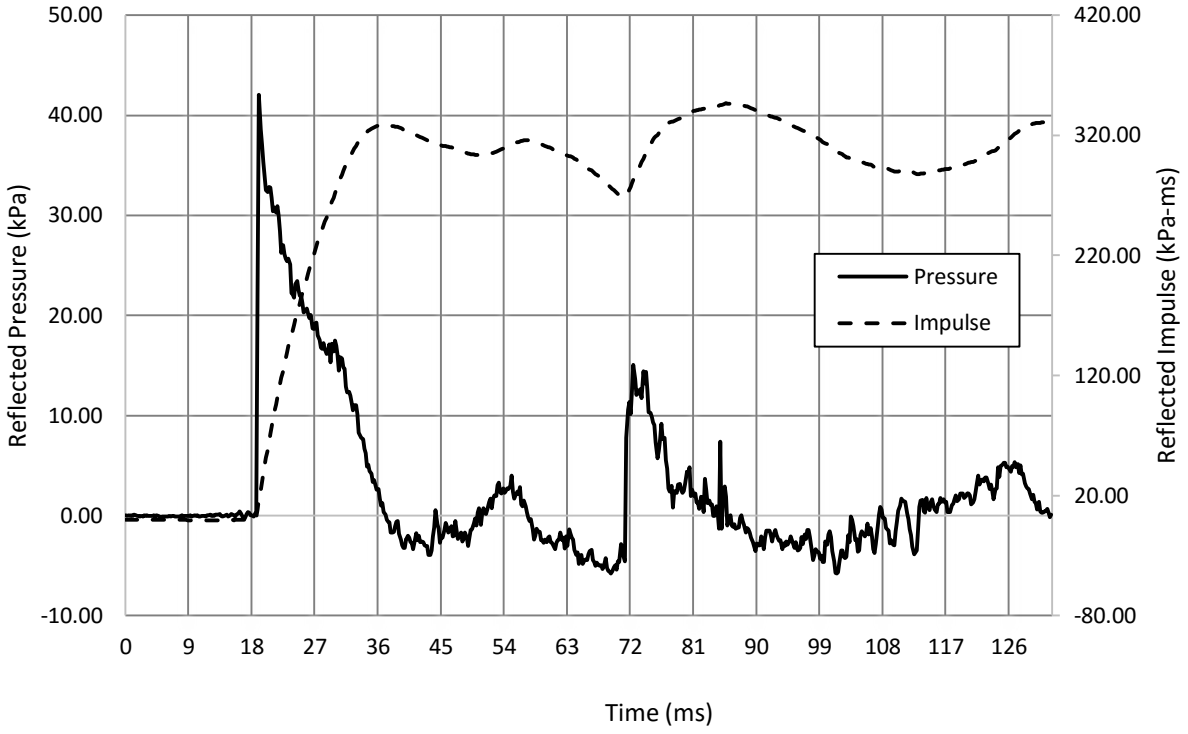

Figure A23.1 : Reflected pressure and impulse time histories for Wall 23 Shot 1

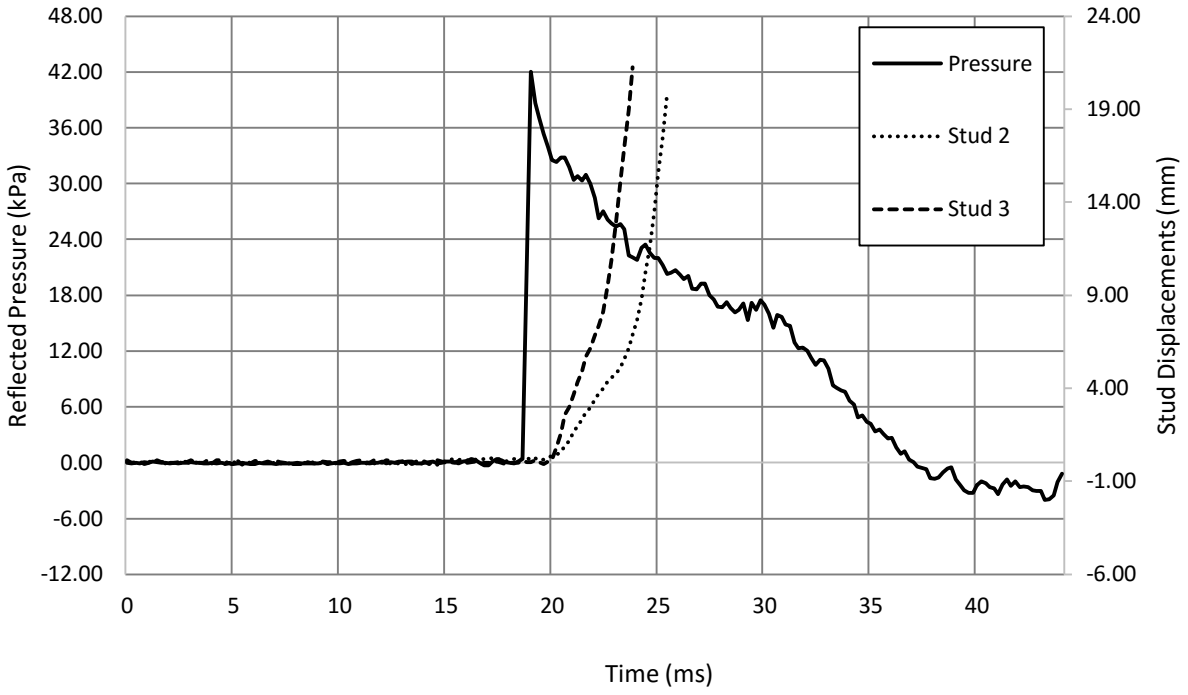

Figure A23.2 : Reflected pressure and displacement time histories for Wall 23 Shot 1

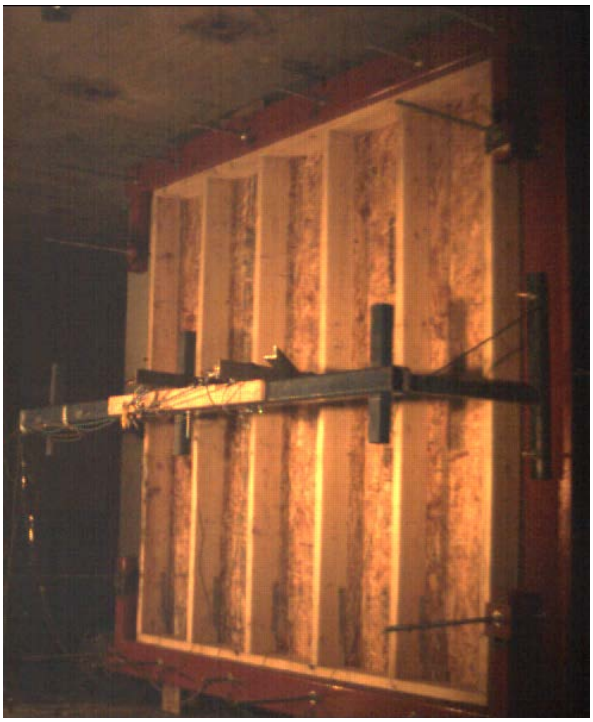

a) t = 0 ms

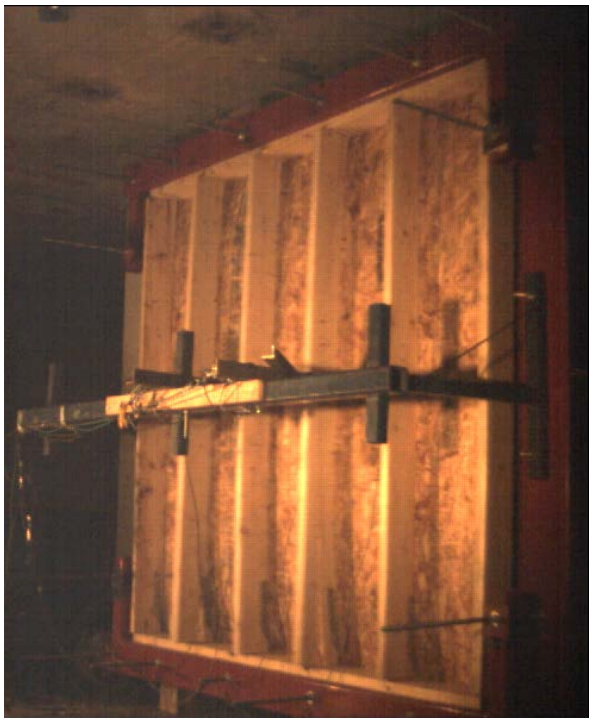

b) t = 6 ms

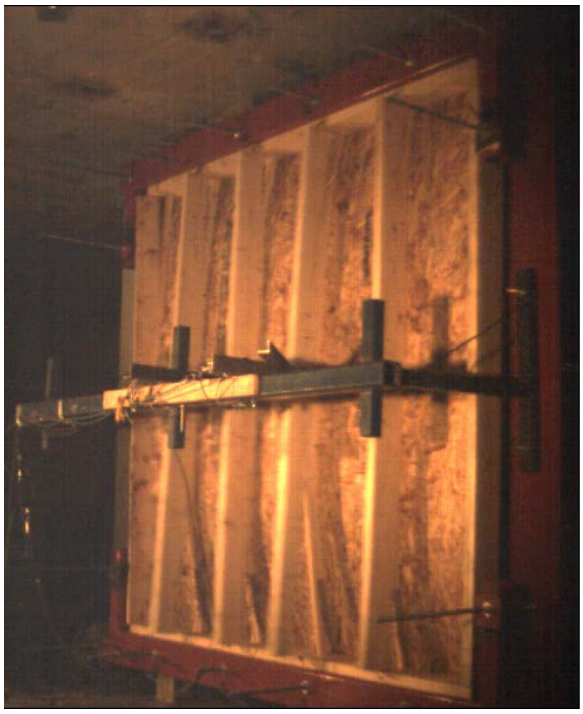

c) t = 10 ms

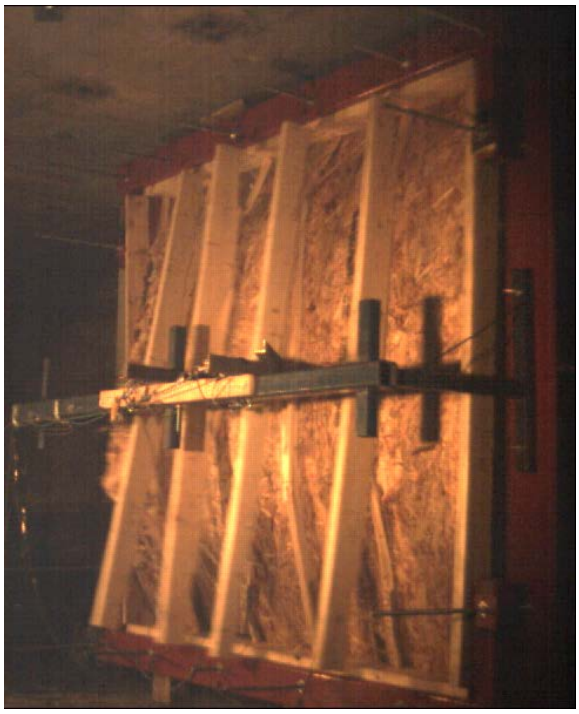

d) t = 20 ms

Figure A23.3 : Evolution of connection failure with time for Wall 23 Shot 1

a) Oblique view

b) Stud 2 Splitting failure

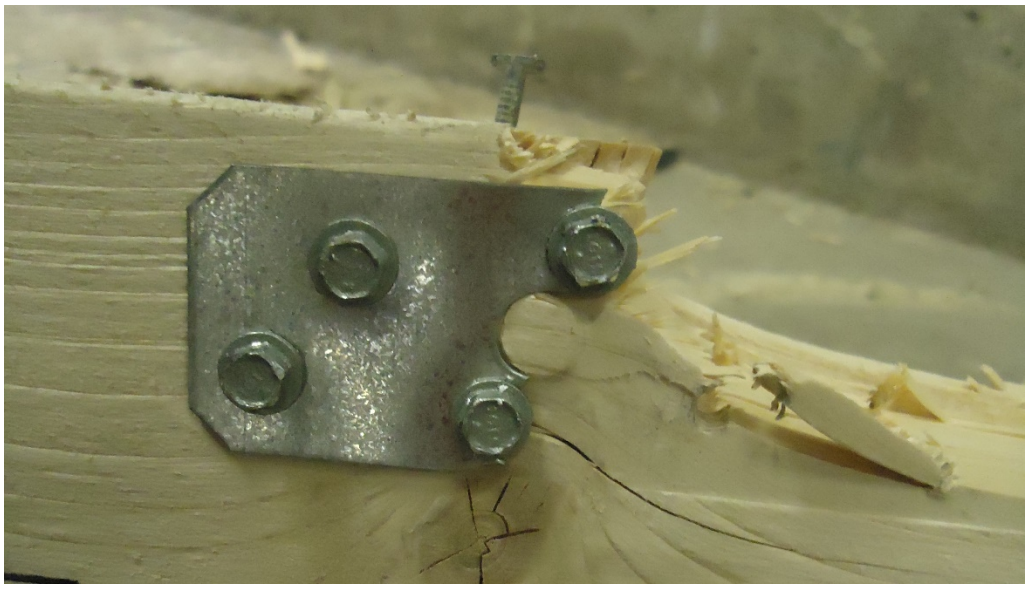

c) Rupturing of LTS18 connector on Stud 5

Figure A23.4 : Damage of Wall 23 after shot 1

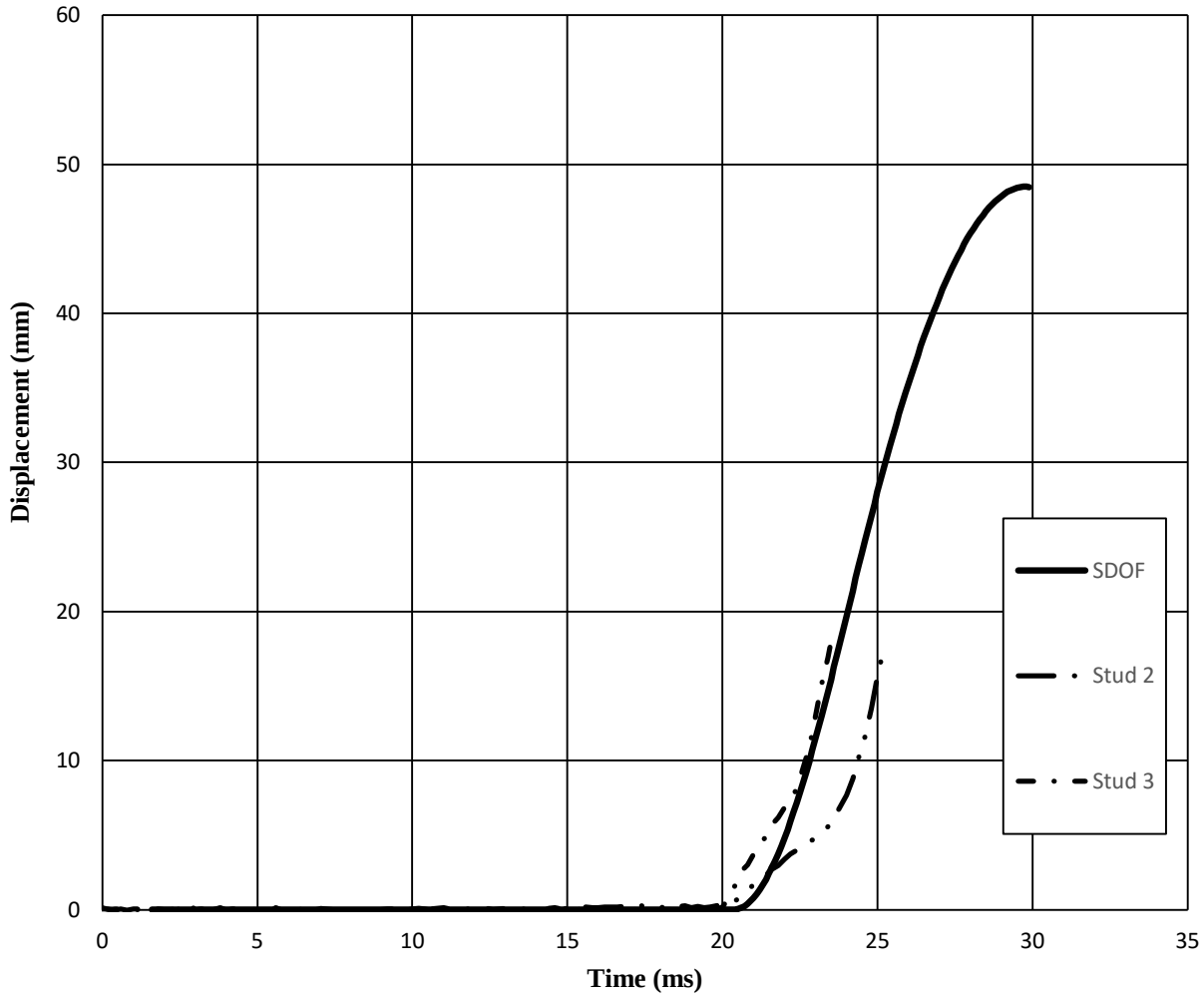

Figure A23.5 : SDOF prediction for Wall 23 Shot 1

Wall 24 Test Summary

Test name: Wall_24_Shot_1 **Test date:** 5/8/2014

Driver length: 2745 mm **Driver pressure:** 215.1 kPa

Wall mass: 72.13 kg

Test specimen properties:

- 6-38 mm x 140 mm No. 2 studs @ 406.4 mm o/c
- Nails, 50 mm x 2.87 mm @ 150 mm o/c (field and edge)
- 2108 mm total length of wall
- 2032 mm long studs
- 2032 mm clear span
- 11 mm OSB
- 12 Simpson Strong-Tie® LTS18 hurricane tie-down-type connectors used to connect wall to blocking

Average maximum reflected pressure: 39.1 kPa **Average max. deflection of wall studs:** 48.81 mm

Average maximum reflected impulse: 318.0 kPa-ms **Average time to max. deflection:** 6.80 ms

Positive phase duration: 18.0 ms **Quantified wall damage level:** Blowout

Table A24.1 : Stud data from Wall 24 Shot 1

Stud number	Stud reference ID	Maximum mid-span displacement	Time to Maximum	Debris projection	Stud damage level
		mm	ms	mm	
1	S-156	-	-	No debris*	Superficial
2	S-335	51.54	7.4	No debris*	Cracking
3	S-186	46.08	8.4	No debris*	Failed
4	S-198	-	6.2	No debris*	Failed
5	S-133	-	5.2	No debris*	Failed
6	S-124	-	-	No debris*	Superficial

* LVDT bracket prevented studs from being blown across the room. While no debris was created, real life conditions would yield extreme amounts of debris.

Comments:

Connection failure occurred at Stud 2, 3, 4, and 5, at both top and bottom ends. The top connector of Stud 2 ruptured, while all other center stud connectors caused row-shear failure/splitting. Twisting effects were observed on Stud 1 and 6 due to the asymmetrical nature of the connectors. Most of the sheathing was ripped from the wall and landed within the shock tube. Viewing of the test video shows the development of a large vertical rip in the sheathing between Stud 1 and 2, as well as Stud 5 and 6. Most of the connectors failed in sync, with all center studs being thrown against the LVDT bracket. Very similar behaviour as the other wall with the LTS18 connectors.

Majority of stud debris stayed within the shock tube due to the LVDT bracket. Nail withdrawal and puncture was observed along Stud 2, 3, 4, and 5. The LVDT on Stud 2 was damaged in the shot and did not record displacement data. Typical failure at the end regions occurred where the connector screws penetrated the stud.

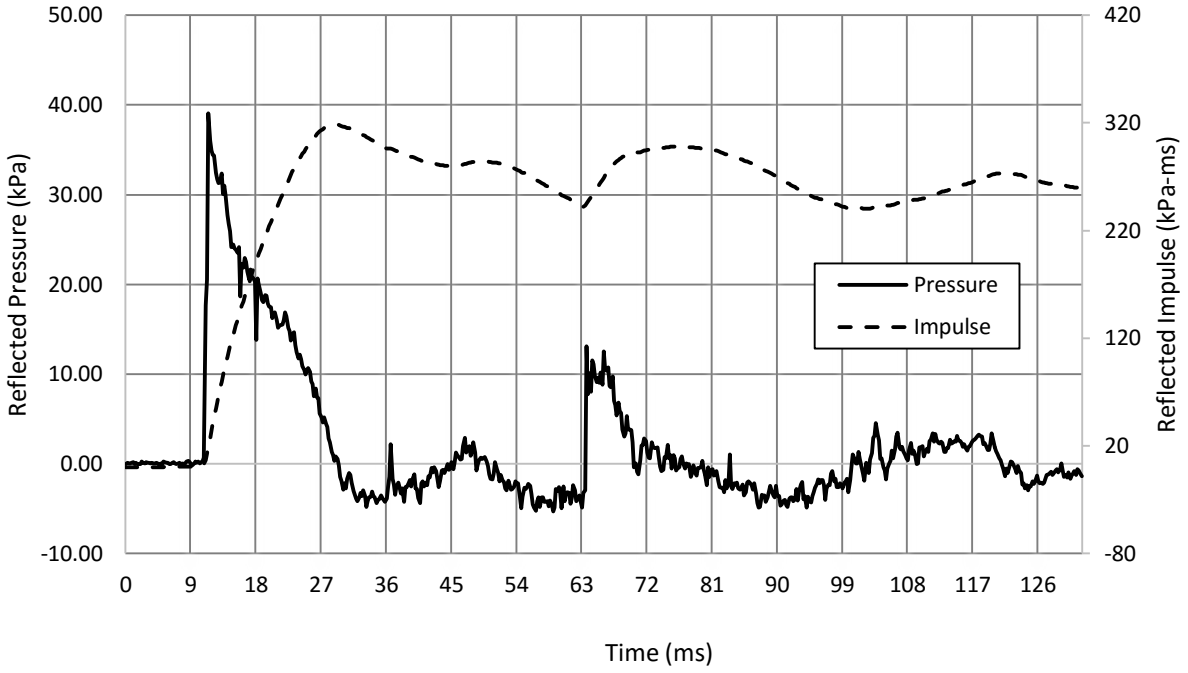

Figure A24.1 : Reflected pressure and impulse time histories for Wall 24 Shot 1

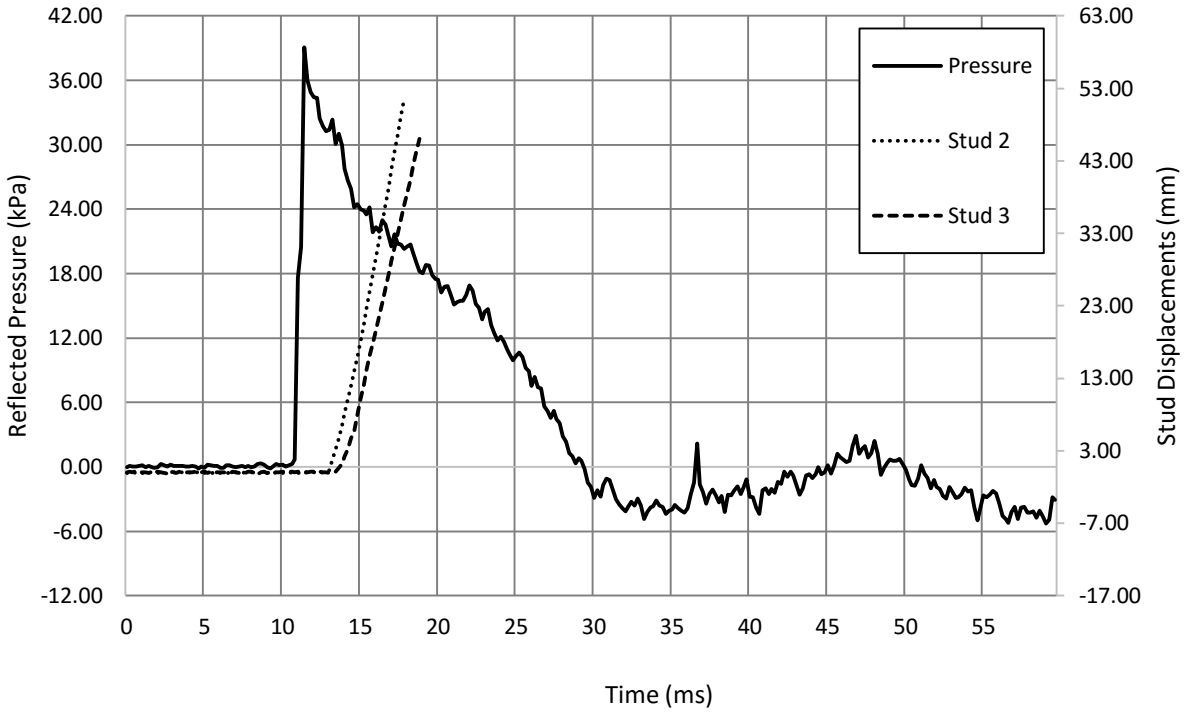

Figure A24.2 : Reflected pressure and displacement time histories for Wall 24 Shot 1

a) t = 0 ms

b) t = 8 ms

c) t = 14 ms

d) t = 20 ms

Figure A24.3 : Evolution of connection failure with time for Wall 24 Shot 1

a) Oblique view

b) Stud 5 Splitting failure

c) Rupturing of LTS18 connector on Stud 2

Figure A24.4 : Damage of Wall 24 after shot 1

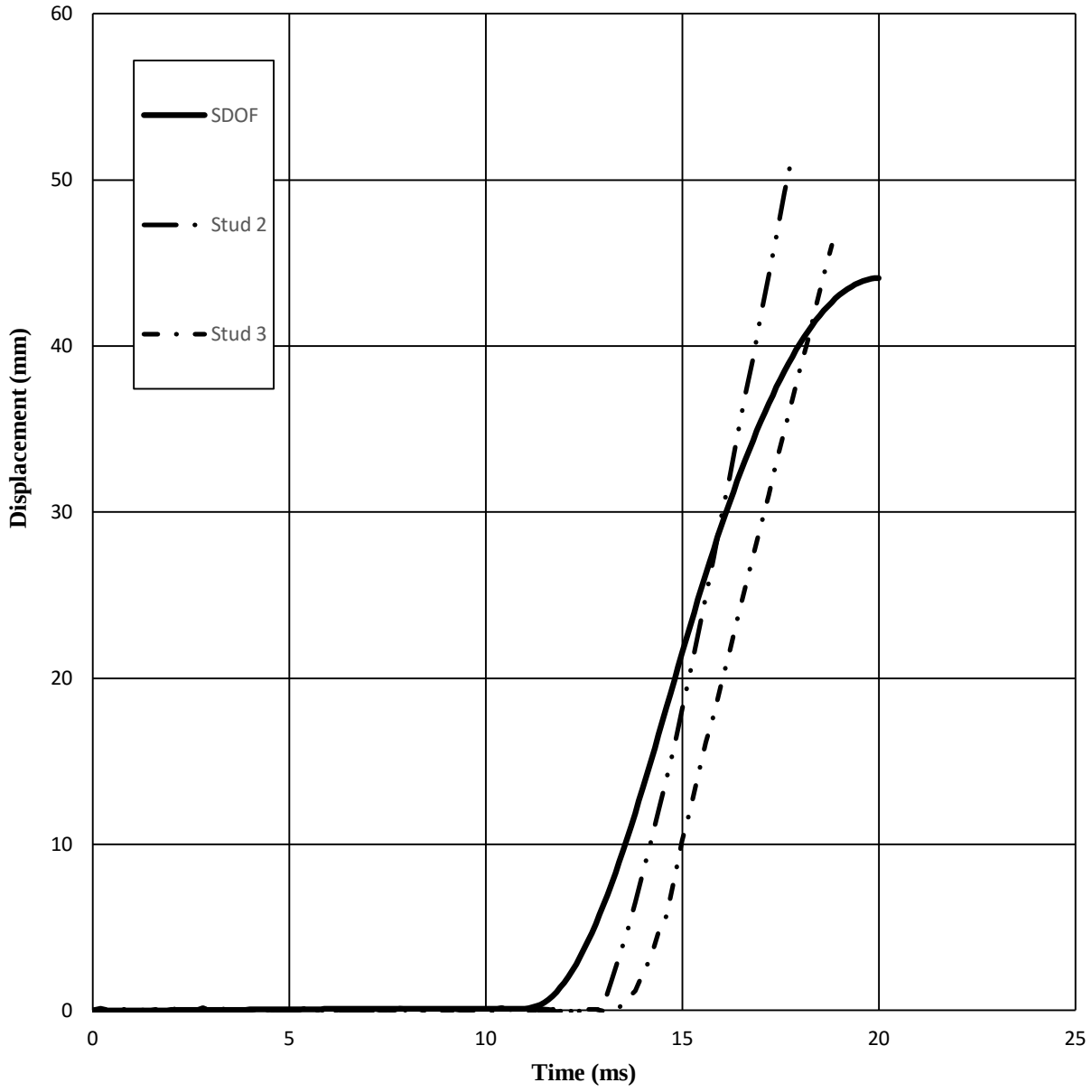

Figure A24.5 : SDOF prediction for Wall 24 Shot 1

Wall 25 Test Summary

Test name: Wall_25_Shot_1 **Test date:** 2/8/2014

Driver length: 2745 mm **Driver pressure:** 211.0 kPa

Wall mass: 72.54 kg

Test specimen properties:

- 6-38 mm x 140 mm No. 2 studs @ 406.4 mm o/c
- Nails, 50 mm x 2.87 mm @ 150 mm o/c (field and edge)
- 2108 mm total length of wall
- 2032 mm long studs
- 2032 mm clear span
- 11 mm OSB
- 12 Simpson Strong-Tie® ML24Z angle-type connectors used to connect wall to blocking

Average maximum reflected pressure: 38.8 kPa **Average max. deflection of wall studs:** 31.66 mm

Average maximum reflected impulse: 377.4 kPa-ms **Average time to max. deflection:** 9.5 ms

Positive phase duration: 15.8 ms **Quantified wall damage level:** Blowout

Table A25.1 : Stud data from Wall 25 Shot 1

Stud number	Stud reference ID	Maximum mid-span displacement	Time to Maximum	Debris projection	Stud damage level
		mm	ms	mm	
1	S-197	-	-	No debris	Failed
2	S-126	33.29	9.8	5500	Failed
3	S-131	30.03	9.2	300	Failed
4	S-248	-	-	No debris	Failed
5	S-112	-	-	5500	Failed
6	S-334	-	-	No debris	Failed

Comments:

Stud 1 failed near the top connection, where a split occurred then travelled down the stud towards the third point. Both connectors showed signs of yielding, but little screw withdrawal. Heavy nail-withdrawal was observed. Stud 2 failed similarly to Stud 1, with the bottom half being ejected. Connectors also showed signs of minor yielding. A rip in the sheathing began to form near the failure site of Stud 2. Stud 3 failed in flexure, with the failure occurring from the bottom connector, travelling upwards to the compression zone at mid-span. Yielding in both connectors was observed. The ripping in sheathing at mid-span was observed, as well as nail withdrawal in the top-half. Stud 4 failed in similar fashion as the other studs, with splitting occurring at the bottom connector and travelling up until the compression zone at mid-span. The same rip observed near Stud 2 and 3 is ongoing near the center of the wall. Large splits were observed at the top connector of Stud 4. The sheathing joint, which is located along Stud 4, showed displacement and a minor gap could be observed. Stud 5 failed similar to the other studs, with its top half being ejected. Splitting could be seen occurring at both connection sites. Significant nail-withdrawal occurred along Stud 5. Stud 6 only suffered damage near the top connector, where splitting caused the stud to dislodge from the sheathing. The bottom connector, however, kept Stud 6 in the wall frame. The bottom Stud 6 connector showed signs of yielding.

A large vertical rip occurred in between Stud 5 and 6, which has been typical in these tests. Typical failure at the end regions occurred where the connector screws penetrated the stud. Some twisting could be observed, due to the asymmetrical design of the connector.

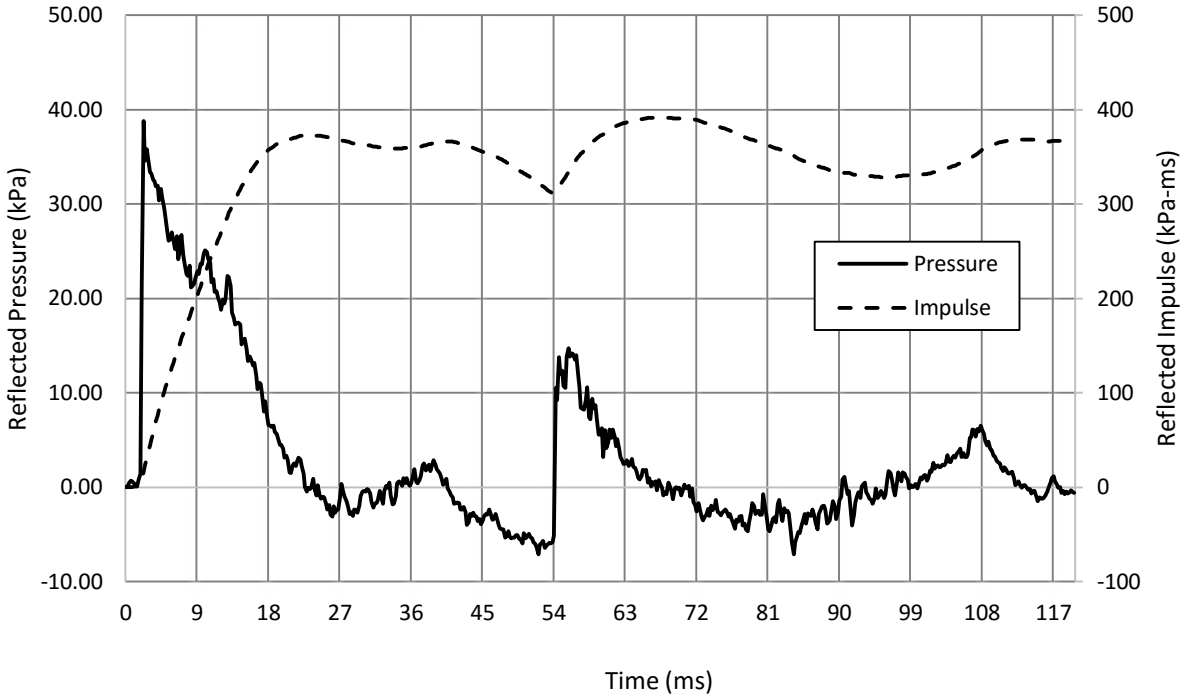

Figure A25.1 : Reflected pressure and impulse time histories for Wall 25 Shot 1

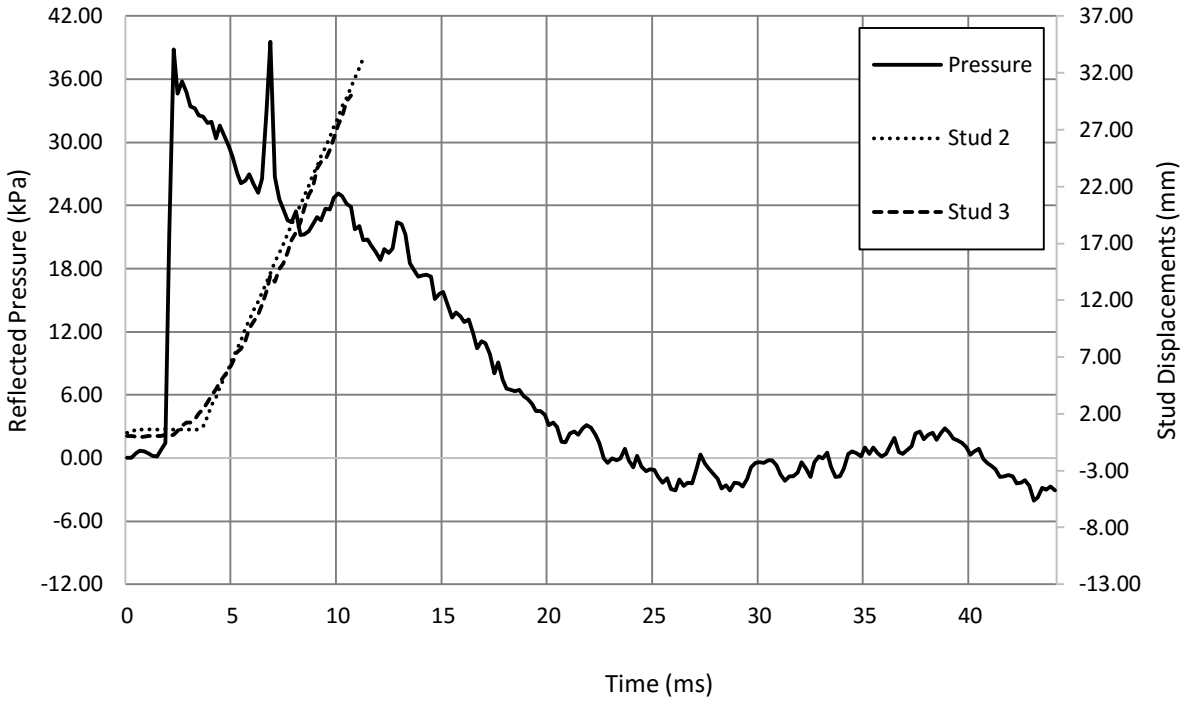

Figure A25.2 : Reflected pressure and displacement time histories for Wall 25 Shot 1

a) t = 0 ms

b) t = 33 ms

c) t = 66 ms

d) t = 99 ms

Figure A25.3 : Evolution of damage with time for Wall 25 Shot 1

a) Oblique view

b) Yielding of connector

c) Side view

Figure A25.4 : Damage of Wall 25 after shot 1

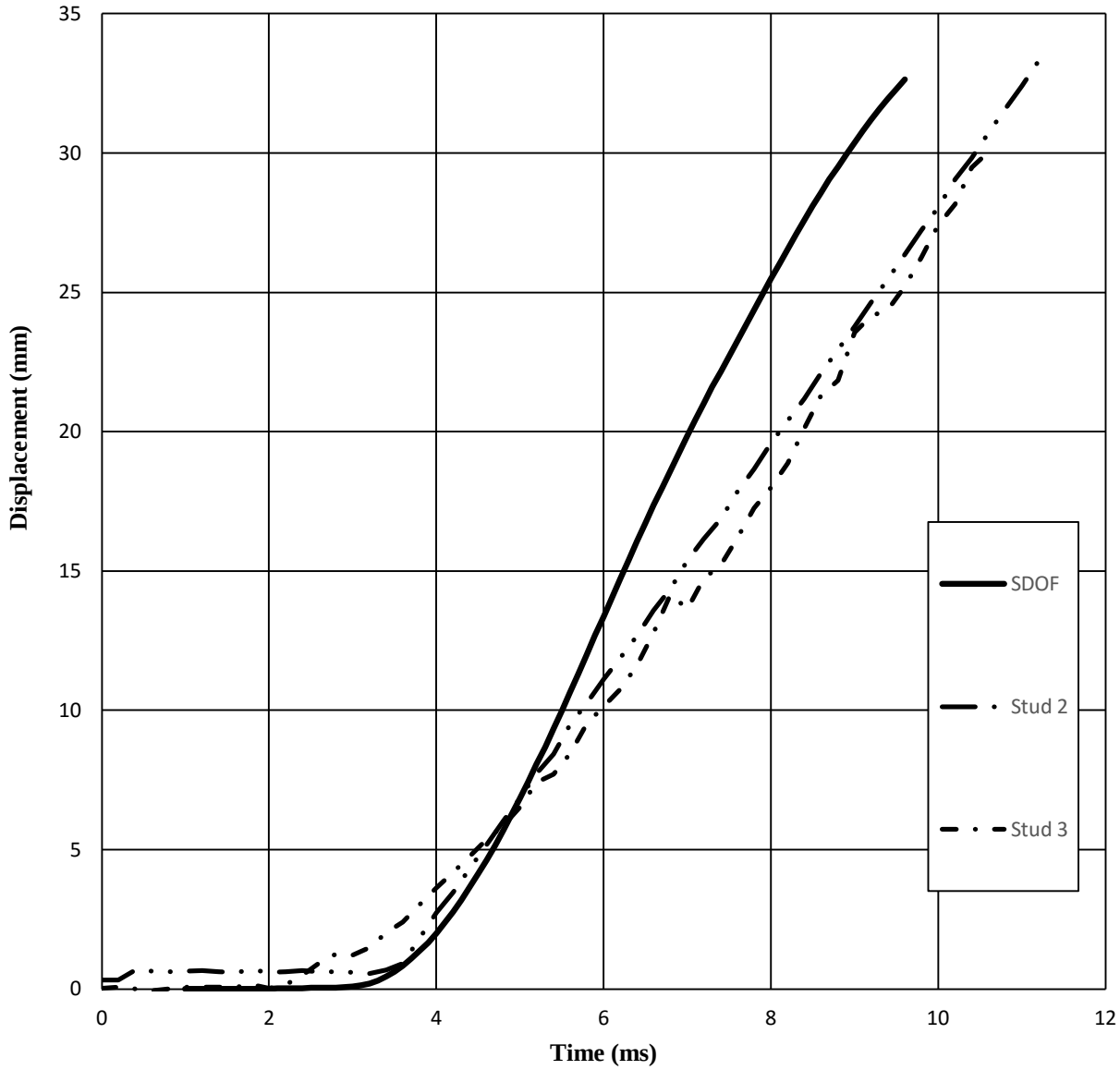

Figure A25.5 : SDOF prediction for Wall 25 Shot 1